Jan Iżykowski

Fault location on power transmission lines

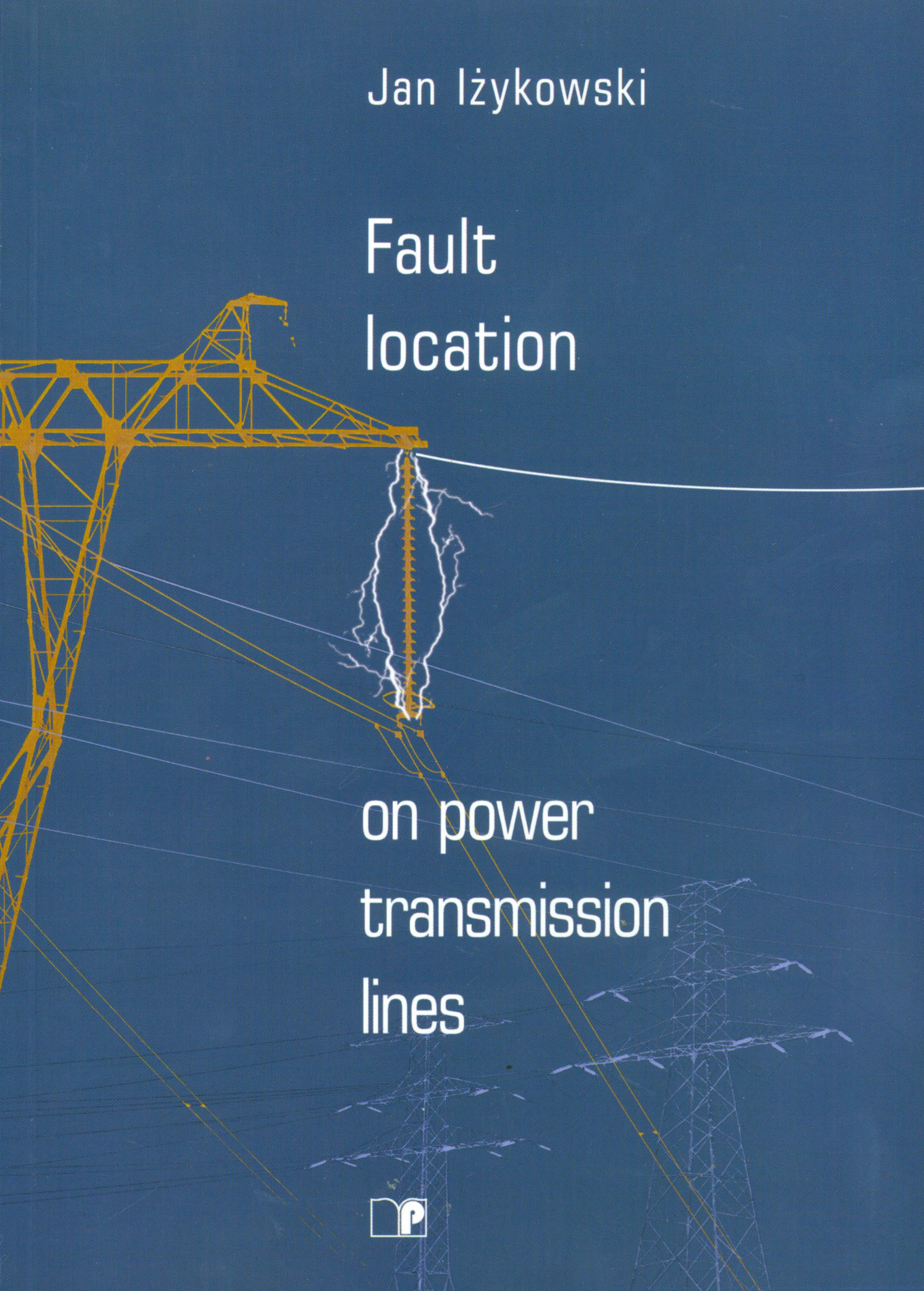

Jan Iżykowski

Fault location on power transmission lines

Oficyna Wydawnicza Politechniki Wrocławskiej
Wrocław 2008

Reviewer
Andrzej WISZNIEWSKI

Editorial layout and proof-reading
Halina MARCINIAK

Cover design
Justyna GODLEWSKA-ISKIERKA

The cover image is based on the original photo by Andrzej Marek CIURASZKIEWICZ.

OFICYNA WYDAWNICZA POLITECHNIKI WROCŁAWSKIEJ
Wybrzeże Wyspiańskiego 27, 50-370 Wrocław
http://www.oficyna.pwr.wroc.pl
e-mail: oficwyd@pwr.wroc.pl

ISBN 978-83-7493-430-5

Drukarnia Oficyny Wydawniczej Politechniki Wrocławskiej. Zam. nr 907/2008.

Contents

Preface

Importance of fault location

Electric power systems have grown rapidly over the past fifty years. This has resulted in a huge increase of the number of overhead power lines in operation and their total length. These lines experience faults due to various causes. In most cases, electrical faults manifest themselves in mechanical damage, which must be repaired before the line is put back to service. The restoration can be expedited if the location of the fault is either known or can be estimated with good accuracy. Fault locators provide estimate for both sustained and transient faults.

The subject of fault location has been of considerable interest to electric power utility engineers and researchers for several decades. Most of the research done to date has been aimed at finding the locations of transmission line faults. This is mainly because of the impact of transmission line faults on the power systems and the time required to physically check the lines is much longer than in the case of faults occurring in other power system components. Recently, the location of faults has received growing attention as many utilities operate in a deregulated environment and compete with each other to increase the availability of power supply to the customers, assuring at the same time adequate quality of power.

Research on fault location conducted at the Wrocław University of Technology

The research into transmission line fault location at the Institute of Electrical Power Engineering of the Wrocław University of Technology (WrUT) has been initiated by Prof. Andrzej Wiszniewski more than 25 years ago. In 1983, Prof. Andrzej Wiszniewski developed the fundamental one-end fault location algorithm, which is still often referred to in the fault location literature worldwide. Then, in 1994, our team of researchers started co-operation with the ABB AB in Västerås (Sweden), under the supervision of Dr. Murari Mohan Saha (ABB) and Prof. Eugeniusz Rosołowski (WrUT). It was a great pleasure for me to be a member of this team and to be given the possibility of joint work on the fault location and protective relaying issues. Also, I appreciate very much the co-operation with Dr. Bogdan Kasztenny, previously affiliated with the WrUT and presently with the GE Multilin–Markham, Canada. For the last three years the research has been governed by the ABB Corporate Research Center in Kraków. A part of the research was conducted within the grants of the Ministry

of Science and Higher Education of Poland, as well as within the Ph.D. theses completed by Dr. Rafał Kawecki, Dr. Przemysław Balcerek and Dr. Rafał Moląg, under my supervision.

Acknowledgements

My sincere gratitude goes to everyone who worked with me during the research on the fault location, within the project conducted in co-operation with ABB AB, especially to Dr. Murari Mohan Saha and Prof. Eugeniusz Rosołowski. Also, I would like to thank warmly all the academic staff members of the Power System Control and Protection Group. This wonderful research group was initially led by Prof. Andrzej Wiszniewski, then by Prof. Janusz Szafran, and lately by Prof. Eugeniusz Rosołowski. It is my great pleasure and satisfaction to belong to the team, in which there is an unusual atmosphere of work and friendship.

Special thanks are due to the reviewer of this book Prof. Andrzej Wiszniewski for his effort in the reviewing and many suggestions as to the changes and improvements.

Finally, my deepest appreciation goes to my family for limitless patience and understanding.

Jan Iżykowski
Wrocław, July 2008

A Note for the Reader

This book deals with fault location on transmission lines. Among many fault location methods, the impedance-based method has been taken for detailed considerations. In this method, the impedance parameters of the faulted line section are considered as a measure of the distance to fault. The impedance-based fault location appears to be still the most popular method. This is so, since impedance-based fault location algorithms exhibit various advantages and can be easily implemented into the products offered by the numerous manufacturers.

The book begins (Chapter 1) with explaining the aim of fault location and its importance. In particular, the fault locators are considered as the devices that differ in many aspects from protective relays. Then, different fault location methods are shortly characterised.

In Chapter 2, the basics of the impedance-based fault location are presented. Division of fault location algorithms with respect to the fault locator input signals is performed and time intervals of fault locator input signals are defined. Then, signal processing methods for fault location are shortly reviewed. In relation to use of distributed digital measurements to fault location, their synchronisation with the aid of the GPS or by analytical synchronisation is described. The fault location error is defined and the sources of errors are characterised.

Chapter 3 reviews different configurations of the networks. The networks containing single-circuit lines, double-circuit lines, multi-terminal and tapped lines, composition of overhead line and cable, and series-compensated lines are presented. Then, the lumped-parameter and distributed-parameter line models are presented. The modal transformations are gathered.

In Chapter 4, the basics of transmission line faults are provided. The fault models are formulated using symmetrical components and phase co-ordinates approach. The analysis of arcing faults, including typical waveforms of current and voltage signals, obtained from the ATP-EMTP simulation, is presented.

Chapter 5 is focused on the measurement chains of fault locators. Transient performance of capacitive voltage transformers and their dynamic compensation are considered. The basics for current transformers are given. It has been shown how to counteract the negative effects of the possible saturation of current transformers, when

deriving fault location algorithms. The design of analogue low-pass filters is addressed.

In Chapter 6, a variety of one-end impedance-based fault location algorithms are presented. To this end, a uniform description of the faults and the fault loops has been applied. The algorithms presented are designed for locating faults on single-circuit lines, double-circuit lines and series-compensated lines. Both transposed and untransposed lines are taken into consideration. The algorithms are formulated for the lumped line models, however, at the end of the chapter, the way of improving fault location accuracy by introducing the distributed-parameter line model is presented.

Chapter 7 is focused on two-end and multi-end fault location algorithms. First, the algorithms utilising two-end synchronised measurements are presented for both phasor-based and time domain approaches. Then, the unsynchronised measurements as applied to fault location are considered in detail. Different options for measuring the synchronisation angle are introduced and various fault location algorithms are presented. Complete and incomplete two-end measurements are taken into account. Algorithms utilising measurements of distance relays from line terminals are described. Fault location on three-terminal and multi-terminal lines is addressed.

The author presents fault location algorithms developed by himself or in cooperation, as well as algorithms selected from the vast literature of the subject. When presenting fault location on series-compensated lines, the considerations are intentionally limited to the basic network configuration with a single-circuit line and to using the one-end measurements. The other fault location algorithms can be found in the literature.

1. Introduction

1.1. Aim of fault location and its importance

Rapid growth of electric power systems over the last decades has resulted in a large increase in the number of transmission and distribution lines [B10, B12, B23] in the world. At the same time, free marketing and de-regulation introduced all over the world impose more and more restrictive requirements on providing a continuous and good quality power supply, without any significant increase in the cost of energy being delivered. The terms such as continuity of power supply, dependability and reliability play a very important role in contemporary power systems. As a result of imposing restrictive requirements, an increased demand for high-quality power system protection and control devices together with their supplementary equipment became a matter of prime importance. Among the different functions of those devices the fault location is considered to be very important [B.7, B.9, B.11, B.16, B19, B20, 21, 162].

Fault location is a process aimed at location of the fault with the highest accuracy possible. **Fault locators** are in general the supplementary protection equipment, which apply the **fault location algorithms** for estimating a distance to the fault. When locating faults on a line consisting of more than one section (multi-terminal line), initially a faulted section has to be identified and then a fault on this section has to be located.

Fault location function can be implemented in [B.9, B.16]:

1. microprocessor-based relays,
2. digital fault recorders (DFRs),
3. stand-alone fault locators,
4. post-fault analysis programs.

Including the fault location as an additional function in microprocessor-based relays is a common practice. In this case, high computational capability and communication with remote sites of modern relays are taken advantage of at little or almost no additional cost. Also, digital fault recorders enable an easy and not costly incorporation of the fault location function. In turn, stand-alone fault locators are applied in the case of using sophisticated fault location algorithms and on condition that higher cost of the implementation is accepted. Yet, there is another possibility which concerns

post-fault analysis programs [64] with fault location algorithms included. Such programs are mainly used for verification of the operation of protective relays.

Transmission and distribution lines experience temporary and permanent faults. Temporary faults, which are most frequent on overhead lines, in many cases could be self-cleared. In consequence, the continuity of power supply is not permanently affected, which is advantageous. In turn, upon the occurrence of permanent fault, the protective relaying equipment, using circuit breakers, enables the faulted sections to be de-energized. If a given line is put out of service, the connected loads are not supplied or, if possible, the other lines are forced to supply the loads of the tripped line. It is also possible that a series of cascading trippings may happen, taking out of service successively larger and larger parts of the system. Under some unfavourable circumstances, this may even lead to blackouts of large power systems, as has recently happened in some countries. Contemporary power systems get closer and closer to their operating limits. Therefore, in order to avoid blackouts special attention must be paid to equipping power systems with protection and control devices, as well as to their settings.

In the case of permanent faults, power supply can be restored after the maintenance crew have finished the repair of the damage caused by the fault. For this purpose, the fault position has to be known, otherwise the whole line has to be inspected for finding the place of damage. Thus, it is important to know the location of a fault or to locate it with possibly high accuracy. This allows us to save money and time spent on inspection and repair, as well as to provide a better service due to the possibility of faster restoration of power supply. Also, blackouts can be avoided this way.

Temporary faults are self-cleared and do not permanently affect the continuity of supply, however, the location of such faults is also important. In this case, the fault location can help pinpoint the weak spots on the line, and therefore, it should be included in maintenance schedules to avoid serious problems in the future.

Even if helicopters are immediately available for patrol following unsuccessful reclosing, fault locators perform a valuable service. Trouble cannot always be found by a routine patrol with no indication of where the fault occurred. For example, tree growth could reduce clearances, resulting in a flashover during severe conductor sagging. By the time the patrol arrives, the conductors have cooled, making the clearance to the tree increase. The weak spot is not well recognized [64].

The importance of fault locators is more obvious where foot patrols are relied upon, particularly on long lines, in rough terrain. Also, these can help where maintenance jurisdiction is divided between different companies or divisions within a company.

Fault locators are valuable even where the line has been restored either automatically or non-automatically. In this category are the faults caused by cranes swinging into the line, brushfires, damaged insulators and vandalism. The locator allows rapid arrival at the site before the evidence is removed or the “trail becomes cold”. Also, the knowledge that repeat faults are occurring in the same area can be valuable in detect-

ing the cause. Weak spots that are not obvious may be found because a more thorough inspection can be focused in the limited area defined by the fault locator.

1.2. Fault locators versus protective relays

Fault locators and protective relays are closely related, however, there are some important differences between them. These differences can be considered as related to the following features [B.16]:

1. accuracy of fault location,
2. speed of determining the fault position,
3. speed of transmitting data from remote site,
4. used data window,
5. digital filtering of input signals and complexity of calculations.

The above can be further explained as follows:

1. Fault locators are used for pinpointing the fault position accurately and not only for indication of the general area (defined by a protective zone) where a fault occurred – which is provided by protective relays.

2. In the case of protective relays, both the measurement and decision making are performed in an *on-line* regime. High speed of operation of protective relays appears as a crucial requirement imposed on them. This is so since in order to prevent spreading out the fault effects, the faulted line has to be switched-off as quickly as possible. Therefore, high speed measuring algorithms are applied in contemporary protective relays, and use of high-speed operating circuit breakers is also of prime importance. Fault clearing time is an important consideration in the selection of protective relays and requirements for relaying speed must be carefully determined. If the relaying is too slow, system instability, excessive equipment damage, and adverse effects on customer service may result. On the other hand, faster protection tends to compromise relay system security and selectivity. The requirement for the fast clearing of faults demands that the decision for tripping transmission lines has to be made in a short time, even faster than in one cycle of the fundamental frequency (20 ms for the systems operating at 50 Hz). In contrast, the calculations of fault locators are performed in an *off-line* mode since the results of these calculations (position of the fault and in the case of some algorithms also the fault resistance involved) are for human users. This implies that the fault location can be longer and take seconds or even minutes.

3. Low-speed data communications or Supervisory Control and Data Acquisition (SCADA) can be applied for fault location purposes, which differs from communication used by protective relays.

4. The best data window segment from the whole available window can be selected for fault location to reduce errors. This is so since the computations are per-

formed in an *off-line* regime and searching for the best data window can be easily applied. The fault interval lasts from a fault incipience up to a fault clearing by a circuit breaker, and usually this takes around three fundamental frequency cycles, which is sufficient for fault location.

5. In the case of the protective relays the high speed required causes that the calculations are not to be too complex nor much time-consuming. In contrast, fault location calculations have no such limitations. Therefore, more accurate phasor calculation for fault location, including rejection of dc components, can be applied. Also, the models of the power line and the fault in fault location algorithms are usually more advanced than for relaying.

Among different types of relays commonly used for protecting power lines, distance relays [B.3, B.18, B.21, B.24, B.25, 18] are the most related to fault locators. These relays are desiged for fast and reliable indication of the general area where a fault occurred. If the fault is recognized as occurring within the pre-defined protective zone, then a trip signal to the corresponding circuit breaker is sent immediately. In consequence, the fault becomes isolated quickly, which minimises the impact of a fault on a power network.

Distance relays have multiple protection zones for providing back capability. The relay that detects the fault in the 1st zone is designed to trip first. Generally, a pair of distance relays is used to protect a two-terminal line. Usually, they can communicate with each other, forming a pilot relaying. As a result of exchanging information between the distance relays from the line terminals, they both could trip within the 1st zone.

The operation of a distance relay may be significantly influenced by the combined effect of load and fault resistance, which is known as **the reactance effect** [18, 31, 182]. The distance relay may misoperate for a forward external fault, or may not operate for an internal fault if the value of the fault resistance is too large. The value of the fault resistance may be particularly large for ground faults, which are the most frequent faults on overhead lines.

The influence of fault resistance on measurement performed by distance relays is explained in Figs. 1.1 and 1.2. The explanation is performed in relation to a single phase case, which can be easily extended to a three-phase one, with different fault types being considered [18, 31, 182]. Figure 1.1 shows a circuit diagram of the transmission network experiencing a fault (F), involving resistance (R_F), on a homogeneous single-phase line with impedance ($\underline{Z}_L$) between buses S and R. For the sake of simplicity, a lumped line model is taken into account, with shunt capacitances being neglected. Parts of the network behind the local (S) and remote (R) terminals are replaced by the Thevenin equivalents containing EMFS and equivalent source impedances [B.1].

The fault loop seen from the bus S can be described with the following formula, using the phasor notation:

$$\underline{V}_S - d\underline{Z}_L \underline{I}_S - R_F \underline{I}_F = 0 \tag{1.1}$$

where:

d – distance from the bus S to fault point F, expressed in relative units (p.u.),

$\underline{V}_S$, $\underline{I}_S$ – voltage and current measured at the measurement point (here at the bus S),

$\underline{I}_F$ – total fault current (flowing through the fault path resistance), which for the assumed lumped line model and neglected shunt capacitances, equals:

$$\underline{I}_F = \underline{I}_S + \underline{I}_R \tag{1.2}$$

The formula (1.1) can be written as:

$$\underline{Z}_S = \frac{\underline{V}_S}{\underline{I}_S} = d\underline{Z}_L + R_F \frac{\underline{I}_F}{\underline{I}_S} \tag{1.3}$$

where $\underline{Z}_S$ – impedance determined on the basis of the voltage and current measured at point S.

From (1.3) it is seen that the impedance $\underline{Z}_S$ is a strict measure of the distance to fault (d), only if the fault resistance is equal to zero or is very low and can be neglected. Otherwise, the fault resistance R_F is seen, in general, as a certain impedance:

$$\underline{R}_F^{\#} = \frac{\underline{I}_S + \underline{I}_R}{\underline{I}_S} R_F \tag{1.4}$$

Depending on the currents at both line ends ($\underline{I}_S$, $\underline{I}_R$), the fault resistance R_F can be seen as $\underline{R}_F^{\#}$, which presents:

- pure resistance (Fig. 1.2a),
- resistance and capacitive reactance (Fig. 1.2b),
- resistance and inductive reactance (Fig. 1.2c).

In the last two cases (Figs. 1.2b and c), the reactance (capacitive or inductive) is observed to contribute to resistance, and that is why such an effect is called “reactance effect” [31, 36, 68, 120].

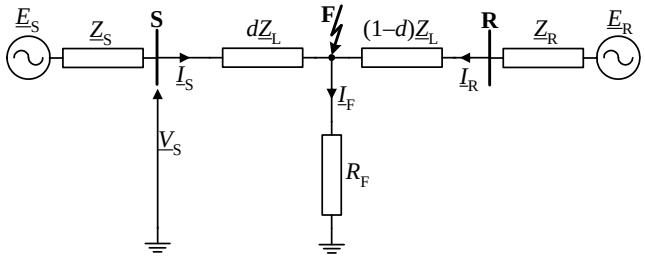

Fig. 1.1. Circuit diagram of transmission network with line S–R affected by fault (F) involving fault resistance R_F

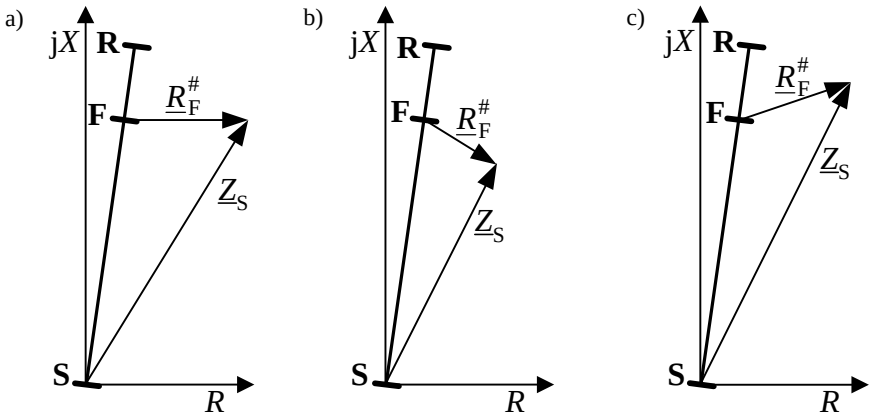

Fig. 1.2. Influence of remote in-feed on one-end fault-loop impedance measurement by protective distance relay

1.3. Fault location methods

In a natural way fault location can be done by foot patrols or by patrols equipped with different transportation means (including helicopters or airplanes) and binoculars. Such a way of the faulted line inspection is considered to be time-consuming. Also, calls from witnesses of damage on the power line, or customer calls, can provide the required knowledge about the fault position. However, such primitive ways do not satisfy the requirements imposed on fault location.

In spite of the various attempts at different techniques, **the automatic fault location** still appears to be the most widely used. It is based on determining the physical location of a fault by processing the voltage and current waveform values. Automatic fault location can be classified under the following main categories:

1. technique based on fundamental frequency currents and voltages, mainly on impedance measurement,
2. technique based on the phenomenon of travelling waves,
3. technique based on measuring high frequency components of currents and voltages generated by faults,
4. pulse methods,
5. use of fault indicators,
6. monitoring the induced radiation from the power system arcing faults, using VLF and VHF reception,
7. knowledge-based approaches.

Making use of the fundamental frequency voltages and currents at the line terminal (or terminals), together with the line parameters, appears to be the simplest way of

determining the fault location. It is assumed that the calculated impedance of the faulted line segment is a measure of the distance to fault. The algorithms belonging to this category are called as **impedance-based fault location algorithms.** Such fault location algorithms are economical and simple to implement. Depending on the input signals of the fault locator, these methods can be further classified. This issue is considered in Chapter 2. Formulation and description of different impedance-based fault location algorithms are presented in Chapters 6 and 7.

Travelling wave methods consider the voltage and current waves, travelling at the speed of light from the fault towards the line terminals. These methods are considered very accurate, being at the same time complex and costly for application, since they require high sampling frequency [109, 173].

The technique based on measuring **high frequency components** of currents and voltages generated by faults, which travel between the fault and the line terminals, is not widely used either. This method is considered expensive and complex, since use of specially tuned filters for measuring high frequency components is required [10, 110].

Pulse methods [B.19, B.20] are the other fault location methods in use. They are based on injecting the testing signals (pulses) into the line. Knowledge of the propagation speed of the pulse signal together with time required for reaching the fault place are the basis for determining fault location. Single- and double-pulse methods are applied for locating permanent and temporary faults, respectively. The testing signal can be injected into the operating line or into the line already switched-off.

Valuable information on fault location can be obtained also from **fault indicators**, installed either in substation or on towers along the transmission or distribution line [173]. Additional use of a radio link allows the information from indicators to be used even during inclement weather.

Another, unconventional fault location system for monitoring transient induced radiation from power system arcing faults, using both **VLF and VHF reception**, has been tested in the experimental installation [179]. In the near future, such systems could compete with the conventional fault location systems.

Recently, a lot of research effort has been focused on fault location techniques using **knowledge-based approaches**, such as artificial neural networks, fuzzy sets theory and expert systems. There is a huge number of scientific papers in journals and conference proceedings dealing with the knowledge-based fault location. This issue, though deserving wide consideration is out of the scope of this book.

2. Impedance-based fault location – basics

2.1. Fault locator input signals

Depending on what input signals of the fault locator are used, the fault location methods can be further classified into respective sub-categories. In the case of a two-terminal and single-circuit line, the methods utilising the following input signals can be distinguished:

- three-phase current and three-phase voltage measured at one line end, Sections 6.2, 6.5–6.7, 6.12, 6.14, 7.4.4,
- three-phase current or three-phase voltage measured at one line end, Sections 6.10, or 6.11, respectively,
- three-phase current and three-phase voltage measured at two line ends, Sections 7.2, 7.3,
- incomplete three-phase current and three-phase voltage measured at two line ends, in particular:
  - three-phase voltage from two line ends, and current from one line end, Section 7.4.2,
  - three-phase current from two line ends, and voltage from one line end, Section 7.4.3,
  - three-phase voltage from two line ends, Section 7.4.1.

Also, different availability of measurements for the fault locator can be considered for double-circuit lines, Sections 6.8, 6.9. Similarly, different availability of the fault locator input signals could be distinguished in application to the three-terminal (Section 7.5), and multi-terminal and tapped (Section 7.6) lines. The above sub-categories can be further sub-divided with respect to other features, as for example, the technique applying two-end measurements can be sub-divided into the methods using:

- unsynchronised measurements, Section 7.3,
- synchronised measurements, Section 7.2.

Various fault location methods, with acceptable accuracy for most of the practical applications, have been developed using one-end techniques. These techniques utilise measurements of three-phase current and three-phase voltage from one line end (Fig. 2.1).

A major advantage of these techniques is that no communication means are needed and simple implementation into digital protective relays or digital fault recorders is possible.

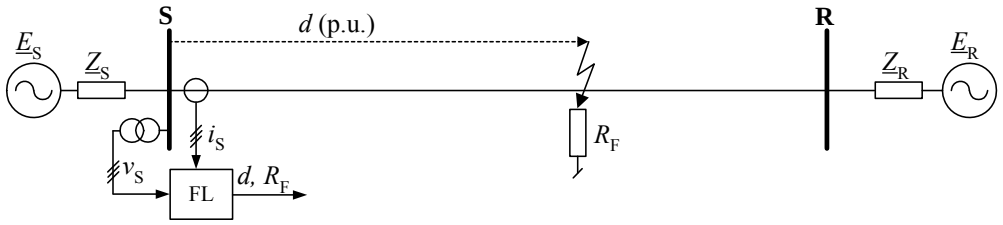

Fig. 2.1. Schematic diagram of one-end fault location

The fault location algorithms could be more accurate if more information about the system were available. Therefore, if communication channels are available, then the two-end fault location methods (Figs. 2.2 and 2.3) may be used. The two-end technique offers improved fault location determination, without any assumptions and information regarding the external networks such as impedances of the equivalent sources. In this way, if the two-terminal technique can be applied, the compensation for the reactance effect becomes immaterial.

Following fault isolation, relays or other digital devices at the substations can transmit the fault data to a substation computer via a modem or other communications link. The fault data can also be transmitted, through the dedicated communication link, directly between the relays or other devices at both ends of the protected line. The substation computer and/or digital relays can process the data and obtain a fault location estimate with minimal assumptions, reducing the estimation error. Only low-speed communication is necessary for this application. If needed, the data could also be retrieved manually for estimation of the fault location and sent via internet or using some other means.

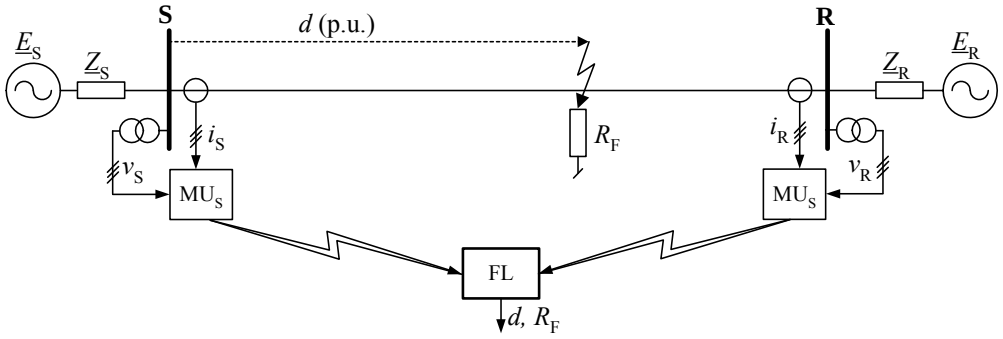

Fig. 2.2. Schematic diagram of two-end unsynchronised fault location

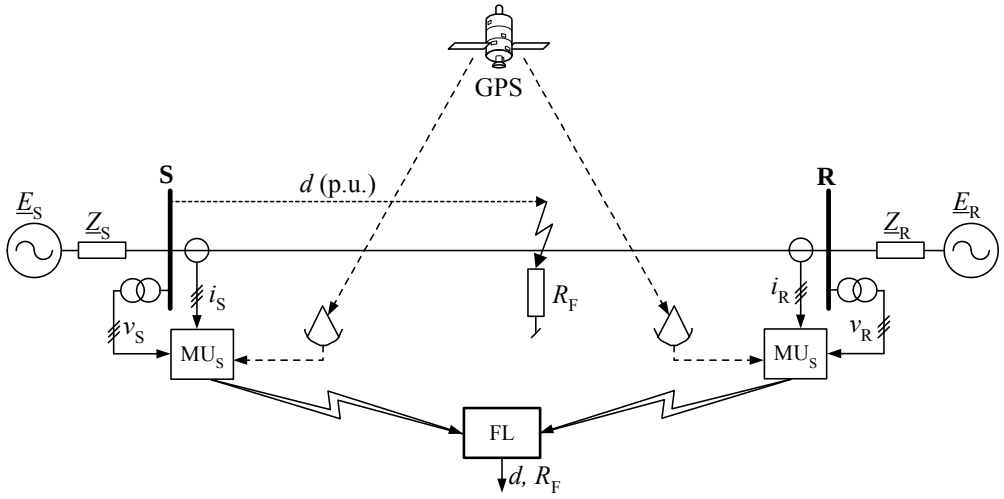

Fig. 2.3. Schematic diagram of two-end synchronised fault location using GPS synchronisation

Figures 2.2 and 2.3 present schematically a two-end fault location on a two-terminal transmission line S–R. The fault locator (FL) is here shown as a stand-alone device, however, it can also be incorporated into the measurement unit at either side of the line (MU_S or MU_R). At both terminals (S, R) there are current transformers and voltage transformers which transform signals to the measurement units.

In the measurement units the digital measurements are performed. It is considered that in the case of Fig. 2.2 the A/D converters in the measurement units are not provided with the GPS signals. Therefore, the determined phasors of currents and voltages, which are the fault locator input signals, do not have common time reference; i.e. the measurements are unsynchronised.

Fault location with two-end synchronised measurements is depicted in Fig. 2.3. This is accomplished with use of technical means for providing a common time reference of the measurements acquired at the line terminals. Here, the satellite Global Positioning System (GPS) [B8, 19] is considered as the synchronisation means.

The satellites of the GPS are owned and operated by the US Department of Defense but civilian users also have access. There are 24 satellites that are positioned in such a way that four or more of them are observable at every location on the earth. Each satellite contains a highly accurate clock. Satellites maintain the so called **Coordinated Universal Time** with the accuracy of ±0.5 μs.

In order to show how high accuracy is assured let us relate the GPS accuracy to:

- *a single cycle* (T_1) *for the fundamental frequency of* 50 Hz:
  - the accuracy of ±0.5 μs corresponds to ± (1/40000)T_1, (note: T_1 = 20 ms);
  - the accuracy of ±0.5 μs corresponds to (±1/40000)360° = ±0.009°, note: $T_1 \rightarrow$ 360°.

• *a single sampling period*, *for example*, *for sampling frequency equal to* 1000 Hz:
  – the accuracy of ±0.5 μs corresponds to $\pm(1/2000)T_s$;
  – the accuracy of ±0.5 μs corresponds to ±(1/40 000)360 = 0.009°, note $T_s \rightarrow$ 360/20 = 18°.

If no GPS signal is received during 8 hrs, the time drift of the backing up crystal oscillator in the application reported [19] does not exceed 20 μs. The ability of GPS to provide a time reference signal, synchronised at widely separated locations has been lately recognised as having great potential for power system applications [B8, 19].

2.2. Time intervals of fault locator input signals

Figure 2.4 presents examples of waveforms of three-phase voltage recorded under a single phase-to-earth fault. The following time intervals can be distinguished considering their position with respect to this fault incipience and its clearance (achieved as a result of the protective relay operation and switching off the line by the circuit breaker):

• **pre-fault interval**: lasting from the beginning of the recording up to the fault incipience instant detected ($t_{\text{flt\_incipience}}$),

• **fault interval**: lasting from the fault incipience instant ($t_{\text{flt\_incipience}}$) up to the fault clearance instant detected ($t_{\text{flt\_clearance}}$),

• **post-fault interval**: lasting from the fault clearance instant ($t_{\text{flt\_clearance}}$) up to the end of the event recorded.

According to the kind of the time interval, one can distinguish:

• **pre-fault quantities** – signals recorded within the pre-fault interval,

• **fault quantities** – signals recorded within the fault interval,

• **post-fault quantities** – signals recorded within the post-fault interval.

However, there is no uniform usage of this nomenclature in the literature related to the fault location issue. Sometimes, instead of "fault interval" and "fault quantities", the terms "post-fault interval" and "post-fault quantities" are used, since the prefix "post-" has the meaning "after the fault (incipience)" and not "after the fault (clearance)".

Usually, it is the fault quantities (voltage and current) that are used in fault location. There are also many fault location approaches in which the pre-fault quantities are additionally included as the fault locator input signals. However, sometimes, usage of the pre-fault measurements is treated as the drawback of the fault location method. This is so, since in some cases the pre-fault quantities could not be recorded or they do not exist, as for example, in the case of the current during some intervals of the auto-

matic reclosure process. Also, the pre-fault quantities may not be of pure sinusoidal shape, due to the appearance of the fault symptoms just before its occurrence. Also, in some hardware solutions, measurement of pre-fault (load) currents is accomplished with lower accuracy than for much higher fault currents. Therefore, if possible, the pre-fault measurements are usually avoided.

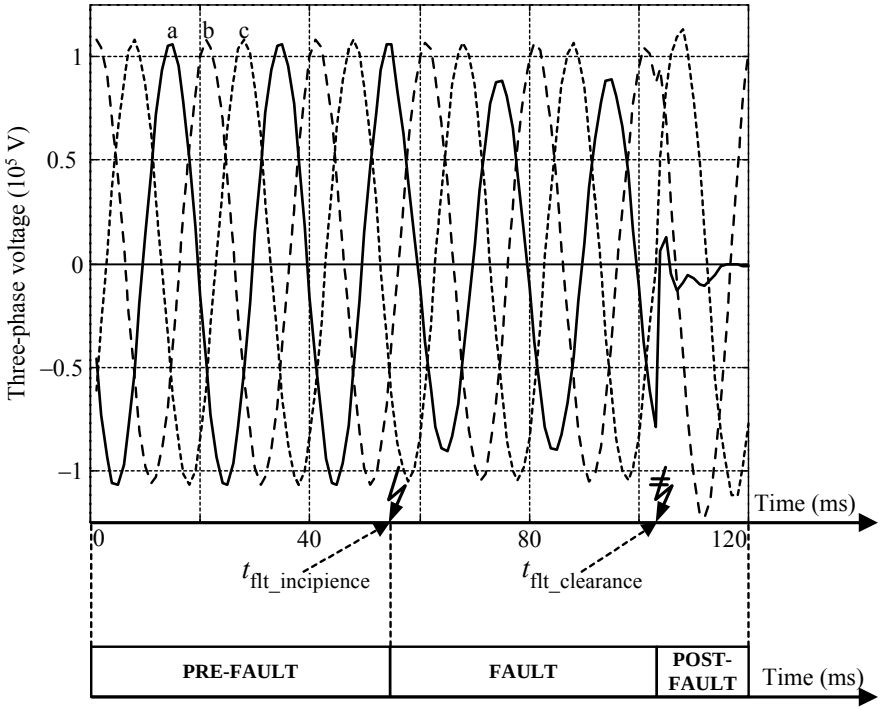

Fig. 2.4. Time interval positions with respect to instances of fault incipience and its clearance

As opposed to the fault and pre-fault quantities, the post-fault quantities are rather rarely used for the fault location purposes. One of such techniques is presented in [169].

2.3. Signal processing methods for fault location

Input signals of the fault locator provide information necessary for determination of a distance to fault. The measurement chains of the fault locator are described in Chapter 5. The continuous-time voltages and signals at the line terminal undergo transformation in these chains (containing instrument transformers, analogue low-pass

filters and A/D converters) to discrete-time signals. These signals are applied for description of the faulted network. One can distinguish the following main methods for description of the state of the faulted network:

- phasor approach,
- instantaneous state of the system representation.

The multi-resolution analysis, which is connected with application of such signal processing tools as the Short Time Fourier Transform (STFT), the Wavelet Transform (WT) and others [B.15, 138] is also utilised for fault location.

In the phasor concept, the post-fault state is assumed to be a steady one. Consequently, the processed voltage and current signals are represented in the form of sinusoidal waveforms with constant magnitude and angle velocity ω. The faulted network may thus be entirely described using the voltage/current phasors and impedance/admittance data of the network. Such a treatment is also called the frequency-domain circuit analysis [B.4].

Applying the phasor approach, the phasors of phase voltages and phase currents are determined. Also, phasors for the voltage and current **symmetrical components** are processed. A vast majority of fault location algorithms are based on the phasor approach.

Symmetrical components approach appears to be a very effective technique for transposed lines and therefore it is advantageous that the fault location algorithm is formulated in terms of these components. In general, the following symmetrical components of the quantities measured can be processed in the algorithm, namely:

- positive-sequence components,
- superimposed positive-sequence components,
- negative-sequence components,
- zero-sequence components.

Due to uncertainty of the impedance data of transmission lines for the zero-sequence as well as the presence of mutual coupling of parallel lines for this sequence, in the case of double circuit lines, usage of the zero-sequence voltages and currents is not advantageous, and whenever possible, they are not included in the fault location algorithm [31]. Therefore, practically, the remaining symmetrical components can be considered as the input quantities of the fault location algorithm, however, with some restrictions. Namely, utilisation of the negative-sequence components is not applicable in the case of three-phase balanced faults. In contrast, the positive- and superimposed positive-sequence components are present in all faults and thus the fault location can be performed without selection of the fault type. It is worth noting that the superimposed (incremental) positive-sequence components are calculated by subtracting the pre-fault quantities from the fault quantities. In certain cases, the pre-fault signals recorded are not in the form of pure sinusoids since the symptoms of the fault can be observed just before its occurrence. Therefore, in such cases use of the superimposed positive-sequence quantities is not recommended either. When utilising the positive-

sequence quantities, higher (than for the other symmetrical components) fault location errors are obtained if the shunt parameters of the line are not taken into account [127]. However, this drawback is overcome if the distributed parameter line model is employed in formulation of the algorithm [60].

In the case of untransposed lines the symmetrical components approach cannot be utilised, however, there is a possibility of determining a transformation matrix, which can be applied for transforming the coupled phase quantities to decoupled modal quantities based on the eigenvalue/eigenvector theory [74].

Besides the phasor approach, the instantaneous-based state of the system representation is commonly applied for description of the state of the faulted network. Dynamical relations are represented by discrete differential equations [153] or partial differential equations [B.2].

Digital signal processing methods deserve wider consideration than presented here, however, this is beyond the scope of this book.

2.4. Synchronisation of distributed digital measurements

Digital measurements at different line terminals can be performed synchronously if a GPS (Global Positioning System) is available. A synchronised measurement system requires that measurements taken at different substations include, in addition to magnitude, the phase angle data with respect to an arbitrary but common reference. Phase information is obtained from knowledge of the absolute time at which the measurements were taken (time tagging). The time for all measurements must be synchronised with a time reference that must be the same for all local systems. This time reference is commonly obtained from the GPS [33].

If there is no GPS synchronisation or in the case of loss of the GPS signal, the digital measurements from the line terminals are performed asynchronously and thus do not have common time reference, as shown in Fig. 2.5.

In two-end unsynchronised measurements [60, 64, 127, 143, 187] the sampling instants (marked in Fig. 2.5 with small circles) of the A/D converters from terminals S and R do not coincide since the converters are not controlled by the GPS. As a result, there is a certain random shift (ΔT_{R-S}) between the sampling instants of the A/D converters at both ends. Moreover, an instant at which the fault is detected, is usually considered as the time stamp: $t_S = 0$ (at terminal S) and $t_R = 0$ (at terminal R), which in general case do not coincide either. In consequence, the measurements from both line ends do not have a common time reference. In order to assure such a common base, one has to take measurements from the particular terminal as the base (for example, from terminal R, as will be assumed in further considerations), while for the other terminal (terminal S) to introduce the respective alignment. When formulating the fault location algorithm in terms of phasors of the measured

quantities, such alignment is done by multiplying all the unsynchronised (the superscript: 'asynchr.') phasors from terminal S by the synchronisation operator exp(jδ), as for example, in the case of positive-sequence voltage (likewise for the remaining phasors of signals from terminal S):

$$\underline{V}_{S1} = \underline{V}_{S1}^{\text{asynchr.}} e^{j\delta} \tag{2.1}$$

where δ is unknown synchronisation angle.

In general, the synchronisation angle can be:

- measured from the pre-fault quantities [3],
- eliminated by mathematical manipulations [187],
- calculated with processing the fault quantities [60, 64, 127].

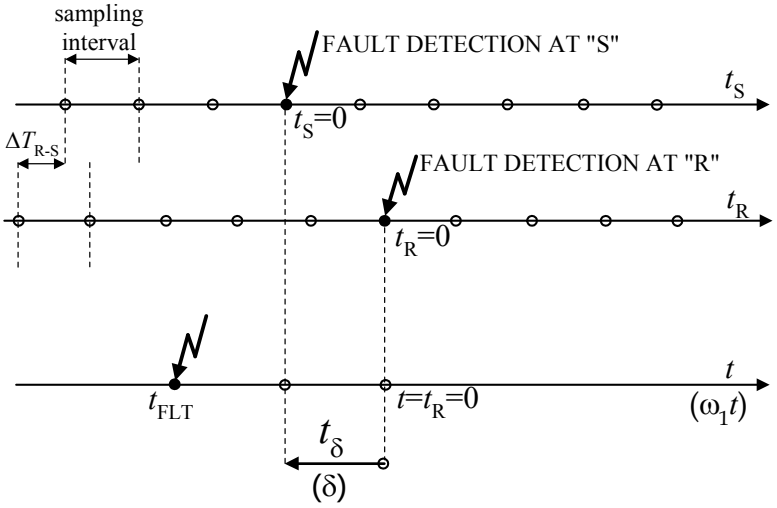

Fig. 2.5. Illustration of the need of phase alignment in the case of two-end unsynchronised measurements

2.5. Fault location errors

In [B.7], and in other numerous references, the following definition of the fault location error is given:

"Percentage error in fault location estimate based on the total line length:
e (error) = (instrument reading – exact distance to the fault) / total line length".

This definition can be written down as the following formula:

$$\text{error}(\%) = \frac{d - d_{\text{exact}}}{\ell} 100\% \tag{2.2}$$

where:

d, d_{exact} – estimated and exact distance to the fault (in km or in relative units: p.u.);

ℓ – total line length (in km, or if relative units are used: $\ell = 1$ p.u.).

In statistical evaluation of the accuracy of particular fault location methods, different measures for the fault location error are determined, as for example, maximum, average, and standard deviation values. It is characteristic that the absolute value is usually taken for the nominator from the definition formula (2.2), thus obtaining [71]:

$$\text{error}(\%) = \frac{|d - d_{\text{exact}}|}{\ell} 100\% \tag{2.3}$$

Note that usage of (2.3) assures that, when for example the average error is determined for a given population of the evaluation tests, the errors having identical magnitude but different signs do not compensate each other.

In evaluation of the fault location accuracy, different factors are taken into account. The main factors commonly considered are the following:

- fault position (location),
- fault type,
- fault resistance including presence of an arc,
- level of pre-fault power flow and its direction,
- strength of equivalent sources behind the line terminals,
- line imbalance due to the lack of transposition,
- inaccuracy in providing impedance data for the overhead line (or underground cable),
- inaccuracy in providing impedance data for the vicinity of the overhead line in question, as for example, the possible mismatch with respect to the source impedances (if they are involved in the evaluated fault location algorithm) is considered,
- presence and status of series and shunt devices in the line, as for example, installations of the banks of series compensating capacitors equipped with Metal Oxide Varistors (MOVs),
- fault inception angle,
- identification of a fault, in terms of the correctness and accuracy of fault incipience detection, fault clarification detection, fault type classification,
- transient and steady errors of instrument voltage and current transformers, including the possibility of CT saturation,
- frequency response of voltage measurement chains,
- accuracy of A/D conversion, etc.

Different factors affect the accuracy of fault location methods. In general, without specifying the fault location method, they can be listed as follows:

- Inaccurate compensation for the reactance effect in the case of fault location algorithms using one-end measurements. This is so, if the vicinity of the line is inaccurately represented in the algorithm, i.e., when providing impedances of equivalent sources behind the line terminals, which do not match the actual strength of the sources.
- Inaccurate fault type (faulted phases) identification for fault locating algorithms based on considering the natural fault loops (phase-to-earth or phase-to-phase loops), similarly as applied in distance relays.
- Inaccurate line parameters, which do not match the actual parameters. Note that, even if the geometry of line conductors is accurately taken to calculate the line impedances, the total line length might be known with some error.
- Uncertainty with respect to the line parameters, particularly for the zero-sequence impedance. It is often difficult to obtain the accurate zero-sequence impedance for the line. This is so, since this impedance is affected by soil resistivity, which may be variable under the whole line route, and is dependent on weather conditions.
- Inaccurate compensation for the mutual effects on the zero-sequence components. This takes place if current required to compensate for the mutual coupling is for some reasons unavailable.
- Insufficient accuracy of the line model, i.e. if untransposed lines are represented as being transposed, and line shunt capacitance is not considered.
- the presence of shunt reactors and capacitors, as well as the presence of series capacitor compensating devices.
- Load flow unbalance.
- Errors of current and voltage instrument transformers and inaccurate reproduction of the primary signals due to their limited bandwidth.
- Insufficient sampling frequency and bit resolution of A/D system.

To improve the fault location estimation, it is important to eliminate, or at least to reduce errors possible to occur in the method considered. Note that a particular factor affecting fault location accuracy has to be considered strictly in relation to the method analysed. If this factor appears important, then the way of its elimination or minimisation has to be considered when formulating the particular fault location algorithm.

3. Transmission network models for fault location studies

3.1. Network configurations

Fault location in transmission networks is based on considering the flow of a fault current. Depending on the availability of measurements for the fault locator, the flow of a fault current within the faulted line itself or also in its vicinity has to be performed. A particular fault location method has to be considered in strict relation to the configuration of the power network and its model.

3.1.1. Networks with single-circuit overhead lines

Single-circuit three-phase overhead lines are the simplest means for transmitting a power energy from the generation centre to the consumption region. Schematic diagram of a power network with a single-circuit overhead line is presented in Fig. 3.1a [B.1]. The line is marked with a graphic symbol typical of an impedance description. Moreover, the description $\underline{Z}_L$, corresponding to general indication of the line impedance is used. The line ends are denoted here by letters: S (sending end), R (receiving end). The fault occurring on the line is marked with a common graphic symbol for the fault and letter F. The vicinity of the line S–R under consideration is represented by the external network. Assuming linearity of the whole circuit, the external network can be equivalented [B.1], as shown in Fig. 3.1b. The obtained equivalent of the external network in a general case consists of:

- two equivalent sources behind the line terminals S, R – consisting of the emfs ($\underline{E}_S$, $\underline{E}_R$) and source impedances ($\underline{Z}_S$, $\underline{Z}_R$),
- extra link ($\underline{Z}_F$) between the line terminals S, R.

Since the load and generation in a power network as well as the network topology undergo changes, the equivalent network of the line external network also changes and is not fixed. As a result, the source impedances ($\underline{Z}_S$, $\underline{Z}_R$) are considered in fault location process to be the uncertain parameters. Therefore, the fault location algorithms which do not require that the source impedances be known are generally more accu-

rate than the algorithms for which this impedance data is used as the input data. The one-end fault location algorithms require setting the source impedances and due to dynamic changes of the network it is difficult to provide the actual values of these impedances. Fortunately, in many applications it is sufficient to provide the representative values of the source impedances, which are obtained for the most typical conditions of the network operation. Possible mismatch between the provided representative source impedances and the actual parameters in many applications does not cause considerable errors in fault location. This is so especially in the case of strong sources, which is the case when the source impedance is much smaller than the line impedance.

If the line ($\underline{Z}_L$) considered is the only connection between the buses S, R, then the extra link ($\underline{Z}_E$) does not exist, and there are only equivalent sources, as shown in Fig. 3.1c. This is the well-known double-machine network.

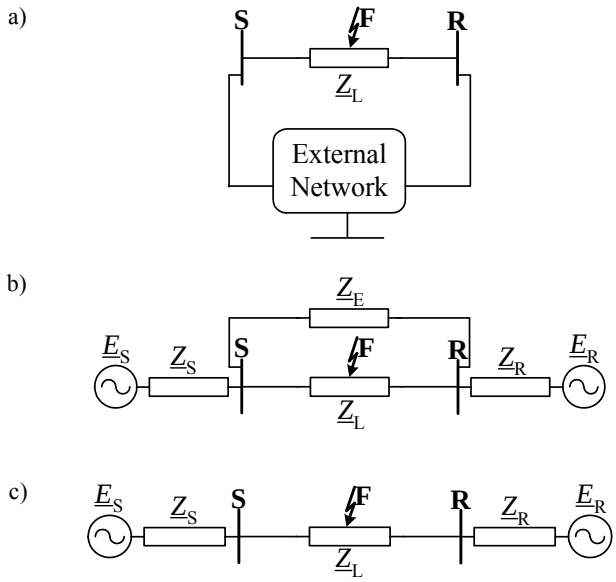

Fig. 3.1. Transmission network with single-circuit overhead line:
a) generic scheme, b) general equivalent scheme,
c) simplified equivalent scheme with the line being the only connection between buses S, R

3.1.2. Networks with double-circuit lines

Both fault location and protective relaying for double-circuit lines (also called parallel lines) are dealt with in numerous references [B.1, B.7, B.9, 3, 8, 34, 41, 47, 57, 58, 62, 63, 70, 76, 87, 114, 115, 123, 158, 163, 164, 167, 190]. Such lines are basically

constructed due to constraints in obtaining new right-of-ways and are very common in power networks. For such lines the two three-phase transmission circuits are arranged on the same tower or follow on adjacent towers the same right-of-way. The circuits may be either of the same or different voltage level. Also more than two three-phase circuits can be arranged in such a way (multi-circuit lines) [B.23].

Due to the nearness of both circuits of a double-circuit line, they are mutually magnetically coupled. The magnetic coupling is related with the effect of a current flowing in one circuit, which influences the voltage profile in the other circuit, and vice versa. This means that the voltage profile of a given circuit is not being entirely dependent on the current flowing in this circuit.

The mutual coupling effect can be expressed in terms of various inter-circuit mutual impedances. Using the symmetrical components approach to the line description, the positive-, negative- and zero-sequence mutual impedances are considered. The positive- and negative-sequence mutual impedances are usually a small fraction of the positive-, negative-sequence self impedances and therefore are usually neglected in the analysis. In contrast, the zero-sequence mutual impedance ($\underline{Z}_{0m}$) is of relatively high value and thus cannot be ignored in the analysis of single phase-to-ground faults. The mutual coupling of double-circuit lines for the zero-sequence is thus important for the fault location based on considering the natural fault loops [B.9].

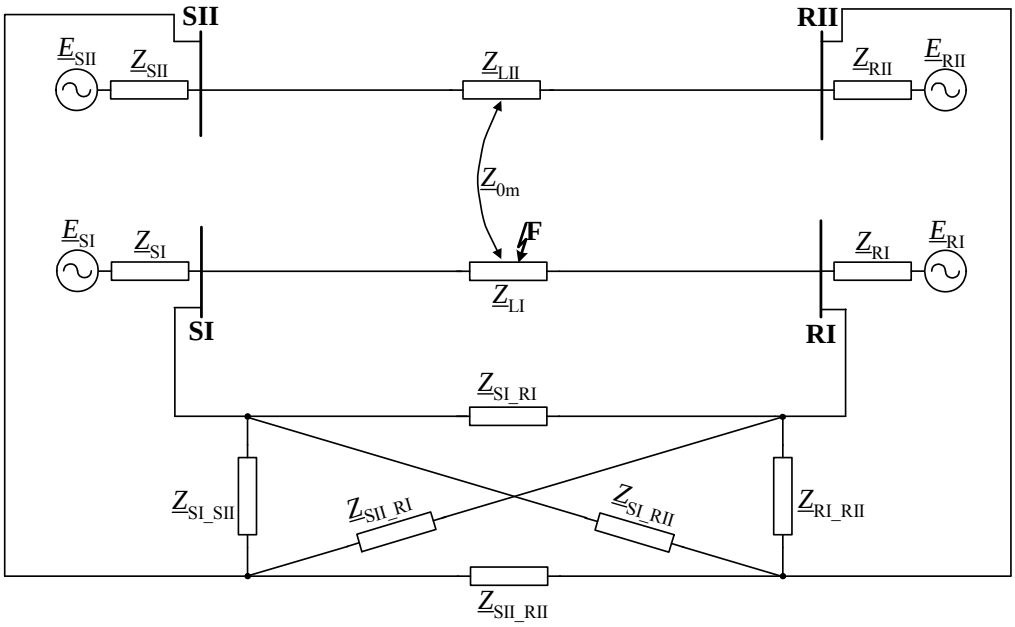

Fig. 3.2. Schematic diagram of power network with double-circuit overhead line terminated at both ends at separate buses

Different configurations of double-circuit lines [B.1, B.9, B.23] are met in power networks. Figure 3.2 presents a general configuration of a power network with a double-circuit overhead line terminated on both sides at the separate buses. The line circuits are denoted by $\underline{Z}_{LI}$, $\underline{Z}_{LII}$ and their mutual coupling for the zero-sequence by $\underline{Z}_{0m}$. The vicinity of the line circuits is represented with:

- equivalent source behind the line terminal SI (emf: $\underline{E}_{SI}$, impedance: $\underline{Z}_{SI}$),
- equivalent source behind the line terminal SII (emf: $\underline{E}_{SII}$, impedance: $\underline{Z}_{SII}$),
- equivalent source behind the line terminal RI (emf: $\underline{E}_{RI}$, impedance: $\underline{Z}_{RI}$),
- equivalent source behind the line terminal RII (emf: $\underline{E}_{RII}$, impedance: $\underline{Z}_{RII}$),
- links between the line terminals SI, SII, RI, RII in the form of a complete tetragonal of impedances: $\underline{Z}_{SI\_SII}$, $\underline{Z}_{SI\_RI}$, $\underline{Z}_{SI\_RII}$, $\underline{Z}_{SII\_RI}$, $\underline{Z}_{SII\_RII}$, $\underline{Z}_{RI\_RII}$.

Figure 3.3 presents the classical case of the network with two line circuits connected at both ends to the common buses. This scheme is obtained from the general scheme of Fig. 3.2, considering the following:

- equivalent source ($\underline{E}_S$, $\underline{Z}_S$) obtained as the resultant for parallel connection of the sources: ($\underline{E}_{SI}$, $\underline{Z}_{SI}$) and ($\underline{E}_{SII}$, $\underline{Z}_{SII}$),
- equivalent source ($\underline{E}_R$, $\underline{Z}_R$) obtained as the resultant for parallel connection of the sources: ($\underline{E}_{RI}$, $\underline{Z}_{RI}$) and ($\underline{E}_{RII}$, $\underline{Z}_{RII}$),
- extra link ($\underline{Z}_E$) obtained as the resultant for parallel connection of the following impedances: $\underline{Z}_{SI\_RI}$, $\underline{Z}_{SI\_RII}$, $\underline{Z}_{SII\_RI}$, $\underline{Z}_{SII\_RII}$.

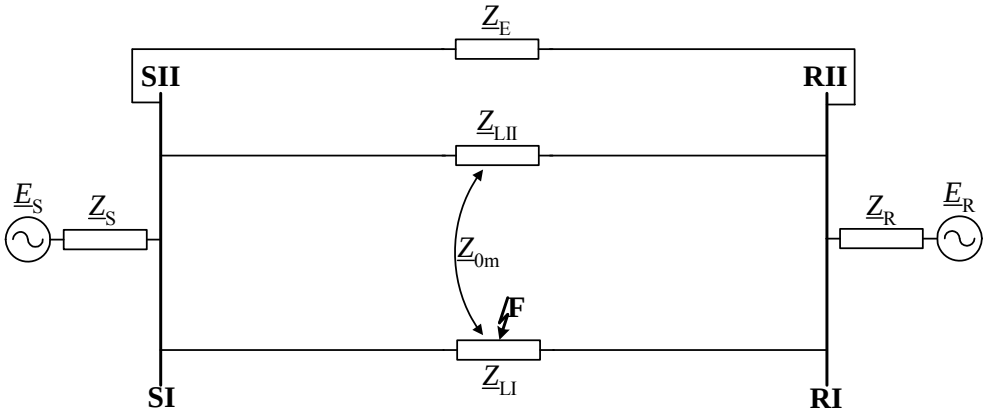

Fig. 3.3. Schematic diagram of power network with double-circuit overhead line terminated at both ends at common buses

The extra link shown in the network of Fig. 3.3 is not always present, especially in high voltage networks which are not highly interconnected.

Operating conditions of a double circuit line could change due to different reasons, such as load dispatch, forced outage, scheduled maintenance, etc. The mutual coupling

of double-circuit lines depends on the mode of operation of the healthy circuit ($\underline{Z}_{LII}$), which is in parallel to the faulted line circuit ($\underline{Z}_{LI}$) considered. In order to present these modes, the status of circuit breakers and earthing connectors of the healthy parallel line has to be considered [112].

Figure 3.4 presents two modes for which the mutual coupling of parallel lines has to be taken into account. In the case of the network from Fig. 3.4a the parallel line is in operation, which is the normal operating mode. The mutual coupling of parallel lines also exists if the parallel line is switched-off and earthed at both ends [58] (Fig. 3.4b).

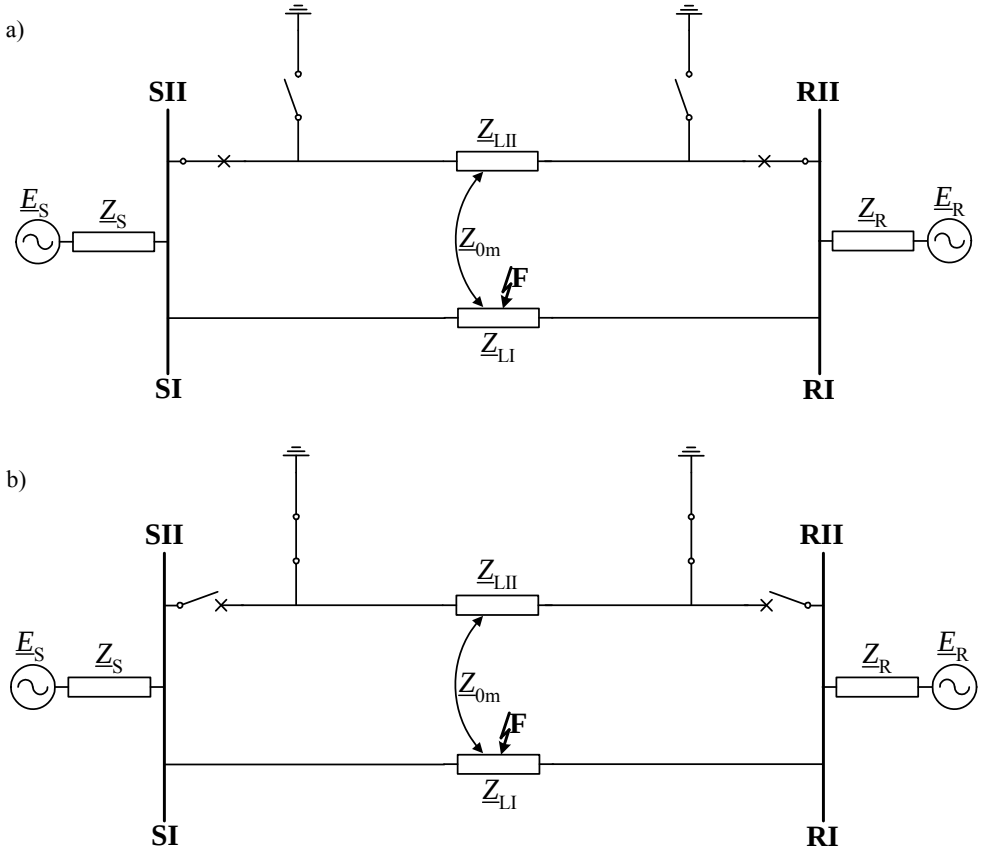

Fig. 3.4. Double-circuit overhead line modes with mutual coupling of parallel lines: a) both lines in operation, b) parallel line is switched-off and earthed at both ends

Figure 3.5 presents three cases for which there is a discontinuity for the current flow in the healthy parallel line, and therefore there is no mutual coupling between the lines.

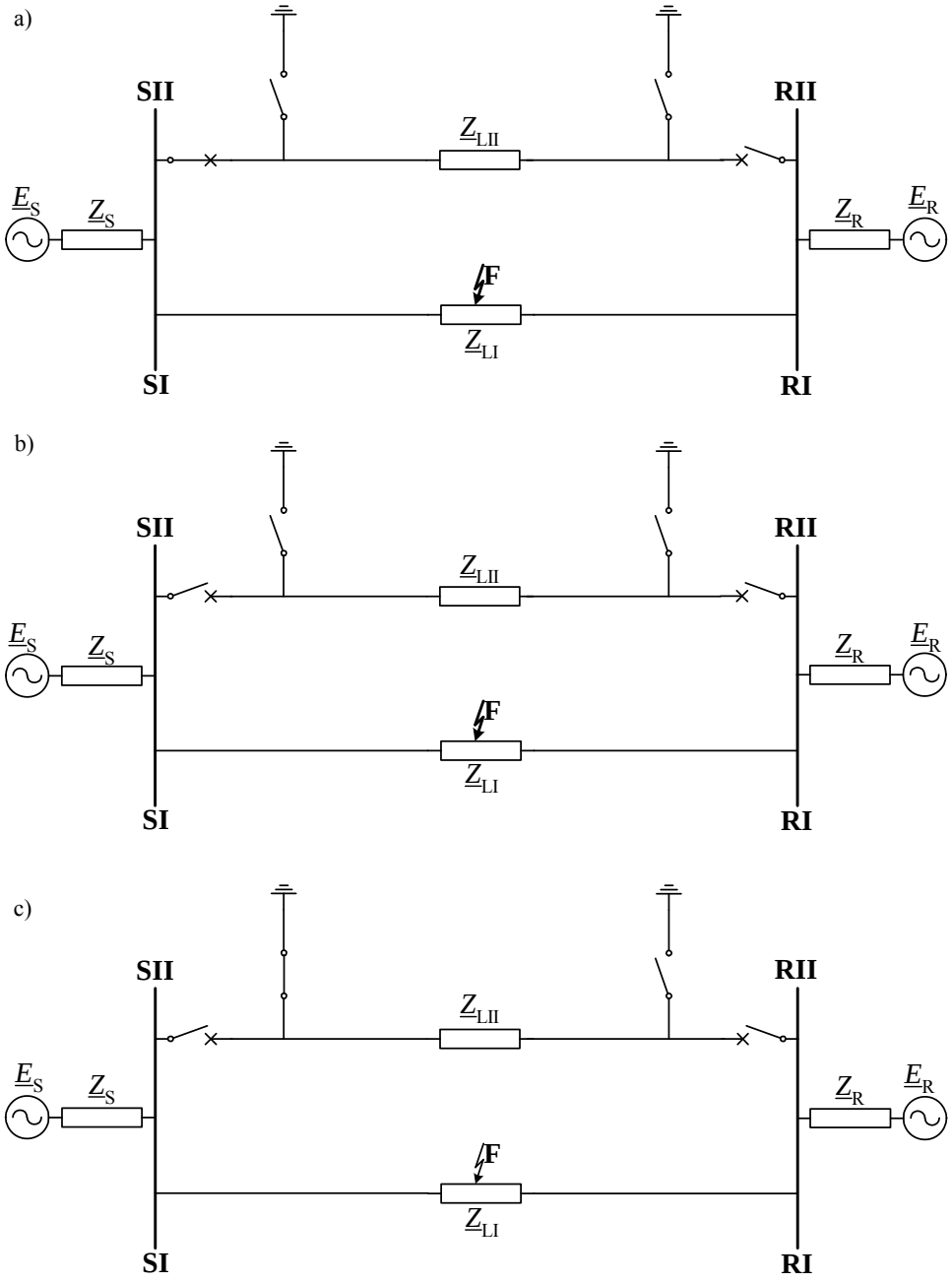

Fig. 3.5. Double-circuit overhead line modes with no mutual coupling of parallel lines: a) parallel line is switched-off at one end (RII) and not earthed, b) parallel line is switched-off at both ends and not earthed, c) parallel line is switched-off at both ends and earthed only at one end

In some cases [B.23, 57], the line circuits may run in parallel only for a part of the route. The circuits for this part are mutually coupled, while for the remaining part of the route, they are hanged on different towers and are terminated at distant substations. Figure 3.6 presents two examples of power networks with partially parallel circuits. The need for taking into account the mutual coupling effect depends on the fault position: Fig. 3.6a – faults F1, F2; Fig. 3.6b – faults F1, F2, F3. Considering the fault loop between bus SI and fault point F1 in the network of Fig. 3.6a, the mutual coupling has to be taken into account along the whole distance. By contrast, as regards the fault loop between bus SI and the fault point F2, the mutual coupling has to be considered for the distance between bus SI and point MI, and not for the remaining part (MI-F2).

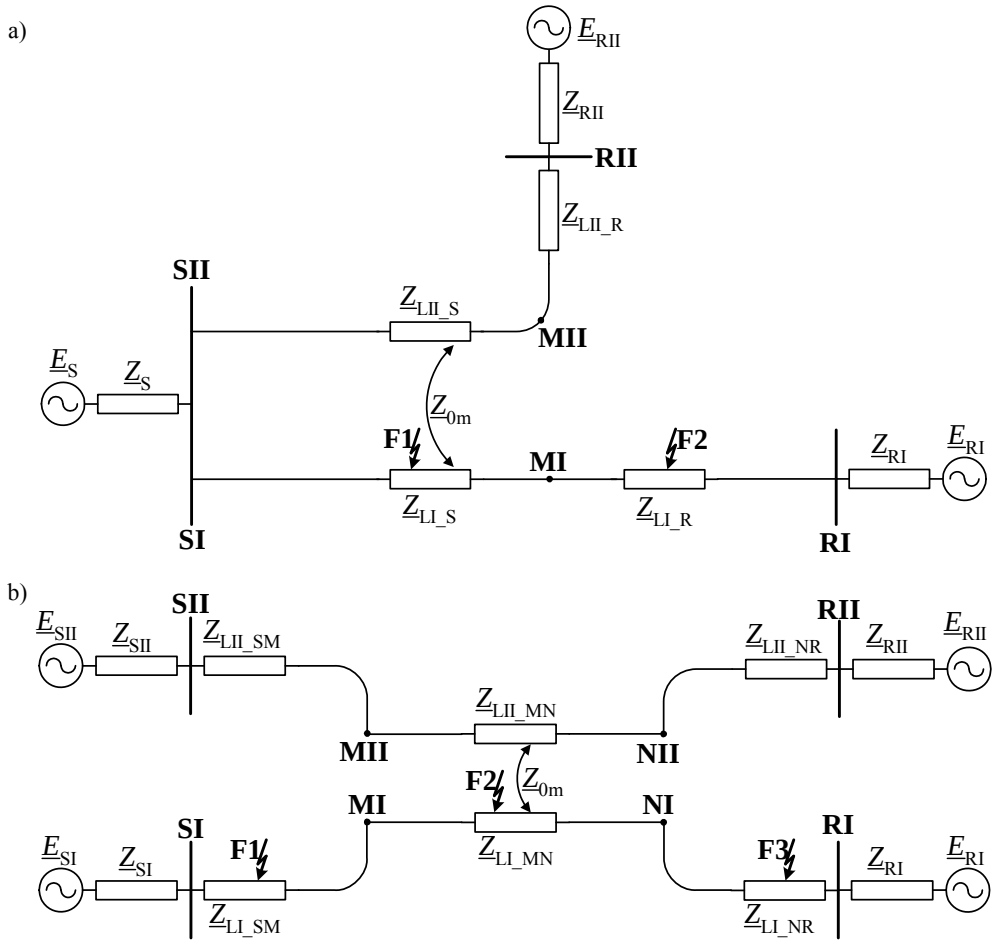

Fig. 3.6. Examples of power networks containing partially parallel line circuits with mutual coupling for: a) $\underline{Z}_{LI\_S}$, $\underline{Z}_{LII\_S}$, b) $\underline{Z}_{LI\_MN}$, $\underline{Z}_{LII\_MN}$

3.1.3. Multi-terminal and tapped lines

It is for economy or environmental protection reasons that use is made of multi-terminal and tapped lines [B.23]. Lines having three or more terminals with substantial generation behind each are called multi-terminal lines. Depending on the number of terminals we can distinguish three-terminal lines having three terminals, four-terminal lines having four terminals, and so on.

Tapped lines are the ones having three or more terminals with substantial power generation behind, at maximum two of them [B.23]. The number of taps per line varies from one to even more than ten. The taps themselves feed only loads, which means that they are terminated by the passive networks, while at the remaining terminals there are active networks (with power generation) [B.23, 43].

Examples of power network configurations with single-circuit three-terminal line are shown in Fig. 3.7. In the case of using double-circuit lines, typical configurations are as shown in Fig. 3.8.

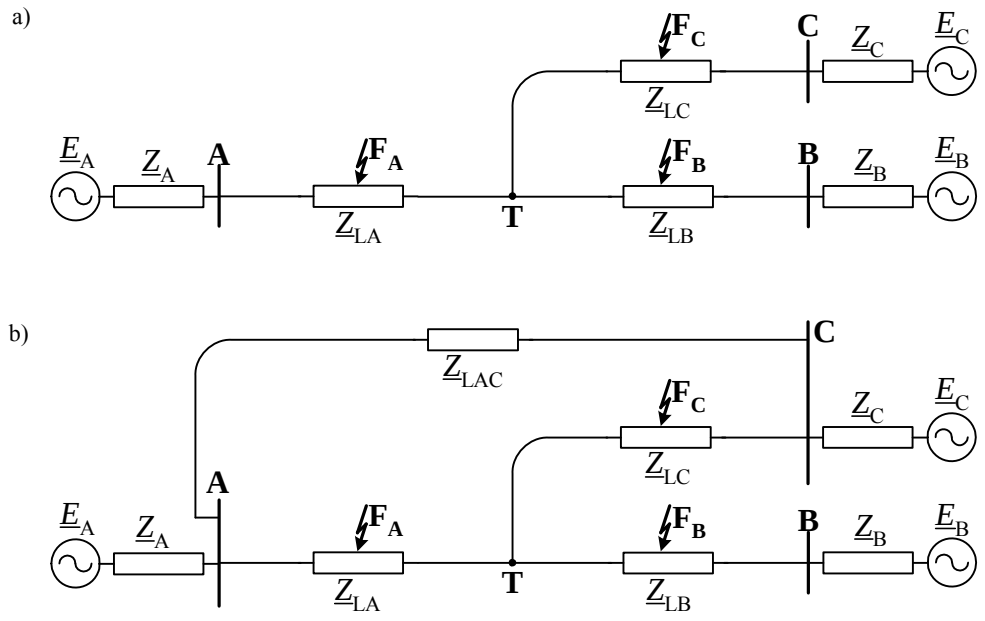

Fig. 3.7. Examples of power network configurations
with single-circuit three-terminal line:
a) basic teed network, b) teed network with extra link between two substations

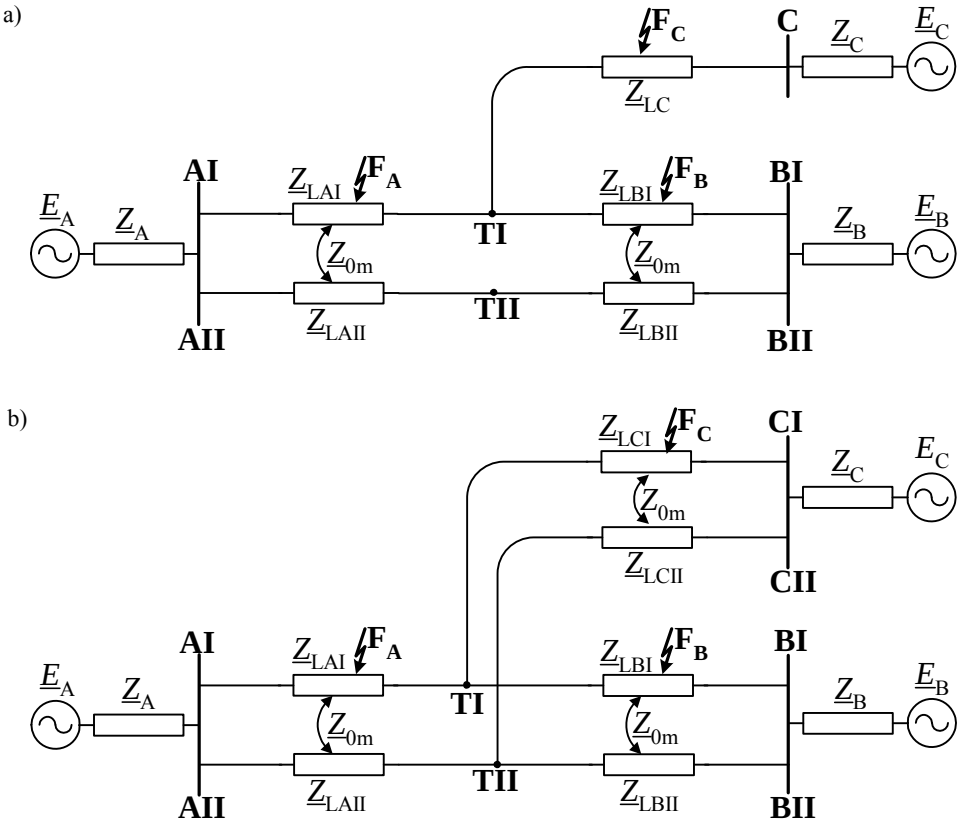

Fig. 3.8. Examples of power network configurations
with parallel three-terminal line:
a) two line sections are of double-circuit type,
b) all three line sections are double-circuits

Figure 3.9 presents typical configurations of power networks with tapped line supplying load in two different ways [B.23]: via a transformer connected to the tap point through a circuit breaker (Fig. 3.9a) and additionally with overhead line section ($\underline{Z}_{LC}$), Fig. 3.9b.

Fault location on multi-terminal and tapped lines relies on:

- identifying the line section at which the fault (F_A or F_B or F_C) occurred,
- determining the distance to fault for the faulted section (usually measured from the respective bus towards the fault point).

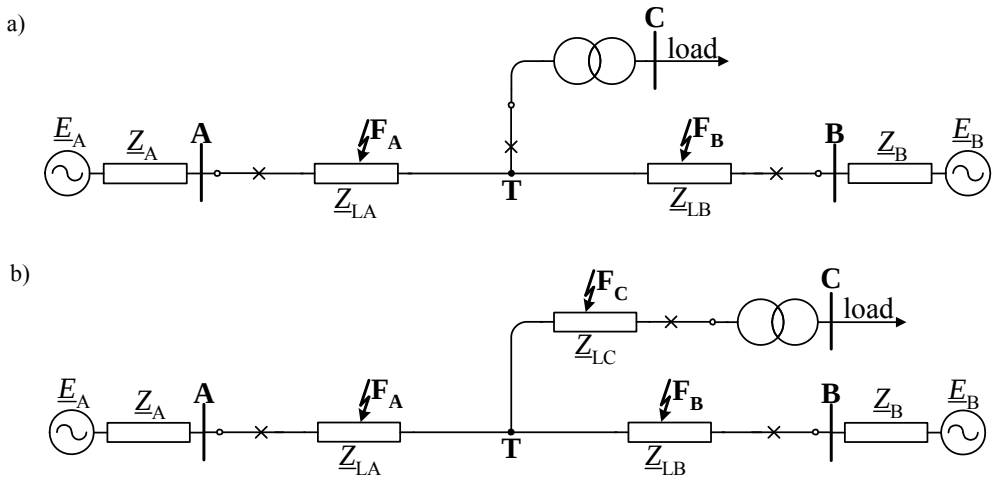

Fig. 3.9. Typical configurations of power networks with tapped line supplying load through: a) transformer, b) overhead line ($\underline{Z}_{LC}$) and transformer

3.1.4. Overhead line and cable composite networks

In Figs. 3.10 and 3.11, examples of configurations of overhead line and cable composite networks [119, 170] are presented. Fault location in such networks is considered to be a difficult task due to large differences in parameters of the line and cable. Moreover, the problem of cable parameters changing, especially changes in its relative permittivity occurring with aging, has to be solved [170].

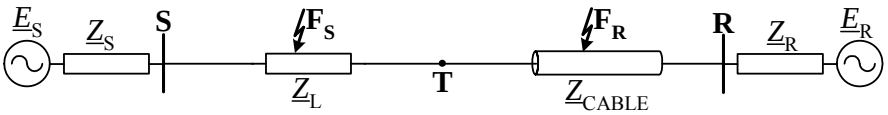

Fig. 3.10. Overhead line in series connection with cable

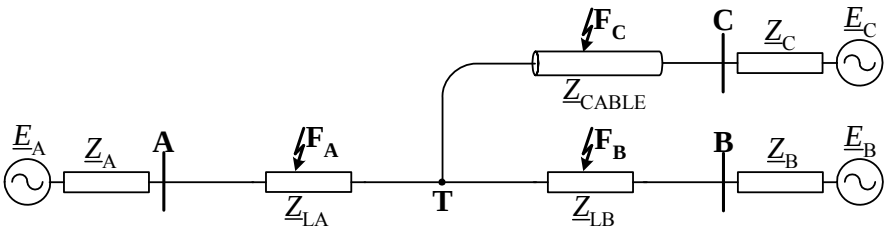

Fig. 3.11. Overhead line tapped with cable

3.1.5. Networks with series-compensated lines

Power (P) transfer capability of a traditional uncompensated transmission line (Fig. 3.1) is determined by the well-known formula (with line resistance and capacitance being neglected):

$$P = \frac{|\underline{V}_S| \cdot |\underline{V}_R|}{X_L} \sin(\delta) \tag{3.1}$$

where:

$\underline{V}_S$, $\underline{V}_R$ – sending and receiving terminal voltage phasors, respectively,
X_L – line reactance,
δ – electric angle between the terminal voltage phasors.

The maximum value of δ is limited by the stability constraints, and thus an increase in the power transfer capability can be obtained by reducing the line reactance. This can be done by adding series capacitors to counteract series inductance. As a result, the total reactance of the series compensated line (X_{total}) is equal to:

$$X_{total} = X_L - X_C \tag{3.2}$$

where X_C is the capacitor reactance.

The compensation degree is expressed by the following ratio:

$$k_{SC} = \frac{X_C}{X_L} 100\% \tag{3.3}$$

and usually falls within the range of 50 up to 90%.

The capacitor compensation in high voltage transmission networks is performed by adding series capacitors of the fixed value or of the value controlled with the thyristor circuits.

Use of the series capacitors besides increasing the power transfer capability brings about several advantages to power system operation [B.23], such as:

- improving power system stability,
- reduced transmission losses,
- enhanced voltage control,
- flexible power flow control.

The environmental concerns are also of importance here since instead of constructing a new line, the power transfer capability of the existing line is increased. The cost of introducing the series capacitor compensation is much lower than that of constructing a new equivalent overhead power line [B.23].

Usually, only one three-phase capacitor bank is installed on a power transmission line. As far as a single line is concerned, the one line circuit diagram of the series-compensated line is as presented in Fig. 3.12. Series capacitors (SCs) are installed on

the line at a distance d_{SC} (p.u.) from the bus S. In order to protect SCs against over-voltages they are equipped with Metal Oxide Varistors (MOVs). The SC and its MOV are the main components of the compensating bank installed in each phase of the line. Therefore, for the sake of simplifying the series-compensated transmission networks presented, only these components are indicated in the schemes (Fig. 3.12 and further figures showing configurations of series-compensated networks).

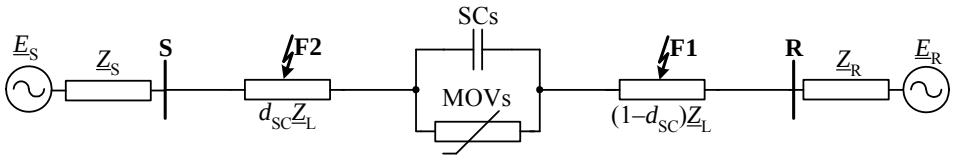

Fig. 3.12. Single transmission line compensated with SCs&MOVs installed at midpoint

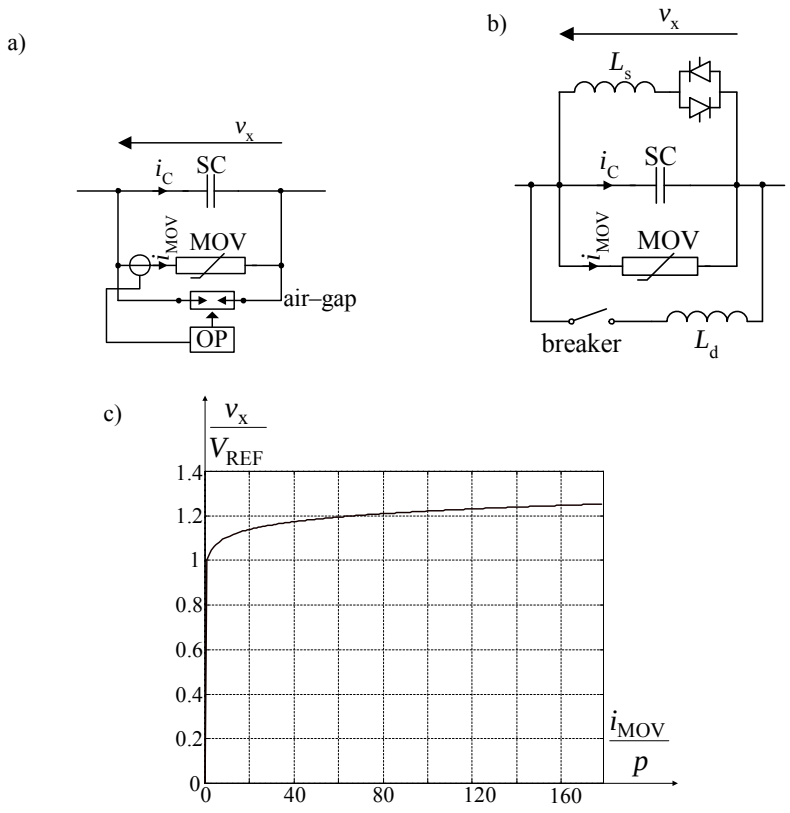

Fig. 3.13. Series capacitor bank: a) scheme of bank with fixed capacitor,
b) scheme of bank with thyristor controlled capacitor, c) typical voltage-current characteristic of MOV

Figure 3.13a presents a scheme of the compensating bank from one phase of a line, which contains a fixed series capacitor [88, 108, 145]. Besides the SC and MOV there is a protection of MOV against overheating. This thermal (overload) protection (OP) measures the current conducted by the MOV. If the energy absorbed by the MOV exceeds its pre-defined limit the MOV becomes shunted by firing the air-gap. Figure 3.13b presents a compensating bank with thyristor controlled capacitor [16, 22, 83, 186].

MOVs are non-linear resistors commonly approximated by the standard exponential formula:

$$\frac{i_{\mathrm{MOV}}}{p} = \left(\frac{v_{\mathrm{x}}}{V_{\mathrm{REF}}} \right)^{q} \tag{3.4}$$

Figure 3.13c shows the voltage-current characteristic for the following parameters of the approximation (3.4): $q = 23$, $p = 1$ kA, $V_{\mathrm{REF}} = 150$ kV.

Series capacitors equipped with MOVs, when set on a transmission line, create certain problems for its protective relays [30, 39, 40, 44, 48, 67, 82, 84, 88, 128, 135, 139, 141, 147, 153, 154] and fault locators [B.7, B.9, 7, 32, 55, 125, 129, 140, 144, 145, 150, 151, 152, 155, 156, 157, 159, 186]. Under faults behind the SCs&MOVs (fault F1 in Fig. 3.26), a fault loop seen from the bus S becomes strongly non-linear, and as a consequence, the nature of transients as well as the steady state situation are entirely different, compared with traditional uncompensated lines. In the case of faults in front of the SCs&MOVs (fault F2 in Fig. 3.12) the SCs&MOVs are outside the fault loop seen from the bus S, however they influence the infeed of the fault from the remote substation R.

Adequate representation of the SCs&MOVs has to be applied for both protective relays and fault location. Form of this representation depends on the type of protection and fault location algorithms. If these algorithms are based on phasor technique, then the SC&MOV from a particular phase can be represented with the fundamental frequency equivalent [B.7, 45, 55, 150, 151, 152, 156, 159] in the form of resistance-capacitive reactance series branch with parameters dependent on an amplitude of the current (fundamental frequency component) measured in the phase of interest. When considering protection and fault location algorithms based on a differential equation approach, the SC&MOV from a particular phase is represented with use of the estimated instantaneous voltage drop across the compensating bank [7, 39, 40, 153, 154, 155].

Figure 3.14 shows operation of SCs&MOVs under the sample fault on a 400 kV, 300 km transmission line compensated at $k_{\mathrm{SC}} = 80\%$. The parameters of the approximation (3.4) are as taken for plotting the voltage-current characteristic from Fig. 3.13c. A single phase-to-earth fault (a–E fault) with fault resistance of 10 Ω was applied just behind SCs&MOVs. In Fig. 3.14a, the three-phase currents entering the SCs&MOVs are shown. The voltage drops across the SCs&MOVs are shown in Fig. 3.14b. It can be observed that the voltage drop in the faulted phase (a) is limited to

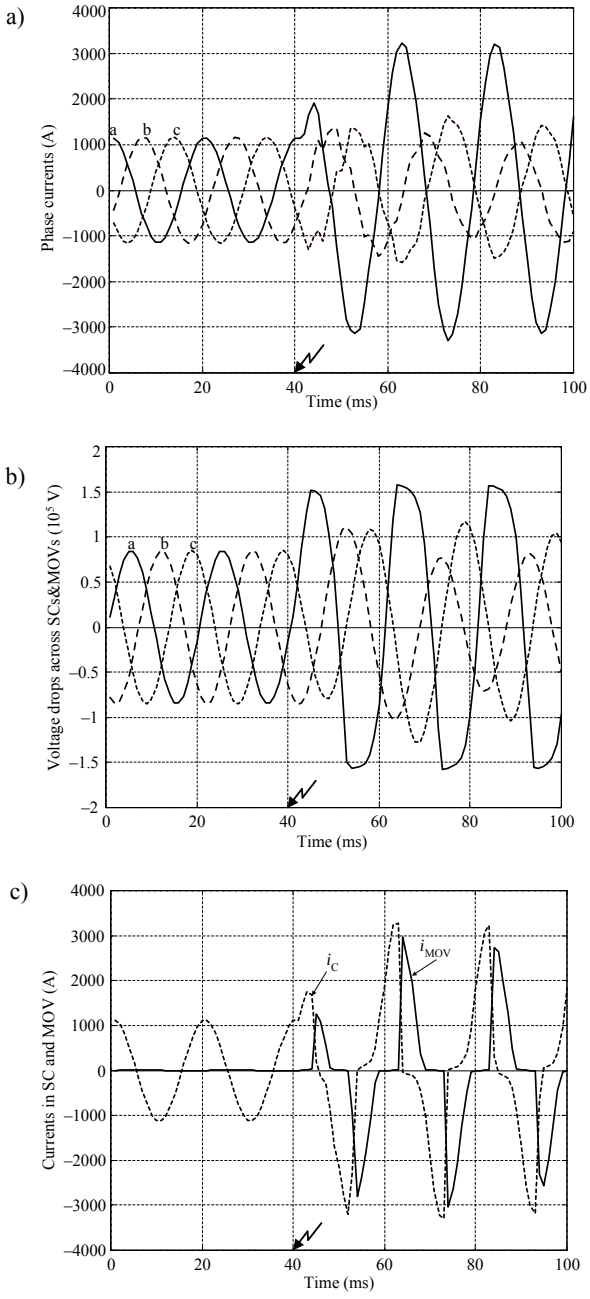

Fig. 3.14. Operation of SCS&MOVs under the sample a–E fault:
a) phase currents entering SCs&MOVs, b) voltage drops across SCs&MOVs,
c) currents flowing in SC (i_C) and MOV (i_{MOV}) from the faulted phase

around ±150 kV, which results from applying the MOVs with the reference voltage: V_{REF} = 150 kV. The waveforms of the voltage drop from the healthy phases (b, c) are distorted by sub-synchronous resonance oscillations. Such oscillations appear since MOVs from these phases operate at the linear range, conducting low current. The sub-synchronous resonance oscillations are also visible in currents entering the SCs&MOVs from the healthy phases (Fig. 3.14a). Figure 3.14c shows division of the fault current from the faulted phase (a) into the parallel branches of the SC and its MOV. The SC and MOV conduct the fault current alternately, around for the quarter of the fundamental period.

Figure 3.15 depicts series capacitors compensation of the transmission line using the compensation banks installed at both ends [B.23, 151]. In the case of such compensation, the placement of current and voltage instrument transformers (CTs – current transformers, CVTs – capacitive voltage transformers) at the line ends is important for considering fault location. The instrument transformers can be placed on the bus side (Fig. 3.16a) or on the line side (Fig. 3.16b) [B.23].

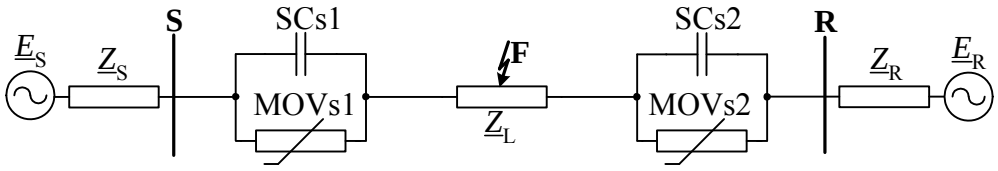

Fig. 3.15. Transmission line compensated with SCs&MOVs banks at both ends

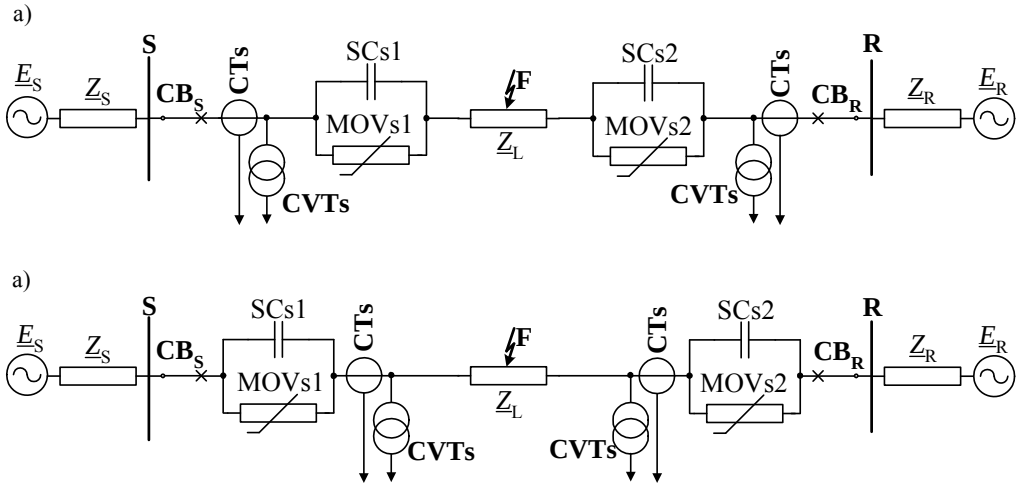

Fig. 3.16. Placement of instrument transformers in the case of double-end series compensation: a) on the bus side, b) on the line side

Similarly, double-circuit transmission lines, analogously to the single line, can be compensated using the capacitor compensating banks installed at the midpoint [155, 156, 157] (Fig. 3.17) or at the line ends (Fig. 3.18).

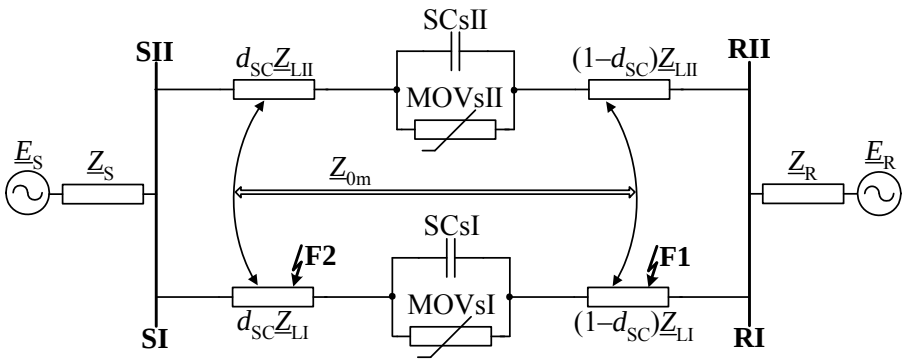

Fig. 3.17. Double-circuit transmission lines with capacitor compensating banks installed at the midpoint in both circuits

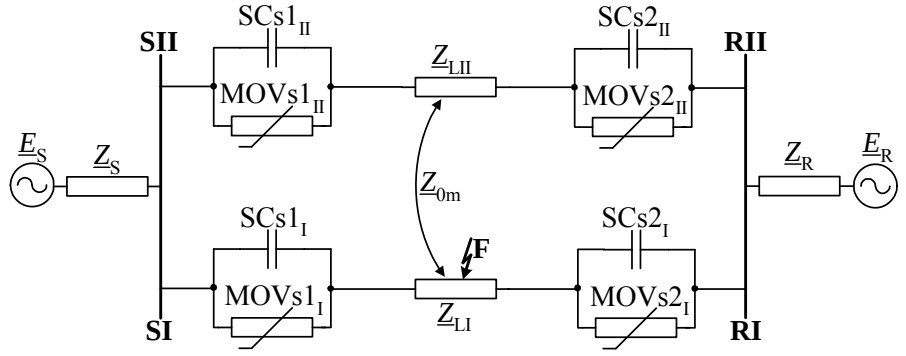

Fig. 3.18. Double-circuit transmission lines with capacitor compensating banks installed at two ends in both circuits

3.2. Models of overhead lines

Models of overhead lines are considered in strict relation to a particular application. Among different applications, the line models are considered in relation to the following:

- representing a faulted line in the fault location algorithm,
- simulating faults for generating the fault data, which is used in evaluation of the fault location algorithms under study [B.5, 28, 113, 116].

In this section, the representation of a faulted line in fault location algorithms is addressed. Assumption of the line model is a starting point for derivation of the fault location algorithms.

In turn, the line models adopted in simulation of line faults are widely described in reference manuals (theory books) of the well-known simulation transients programs, such as ATP-EMTP [B.5] and others, and therefore are not considered here.

Overhead line parameters are calculated using supporting routines available in simulation programs. Also, an on-line measurement of transmission line impedance performed either during normal operation or during faults is used in practice.

In general, there are two-types of line models:

- lumped-parameter models,
- distributed-parameter models.

Lumped-parameter models represent a line by lumped elements, whose parameters are calculated at a single frequency, predominantly the fundamental power frequency. Using these models, steady-state calculations for fault location or transient simulations in the neighbourhood of the frequency considered can be performed.

As opposed to the lumped-parameter, the distributed-parameter line models are used for more accurate representation of the lines. Two categories of distributed-parameter line models can be distinguished:

- constant-parameter model,
- frequency-dependent parameter model.

Series parameters: resistance (R), inductance (L), and shunt parameters: capacitance (C) and conductance (G) characterize the line. Usually, line conductance, which accounts for the leakage currents along the insulators and in the air, can be neglected, except at very low frequencies. Shunt capacitance can usually be assumed as frequency-independent. In turn, series resistance and inductance can be considered to be frequency-dependent. However, this is considered rather for the simulation [B.5, 111] and not for representing lines in fault location algorithms.

3.2.1. Lumped-parameter models

In the simplest lumped-parameter model of an overhead line, only the series resistance (R_L) and reactance (X_L) are included (Fig. 3.19). Such a model is considered adequate for representing a short line, usually less than 80 km long [B.6].

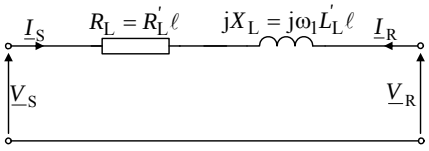

Fig. 3.19. Model of short unfaulted overhead line

In Fig. 3.19, the following signals and parameters are used:
$\underline{V}_S$, $\underline{V}_R$ – sending (S) and receiving (R) end voltage,
$\underline{I}_S$, $\underline{I}_R$ – sending (S) and receiving (R) end current,
R'_L, L'_L – line resistance and inductance per unit length,
ℓ – line length,
ω_1 – angular fundamental frequency.

The circuit of Fig. 3.19 applies either to single-phase or completely transposed three-phase lines operating under balanced conditions. For a completely transposed three-phase line and balanced conditions, line resistance and inductance are considered for the positive-sequence. In turn, $\underline{V}_S$, $\underline{V}_R$ are the positive-sequence line-to-neutral voltages; $\underline{I}_S$, $\underline{I}_R$ are the positive-sequence line currents.

Under unbalanced conditions, mainly under faults, a three-phase line representation has to be considered. Figure 3.20 presents a faulted line together with the equivalent sources behind the line terminals S, R. A fault (occurring at a point marked by F) divides the line into two segments:

- S–F of the relative length d (p.u.),
- F–R of the relative length $(1 - d)$ (p.u.).

All signals (voltages and currents) in the circuit of Fig. 3.20 are three-phase (note that particular phases are marked in subscripts with letters: a, b, c), and thus are represented by 3×1 column matrices, as for example, the sending end voltage $\mathbf{V}_S$:

$$\mathbf{V}_S = \begin{bmatrix} \underline{V}_{Sa} \\ \underline{V}_{Sb} \\ \underline{V}_{Sc} \end{bmatrix} \tag{3.5}$$

All impedances are described by 3×3 matrices, as for example, the line impedance:

$$\mathbf{Z}_L = \begin{bmatrix} \underline{Z}_{Laa} & \underline{Z}_{Lab} & \underline{Z}_{Lac} \\ \underline{Z}_{Lba} & \underline{Z}_{Lbb} & \underline{Z}_{Lbc} \\ \underline{Z}_{Lca} & \underline{Z}_{Lcb} & \underline{Z}_{Lcc} \end{bmatrix} \tag{3.6}$$

where:

- diagonal elements present the self-impedances of the phase conductors,
- off-diagonal elements present the mutual impedances between two phase conductors, for which the following is satisfied: $\underline{Z}_{Lba} = \underline{Z}_{Lab}$, $\underline{Z}_{Lca} = \underline{Z}_{Lac}$, $\underline{Z}_{Lcb} = \underline{Z}_{Lbc}$

Note that the line in Fig. 3.20 is represented with only series parameters, while shunt parameters are here neglected.

At the fault point there is a three-phase fault model marked by $\mathbf{Z}_F$, while $\mathbf{I}_F$, $\mathbf{V}_F$ denote the total fault current and voltage at the fault, respectively. Detailed considerations for the fault models are presented in Chapter 4.

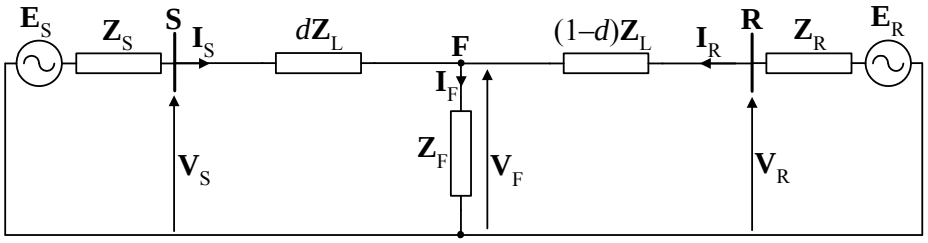

Fig. 3.20. Circuit diagram of three-phase faulted line using matrices for presenting components and column matrices for signals

The self and mutual impedances and admittances of each phase of overhead lines are determined by line geometry and they are not identical for all phases. In general, the line impedance matrix $\mathbf{Z}_L$ is not symmetrical. For a symmetrical impedance matrix the diagonal elements are equal and the off-diagonal elements are equal, too. This is satisfied if the line is completely transposed. A complete transposition (Fig. 3.21) is achieved by exchanging the conductor positions along the line in such a way that each phase (a, b and c) occupies each position for one-third of the line length.

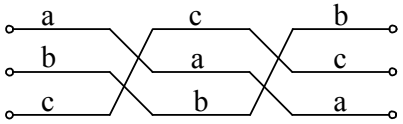

Fig. 3.21. Completely transposed section of three-phase line

For a completely transposed three-phase line the impedance matrix is symmetrical:

$$\mathbf{Z}_L = \begin{bmatrix} \underline{Z}_{Ls} & \underline{Z}_{Lm} & \underline{Z}_{Lm} \\ \underline{Z}_{Lm} & \underline{Z}_{Ls} & \underline{Z}_{Lm} \\ \underline{Z}_{Lm} & \underline{Z}_{Lm} & \underline{Z}_{Ls} \end{bmatrix} \tag{3.7}$$

where in the last position of the subscript for the matrix impedance elements the character of the impedance is denoted by s – self impedance of the phase conductor and by m – mutual impedance between phase conductors.

If the transposition technique is not applied, the impedance matrix is no longer a symmetrical one, however, the following simplification is sometimes made. It relies on using the averaged value for the diagonal and the average for the off-diagonal elements. In this case, additional ramifications with respect to accuracy of the calculation results occur. Applying this simplification one gets:

$$\underline{Z}_{Ls} = \frac{1}{3}(\underline{Z}_{Laa} + \underline{Z}_{Lbb} + \underline{Z}_{Lcc}) \tag{3.8}$$

$$\underline{Z}_{\mathrm{Lm}} = \frac{1}{3}(\underline{Z}_{\mathrm{Lab}} + \underline{Z}_{\mathrm{Lbc}} + \underline{Z}_{\mathrm{Lca}}) \tag{3.9}$$

As a result, one obtains a symmetrical impedance matrix (3.7), whose symmetry is of advantage, however one must accept certain deterioration of accuracy.

Owing to this symmetry, it is possible to apply a method of symmetrical components, developed by C.L. Fortescue in 1918, which is now known from numerous references. Based on this method, a linear transformation from phase components to a set of symmetrical components, as for example for the sending end voltage $\underline{V}_{\mathrm{S}}$, is performed according to:

$$\begin{bmatrix} \underline{V}_{\mathrm{S0}} \\ \underline{V}_{\mathrm{S1}} \\ \underline{V}_{\mathrm{S2}} \end{bmatrix} = \frac{1}{3}\begin{bmatrix} 1 & 1 & 1 \\ 1 & \underline{a} & \underline{a}^2 \\ 1 & \underline{a}^2 & \underline{a} \end{bmatrix} \cdot \begin{bmatrix} \underline{V}_{\mathrm{Sa}} \\ \underline{V}_{\mathrm{Sb}} \\ \underline{V}_{\mathrm{Sc}} \end{bmatrix} \tag{3.10}$$

where:

$\underline{V}_{\mathrm{Sa}}$, $\underline{V}_{\mathrm{Sb}}$, $\underline{V}_{\mathrm{Sc}}$ – voltage from phases: a, b, c,

$\underline{V}_{\mathrm{S0}}$, $\underline{V}_{\mathrm{S1}}$, $\underline{V}_{\mathrm{S2}}$ – zero-, positive- and negative-sequence voltage,

$\underline{a} = 1\angle 120° = -\frac{1}{2} + \mathrm{j}\frac{\sqrt{3}}{2}$ is a complex number with unit magnitude and 120° phase angle.

Note that multiplying any phasor by $\underline{a}$ results in rotating it by 120° counter-clockwise.

For the transformation (3.10) the sequence of phases: (a, b, c) is assumed to be the base, in which phase (a) is considered as the first one in this sequence. Sometimes it is convenient to apply the transformation from phase components into the symmetrical components with assuming the other sequences of phases: (b, c, a) or (c, a, b), in which the phase b or phase c starts the sequence, respectively.

Transformation from symmetrical components into the phase components is defined as follows:

$$\begin{bmatrix} \underline{V}_{\mathrm{Sa}} \\ \underline{V}_{\mathrm{Sb}} \\ \underline{V}_{\mathrm{Sc}} \end{bmatrix} = \frac{1}{3}\begin{bmatrix} 1 & 1 & 1 \\ 1 & \underline{a}^2 & \underline{a} \\ 1 & \underline{a} & \underline{a}^2 \end{bmatrix} \cdot \begin{bmatrix} \underline{V}_{\mathrm{S0}} \\ \underline{V}_{\mathrm{S1}} \\ \underline{V}_{\mathrm{S2}} \end{bmatrix} \tag{3.11}$$

Use of symmetrical components method to a three-phase network, which is represented by the symmetrical impedance matrix, such as (3.7), allows this network to be decoupled into three sequence networks, which are simpler to analyse. These are called the zero-sequence, positive-sequence and negative-sequence networks. The sequence networks results can then be superposed to obtain three-phase network results by using (3.11).

In the sequence networks, the line is represented by its respective sequence impedances:

- positive- and negative-sequence impedance:

$$\underline{Z}_{1L} = \underline{Z}_{2L} = \underline{Z}_{Ls} - \underline{Z}_{Lm} \tag{3.12}$$

- zero-sequence impedance:

$$\underline{Z}_{0L} = \underline{Z}_{Ls} + 2\underline{Z}_{Lm} \tag{3.13}$$

Note that the positive- and negative-sequence impedances, as stated in (3.12), are equal. This is so for linear, symmetric impedances representing non-rotating power system items such as overhead lines and transformers.

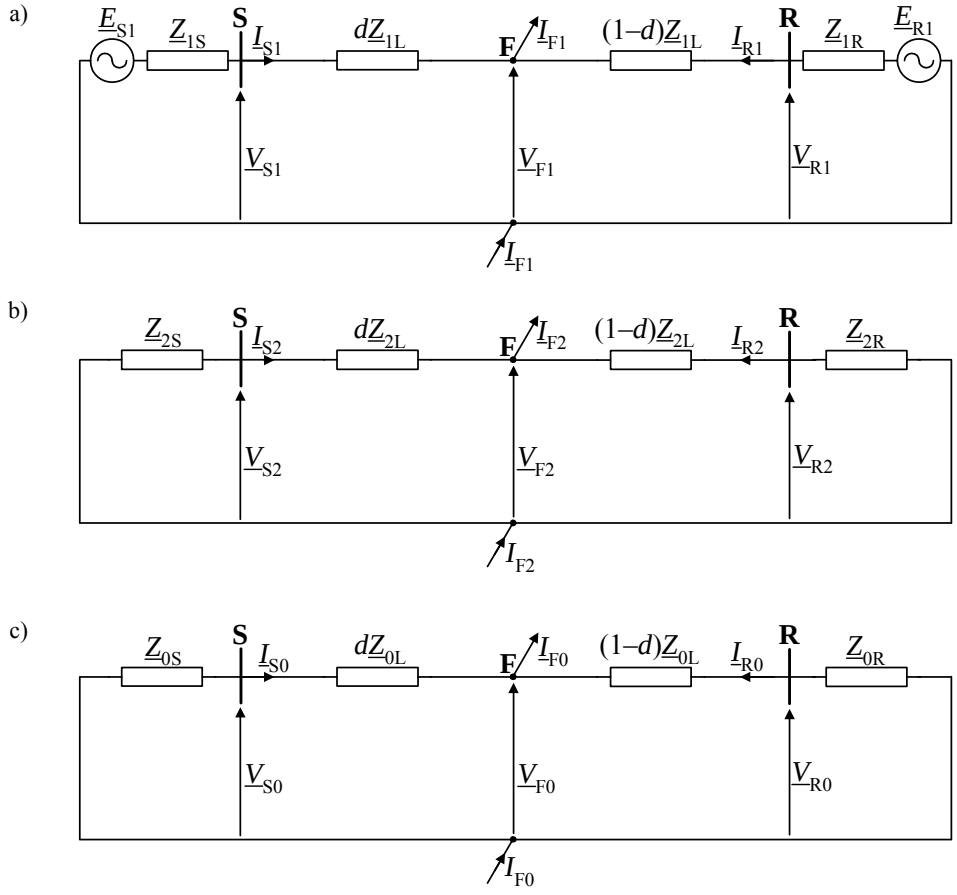

Fig. 3.22. Equivalent networks of single-circuit faulted line for:
a) positive-sequence, b) negative-sequence, c) zero-sequence

Figure 3.22 presents models of a faulted single-circuit overhead line, together with the equivalent sources behind the line terminals, for the respective sequences. There are three circuits, which can be analysed separately. These circuits can be composed into one resultant circuit by connecting them at points of unbalance and including the fault path resistance R_F. At these points of unbalance, the respective sequence components of the total fault current ($\underline{I}_{F1}$, $\underline{I}_{F2}$, $\underline{I}_{F0}$) flow into the sequence circuit, and flow out of the respective circuit. The particular sequence networks are connected in such a way as to satisfy the particular fault type constraints.

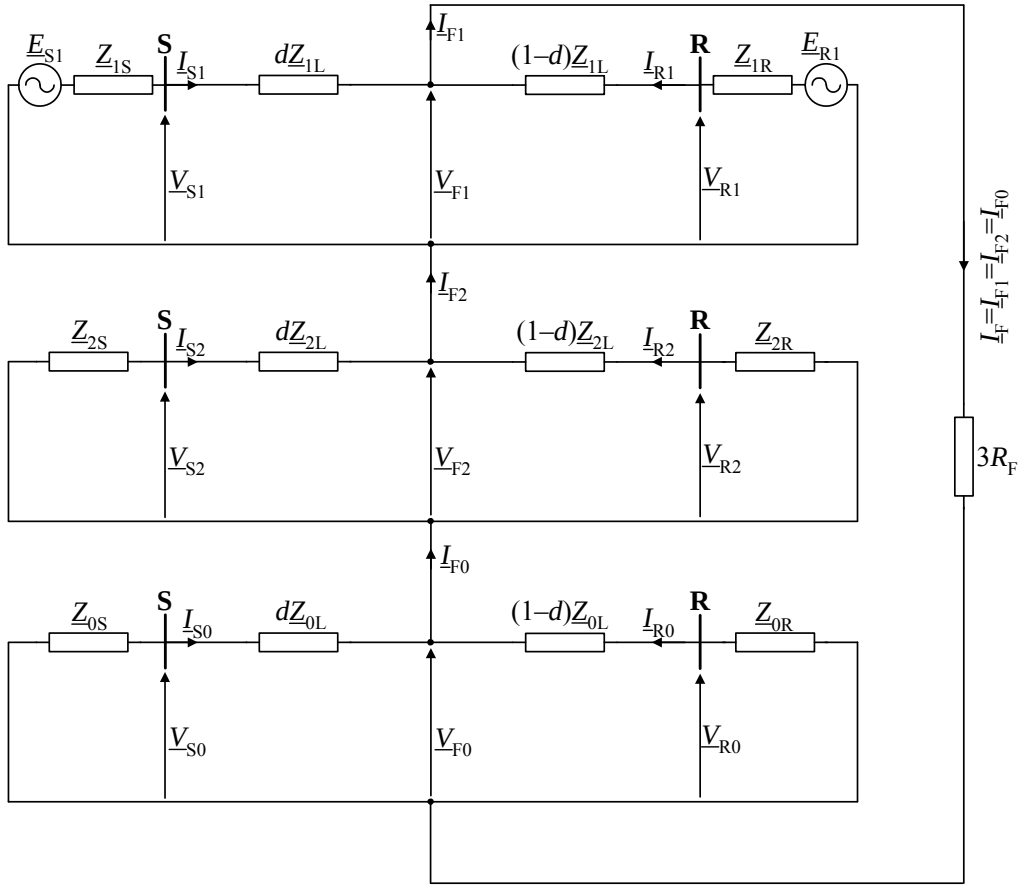

Fig. 3.23. Connection of sequence networks for single phase-to-earth fault (a–E fault) involving fault resistance R_F

Figure 3.23 shows the connection of the sequence networks for a single phase-to-earth fault: a–E fault. The sequence networks are connected in series and the triple fault resistance ($3R_F$) is included in series as well. The series connection of Fig. 3.23

can also be applied for the remaining single phase-to-earth faults: b–E, c–E, however this makes it necessary to use the following sequences of phases: (b, c, a) and (c, a, b), respectively.

In Fig. 3.24, equivalent circuit diagrams of double-circuit line for the positive- and negative-sequence are shown.

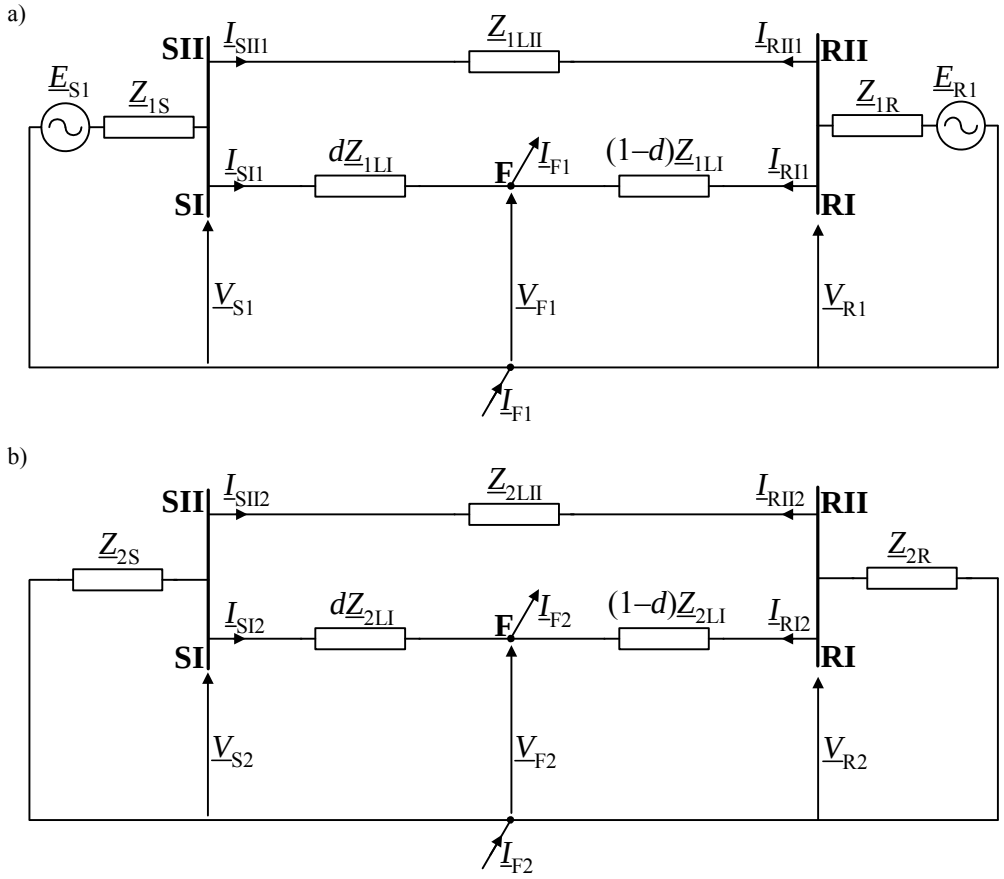

Fig. 3.24. Equivalent networks of double-circuit faulted line for:
a) positive-sequence, b) negative-sequence

In Fig. 3.25, equivalent circuits of double-circuit line, with both circuits in operation [B.1, B.9, 58, 63, 76, 158, 163, 189], for the zero-sequence are presented. As a result of mutual coupling of the line circuits, the current flowing in the faulted line SI–RI influences the voltage profile in the healthy parallel line SII–RII, and vice versa. In particular, in the faulted line (SI–RI) one can distinguish the following voltage drops (Fig. 3.25a):

• voltage drops resulting from the flow of the faulted line current:

$$\underline{V}_0^{\mathrm{A}} = d\,\underline{Z}_{0\mathrm{LI}}\underline{I}_{\mathrm{SI0}} \tag{3.14}$$

$$\underline{V}_0^{\mathrm{B}} = (1-d)\underline{Z}_{0\mathrm{LI}}(\underline{I}_{\mathrm{SI0}} - \underline{I}_{\mathrm{F0}}) \tag{3.15}$$

• voltage drops resulting from the flow of the current in the healthy parallel line:

$$\underline{V}_0^{\mathrm{C}} = d\,\underline{Z}_{0\mathrm{m}}\underline{I}_{\mathrm{SII0}} \tag{3.16}$$

$$\underline{V}_0^{\mathrm{D}} = (1-d)\underline{Z}_{0\mathrm{m}}\underline{I}_{\mathrm{SII0}} \tag{3.17}$$

In the healthy line (SII–RII) there are the following voltage drops (Fig. 3.25a):
• voltage drops resulting from the flow of the healthy line current:

$$\underline{V}_0^{\mathrm{E}} = d\,\underline{Z}_{0\mathrm{LII}}\underline{I}_{\mathrm{SII0}} \tag{3.18}$$

$$\underline{V}_0^{\mathrm{F}} = (1-d)\underline{Z}_{0\mathrm{LII}}\underline{I}_{\mathrm{SII0}} \tag{3.19}$$

• voltage drops resulting from the flow of the current in the faulted line:

$$\underline{V}_0^{\mathrm{G}} = d\,\underline{Z}_{0\mathrm{m}}\underline{I}_{\mathrm{SI0}} \tag{3.20}$$

$$\underline{V}_0^{\mathrm{H}} = (1-d)\underline{Z}_{0\mathrm{m}}(\underline{I}_{\mathrm{SI0}} - \underline{I}_{\mathrm{F0}}) \tag{3.21}$$

The circuit of Fig. 3.25a can be transformed to the form shown in Fig. 3.25b, which is more convenient for use. For this purpose the voltage drop between the bus SI and fault point F is determined, taking into account (3.14), (3.16):

$$\underline{V}_0^{(\mathrm{SI-F})} = d\,\underline{Z}_{0\mathrm{LI}}\underline{I}_{\mathrm{SI0}} + d\,\underline{Z}_{0\mathrm{m}}\underline{I}_{\mathrm{SII0}} \tag{3.22}$$

Adding and subtracting the term $d\,\underline{Z}_{0\mathrm{m}}\underline{I}_{\mathrm{SI0}}$ to the right-hand side of (3.22) leads to the following alternative form of (3.22):

$$\underline{V}_0^{(\mathrm{SI-F})} = d\,\underline{Z}_{0\mathrm{m}}(\underline{I}_{\mathrm{SI0}} + \underline{I}_{\mathrm{SII0}}) + d(\underline{Z}_{0\mathrm{LI}} - \underline{Z}_{0\mathrm{m}})\underline{I}_{\mathrm{SI0}} \tag{3.23}$$

Analogously, after taking (3.15) and (3.17), one obtains for the voltage drop between the fault point F and the bus RI:

$$\underline{V}_0^{(\mathrm{F-RI})} = (1-d)(\underline{Z}_{0\mathrm{LI}} - \underline{Z}_{0\mathrm{m}})(\underline{I}_{\mathrm{SI0}} - \underline{I}_{\mathrm{F0}}) + (1-d)\underline{Z}_{0\mathrm{m}}(\underline{I}_{\mathrm{SI0}} + \underline{I}_{\mathrm{SII0}} - \underline{I}_{\mathrm{F0}}) \tag{3.24}$$

Similarly, for the healthy line path (between buses SII, RII) one obtains:

$$\underline{V}_0^{(\mathrm{SII-RII})} = d\,\underline{Z}_{0\mathrm{m}}(\underline{I}_{\mathrm{SI0}} + \underline{I}_{\mathrm{SII0}}) + (\underline{Z}_{0\mathrm{LII}} - \underline{Z}_{0\mathrm{m}})\underline{I}_{\mathrm{SII0}} + (1-d)\underline{Z}_{0\mathrm{m}}(\underline{I}_{\mathrm{SI0}} + \underline{I}_{\mathrm{SII0}} - \underline{I}_{\mathrm{F0}}) \quad (3.25)$$

Taking into account (3.23)–(3.25), the circuit of Fig. 3.25b is obtained.

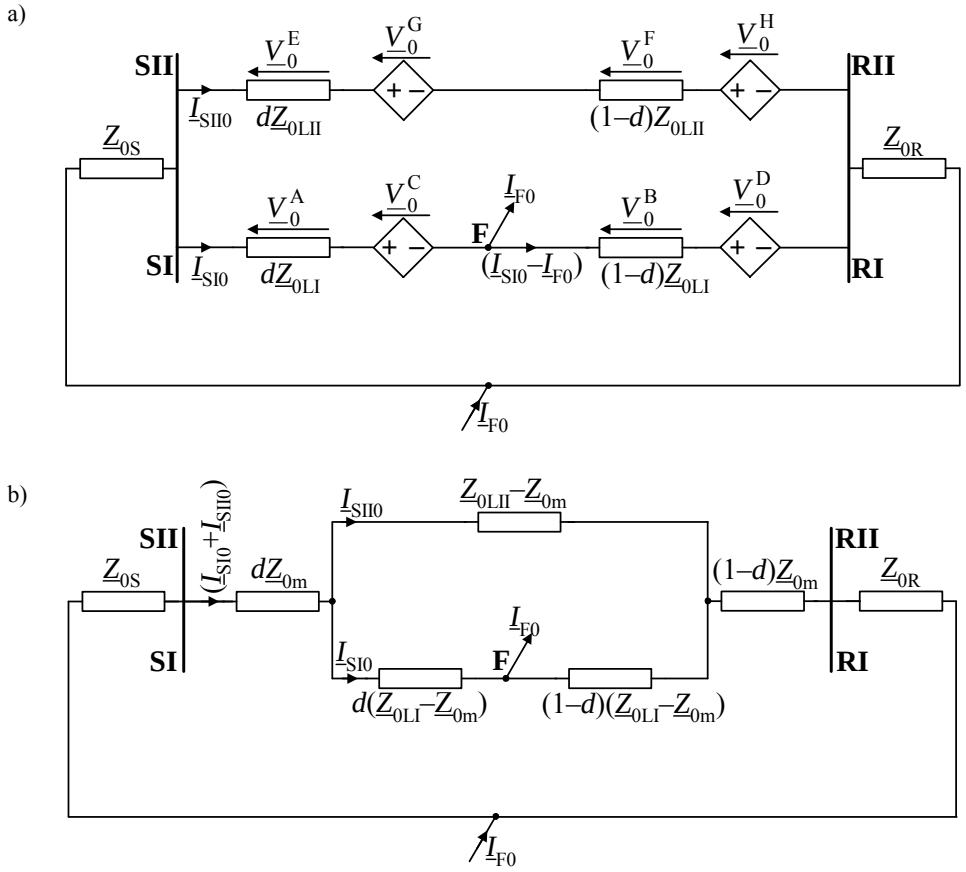

Fig. 3.25. Equivalent networks of double-circuit faulted line with both lines in operation for zero-sequence: a) general circuit, b) alternative circuit

In Fig. 3.26, the mutual coupling effect is depicted for a double circuit line with the healthy parallel line switched-off and earthed at both ends [58]. The particular voltage drops for both lines are expressed in the same way as for the case of both lines in operation (3.14)–(3.21). Usual unavailability of the zero sequence current from the healthy parallel line $\underline{I}_{\mathrm{SII0}}$ causes difficulty in reflecting the mutual coupling effect in the fault location algorithms for this mode of operation. Therefore, it remains to estimate this current, based on other measurements available [58].

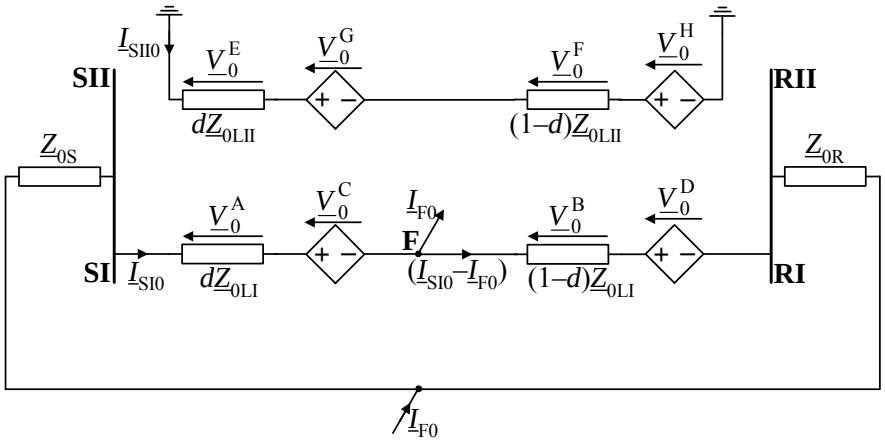

Fig. 3.26. Zero-sequence equivalent network for double-circuit line with faulted line in operation and parallel healthy line switched-off and earthed at both ends

In the models presented so far (Figs. 3.19–3.20 and Figs. 3.22–3.26), only the series parameters of the line have been accounted for. These models can be used for short lines. For medium-length lines, typically ranging from 80 to 250 km, it is common to incorporate the shunt admittance to the line model [B.6]. Shunt conductance is usually neglected and only shunt capacitances of the line are considered for that. It is a common practice to lump the total shunt capacitance and insert half at each of the line section. In this way the nominal π circuit is obtained [B.6].

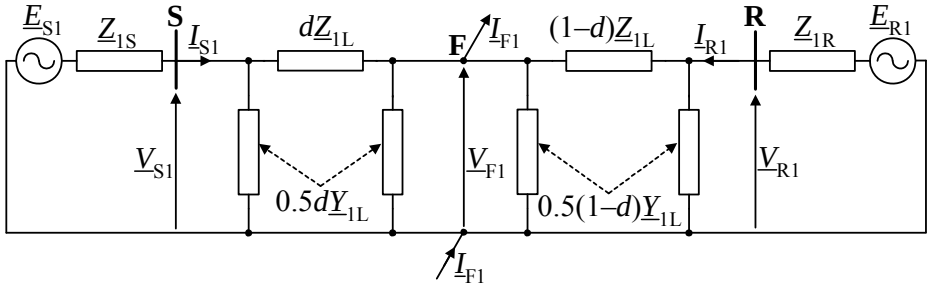

Fig. 3.27. Equivalent circuit diagram of the network for the positive-sequence with the use of nominal π circuit for faulted line

Figure 3.27 shows a positive-sequence circuit of the faulted line, for which both sections (S–F and F–R) are represented using the nominal π circuits. The parameter $\underline{Y}_{1L}$ used in describing admittances of shunt branches denotes:

$$\underline{Y}_{1L} = \mathrm{j}\omega_1 C'_{1L}\ell \tag{3.26}$$

where:

C'_{1L} – line capacitance for the positive-sequence per unit length,

ℓ – line length,

ω_1 – angular fundamental frequency.

The equivalent circuit diagrams for the remaining sequences are obtained analogously.

Figure 3.28a presents a model of the line section between the bus S and the fault point F (as applied in Fig. 3.27). Note that a sought distance to fault (d) is used for determining both the series impedance $d\underline{Z}_{1L}$ and shunt admittance $0.5d\underline{Y}_{1L}$. However, it is inconvenient for performing fault location calculations. In order to make the calculation simpler, the iterative calculations are usually performed in such a way that the unknown fault distance is left in the current iteration (n) as related to the series impedance $d_{(n)}\underline{Z}_{1L}$ (Fig. 3.28b). On the other hand, the shunt admittance is determined using the fault distance from the previous iteration ($n-1$): $0.5d_{(n-1)}\underline{Y}_{1L}$ at both ends of the faulted section (Fig. 3.28b). When starting the iterative calculations (iteration number: $n = 1$) one takes the fault distance obtained under neglecting the shunt admittance ($\underline{Y}_{1L} = 0$) as the fault distance from the previous iteration (iteration number: $n - 1 = 0$).

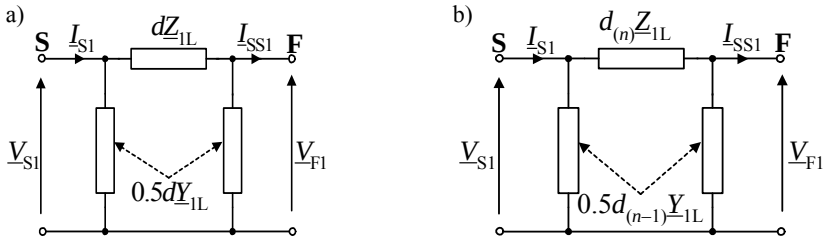

Fig. 3.28. Model of faulted line section from the side S for the positive-sequence: a) basic model, b) model used in simple iterative fault location calculations

3.2.2. Distributed-parameter models

For short and medium-length lines using the lumped-model is usually sufficient. In order to improve fault location accuracy, especially in the case of long-length lines, the distributed nature of overhead line parameters has to be considered.

In the distributed parameter-parameter line model the voltage and current along the line are functions of the distance x (point X) from the sending end (S) of the line and the time t (Fig. 3.29). The voltage $v(x, t)$ and current $i(x, t)$ are related with the parameters of the line (R'_L, L'_L, C'_L – resistance, inductance and capacitance of the line per unit length) by the so called **Telegrapher's Equations** [B.2, B.11, 46]:

$$\frac{\partial v(x,t)}{\partial x} + L'_{\mathrm{L}} \frac{\partial i(x,t)}{\partial t} = -R'_{\mathrm{L}} i(x,t) \tag{3.27}$$

$$C'_{\mathrm{L}} \frac{\partial v(x,t)}{\partial t} + \frac{\partial i(x,t)}{\partial x} = 0 \tag{3.28}$$

Note that in (3.28) the line conductance is neglected, which is a common practice.

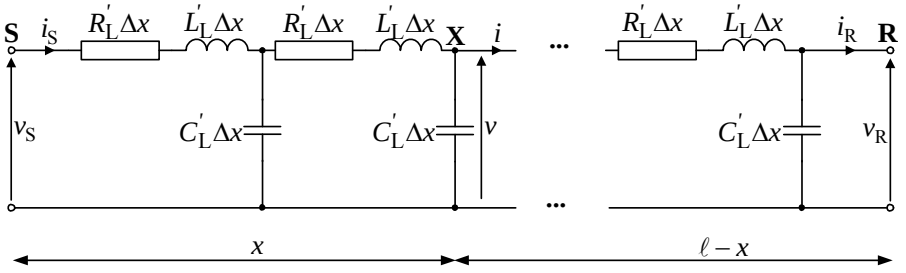

Fig. 3.29. Distributed-parameter model of unfaulted long overhead line

Partial differential equations (3.27)–(3.28) can be solved using the method of characteristics developed by Collatz [B.2]. For this purpose **the modified Telegrapher's Equations** are formulated:

$$\frac{\partial u(x,t)}{\partial x} - \chi^2 \frac{\partial i(x,t)}{\partial t} = -\eta i(x,t) \tag{3.29}$$

$$\frac{\partial u(x,t)}{\partial t} - \frac{\partial i(x,t)}{\partial x} = 0 \tag{3.30}$$

where:

$u(x,t) = -C'_{\mathrm{L}} v(x,t)$,

$\chi = \sqrt{L'_{\mathrm{L}} C'_{\mathrm{L}}}$,

$\eta = R'_{\mathrm{L}} C'_{\mathrm{L}}$.

The travelling waves method is applied as the alternative to solving the partial differential equations (3.29)–(3.30). In this method, the voltage and current are considered as two components: the forward and backward travelling waves [B.11].

A distributed-parameter model of an overhead line can also be applied for phasors. In this case, the so-called equivalent π circuit [B.6] is utilised. In Fig. 3.30, two such circuits are used for representing both line sections S–F and F–R. The model of Fig. 3.30 is for the general case, i.e. for the *i*-th symmetrical component, where: *i* = 1 – positive-sequence, *i* = 2 – negative-sequence, *i* = 0 – zero-sequence.

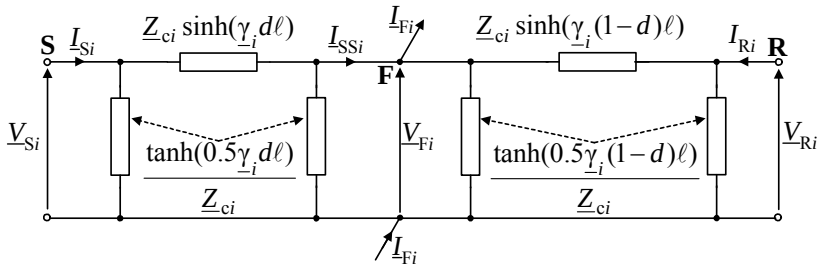

Fig. 3.30. Distributed-parameter model of faulted line for the *i*-th symmetrical component

In Figure 3.30, both the series and shunt parameters of the line are distributed-parameters and are expressed using:

- surge impedance of the line for the *i*-th sequence:

$$\underline{Z}_{ci} = \sqrt{\frac{\underline{Z}'_{iL}}{\underline{Y}'_{iL}}} \tag{3.31}$$

- propagation constant of the line for the *i*-th sequence:

$$\underline{\gamma}_i = \sqrt{\underline{Z}'_{iL}\underline{Y}'_{iL}} \tag{3.32}$$

Using the equivalent π circuit model, the voltage and current, for example, from the sending end S can be analytically transferred to the fault point F (Fig. 3.30) according to:

$$\underline{V}_{Fi} = \cosh(\underline{\gamma}_i d\ell)\underline{V}_{Si} - \underline{Z}_{ci}\sinh(\underline{\gamma}_i d\ell)\underline{I}_{Si} \tag{3.33}$$

$$\underline{I}_{SSi} = -\frac{1}{\underline{Z}_{ci}}\sinh(\underline{\gamma}_i d\ell)\underline{V}_{Si} + \cosh(\underline{\gamma}_i d\ell)\underline{I}_{Si} \tag{3.34}$$

Alternative representation of the faulted line, based on the distributed-parameter line model is depicted in Fig. 3.31 [B.6]. Both the series impedances and shunt admittances are expressed as the lumped parameter multiplied by the respective correction factor:

- correction factors for series impedances:

$$\underline{A}_i^{\text{sh}} = \frac{\sinh(\underline{\gamma}_i d\ell)}{\underline{\gamma}_i d\ell} \tag{3.35}$$

$$\underline{B}_i^{\text{sh}} = \frac{\sinh(\underline{\gamma}_i(1-d)\ell)}{\underline{\gamma}_i(1-d)\ell} \tag{3.36}$$

• correction factors for shunt admittances:

$$\underline{A}_i^{\text{th}} = \frac{\tanh(0.5\underline{\gamma}_i d\ell)}{0.5\underline{\gamma}_i d\ell} \tag{3.37}$$

$$\underline{B}_i^{\text{th}} = \frac{\tanh(0.5\underline{\gamma}_i (1-d)\ell)}{0.5\underline{\gamma}_i (1-d)\ell} \tag{3.38}$$

Using the correction factors (3.35)–(3.38) allows us to recalculate the lumped parameters into the distributed ones.

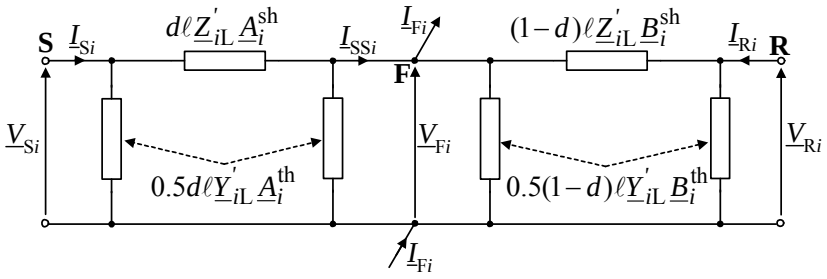

Fig. 3.31. Distributed-parameter model of faulted line for the *i*-th symmetrical component, with use of the correction factors for representing series and shunt parameters

In Fig. 3.32, the distributed-parameter model of faulted line for the *i*-th symmetrical component for application to simplified iterative fault location calculations is presented. The model of Fig. 3.32 is simpler in comparison to the strict model of Fig. 3.31. The unknown fault distance in the model of Fig. 3.32, which is calculated in the current iteration (iteration number n): $d_{(n)}$, is involved only to represent the series impedances. The shunt parameters are represented by the fault distance value obtained in the previous iteration: $d_{(n-1)}$. Also this value of fault distance is used for calculating all correction factors:

$$\underline{A}_{i_{(n-1)}}^{\text{sh}} = \frac{\sinh(\underline{\gamma}_i d_{(n-1)}\ell)}{\underline{\gamma}_i d_{(n-1)}\ell} \tag{3.39}$$

$$\underline{B}_{i_{(n-1)}}^{\text{sh}} = \frac{\sinh(\underline{\gamma}_i (1-d_{(n-1)})\ell)}{\underline{\gamma}_i (1-d_{(n-1)})\ell} \tag{3.40}$$

$$\underline{A}_{i_{(n-1)}}^{\text{th}} = \frac{\tanh(0.5\underline{\gamma}_i d_{(n-1)}\ell)}{0.5\underline{\gamma}_i d_{(n-1)}\ell} \tag{3.41}$$

$$\underline{B}^{\mathrm{th}}_{i_{(n-1)}} = \frac{\tanh(0.5\underline{\gamma}_i(1-d_{(n-1)})\ell)}{0.5\underline{\gamma}_i(1-d_{(n-1)})\ell} \tag{3.42}$$

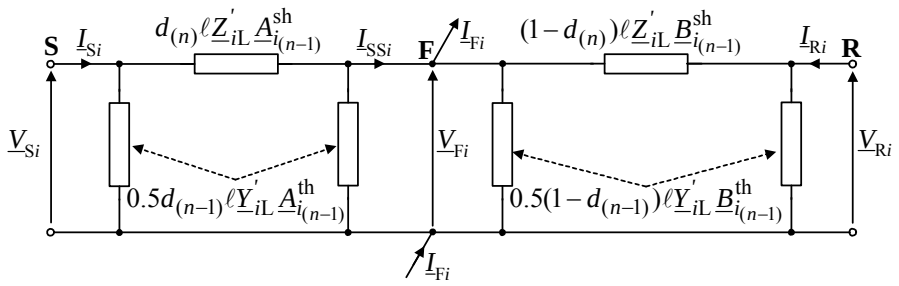

Fig. 3.32. Distributed-parameter model of faulted line for the *i*-th symmetrical component for application to simplified iterative calculations in fault location

3.2.3. Modal transformation

The symmetrical components approach was used in the preceding sections for presenting different line models. Yet, there is another technique based on modal transformation which considers the general case of untransposed line [B.5].

Using the modal transformation [B.5, 74] the line impedance matrix **Z** and admittance matrix **Y** are transformed into the matrices $\mathbf{Z}_{\mathrm{mode}}$, $\mathbf{Y}_{\mathrm{mode}}$:

$$\mathbf{Z}_{\mathrm{mode}} = \mathbf{T}_{\mathrm{v}}^{-1}\mathbf{Z}\mathbf{T}_{\mathrm{i}} \tag{3.43}$$

$$\mathbf{Y}_{\mathrm{mode}} = \mathbf{T}_{\mathrm{i}}^{-1}\mathbf{Y}\mathbf{T}_{\mathrm{v}} \tag{3.44}$$

where the superscript (–1) denotes the matrix inversion.

The transformation (3.43)–(3.44) is performed in such a way that the matrices $\mathbf{Z}_{\mathrm{mode}}$, $\mathbf{Y}_{\mathrm{mode}}$ are diagonal, which means that the three-phase coupled network becomes decoupled into three decoupled single phase networks.

Three-phase voltage **V** and current **I** matrices are transformed into the modal matrices $\mathbf{V}_{\mathrm{mode}}$, $\mathbf{I}_{\mathrm{mode}}$. This is performed using the matrices $\mathbf{T}_{\mathrm{i}}$, $\mathbf{T}_{\mathrm{v}}$ (used in (3.43) and (3.44)):

$$\mathbf{V}_{\mathrm{mode}} = \mathbf{T}_{\mathrm{v}}^{-1}\mathbf{V} \tag{3.45}$$

$$\mathbf{I}_{\mathrm{mode}} = \mathbf{T}_{\mathrm{i}}^{-1}\mathbf{I} \tag{3.46}$$

For balanced (equally transposed) three-phase lines, both matrices $\mathbf{T}_{\mathrm{i}}$, $\mathbf{T}_{\mathrm{v}}$ are identical and are composed of the different real value elements such as:

- Clarke transformation (also called the α–β transform):

$$\mathbf{T}_{\mathrm{v}} = \mathbf{T}_{\mathrm{i}} = \begin{bmatrix} 1 & 1 & 0 \\ 1 & -\frac{1}{2} & \frac{\sqrt{3}}{2} \\ 1 & -\frac{1}{2} & -\frac{\sqrt{3}}{2} \end{bmatrix} \tag{3.47}$$

$$\mathbf{T}_{\mathrm{v}}^{-1} = \mathbf{T}_{\mathrm{i}}^{-1} = \frac{1}{3}\begin{bmatrix} 1 & 1 & 1 \\ 2 & -1 & -1 \\ 0 & \sqrt{3} & -\sqrt{3} \end{bmatrix} \tag{3.48}$$

- Karrenbauer transformation:

$$\mathbf{T}_{\mathrm{v}} = \mathbf{T}_{\mathrm{i}} = \begin{bmatrix} 1 & 1 & 1 \\ 1 & -2 & 1 \\ 1 & 1 & -2 \end{bmatrix} \tag{3.49}$$

$$\mathbf{T}_{\mathrm{v}}^{-1} = \mathbf{T}_{\mathrm{i}}^{-1} = \frac{1}{3}\begin{bmatrix} 1 & 1 & 1 \\ 1 & -1 & 0 \\ 1 & 0 & -1 \end{bmatrix} \tag{3.50}$$

- Wedepohl transformation:

$$\mathbf{T}_{\mathrm{v}} = \mathbf{T}_{\mathrm{i}} = \begin{bmatrix} 1 & 1 & 1 \\ 1 & 0 & -2 \\ 1 & -1 & 1 \end{bmatrix} \tag{3.51}$$

$$\mathbf{T}_{\mathrm{v}}^{-1} = \mathbf{T}_{\mathrm{i}}^{-1} = \frac{1}{3}\begin{bmatrix} 1 & 1 & 1 \\ \frac{3}{2} & 0 & -\frac{3}{2} \\ \frac{1}{2} & -1 & \frac{1}{2} \end{bmatrix} \tag{3.52}$$

In the case of untransposed lines, there is also a possibility of determining the transformation matrices $\mathbf{T}_{\mathrm{v}}$, $\mathbf{T}_{\mathrm{i}}$, which are not identical. They can be applied for transforming the coupled phase quantities to decoupled modal quantities based in eigenvalue/eigenvector theory [74].

4. Transmission line faults

4.1. Introduction

There are various causes of faults occurring in power systems. Breakdown of the insulation can be caused by lightning strokes on overhead lines. As a result, the connection with earth via an earth wire is established. Also such earth connection occurs when a tree or a man-made object provides the connecting path. Some faults are also caused by switching mistakes of the station personnel.

Power system faults can be shunt, series or a combination of shunt and series faults. Under a shunt fault there is a flow of current between two or more phases, or between phase(s) and earth. A series fault is an abnormality at which the impedances of the three phases are not equal, usually caused by the interruption of one or two phases.

Most of the power system faults occur in transmission networks, especially on overhead lines. Lines are the elements in the system that are in charge of transporting important bulks of energy from generator plants to load centres. Due to their inherent characteristic of being exposed to atmospheric conditions, transmission lines have the highest fault rate in the system. Therefore, a number of researchers have devoted great effort to the line protection and fault location.

There are known various fault statistics, which are related to different voltage levels, technical and weather conditions. All of them unambiguously indicate that around 75% of the total number of power system faults occur in transmission networks. This fact reveals very high importance of fault analysis for transmission networks.

4.2. Fault types

Faults on EHV/UHV overhead lines are in majority single-phase-to-ground arcing faults and are temporary in most cases. Therefore, protective relays are provided with the automatic reclosing function [6, 25, 166]. This function allows the line to be reclosed and kept in operation after the fault has disappeared because the arc can self-extinguish. The circuit breakers can operate on a single phase (single pole) or on all

three phases. For applying a proper autoreclosing option the fault type is required to be correctly recognized by the fault location techniques [27, 95, 101].

The main characteristic of faults is related with the fault impedance involved, which can basically be considered as fault resistance. In this respect, the faults are categorized as bold and resistive ones, respectively. Usually, for inter-phase faults, fault resistances are small and in general do not exceed 0.5 Ω. They may, however, become much higher during earth faults, because tower footing resistance may be as high as 10 Ω [98]. If there is a flashover of an insulator, the connection of towers with earth wires makes the resulting fault resistance smaller. In practice, it seldom exceeds 3 Ω. For some earth faults the fault resistances may become much higher, which happens in cases of fallen trees, or if a broken conductor lays on the high-resistive soil.

For formulating fault location algorithms mostly the basic linear models of faults, such as presented in Fig. 4.1, are considered. The fault resistance involved is denoted by R_F and the resistance connected to an earth in the case of inter-phase faults involving earth (Fig. 4.1c, e) by R_E. Note that it is assumed that the fault resistance R_F for inter-phase faults (Fig. 4.1.b–e) is identical in all phases. Such basic fault models are considered for both the symmetrical components approach and the phase co-ordinates approach as well.

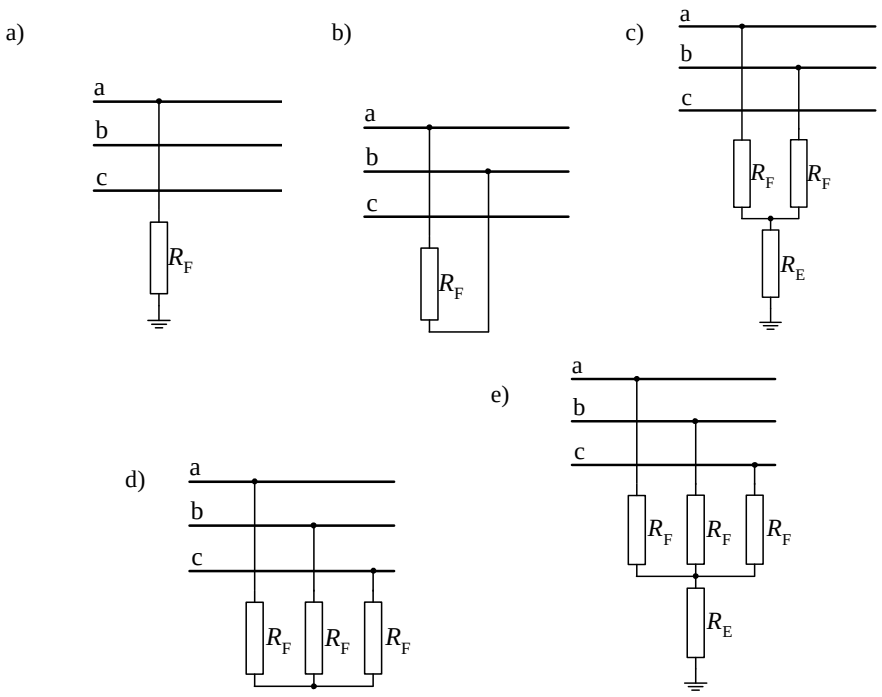

Fig. 4.1. Typical shunt faults: a) phase-to-earth, b) phase-to-phase, c) phase-to-phase-to-earth, d) three-phase, e) three-phase-to-earth

Besides numerous fault location techniques considering the basic linear fault models, there have also been developed some algorithms treating faults as of non-linear character, i.e. considering the electric arc phenomenon [24, 26, 105, 106, 136]. Also, this phenomenon is widely used in digital simulations [93, 94, 122] aimed at evaluating the performance of the algorithms based on the linear fault models.

Broken conductor or open conductor failure in one phase (phase a) is shown in Fig. 4.2a. However, such failure may also happen in two phases. Broken conductor failure may also occur as coupled with this phase-to-earth fault (Fig. 4.2b, c). For such combined faults, different sequences, as seen from the measuring point (M in Fig. 4.2b, c) can be considered. For a fault from Fig. 4.2b, an open conductor failure is located outside the fault loop seen from the measuring point, while inside it for the case of Fig. 4.2c. Such two combined faults (Fig. 4.2b, c) impose different conditions on fault location [54].

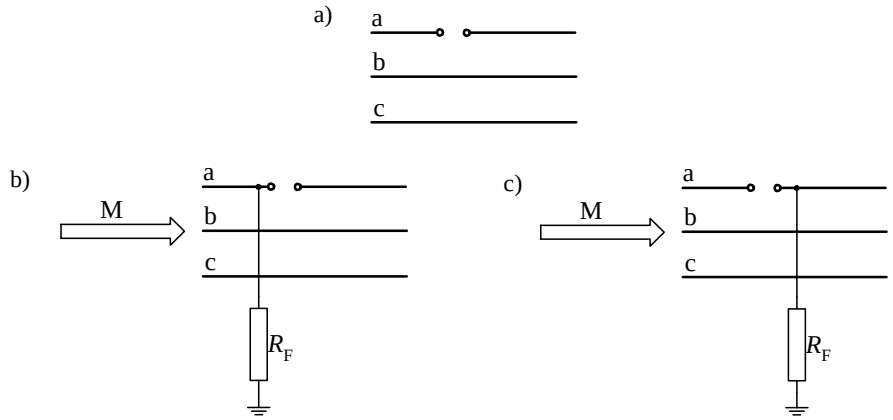

Fig. 4.2. Broken conductor faults: a) broken conductor failure alone,
b) phase-to-earth fault with broken conductor, c) broken conductor with phase-to-earth fault

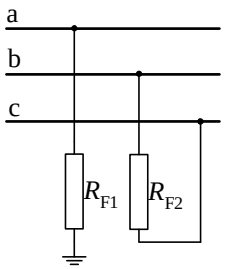

Fig. 4.3. Phase-to-earth fault combined with phase-to-phase fault

Sometimes more than one fault can occur simultaneously. For example, these may all be shunt faults, as shown in Fig. 4.3, where phase-to-earth fault occurs in combina-

tion with phase-to-phase fault for the remaining phases. In general, different fault resistances (R_{F1}, R_{F2}) can be involved in these faults.

Double faults [134] are considered as faults to earth, occurring simultaneously at two different locations in one or several circuits. In Fig. 4.4a, such a fault, also called a cross-country fault is shown as occurring on double-circuit line.

Flashover faults on double-circuit line (Fig. 4.4b) are usually caused by lightning stroke to an earth wire or tower, or due to a direct lightning stroke to a phase conductor [B.3].

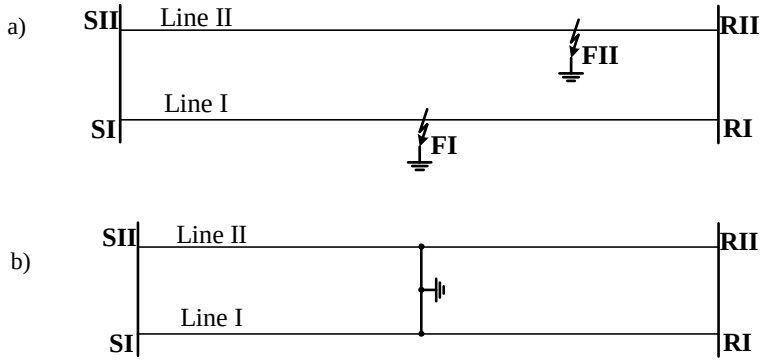

Fig. 4.4. Faults on double-circuit lines:
a) cross-country earth fault, b) flashover fault to earth

A fault involving two different nominal power system voltages is called an intersystem fault. Such faults can occur on transmission lines hanged on the same tower and rated at different voltages.

Besides the faults described, there are also multiple faults, as for example, faults to earth occurring simultaneously at more than two different locations in one or several circuits originated from a common source.

4.3. Fault statistics

Numerous statistics data concerning power system faults are available in the literature and internet. They differ depending on which power system element is considered and on voltage level. In order to be acquainted briefly with the fault statistics for power transmission lines, in Tables 4.1 and 4.2 the representative data [B.9], [B.10] is provided. In general, the number of faults decreases with an increase of the voltage level (Table 4.1). As regards the fault type, it is the single phase-to-earth faults that most frequently occur (Table 4.2).

Table 4.1. Number of faults on lines of different voltage levels (fault/year/100 km)

Source of information	Voltage level	
	200÷250 kV	300÷500 kV
Poland	3÷5	1÷3
CIGRE	0.4÷10.4	0.4÷4.68
IEEE	1.24	0.83
NORDEL (Denmark, Norway, Iceland, Finland, Sweden)*	1.0	0.3
Former Soviet Union	1.5	1
* NORDEL statistics is available at: *www.nordel.org*		

Table 4.2. Statistics of different fault types occurring on lines of different voltage levels (fault/year/100 km)

Fault type	Voltage level	
	200÷250 kV	300÷500 kV
Single phase-to-earth faults	2.64	2.2
Phase-to-phase-to-earth faults	0.56	0.16
Faults involving more than one circuit of a line	0.11	0.06
Faults involving circuits of lines of different voltage levels	0.005	0.004

4.4. Models of resistive faults in symmetrical components

There is a wide group of fault location algorithms which require determining the total fault current ($\underline{I}_F$), i.e. the current flowing through the fault path resistance. These are mainly fault location algorithms utilising one-end measurement. Also majority of two-end or multi-end fault location algorithms, but not utilising complete three-phase voltage and current measurements, belong to this group. Use of complete measurements of three-phase voltage and current at both ends, or at all ends in the case of multi-terminal lines, allows avoiding determination of the total fault current.

In general, since the total fault current ($\underline{I}_F$) is immeasurable quantity, therefore it can be calculated [59, 66] or estimated [B.9, 31, 63] by expressing it with the measured quantities, the network parameters and the unknown distance to fault. If the currents from all line terminals are available, then the total fault current can be calculated. However, since the required total fault current is calculated with use of the distant measurements, a special calculation method aimed at minimizing the influence of the line shunt capacitances charging has to be applied [66]. In case the currents from all line terminals are not available, then the total fault current has to be estimated.

However, for both the above mentioned cases (calculation or estimation of the total fault current) the total fault current can be expressed as the following weighted sum of its symmetrical components:

$$\underline{I}_{\mathrm{F}} = \underline{a}_{\mathrm{F0}}\underline{I}_{\mathrm{F0}} + \underline{a}_{\mathrm{F1}}\underline{I}_{\mathrm{F1}} + \underline{a}_{\mathrm{F2}}\underline{I}_{\mathrm{F2}} \tag{4.1}$$

where:

$\underline{a}_{\mathrm{F0}}$, $\underline{a}_{\mathrm{F1}}$, $\underline{a}_{\mathrm{F2}}$ – weighting coefficients (complex numbers), dependent on fault type and the assumed priority for using particular symmetrical components,

$\underline{I}_{\mathrm{F0}}$, $\underline{I}_{\mathrm{F1}}$, $\underline{I}_{\mathrm{F2}}$ – zero-, positive- and negative-sequence components of total fault current, which are to be calculated or estimated.

Determination of the total fault current (4.1) is required for reflecting the voltage drop across the fault path ($\underline{V}_{\mathrm{F}}$) in the fault loops considered in the fault location algorithms:

$$\underline{V}_{\mathrm{F}} = R_F \underline{I}_{\mathrm{F}} \tag{4.2}$$

Depending on the fault type, the phase-to-earth or phase-to-phase fault loops are considered, as for the protective distance relays [B.3, B.9, 31, 63].

It appears that there is some freedom in setting the weighting coefficients in (4.1). Example 4.1 illustrates this for a phase ‘a’ to earth fault.

Example 4.1. Determination of the weighting coefficients for a–E fault

At the place of the fault occurring in the phase ‘a’ there is a flow of the total fault current: $\underline{I}_{\mathrm{F}} = \underline{I}_{\mathrm{Fa}}$, while in the remaining phases $\underline{I}_{\mathrm{Fb}} = 0$, $\underline{I}_{\mathrm{Fc}} = 0$. Calculating the symmetrical components of the total fault current and taking into account the constraints for the fault considered, one obtains:

$$\begin{bmatrix} \underline{I}_{\mathrm{F0}} \\ \underline{I}_{\mathrm{F1}} \\ \underline{I}_{\mathrm{F2}} \end{bmatrix} = \frac{1}{3}\begin{bmatrix} 1 & 1 & 1 \\ 1 & \underline{\mathrm{a}} & \underline{\mathrm{a}}^2 \\ 1 & \underline{\mathrm{a}}^2 & \underline{\mathrm{a}} \end{bmatrix}\begin{bmatrix} \underline{I}_{\mathrm{Fa}} \\ 0 \\ 0 \end{bmatrix} = \frac{1}{3}\begin{bmatrix} \underline{I}_{\mathrm{Fa}} \\ \underline{I}_{\mathrm{Fa}} \\ \underline{I}_{\mathrm{Fa}} \end{bmatrix}$$

which results in:

$$\underline{I}_{\mathrm{F0}} = \underline{I}_{\mathrm{F1}} = \underline{I}_{\mathrm{F2}} = \frac{1}{3}\underline{I}_{\mathrm{Fa}} .$$

It follows from the above that the total fault current ($\underline{I}_{\mathrm{F}} = \underline{I}_{\mathrm{Fa}}$) can be expressed in the following alternative ways, depending on which symmetrical component is preferred:

- $\underline{I}_{\mathrm{F}} = \underline{I}_{\mathrm{F0}} + \underline{I}_{\mathrm{F1}} + \underline{I}_{\mathrm{F2}}$,
- $\underline{I}_{\mathrm{F}} = 3\underline{I}_{\mathrm{F1}}$,
- $\underline{I}_{\mathrm{F}} = 3\underline{I}_{\mathrm{F2}}$,
- $\underline{I}_{\mathrm{F}} = 3\underline{I}_{\mathrm{F0}}$,

- $\underline{I}_{\mathrm{F}} = 1.5\underline{I}_{\mathrm{F1}} + 1.5\underline{I}_{\mathrm{F2}}$, and
- others not listed here.

Different priority with respect to using the particular symmetrical components [B.9, 31, 63] can be applied, as for example:

- use of the zero-sequence is generally avoided since the zero-sequence impedance for the overhead line is considered as uncertain parameter,
- use of the negative-instead of positive-sequence is preferred, because the line shunt capacitance charging is more extensive for the positive-sequence,
- use of both positive- and negative-sequence, excluding the zero-sequence ($\underline{I}_{\mathrm{F}} = 1.5\underline{I}_{\mathrm{F1}} + 1.5\underline{I}_{\mathrm{F2}}$ for the fault considered in the above example) is preferred, as it allows the calculations to be made simpler [31, 62],
- instead of using the positive-sequence components, which for three-phase balanced faults are present alone, the superimposed positive-sequence components are recommended due to less shunt capacitance effect [2, 3, 4, 127].

Tables 4.3–4.6 gather alternative sets of the weighting coefficients for different faults, depending on the assumed priority for using respective sequences.

Table 4.3. Set of weighting coefficients from (4.1) with eliminating zero-sequence and giving priority to using negative- over positive-sequence

Fault type	Total fault current	$\underline{a}_{\mathrm{F1}}$	$\underline{a}_{\mathrm{F2}}$	$\underline{a}_{\mathrm{F0}}$
a–E	$\underline{I}_{\mathrm{Fa}}$	0	3	0
b–E	$\underline{I}_{\mathrm{Fb}}$	0	$-1.5 + \mathrm{j}1.5\sqrt{3}$	0
c–E	$\underline{I}_{\mathrm{Fc}}$	0	$-1.5 - \mathrm{j}1.5\sqrt{3}$	0
a–b	$\underline{I}_{\mathrm{Fa}}-\underline{I}_{\mathrm{Fb}}$	0	$1.5 - \mathrm{j}1.5\sqrt{3}$	0
b–c	$\underline{I}_{\mathrm{Fb}}-\underline{I}_{\mathrm{Fc}}$	0	$\mathrm{j}0.5\sqrt{3}$	0
c–a	$\underline{I}_{\mathrm{Fc}}-\underline{I}_{\mathrm{Fa}}$	0	$-1.5 - \mathrm{j}0.5\sqrt{3}$	0
a–b–E	$\underline{I}_{\mathrm{Fa}}-\underline{I}_{\mathrm{Fb}}$	$1.5 + \mathrm{j}0.5\sqrt{3}$	$1.5 - \mathrm{j}0.5\sqrt{3}$	0
b–c–E	$\underline{I}_{\mathrm{Fb}}-\underline{I}_{\mathrm{Fc}}$	$-\mathrm{j}\sqrt{3}$	$\mathrm{j}\sqrt{3}$	0
c–a–E	$\underline{I}_{\mathrm{Fc}}-\underline{I}_{\mathrm{Fa}}$	$-1.5 + \mathrm{j}0.5\sqrt{3}$	$-1.5 - \mathrm{j}0.5\sqrt{3}$	0
a–b–c (a–b–c–E)*	$\underline{I}_{\mathrm{Fa}}-\underline{I}_{\mathrm{Fb}}$	$1.5 + \mathrm{j}0.5\sqrt{3}$	$1.5 - \mathrm{j}0.5\sqrt{3}$ **	0
	* – inter-phase fault loop (a–b) is considered, however, the other fault loops (b–c), (c–a) can be taken as well, ** – this coefficient is different from zero, however the negative-sequence is not present in signals.			

Table 4.4. Set of weighting coefficients from (4.1) with eliminating zero-sequence and giving priority to using positive- over negative-sequence

Fault type	Total fault current	$\underline{a}_{F1}$	$\underline{a}_{F2}$	$\underline{a}_{F0}$
a–E	$\underline{I}_{Fa}$	3	0	0
b–E	$\underline{I}_{Fb}$	$-1.5 - j1.5\sqrt{3}$	0	0
c–E	$\underline{I}_{Fc}$	$-1.5 + j1.5\sqrt{3}$	0	0
a–b	$\underline{I}_{Fa}$–$\underline{I}_{Fb}$	$1.5 + j0.5\sqrt{3}$	0	0
b–c	$\underline{I}_{Fb}$–$\underline{I}_{Fc}$	$-j\sqrt{3}$	0	0
c–a	$\underline{I}_{Fc}$–$\underline{I}_{Fa}$	$-1.5 + j0.5\sqrt{3}$	0	0
a–b–E	$\underline{I}_{Fa}$–$\underline{I}_{Fb}$	$1.5 + j0.5\sqrt{3}$	$1.5 - j0.5\sqrt{3}$	0
b–c–E	$\underline{I}_{Fb}$–$\underline{I}_{Fc}$	$-j\sqrt{3}$	$j\sqrt{3}$	0
c–a–E	$\underline{I}_{Fc}$–$\underline{I}_{Fa}$	$-1.5 + j0.5\sqrt{3}$	$-1.5 - j0.5\sqrt{3}$	0
a–b–c (a–b–c–E)*	$\underline{I}_{Fa}$–$\underline{I}_{Fb}$	$1.5 + j0.5\sqrt{3}$	$1.5 - j0.5\sqrt{3}$ **	0
	* and ** – remarks as in Table 4.3.			

Table 4.5. Set of weighting coefficients from (4.1) with eliminating zero-sequence and using both positive- and negative-sequence

Fault type	Total fault current	$\underline{a}_{F1}$	$\underline{a}_{F2}$	$\underline{a}_{F0}$
a–E	$\underline{I}_{Fa}$	1.5	1.5	0
b–E	$\underline{I}_{Fb}$	$-0.75 - j0.75\sqrt{3}$	$-0.75 + j0.75\sqrt{3}$	0
c–E	$\underline{I}_{Fc}$	$-0.75 + j0.75\sqrt{3}$	$-0.75 - j0.75\sqrt{3}$	0
a–b	$\underline{I}_{Fa}$–$\underline{I}_{Fb}$	$0.75 + j0.25\sqrt{3}$	$0.75 - j0.25\sqrt{3}$	0
b–c	$\underline{I}_{Fb}$–$\underline{I}_{Fc}$	$-j0.5\sqrt{3}$	$j0.5\sqrt{3}$	0
c–a	$\underline{I}_{Fc}$–$\underline{I}_{Fa}$	$0.75 - j0.25\sqrt{3}$	$-0.75 - j0.25\sqrt{3}$	0
a–b–E	$\underline{I}_{Fa}$–$\underline{I}_{Fb}$	$1.5 + j0.5\sqrt{3}$	$1.5 - j0.5\sqrt{3}$	0
b–c–E	$\underline{I}_{Fb}$–$\underline{I}_{Fc}$	$-j\sqrt{3}$	$j\sqrt{3}$	0
c–a–E	$\underline{I}_{Fc}$–$\underline{I}_{Fa}$	$-1.5 + j0.5\sqrt{3}$	$-1.5 - j0.5\sqrt{3}$	0
a–b–c (a–b–c–E)*	$\underline{I}_{Fa}$–$\underline{I}_{Fb}$	$1.5 + j0.5\sqrt{3}$	$1.5 - j0.5\sqrt{3}$ **	0
	* and ** – remarks as in Table 4.3.			

Table 4.6. Set of weighting coefficients from (4.1) with possible elimination of using positive-sequence

Fault type	Total fault current	$\underline{a}_{F1}$	$\underline{a}_{F2}$	$\underline{a}_{F0}$
a–E	$\underline{I}_{Fa}$	0	3	0
b–E	$\underline{I}_{Fb}$	0	$1.5 + j1.5\sqrt{3}$	0
c–E	$\underline{I}_{Fc}$	0	$-1.5 - j1.5\sqrt{3}$	0
a–b	$\underline{I}_{Fa}-\underline{I}_{Fb}$	0	$1.5 - j0.5\sqrt{3}$	0
b–c	$\underline{I}_{Fb}-\underline{I}_{Fc}$	0	$j\sqrt{3}$	0
c–a	$\underline{I}_{Fc}-\underline{I}_{Fa}$	0	$-1.5 - j0.5\sqrt{3}$	0
a–b–E	$\underline{I}_{Fa}-\underline{I}_{Fb}$	0	$3 - j\sqrt{3}$	$j\sqrt{3}$
b–c–E	$\underline{I}_{Fb}-\underline{I}_{Fc}$	0	$j2\sqrt{3}$	$j\sqrt{3}$
c–a–E	$\underline{I}_{Fc}-\underline{I}_{Fa}$	0	$-3 - j\sqrt{3}$	$j\sqrt{3}$
a–b–c (a–b–c–E)*	$\underline{I}_{Fa}-\underline{I}_{Fb}$	$1.5 + j0.5\sqrt{3}$	$1.5 - j0.5\sqrt{3}$ **	0
	* and ** – remarks as in Table 4.3.			

In some fault location algorithms [23] the following relation between the zero-sequence component of the total fault current and the remaining components for faults involving earth is utilised:

$$\underline{I}_{F0} = \underline{b}_{F1}\underline{I}_{F1} + \underline{b}_{F2}\underline{I}_{F2} \tag{4.3}$$

where $\underline{b}_{F1}$, $\underline{b}_{F2}$ – coefficients dependent on fault type (Table 4.7). They are derived taking into account the constraints of the particular fault (Example 4.2 for b–c–E fault). There are two alternative sets (SET I and SET II in Table 4.7).

Table 4.7. Coefficients used in relation (4.3)

Fault type	SET I		SET II	
	$\underline{b}_{F1}$	$\underline{b}_{F2}$	$\underline{b}_{F1}$	$\underline{b}_{F2}$
a–E	0	1	1	0
b–E	0	$-0.5 + j0.5\sqrt{3}$	$-0.5 - j0.5\sqrt{3}$	0
c–E	0	$-0.5 - j0.5\sqrt{3}$	$-0.5 + j0.5\sqrt{3}$	0
a–b–E	$0.5 - j0.5\sqrt{3}$	$0.5 + j0.5\sqrt{3}$	as in SET I	
b–c–E	–1	–1		
c–a–E	$0.5 + j0.5\sqrt{3}$	$0.5 - j0.5\sqrt{3}$		

Example 4.2. Determination of the coefficients involved in (4.3) for b–c–E fault

At the fault place in the healthy phase 'a' there is no current, $\underline{I}_{Fa} = 0$. Taking this, the symmetrical components of the total fault current are as follows:

$$\begin{bmatrix} \underline{I}_{F0} \\ \underline{I}_{F1} \\ \underline{I}_{F2} \end{bmatrix} = \frac{1}{3}\begin{bmatrix} 1 & 1 & 1 \\ 1 & \underline{a} & \underline{a}^2 \\ 1 & \underline{a}^2 & \underline{a} \end{bmatrix}\begin{bmatrix} 0 \\ \underline{I}_{Fb} \\ \underline{I}_{Fc} \end{bmatrix} = \frac{1}{3}\begin{bmatrix} \underline{I}_{Fb} + \underline{I}_{Fc} \\ \underline{a}\underline{I}_{Fb} + \underline{a}^2\underline{I}_{Fc} \\ \underline{a}^2\underline{I}_{Fb} + \underline{a}\underline{I}_{Fc} \end{bmatrix}$$

The sum of positive- and negative-sequence currents equals:

$$\underline{I}_{F1} + \underline{I}_{F2} = \frac{1}{3}((\underline{a} + \underline{a}^2)\underline{I}_{Fb} + (\underline{a}^2 + \underline{a})\underline{I}_{Fc})$$

Taking into account the identity $1 + \underline{a} + \underline{a}^2 = 0$, one obtains:

$$\underline{I}_{F1} + \underline{I}_{F2} = \frac{1}{3}(-\underline{I}_{Fb} - \underline{I}_{Fc})$$

Finally, one obtains:

$$\underline{I}_{F0} = -\underline{I}_{F1} - \underline{I}_{F2}$$

The coefficients for the b–c–E fault considered are thus: $\underline{b}_{F1} = -1$, $b_{F2} = -1$.

4.5. Models of resistive faults in phase co-ordinates

If a line considered is untransposed or if there are devices switched into the line which during faults introduce additional asymmetry, a description of the faulted network can be performed using **the phase co-ordinates approach** [74, 75, 121, 150]. Series capacitors equipped with metal-oxide varistors are such devices [45, 55, 150].

Figure 4.5 presents a general fault model [B.9, 151, 157, 158, 159]. It allows different faults to be represented by assuming for the resistors R:

- $R = R_F$, if the particular connection exists due to the fault (R_F denotes the fault resistance),
- normally-open switch, if there is no such connection.

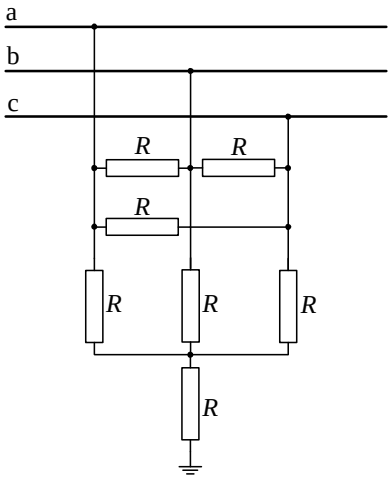

Fig. 4.5. General fault model

Using the phase co-ordinates approach, a fault can be described with the following matrix formula:

$$\mathbf{I}_{\mathrm{F}} = \frac{1}{R_{\mathrm{F}}} \mathbf{K}_{\mathrm{F}} \mathbf{V}_{\mathrm{F}} \tag{4.4}$$

where:

$\mathbf{I}_{\mathrm{F}} = \begin{bmatrix} \underline{I}_{\mathrm{Fa}} \\ \underline{I}_{\mathrm{Fb}} \\ \underline{I}_{\mathrm{Fc}} \end{bmatrix}$, $\mathbf{V}_{\mathrm{F}} = \begin{bmatrix} \underline{V}_{\mathrm{Fa}} \\ \underline{V}_{\mathrm{Fb}} \\ \underline{V}_{\mathrm{Fc}} \end{bmatrix}$ – total fault current and voltage drop at fault column matrices,

$\mathbf{K}_{\mathrm{F}} = \begin{bmatrix} k_{\mathrm{aa}} & k_{\mathrm{ab}} & k_{\mathrm{ac}} \\ k_{\mathrm{ba}} & k_{\mathrm{bb}} & k_{\mathrm{bc}} \\ k_{\mathrm{ca}} & k_{\mathrm{cb}} & k_{\mathrm{cc}} \end{bmatrix}$ – fault matrix, the elements of which are dependent on fault type,

R_{F} – fault resistance (Fig. 4.5).

Fault matrix $\mathbf{K}_{\mathrm{F}}$ for different fault types is built in the following two-step procedure:

Step I – calculate the diagonal and off-diagonal elements of the auxiliary matrix ($\mathbf{K}_{\mathrm{F}}$):

$$k_{ij} = \begin{cases} -1, & \text{if phases } i,\ j \text{ are involved in the fault} \\ 0, & \text{otherwise} \end{cases} \qquad i,\ j = \mathrm{a}, \mathrm{b}, \mathrm{c}\,. \tag{4.5}$$

Note that the diagonal elements of the auxiliary matrix, which is to be recalculated in Step II, are given in parentheses (...).

Step II – substitute the result of summing of absolute values in the respective column for each diagonal element of the auxiliary matrix obtained in Step I:

$$k_{ii} = \sum_{j=\mathrm{a}}^{j=\mathrm{c}} | k_{ij} | \qquad i = \mathrm{a,b,c}\,. \tag{4.6}$$

Use of this two-step procedure is explained in detail in Example 4.3.

Example 4.3. Determination of the fault matrix $\mathbf{K}_\mathrm{F}$ for a–b–E fault

Phases ‘a’ and ‘b’ are involved in this fault and thus the following settings in the auxiliary matrix ($\mathbf{K}_\mathrm{F}$) are made:

$k_{\mathrm{aa}} = -1$, $k_{\mathrm{bb}} = -1$ (since there are connections of phases ‘a’ and ‘b’ to earth),

$k_{\mathrm{ab}} = k_{\mathrm{ba}} = -1$ (since there is an interconnection between phases ‘a’ and ‘b’),

while the remaining elements are set to zero.

As a result, one obtains the auxiliary matrix in the form:

$$(\mathbf{K}_\mathrm{F}) = \begin{bmatrix} (-1) & -1 & 0 \\ -1 & (-1) & 0 \\ 0 & 0 & (0) \end{bmatrix}$$

The sums of absolute values of the elements in the respective columns are substituted for the related diagonal elements of the auxiliary matrix:

- 1st column: $|(-1)| + |-1| + 0 = 2 = k_{\mathrm{aa}}$,
- 2nd column: $|-1| + |(-1)| + 0 = 2 = k_{\mathrm{bb}}$,
- 3rd column: $0 + 0 + (0) = 0 = k_{\mathrm{cc}}$.

Making these substitutions, one obtains the final form of the fault matrix for a–b–E fault:

$$\mathbf{K}_\mathrm{F} = \begin{bmatrix} 2 & -1 & 0 \\ -1 & 2 & 0 \\ 0 & 0 & 0 \end{bmatrix}$$

Table. 4.8. Steps I and II of determining fault matrix $\mathbf{K}_\mathrm{F}$ for different faults

Fault type	STEP I (4.5)	STEP II (4.6)
a–E	$(\mathbf{K}_\mathrm{F}) = \begin{bmatrix} (-1) & 0 & 0 \\ 0 & (0) & 0 \\ 0 & 0 & (0) \end{bmatrix}$	$\mathbf{K}_\mathrm{F} = \begin{bmatrix} 1 & 0 & 0 \\ 0 & 0 & 0 \\ 0 & 0 & 0 \end{bmatrix}$

(to be continued)

(Table 4.8 continued)

b–E	$(\mathbf{K}_F)=\begin{bmatrix}(0) & 0 & 0\\ 0 & (-1) & 0\\ 0 & 0 & (0)\end{bmatrix}$	$\mathbf{K}_F=\begin{bmatrix}0 & 0 & 0\\ 0 & 1 & 0\\ 0 & 0 & 0\end{bmatrix}$
c–E	$(\mathbf{K}_F)=\begin{bmatrix}(0) & 0 & 0\\ 0 & (0) & 0\\ 0 & 0 & (-1)\end{bmatrix}$	$\mathbf{K}_F=\begin{bmatrix}0 & 0 & 0\\ 0 & 0 & 0\\ 0 & 0 & 1\end{bmatrix}$
a–b	$(\mathbf{K}_F)=\begin{bmatrix}(0) & -1 & 0\\ -1 & (0) & 0\\ 0 & 0 & (0)\end{bmatrix}$	$\mathbf{K}_F=\begin{bmatrix}1 & -1 & 0\\ -1 & 1 & 0\\ 0 & 0 & 0\end{bmatrix}$
b–c	$(\mathbf{K}_F)=\begin{bmatrix}(0) & 0 & 0\\ 0 & (0) & -1\\ 0 & -1 & (0)\end{bmatrix}$	$\mathbf{K}_F=\begin{bmatrix}0 & 0 & 0\\ 0 & 1 & -1\\ 0 & -1 & 1\end{bmatrix}$
c–a	$(\mathbf{K}_F)=\begin{bmatrix}(0) & 0 & -1\\ 0 & (0) & 0\\ -1 & 0 & (0)\end{bmatrix}$	$\mathbf{K}_F=\begin{bmatrix}1 & 0 & -1\\ 0 & 0 & 0\\ -1 & 0 & 1\end{bmatrix}$
a–b–E	$(\mathbf{K}_F)=\begin{bmatrix}(-1) & -1 & 0\\ -1 & (-1) & 0\\ 0 & 0 & (0)\end{bmatrix}$	$\mathbf{K}_F=\begin{bmatrix}2 & -1 & 0\\ -1 & 2 & 0\\ 0 & 0 & 0\end{bmatrix}$
b–c–E	$(\mathbf{K}_F)=\begin{bmatrix}(0) & 0 & 0\\ 0 & (-1) & -1\\ 0 & -1 & (-1)\end{bmatrix}$	$\mathbf{K}_F=\begin{bmatrix}0 & 0 & 0\\ 0 & 2 & -1\\ 0 & -1 & 2\end{bmatrix}$
c–a–E	$(\mathbf{K}_F)=\begin{bmatrix}(-1) & 0 & -1\\ 0 & (0) & 0\\ -1 & 0 & (-1)\end{bmatrix}$	$\mathbf{K}_F=\begin{bmatrix}2 & 0 & -1\\ 0 & 0 & 0\\ -1 & 0 & 2\end{bmatrix}$
a–b–c	$(\mathbf{K}_F)=\begin{bmatrix}(0) & -1 & -1\\ -1 & (0) & -1\\ -1 & -1 & (0)\end{bmatrix}$	$\mathbf{K}_F=\begin{bmatrix}2 & -1 & -1\\ -1 & 2 & -1\\ -1 & -1 & 2\end{bmatrix}$
a–b–c–E	$(\mathbf{K}_F)=\begin{bmatrix}(-1) & -1 & -1\\ -1 & (-1) & -1\\ -1 & -1 & (-1)\end{bmatrix}$	$\mathbf{K}_F=\begin{bmatrix}3 & -1 & -1\\ -1 & 3 & -1\\ -1 & -1 & 3\end{bmatrix}$

4.6. Arcing faults

According to the fault current state, the fault arc [73, 94, 166] is classified as:

- primary arc,
- secondary arc.

Primary arc occurs during flash-over of the line insulator string, caused by lightning stroke or other reasons. **Secondary arc** follows the primary one when the faulted phase circuit breaker trips, as is sustained by mutual coupling between the healthy and faulted phases.

Primary arc appears after fault inception and lasts until single-phase tripping of the faulted phase. It shows generally a deterministic behaviour as observed in the field and laboratory arc tests [174]. After isolating the fault (by single-phase tripping) there is a secondary arc, which is sustained by the capacitive and inductive coupling to the sound phases. The secondary arc usually self-extinguishes. The secondary arc has extremely random characteristics affected by the external conditions around the arc channel.

A vast majority of fault location algorithms process current and voltage signals of the fault interval (starting from the fault inception until the circuit breaker operation) and in some cases of the pre-fault interval (just before the fault inception). For these algorithms the primary arc is of interest. However, it mainly concerns simulations performed for evaluating the fault location algorithms under study. This is so since vast majority of fault location algorithms apply linear model of the fault path for their formulation. Only few fault location algorithms take into account the primary arc model.

In [169], it is shown that by measuring voltage on the line-side of a circuit breaker, the location of a permanent fault can be calculated using the transient caused by the fault clearing operation of the circuit breaker. Due to the fault clearing operation of the circuit breaker, a surge is initiated and travels between the opened circuit breaker and the fault, if the latter is still present. The distance to fault is determined by measuring the propagation time of the surge from the opened circuit breaker to the fault. In this relation, modelling the secondary arc is important.

4.6.1. Dynamic model of arc

The dynamic voltage-current characteristics of the electric arc have features of hysteresis. Extensive studies in [73, 94, 166] have shown that the dynamic volt-ampere characteristics of the electric arc can be exactly simulated by the empirical differential equation:

$$\frac{\mathrm{d}\, g_k}{\mathrm{d}\, t} = \frac{1}{T_k}(G_k - g_k) \tag{4.7}$$

where:

the subscript k indicates the kind of arc (k = p for primary arc, k = s for secondary arc),

g_k – dynamic arc conductance,

G_k – stationary arc conductance,

T_k – time constant.

The stationary arc conductance G_k can be physically interpreted as the arc conductance value when the arc current is maintained for a sufficiently long time under constant external conditions. So, G_k is the static characteristic of the arc, which can be evaluated from:

$$G_k = \frac{|i|}{(v_{0k} + R|i|)l_k} \tag{4.8}$$

where:

i – instantaneous arc current,

v_{0k}– arc voltage drop per unit length along the main arc column,

R – characteristic arc resistance per unit length,

l_k – arc length.

For the primary arc v_{0p} is constant and equal to about 15 V/cm for the range of current 1.3÷24.0 kA [29] and l_p may be assumed constant and somehow wider than the length of the line insulator string. The value of the constant voltage parameter of the secondary arc v_{0s} is evaluated empirically on the basis of numerous investigation results in the range of low values of current, collected in [29]. For the range of peak currents I_s, from approximately 1÷55 A it can be roughly defined as $v_{0s} = 75I_s^{-0.4}$ V/cm [166].

The arc length of the secondary current l_s changes with time, and for relatively low wind velocities (up to 1 m/s), it can be approximated as $l_s = 10 l_p t_r$ for $t_r > 0.1\,\text{s}$ but when the secondary arc re-ignition time $t_r \le 0.1\,\text{s}$: $l_s = l_p$.

The secondary arc re-ignition voltage (in V/cm) can be calculated using the empirical formula [166]:

$$v_r = \frac{5 + 1620T_e}{(2.15 + I_s)(t_r - T_e)} \tag{4.9}$$

where:

T_e – secondary arc extinguishing time (when $t_r \le T_e$, $v_r = 0$),

I_s – peak value of current on the volt-ampere arc characteristic.

Time constants are determined as follows [166]:

$$T_k = \frac{\alpha_k I_k}{l_k} \tag{4.10}$$

where α_k – empirical coefficients.

The empirical coefficients α_k can be obtained by fitting equation (4.7) with equations (4.8) and (4.10) to match the experimental dynamic volt-ampere characteristics of the heavy- and low-current arcs, accordingly.

The model (4.7) allows the arc conductance g(t) to be determined, from which the arc resistance $r_{arc}(t) = 1/g(t)$ is calculated.

Using the ATP-EMTP program [B.5] for arc fault simulation, the arc can be reflected with the non-linear resistor – defined in the ELECTRICAL NETWORK unit, while the arc model – in the MODELS (Fig. 4.6). The arc current as the input quantity is measured on-line and the non-linear differential equation (4.7) is being solved. As a result, the arc resistance is determined and transferred for fixing the resistance of the resistor modelling the arc.

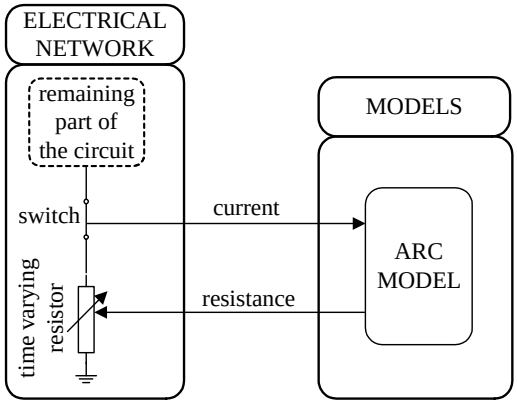

Fig. 4.6. Modelling of primary arc with ATP-EMTP – interaction between the program units

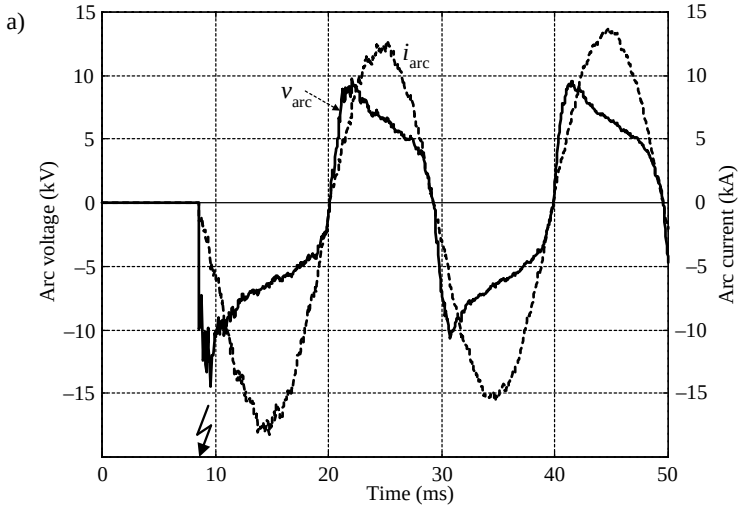

(Fig. 4.7 to be continued)

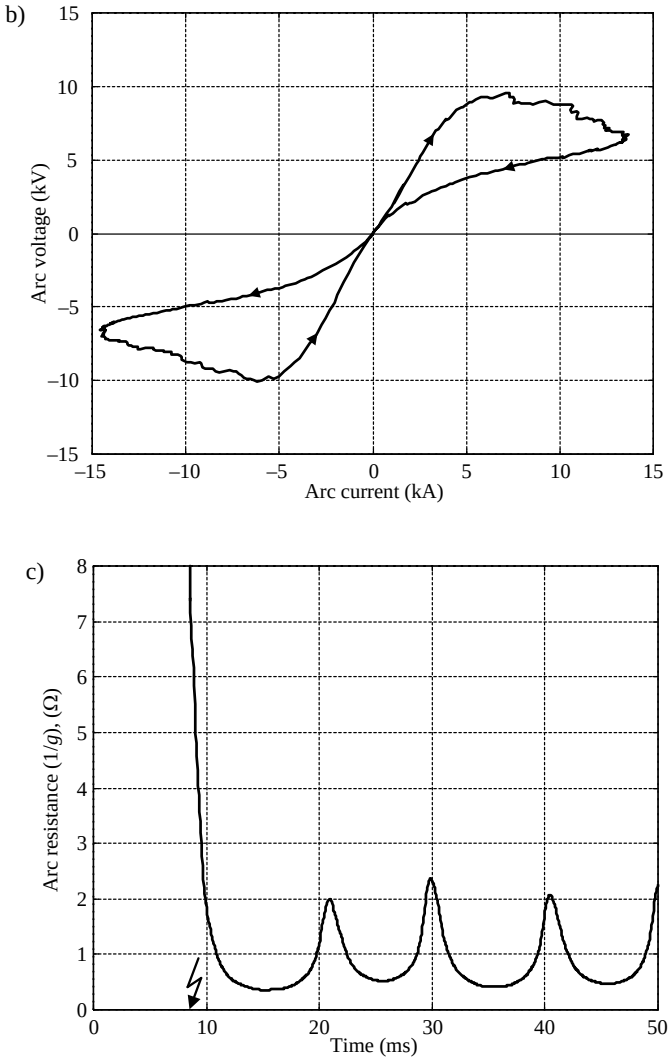

Fig. 4.7. Modelling of primary arc with ATP-EMTP:
a) arc current and voltage, b) arc voltage vs. arc current (for a single cycle), c) arc resistance

4.6.2. Static model of primary arc

For many applications a simpler static model of the primary arc is utilised [24, 25]. Voltage drop across an arc is determined as:

$$v(t) = V_{\mathrm{a}}\,\mathrm{signum}[i(t)] + \xi(t)\,, \tag{4.11}$$

where:

$V_{\mathrm{a}} = V_{\mathrm{p}} l_{\mathrm{p}}$ – magnitude of rectangular wave (V_{p}, l_{p} – as in (4.8)),

$\xi(t)$ – Gaussian noise with zero average value.

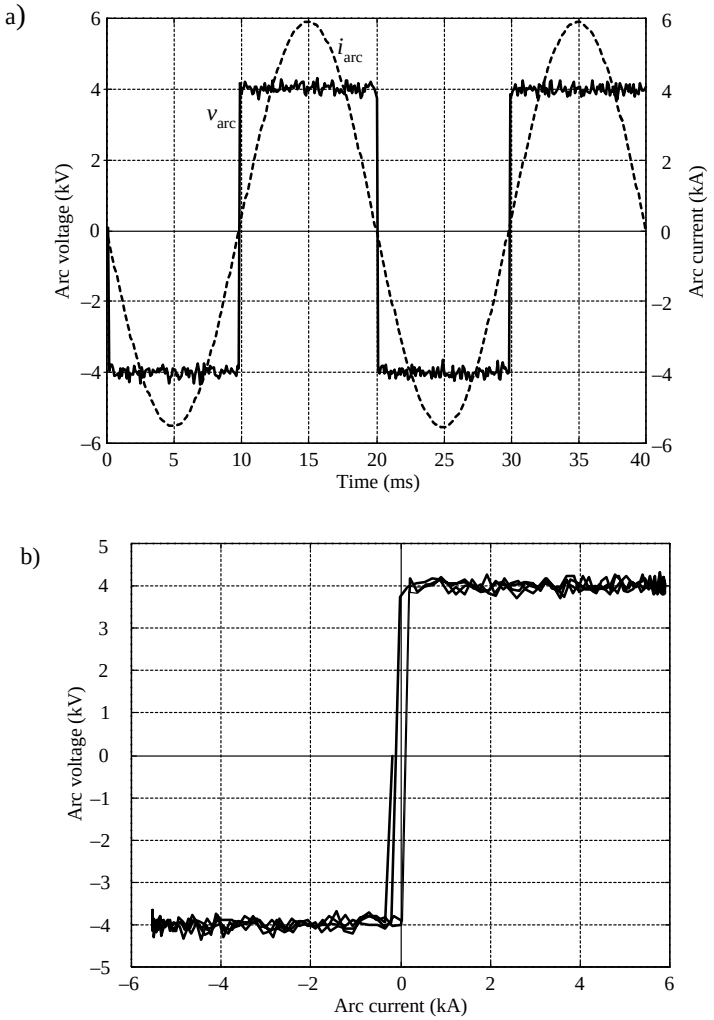

Fig. 4.8. Static model of primary arc:
a) arc current and voltage, b) arc voltage versus arc current

Figures 4.8a and b present typical shapes of the arc voltage and current, and the arc voltage versus arc current, respectively.

5. Measurement chains of fault locators

5.1. Introduction

The input signals of fault locators bring information on a fault, which is an abnormal power system state. Power system faults cause a change in the current and voltage signals, with respect to both steady and transient states. These signals with the abrupt steady state level change, and being contaminated with the transient components, are delivered to fault locator inputs via the measuring chains.

Functional structure of voltage and current measurement chains of a fault locator is shown in Fig. 5.1. Three-phase voltage and current from a power system are transformed with use of instrument voltage and current transformers to the reduced level. The secondary signals of these transformers are rated at around 100 V (voltage) and 1 A or 5 A (current). Then, matching transformers provide adequate level of the signals to electronic devices. Prior to the analogue to digital (A/D) conversion, analogue low-pass filters are used for both voltage and current signals.

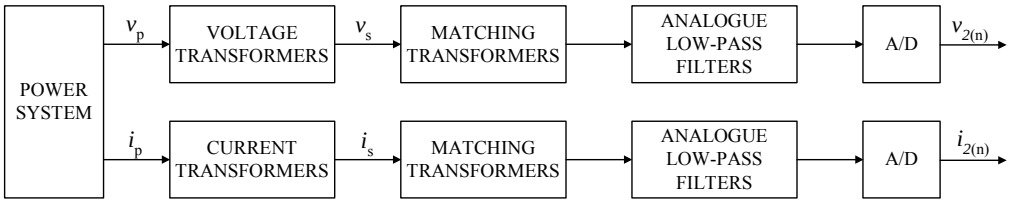

Fig. 5.1. Structure of voltage and current measurement chains

Since in the majority of applications, classical electromagnetic voltage and current instrument transformers are utilised, our attention will be solely paid to them. There is a common opinion that a long time is still to pass before new unconventional instrument transformers [96, 97, 99, 124] become predominant in transforming signals from a power system to protection, monitoring, control and measuring devices.

Due to certain construction limitations both the instrument voltage (CVTs) and current (CTs) transformers exhibit undesired dynamic behaviour under short-circuits

in the power system. As a result, malfunction or substantial delay in the tripping of protective relays may take place [37, 50, 51, 56, 86, 175, 185]. Undesired steady state and dynamic behaviour of instrument transformers influence a fault location as well [4, 65, 100, 131, 137, 149]. A lot of effort has recently been taken towards compensating the protective transformers for their transient errors. The aim of such compensation is to obtain reasonably accurate replica of the primary currents and voltages. The other possibility is based on minimising the influence of transient errors of instrument transformers on operation of both relaying and fault location algorithms.

5.2. Voltage transformers

At transmission and sub-transmission voltage levels the instrument-level voltage signals for protective, monitoring and measuring devices is provided by means of capacitive voltage transformers (CVTs). A CVT provides a cost-effective way of obtaining secondary voltage for HV and EHV systems [56, 86, 90, 176]. Its functional scheme is depicted in Fig. 5.2. Besides the primary (v_p) and secondary (v_s) voltages one can also distinguish the intermediate voltage (v_i), which is usually at the level of around 20 kV.

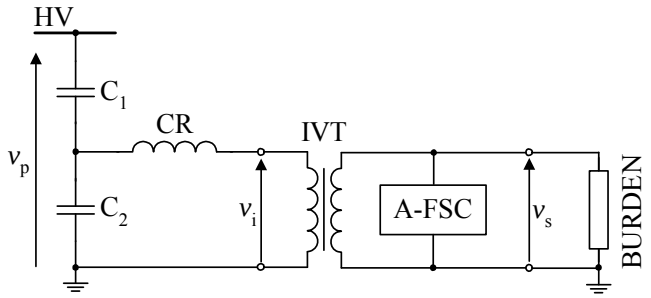

Fig. 5.2. Schematic diagram of CVT: C1, C2 – stack capacitors; CR – compensating reactor; IVT – inductive step-down transformer; A-FSC – anti-ferroresonance suppressing circuit; BURDEN – CVT burden imposed by connected protective and other devices

5.2.1. Transient performance of capacitive voltage transformers

The dynamics of a CVT is determined by two factors [56, 86]:

- non-linear oscillations under saturation of magnetic core of the CVT step-down inductive voltage transformer,
- discharging of the CVT internal energy during short circuits on the transmission line.

Non-linear oscillations can appear when the operating point of the magnetizing characteristic of the step-down transformer is shifted to the saturation region. CVTs are therefore equipped with special anti-ferroresonance circuits (Fig. 5.3) for avoiding stabilization of the sub-harmonics [90, 184]. In Figs. 5.4 and 5.5, examples of waveforms of CVT secondary voltage under interruption of the short-circuit of the secondary terminals are shown. For a CVT unequipped with anti-ferroresonance circuit (Fig. 5.4) intensive contamination with the third sub-harmonic component is observed. Equipping a CVT with properly designed anti-ferroresonance circuit allows effective damping of non-linear oscillations (Fig. 5.5).

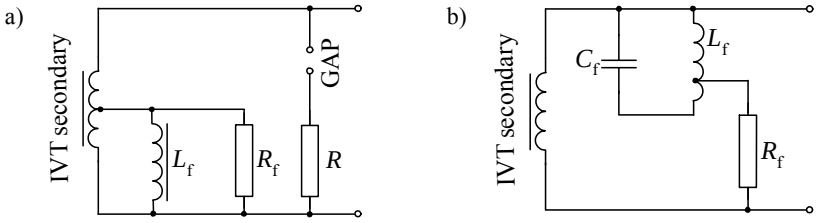

Fig. 5.3. Examples of anti-ferroresonance suppressing circuits: a) passive, b) active

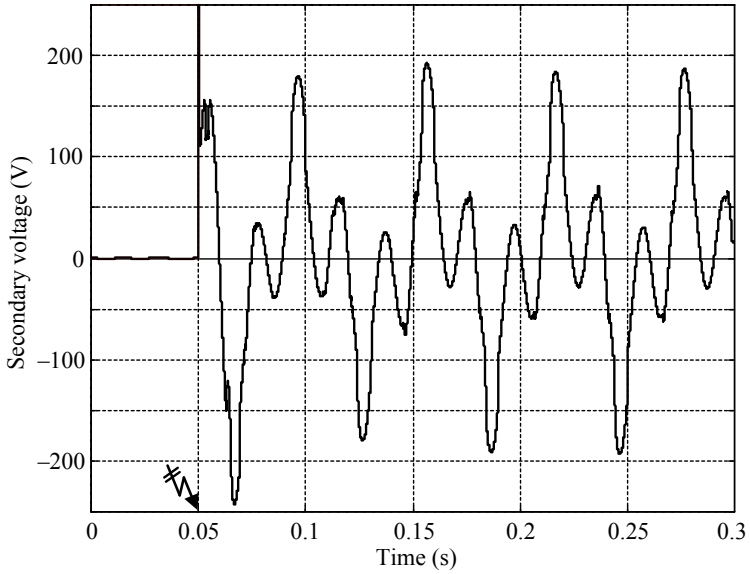

Fig. 5.4. Example of the waveform of CVT secondary voltage for CVT unequipped with anti-ferroresonance suppressing circuit under interruption of short-circuit of secondary terminals

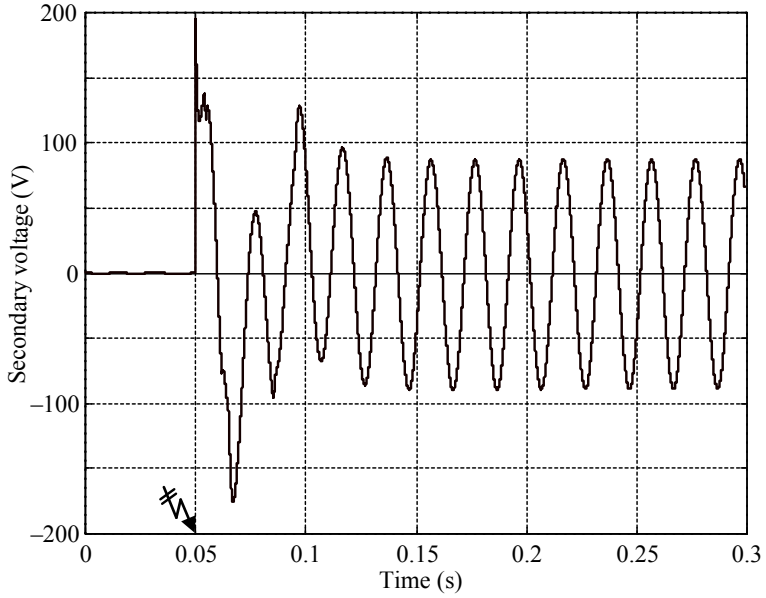

Fig. 5.5. Example of the waveform of CVT secondary voltage for CVT equipped with anti-ferroresonance circuit suppressing effectively ferroresonance under interruption of short-circuit of secondary terminals

Anti-ferroresonance circuits, however, affect the transients of the second kind. Discharging the CVT internal energy (accumulated in the stack capacitors and the compensating reactor of a CVT during the pre-fault state) – to the level determined by the reduced post-fault primary voltage – results in considerable distortion of the secondary wave [50, 56, 86, 90, 146]. The higher the reduction of the primary voltage, the more extensive transients induced by the CVT itself occur (Figs. 5.6 and 5.7). Especially, faults at zero crossing of the primary voltage result in substantial transient errors that, in turn, affect the operation of supplied protective relays. CVT transients may occur during changes in system operating states either due to normal switching operations or due to the occurrence of faults.

Among different CVT parameters, the stack capacitances influence the CVT-generated transients. In reference [86], two types of a CVT are distinguished:

- "high-C CVT" – the sum of stack capacitances below some 100 nF,
- "extra high-C CVT" – the sum of stack capacitances above some 100 nF.

Typical CVT-generated transients for these CVT types are shown in Figs. 5.6 and 5.7. A detailed analysis of these transients is made in [86].

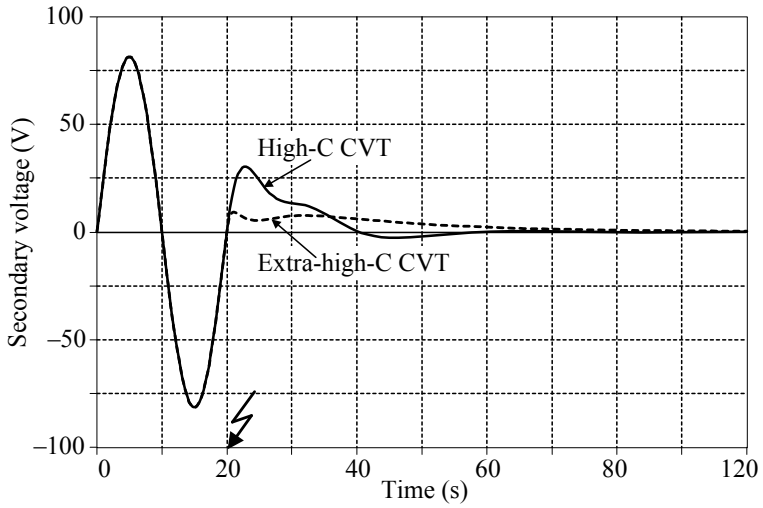

Fig. 5.6. Sample transients for high- and extra-high-C CVTs when primary voltage drops to zero under zero crossing

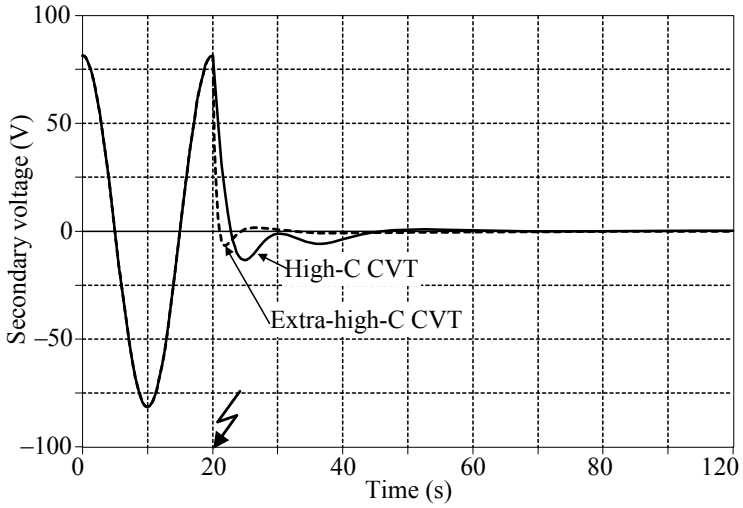

Fig. 5.7. Sample transients for high- and extra-high-C CVTs when primary voltage drops to zero from the voltage peak

5.2.2. Dynamic compensation of capacitive voltage transformers

In [56], it has been proposed to reject the CVT induced transients from the voltage signal with the use of digital compensation algorithm based on inversion of the CVT

simplified transfer function. In Fig. 5.8, a general CVT equivalent circuit diagram [90] is shown. Simplifying this model one obtains a model as shown in Fig. 5.9.

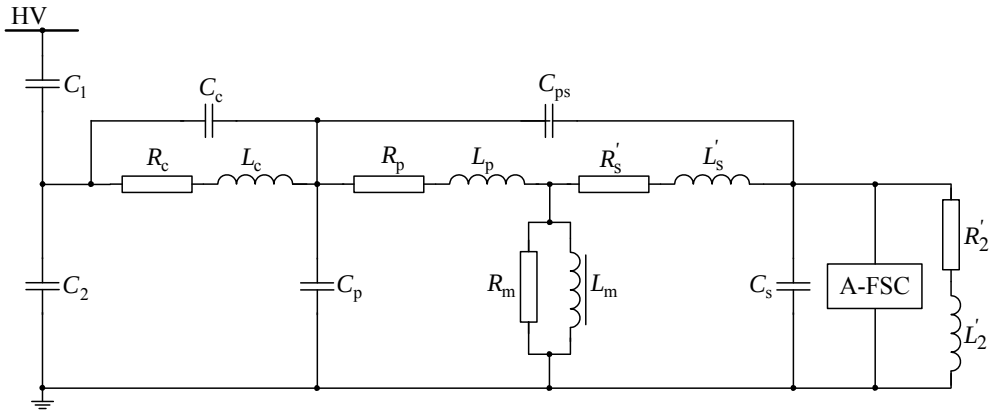

Fig. 5.8. General equivalent circuit diagram of CVT

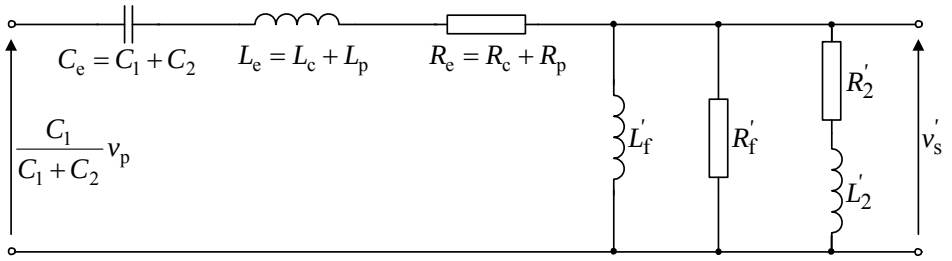

Fig. 5.9. Simplified circuit diagram of CVT equipped with passive anti-ferroresonance circuit

The following simplifications have been made for obtaining a simplified circuit diagram of Fig. 5.9, i.e. in order to facilitate the design of the compensating algorithm:

- The saturation of the step-down inductive transformer is neglected since short-circuits result rather in reduction of the primary voltage, which moves the operating point of the magnetic core down from the rated position.
- The ideal transformation of the step-down transformer is assumed, which means that the parameters L_p, R_p, L_m, R_{Fe}, L_s, R_s and all stray capacitances in the equivalent circuit diagram from Fig. 5.8 are neglected.
- All the remaining parameters are related to the primary side of the step-down inductive transformer.
- The Thevenin theorem is applied to the primary voltage and the capacitor stack.

Under these assumptions, the model from Fig. 5.8 reduces to a simple circuit displayed in Fig. 5.9, for which the transfer function takes the form:

$$G_{CVT}(s) = \frac{A_3 s^3 + A_2 s^2}{B_4 s^4 + B_3 s^3 + B_2 s^2 + B_1 s + B_0} \tag{5.1}$$

where A_3, A_2, B_4, B_3, B_2, B_1, B_0 – coefficients duly expressed by the equivalent circuit diagram parameters.

In order to exactly reproduce the primary voltage, the ideal compensator at the CVT output must be applied in such a way that:

$$G_{COMP\_ideal}(s) = \frac{1}{G_{CVT}(s)} \tag{5.2}$$

Direct inversion of the transfer function (5.1) appears troublesome due to its double zero at the origin. Therefore, the following modified transfer function of the compensator has been proposed:

$$G_{COMP}(s) = \frac{(B_4 s^4 + B_3 s^3 + B_2 s^2 + B_1 s + B_0)}{(A_3 s + A_2)(A_4 s^3 + A_5 s^2 + A_6 s + A_7)} \tag{5.3}$$

where A_4, A_5, A_6, A_7 – coefficients to be selected.

Applying the compensator of the transfer function (5.3) allows all the poles of the CVT transfer function (5.1) to be compensated, while only the single zero ($s = -A_2/A_3$) is cancelled. So, the double zero at the origin is left and some extra three poles are added. In consequence, the transfer function between the primary voltage and the secondary compensated voltage being the result of compensation in as follows:

$$G_{CVT}(s) \cdot G_{COMP}(s) = \frac{s^2}{A_4 s^3 + A_5 s^2 + A_6 s + A_7} \tag{5.4}$$

Selection of the coefficients A_4, A_5, A_6, A_7 may be done in a number of ways with the objective to obtain the desired dynamics of the compensated CVT [56]. Different numeric procedures can be applied for obtaining a discrete form of the compensator (5.3). In [56], the following trapezoidal rule was applied:

$$s \Rightarrow \frac{\omega_1}{\tan(0.5\omega_1 T_s)} \cdot \frac{(1 - z^{-1})}{(1 + z^{-1})} \tag{5.5}$$

where:

ω_1 – fundamental radian frequency,

T_s – sampling period,

z^{-1} – operator representing a time delay of a single sampling period.

The advantage of using (5.5) is that it gives the gain and the phase displacement at the fundamental frequency exactly the same as under continuous differentiation. After applying (5.5) to (5.3) and transforming to the time domain, the following digital compensator COMP (Fig. 5.10) in the form of a recursive filter is obtained:

$$v_{2\mathrm{cc}(n)} = \sum_{i=0}^{i=4} \frac{\mathrm{N}_i}{\mathrm{M}_0} v_{2(n-i)} - \sum_{i=1}^{i=4} \frac{\mathrm{M}_i}{\mathrm{M}_0} v_{2\mathrm{cc}(n-i)} \tag{5.6}$$

where:

n – current sampling instant,

v_2 – uncompensated secondary voltage (as supplied by an A/D converter),

$v_{2\mathrm{cc}}$ – compensated secondary voltage – the output from the compensator (5.6).

The filter (5.6) constitutes the simplest compensator (COMP) for a CVT. This compensator may be even more optimised. The improved compensator $\mathrm{COMP}_{\mathrm{impr.}}$ (Fig. 5.10) is a cascade of the original compensator COMP, given by (5.6), and a short window non-recursive digital filter (F3) added to its output, as shown in Fig. 5.10. The self-explanatory assumptions for such a filter (F3) are summarized as follows:

- zero gain at half the sampling frequency,
- unity gain and zero phase displacement for the fundamental frequency,
- possibly short data window.

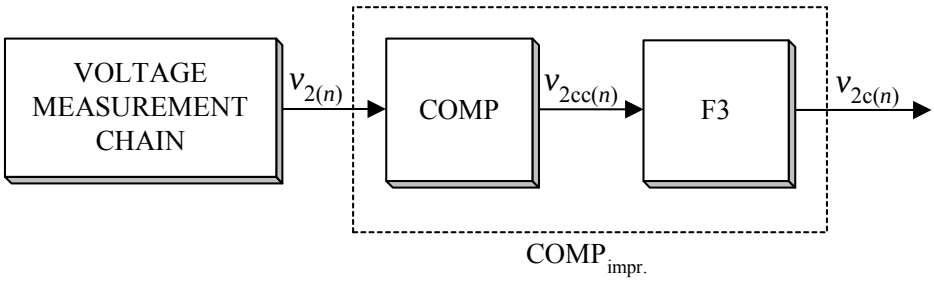

Fig. 5.10. Generic scheme of digital series compensation of CVT (COMP – original compensator, F3 – low-pass three-sample filter, $\mathrm{COMP}_{\mathrm{impr.}}$ – compensator with improved frequency response)

In [56], a three-sample filter has been recommended. The output from the improved compensator ($v_{2\mathrm{c}}$) is thus computed as:

$$v_{2\mathrm{c}(n)} = A(v_{2\mathrm{cc}(n)} + Bv_{2\mathrm{cc}(n-1)} + Cv_{2\mathrm{cc}(n-2)}) \tag{5.7}$$

where:

$$B = \frac{2\cos(\omega_1 T_\mathrm{s})}{1+2\cos(\omega_1 T_\mathrm{s})}, \quad C = \frac{-1}{1+2\cos(\omega_1 T_\mathrm{s})}, \quad A = \frac{1}{1+B\cos(\omega_1 T_\mathrm{s})+C\cos(2\omega_1 T_\mathrm{s})}.$$

The cascade of the original compensator (5.6) and the low-pass filter (5.7) gives the resultant compensation algorithm ($COMP_{impr.}$) of the following recursive form:

$$v_{2c(n)} = \sum_{i=0}^{i=6} P_i v_{2(n-i)} - \sum_{i=1}^{i=4} Q_i v_{2c(n-i)} \tag{5.8}$$

where P_i, Q_i – resultant coefficients of the improved compensator, dependent on CVT parameters and sampling period.

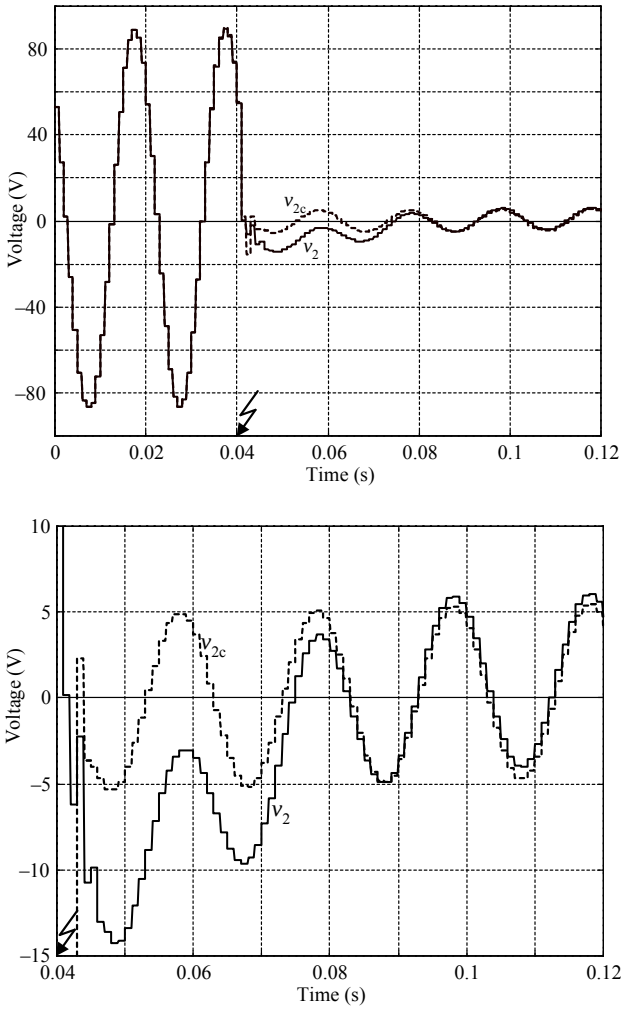

Fig. 5.11. Examples of voltage waveforms (staircase forms): v_2 – CVT secondary voltage, v_{2c} – compensated secondary voltage

Both the original (5.6) and the improved (5.8) compensators, as the recursive digital filters require a kind of a starting procedure. To initiate the filters (5.6) or (5.8) one needs the last four samples of the compensated voltage. For this purpose the pure uncompensated secondary voltage may be used. The initiation is done once just after fault detection with the use of the frozen pre-fault data. However, to its advantage, the algorithm may be launched with the zero initial conditions, but necessarily at the maximum of the voltage wave.

Figures 5.11 through 5.14 present examples of performance of the improved compensator (5.8) for the simulated CVT transients appearing under a decrease of the primary voltage during the transmission line fault. The applied compensation effectively removes the CVT-generated transients (Fig. 5.11). As a result, improved performance of the calculation of voltage magnitude (Fig. 5.12) and impedance components (resistance: Fig. 5.13, reactance: Fig. 5.14) is achieved. An application of the compensation to fault location is depicted in Fig. 5.15. The compensation of the CVT secondary voltage results in decreased oscillations of the distance to fault (d_c). Averaging the fault distance exhibiting lower oscillations results in a more accurate final result. This is especially important when the fault quantities are recorded from a relatively short fault interval.

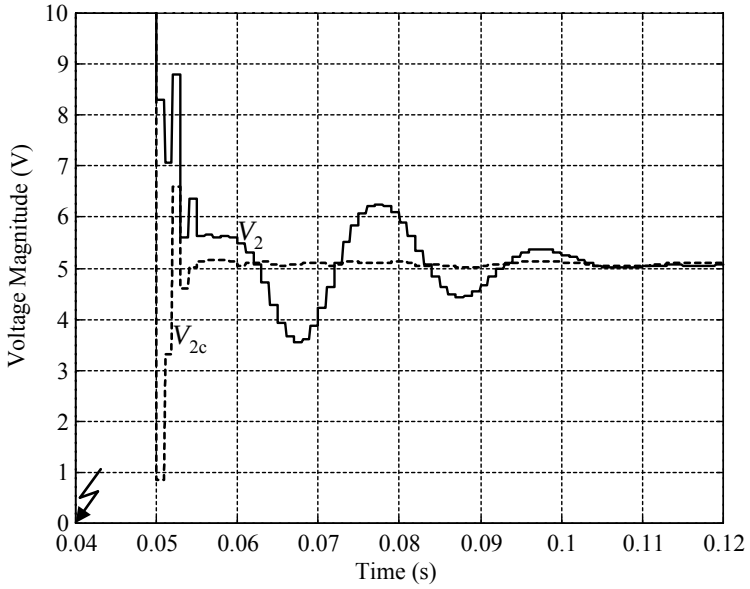

Fig. 5.12. Full-cycle Fourier calculation of voltage magnitude:
V_2 – magnitude of CVT secondary voltage,
V_{2c} – magnitude of compensated voltage

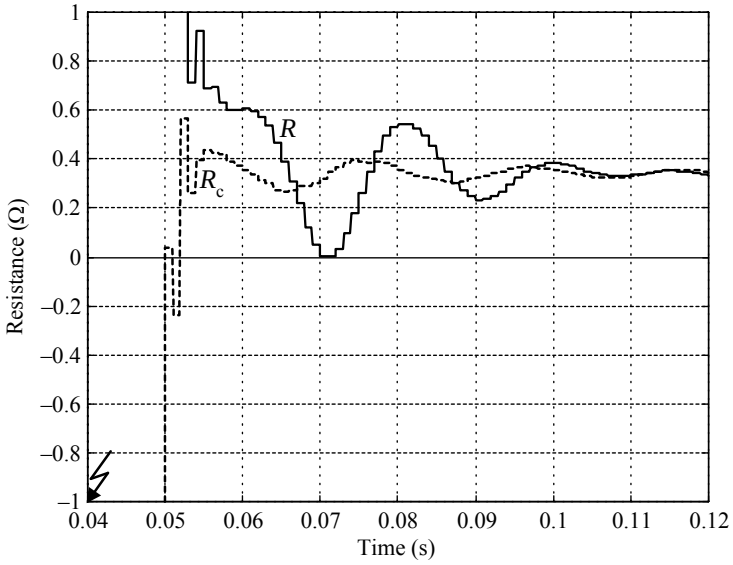

Fig. 5.13. Full-cycle Fourier calculation of the fault loop resistance using secondary current and CVT secondary voltage (resistance R) or compensated voltage (resistance R_c)

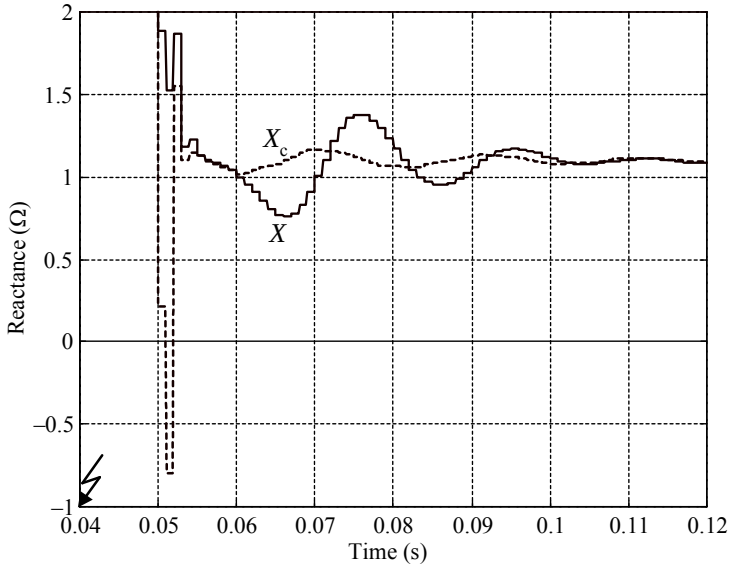

Fig. 5.14. Full-cycle Fourier calculation of the fault loop reactance using secondary current and CVT secondary voltage (reactance X) or compensated voltage (reactance X_c)

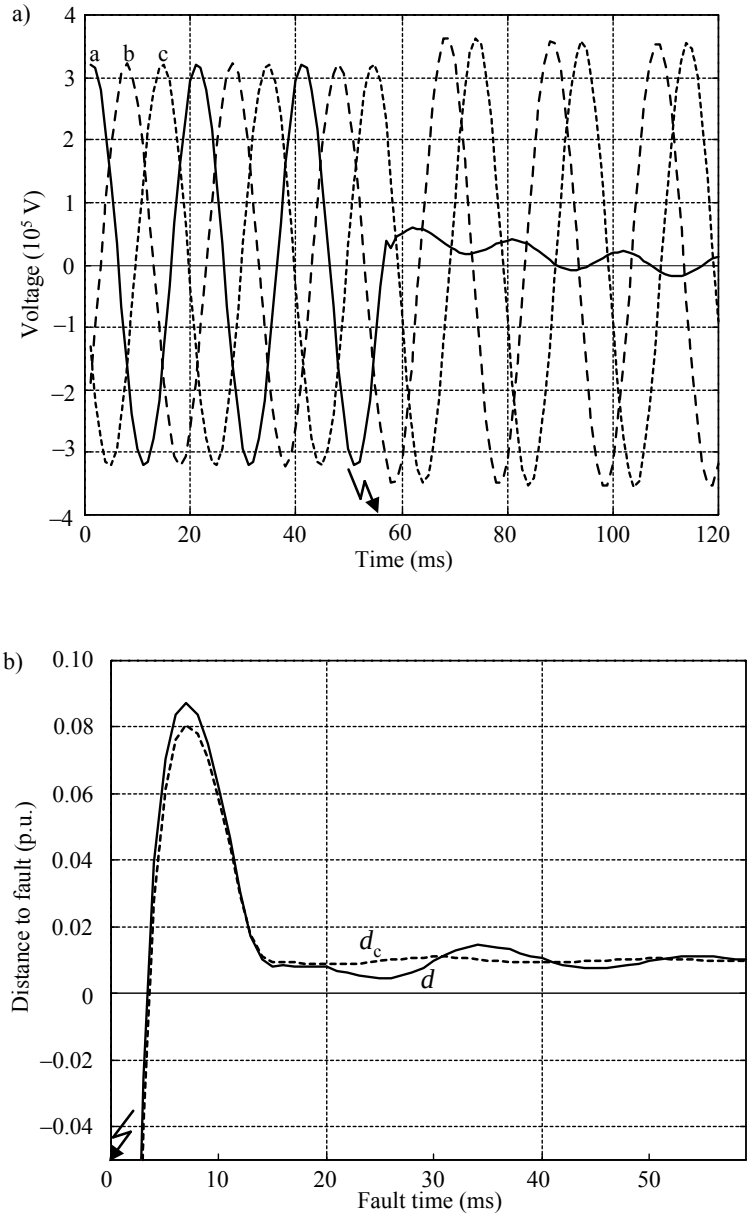

Fig. 5.15. Application of CVT compensation to fault location:
a) three-phase voltage under single-phase to ground fault,
b) distance to fault: d – under no CVT dynamic compensation,
d_c – with CVT compensation

5.3. Current transformers

5.3.1. Basics of current transformers

Instrument current transformers (CTs) transform power system currents to the secondary level rated typically at 1 A or 5 A. The CT secondary current is substantially proportional to the primary current under normal conditions of operation, and differs in phase from it by an angle which is approximately zero for an appropriate direction of the connections. The steady state error of a CT is classified into two: the current or ratio error, and the phase error. Both steady state and transient performance of CTs is covered by IEC Standard, as well as by national standards.

Figure 5.16 depicts a CT circuit model [89, 176], which includes:

i_p, i'_s – primary and secondary (re-calculated to primary side) currents,

i_e, i_r, i_m – exciting current and its active and reactive components,

R_p, L_p – primary winding resistance and leakage inductance,

R'_s, L'_s – secondary winding resistance and leakage inductance, re-calculated to primary side,

R_m, L_m – iron loss equivalent resistance, magnetizing non-linear inductance,

R'_2, L'_2 – load resistance and inductance, re-calculated to primary side.

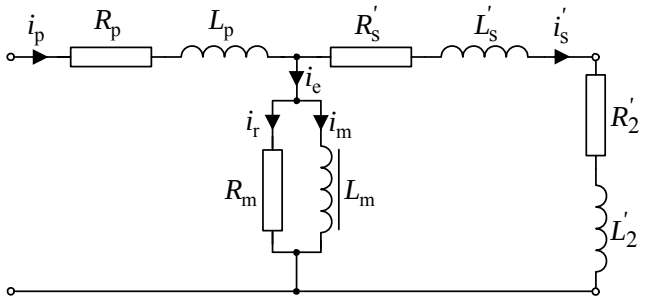

Fig. 5.16. Generic CT circuit model

CTs are designed to operate under load conditions, i.e. on the lower part of the linear region of the *V–I* characteristic of the magnetizing branch. The knee point of the magnetizing characteristic divides it into the linear and the non-linear regions. The **knee point voltage** is understood as the point on the magnetizing curve where an increase of 10% in the flux density (voltage) causes an increase of 50% in the magnetizing force (current). For high fault primary currents without the DC component, the operating point remains in the linear range without exceeding the knee point of the characteristic.

However, if the fault conditions are such that the DC component is present in the CT primary current, then a considerable increase of a flux in the CT magnetic core can take place. As a consequence of such a flux increase, the CT magnetic core gets saturated. Also, CTs can retain the remanent flux that may be left on the core after the fault is cleared [B.22, B.24, 77, 78]. The remanent flux can either oppose or aid the build-up of the CT core flux, depending on the remanent flux polarity.

When a CT gets saturated, its secondary signal becomes distorted. An example of waveforms of primary and secondary currents under CT transient saturation is shown in Fig. 5.17. Besides transient saturation CTs may suffer permanent saturation, under which there is no linear CT transformation at all.

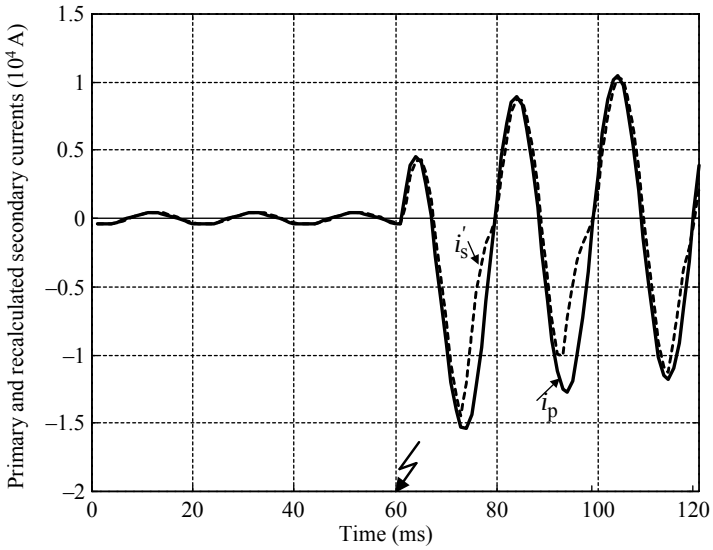

Fig. 5.17. CT saturation – primary and secondary (re-calculated to primary side) waveforms of currents

5.3.2. Fault location under saturation of current transformers

Many studies related to the analysis of the steady-steady and transient behaviour of CTs have been reported so far. In the focus of attention is the problem of how distorted secondary currents due to CT saturation can cause malfunction or operating delays of protection relays and how to prevent saturation or to design protective algorithm insensitive to the effects of saturation [14, 185]. An issue of fault location in relation to CT saturation has been considered as well [183].

The remedies for assuring adequately high accuracy under CT saturation can be categorized as follows:

- use of hardware means for preventing CT saturation [11],
- use of voltage signals alone [12, 13, 130, 187],
- use of voltage signals and current signals, but excluding currents from saturated CTs [65, 131, 149],
- minimizing fault location errors caused by CT saturation and application of digital algorithms for reconstructing the CT primary current [78, 81, 102, 137],
- allowing currents from saturated CTs to be used but only from intervals of linear transformation (when there is no saturation) [85].

All the remedies listed, except intentional use of voltage signals alone, require identifying the CT saturation. In general, the CT saturation identification (detection) is understood as recognizing instants when the saturation starts and when it ends. For this purpose saturation detectors are utilised.

In general, we distinguish two families of methods for saturation detection:

- Hardware oriented methods based on superimposing an extra low power, and high frequency signal to the secondary circuit of a CT and monitoring the core inductance using the superimposed signal. The value of the inductance indicates whether or not and to what degree the supervised CT is saturated.
- Waveform oriented methods based on analysing only the waveform of the secondary current of a CT.

McLaren et al. [117] proposed a scheme in which a 15 kHz signal is superimposed to the secondary current of a CT. The apparent impedance for this signal depends directly on the incremental inductance of the CT core, and consequently, on the degree of saturation. Therefore, the amplitude of the high frequency current driven by an external voltage source acts as the saturation detector.

A similar approach was presented by Sanderson et al. in [160]. The authors use a 10 kHz externally driven signal to monitor the value of the equivalent magnetizing inductance of a CT. Keeping the 10 kHz driving force constant, the authors use a 10 kHz current as the indicator of saturation.

The obvious disadvantage of this family of methods is the need of connecting an extra circuit between the main CTs and the relay (fault locator). The methods from this group process directly the waveform of the CT secondary current in order to distinguish between the linear and saturated operation of a CT. They are investigated as numerical procedures to be run exclusively on digital relays and fault locators. They call for comparatively high sampling frequencies in order to assure adequately short delays in detecting instants when a saturation starts and when stops. Another saturation detector which is based on processing the secondary current with use of an algorithm that evaluates the first, second and third difference functions is presented in [79, 80].

Besides digital algorithms, also analogue (hardware) methods for compensating the distortion in the secondary current have been developed.

In [11], an analogue circuit is connected to the secondary terminals of the CT and used to generate a DC component equal and opposite to that seen in the primary one.

Then, by injecting the generated DC component into the secondary winding component prevents saturation of the CT.

A digital algorithm for compensating the secondary current is put forward in [81]. Then, an advanced compensating algorithm of the distorted secondary current immune to the remanent flux is proposed in [77, 78]. These algorithms estimate the secondary current corresponding to the CT ratio under CT saturation using the flux-current curve. In addition, it is stated that this approach allows for successful compensation of the secondary current even when a smaller CT than the rated size is used, resulting in secondary currents being more severely distorted. Moreover, it is shown [77, 78] that the proposed compensating algorithm can be implemented in real time into a digital-signal-processor hardware as part of the main protective relaying algorithm.

5.4. Analogue anti-aliasing filters

The sampling of analogue signals is performed in A/D converters. Digital information contained in the set of samples obtained differs from that provided by analogue signals [B.14, B.17]. Digital frequency is equal to analogue frequency if the frequency of the sampled analogue signal is smaller than half of the sampling frequency ($0.5\,f_s$). This threshold value is commonly called **the Nyquist frequency**. Sampling the sine analogue wave of the frequency higher than this threshold value results in obtaining a set of samples which represent the sine wave of the frequency different than that at the input of the A/D converter. Figure 5.18 shows the digital frequency versus the analogue frequency. Suppose that the calculations are based on fundamental frequency (f_1) components of the processed signals. It is seen (Fig. 5.18) that the sine analogue waves of different frequencies: f_1, $f_s - f_1$, $f_s + f_1$, $2f_s - f_1$, $2f_s + f_1$, …, after sampling give

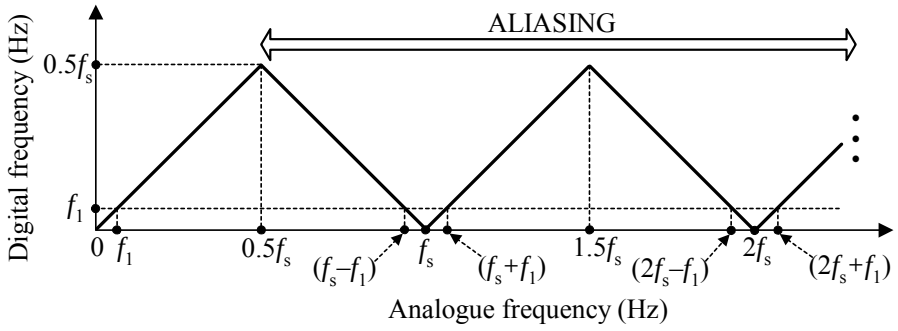

Fig. 5.18. Illustrating the fact that digital data is no uniquely related to a particular analogue signal with respect to frequency

sets of samples representing the sine wave of the fundamental frequency (f_1). So, the sampled sinusoids assume the frequency which is not their own. This phenomenon of sinusoids changing frequency during sampling is called **aliasing**. The term 'aliasing' is originated here from comparing the effect of the frequency change to the crime on an identity (an alias), which is understood here as the frequency of analogue sine wave. In addition to the frequency change effect, the aliasing also changes the phase of the signal by π for the respective ranges of frequencies of the analogue signal, as shown in Fig. 5.19.

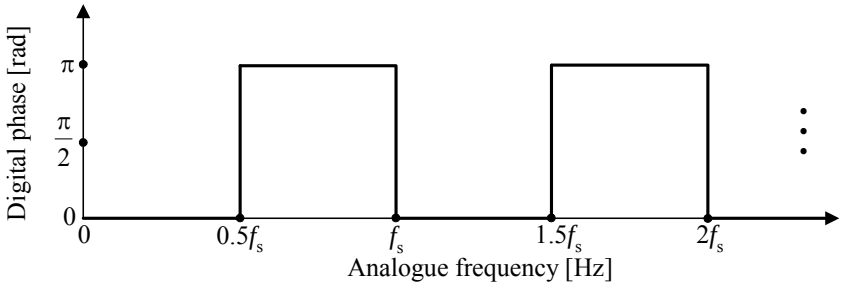

Fig. 5.19. Digital phase versus analogue frequency

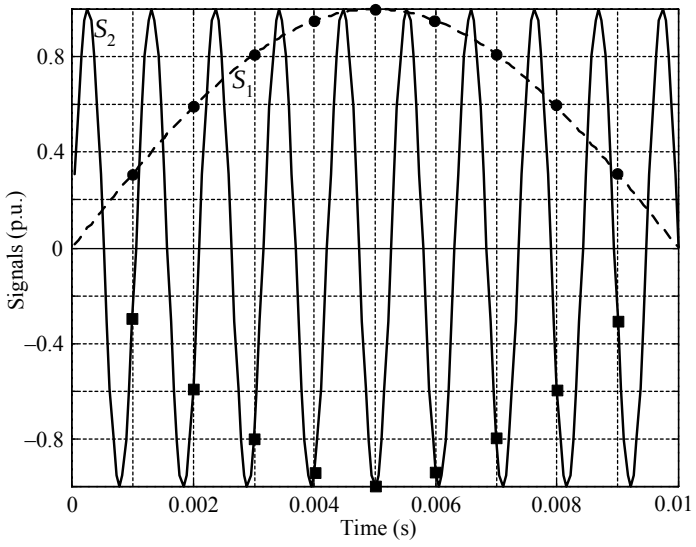

Fig. 5.20. Example of sampling two analogue sine signals with sampling frequency f_s = 1000 Hz: sampled sine signals: • S_1: signal of frequency f_1 = 50 Hz, samples denoted by circles, • S_2: signal of frequency $f_2 = f_s - f_1$ = 950 Hz, samples denoted by squares

Figure 5.20 shows an example of sampling two analogue sine signals. The sampling frequency is f_s = 1000 Hz. The first signal (S_1) is of frequency f_1 = 50 Hz (thus, below the Nyquist frequency) while the second signal (S_2) has the frequency $f_2 = f_s - f_1$ = 950 Hz (thus, above the Nyquist frequency). The aliasing is present in the case of sampling the signal S_2. As a result, both sampled signals give the sets of samples which represent the sinusoids of the fundamental frequency, shifted by angle π. The set of samples for the signal S_1 allows its analogue form to be reconstructed, while information contained in analogue signal S_2 is lost completely. Sampling the signal of frequency 950 Hz at 1000 Hz sampling frequency creates new frequency of 50 Hz for the digital signal. In this case, sampling destroys information encoded in the frequency domain of the analogue signal S_2.

In order not to lose information contained in analogue signals proper sampling frequency of Analogue-to-Digital (A/D) converters has to be applied. Claude E. Shanon in 1949 in his famous **sampling theorem** [B.14, B.17] proved that if the signal contains no frequencies above f_{mx}, then the continuous time signal can be reconstructed from a periodically sampled sequence, provided that the sampling frequency f_s satisfies the condition:

$$f_s > 2 f_{mx} \tag{5.9}$$

The sampling theorem indicates that a continuous signal can be properly sampled, *only if it does not contain frequency components above one-half of the sampling frequency* (the Nyquist frequency). The other possibility calls for removing the frequencies higher than Nyquist frequency from the analogue signal. This can be obtained by applying, prior to sampling, an analogue low pass filter, which is referred to as an anti-aliasing filter.

Figure 5.21 presents a simple R–C four-port network of low-pass transfer function, which can be applied as the anti-aliasing filter. Assuming for the circuit burden impedance $Z_B \to \infty$, the transfer function of the circuit from Fig. 5.21 is obtained as:

$$G(s) = \frac{1}{(RC)^2 s^2 + 3RCs + 1} \tag{5.10}$$

The anti-aliasing cut-off frequency (f_c) of the filter is defined as:

$$|G_{AF}(j\omega_c)| = \frac{\sqrt{2}}{2} \tag{5.11}$$

where $\omega_c = 2\pi f_c$.

From (5.11) one obtains:

$$\omega_c{}^4 (RC)^4 + 7\omega_c{}^2 (RC)^2 - 1 = 0 \tag{5.12}$$

After solving (5.12) and taking the solution for which: $(RC)^2 > 0$, the following formula for the circuit parameters is obtained:

$$RC = \frac{\sqrt{2\sqrt{53} - 14}}{4\pi f_c} \tag{5.13}$$

The time constant (RC) can be calculated from (5.13) after assuming the required cut-off frequency, which is usually set in the range: one-third up to one-half of the sampling rate: $\left(\frac{1}{3} \div \frac{1}{2}\right) f_s$.

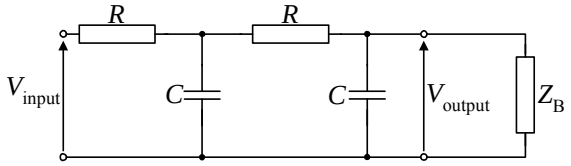

Fig. 5.21. R–C four-port network of low-pass transfer function

Figures 5.22 and 5.23 show common building blocks: Sallen–Key circuits with operational amplifiers for analogue anti-aliasing filters and their transfer functions [B.17].

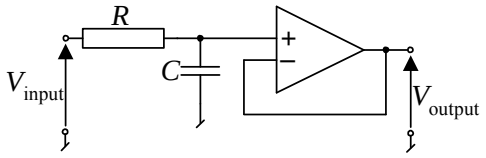

$$G(s) = \frac{1}{RCs + 1}$$

Fig. 5.22. First order Sallen–Key low-pass circuit

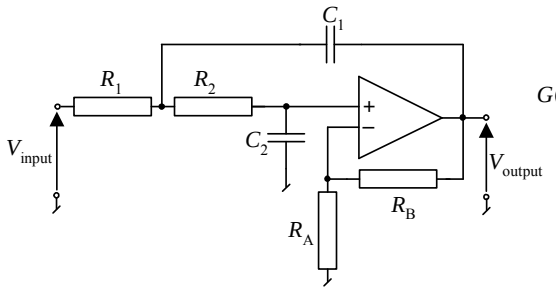

$$G(s) = \frac{\frac{K}{R_1 R_2 C_1 C_2}}{s^2 + \left[\frac{1}{R_1 C_1} + \frac{1}{R_2 C_1} + \frac{1-K}{R_2 C_2}\right] s + \frac{1}{R_1 R_2 C_1 C_2}}$$

$$K = \frac{R_A + R_B}{R_A}$$

Fig. 5.23. Second order Sallen–Key low-pass circuit

Using the first order (Fig. 5.22) and the second order (Fig. 5.23) Sallen–Key low-pass circuits one can build higher order anti-aliasing analogue filters. Another option in this respect are the switched capacitor filters, which are composed of capacitors and electronic switches.

Design of the analogue anti-aliasing filter with the given cut-off frequency requires assuming the respective standard approximation of the transfer function and its order. Three types of analogue filters are commonly used: Butterworth, Chebyshev, and Bessel (also called as Thompson filter) [B.17]. A transfer function of each of them is obtained as a result of optimising a different performance parameter.

6. One-end impedance-based fault location algorithms

6.1. Introduction

One-end fault location algorithms are designed for estimating the location of transmission line faults with use of currents and voltages measured at one terminal of a line. Also, there are some algorithms which use voltages or currents from one terminal only. Besides the fundamental frequency voltages and currents at the terminals of a line, the impedance parameters of the line are required for determining a distance to fault as well. The one-end fault location algorithms are simple and economical compared to two-end methods and those based on the travelling wave and high frequency component techniques. Therefore, they are still popular among electric power utilities.

6.2. Fault location based on impedance measurement

The impact of fault resistance on one-end impedance measurement is a key factor in deriving majority of one-end fault location algorithms. Let us start with considering a single phase line (S–R) connected to a source at one end (S) only, i.e. the line which supplies no load at the end R (Fig. 6.1). The line is affected by a fault (F), which is at unknown distance d (p.u.) from the bus S, where the fault locator (FL) is installed. If the line charging current is neglected, then the current at the fault locator ($\underline{I}_S$) is equal to the current at the fault ($\underline{I}_F$). The impedance seen from the fault locator terminal, i.e. calculated from the measured voltage ($\underline{V}_S$) and current ($\underline{I}_S$), can be mathematically expressed as:

$$\underline{Z}_{FL} = \frac{\underline{V}_S}{\underline{I}_S} = d\,\underline{Z}_L + R_F \tag{6.1}$$

Taking the imaginary part of (6.1) one obtains the distance to fault as:

$$d = \frac{\mathrm{imag}(\underline{Z}_{FL})}{\mathrm{imag}(\underline{Z}_L)} \tag{6.2}$$

This formula is a predecessor of the one-end impedance-based fault location algorithms [161]. It allows accurate determination of distance to fault in the case of one-end supply of the fault (Fig. 6.1). This is so since the fault resistance (R_F) is seen from the fault locator terminal as pure resistance, as shown in Fig. 1.2a.

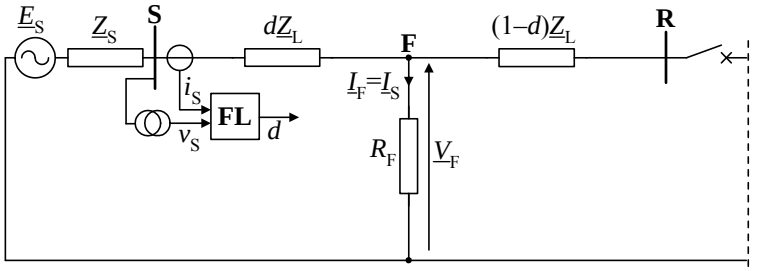

Fig. 6.1. Fault location based on impedance measurement for faulted line connected to the source at one end

However, if there is a two-end supply (Fig. 6.2), the current at the fault ($\underline{I}_F$) is not equal to the current at the fault locator ($\underline{I}_S$) since also the remote current ($\underline{I}_R$) contributes to the total fault current ($\underline{I}_F = \underline{I}_S + \underline{I}_R$). As a result, there is a contribution of the reactance in the impedance seen from the fault locator terminal (the reactance effect), as shown in Fig. 1.2b, c.

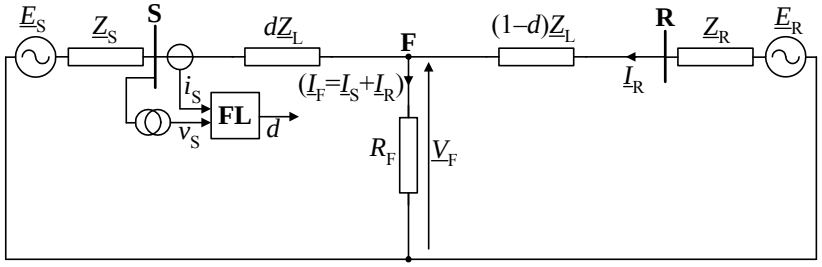

Fig. 6.2. Fault location based on impedance measurement for faulted line connected to the sources at two ends

Formulating Kirchoff's voltage law for the fault loop seen from the terminal S, i.e. the loop containing the faulted line segment ($d\underline{Z}_L$) and fault path resistance (R_F), one obtains the complex scalar equation:

$$\underline{V}_S - d\,\underline{Z}_L\,\underline{I}_S - R_F\,\underline{I}_F = 0 \tag{6.3}$$

This equation can be resolved into the real and imaginary parts (two equations), however, there are four unknowns: d, R_F, real($\underline{I}_F$), imag($\underline{I}_F$) and thus the number of unknowns exceeds the number of equations. In order to assure solvability of the fault location prob-

lem, Takagi et al. in their original work [171] proposed to decompose, using **the Thevenin theorem**, the faulted network (Fig. 6.3a) into the pre-fault network (Fig. 6.3b) and 'pure fault', i.e. superimposed network (Fig. 6.3c). They started the fault location derivation with considering the distributed parameter line model. However, they finally introduced some simplifications, which correspond to use of the simple lumped line model. Therefore, in what follows the lumped line model will be taken into account.

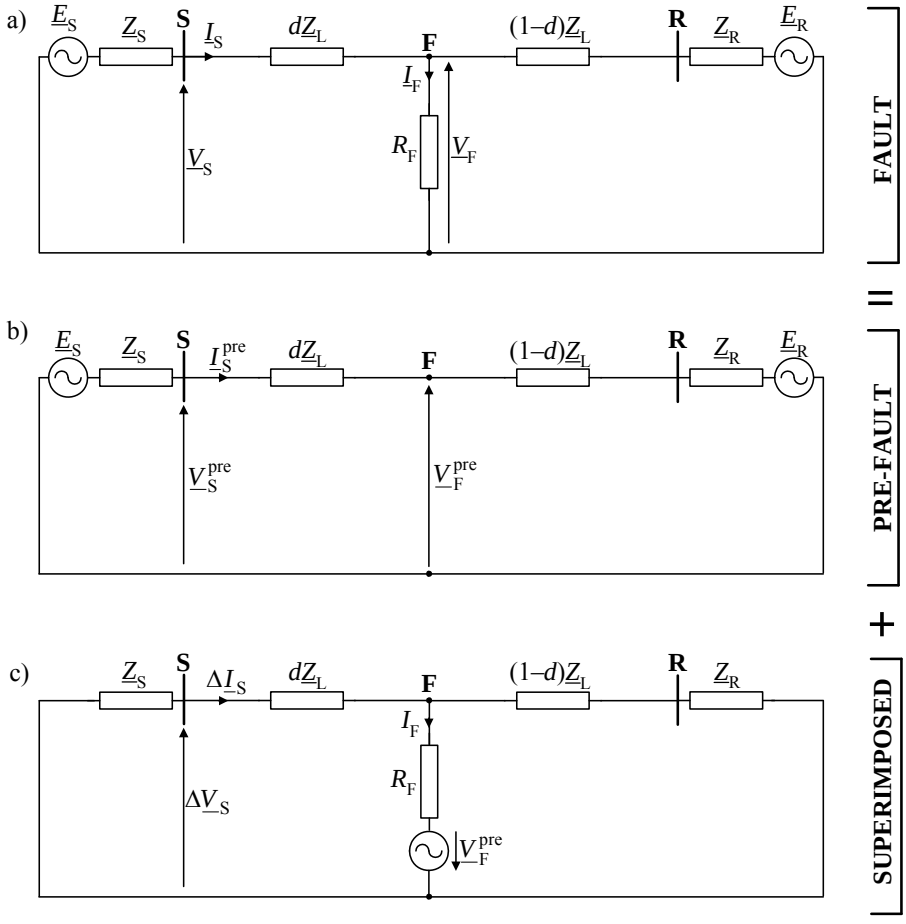

Fig. 6.3. Application of the Thevenin theory to faulted network:
a) faulted network, b) pre-fault network, c) superimposed component network

The superimposed circuit (Fig. 6.3c) is a current divider of the fault current and thus:

$$\Delta \underline{I}_S = \frac{(1-d)\underline{Z}_L + \underline{Z}_R}{\underline{Z}_S + \underline{Z}_L + \underline{Z}_R} \underline{I}_F \tag{6.4}$$

where $\Delta\underline{I}_S = \underline{I}_S - \underline{I}_S^{pre}$ – superimposed current determined from the moment of the fault inception occurrence (thus in the fault interval), and obtained by taking the fault current and subtracting the pre-fault current (present before fault inception). Note that the recordings of the pre-fault current have to be available.

This allows the total fault current to be determined as:

$$\underline{I}_F = \frac{\Delta\underline{I}_S}{\underline{k}_F} \tag{6.5}$$

where the fault current distribution factor ($\underline{k}_F$) [B.7, B.9, 31, 182] is determined as:

$$\underline{k}_F = |\underline{k}_F| e^{j\gamma} = \frac{-d\underline{Z}_L + \underline{Z}_L + \underline{Z}_R}{\underline{Z}_S + \underline{Z}_L + \underline{Z}_R} \tag{6.6}$$

Substituting (6.5)–(6.6) into (6.3) results in:

$$\underline{V}_S - d\underline{Z}_L\underline{I}_S - \frac{R_F}{|\underline{k}_F| e^{j\gamma}}\Delta\underline{I}_S = 0 \tag{6.7}$$

Multiplying (6.7) by the element ($e^{j\gamma}\Delta\underline{I}_S^*$) and taking the imaginary part yields the following formula for the distance to fault:

$$d = \frac{\text{imag}(\underline{V}_S\Delta\underline{I}_S^* e^{j\gamma})}{\text{imag}(\underline{Z}_L\underline{I}_S\Delta\underline{I}_S^* e^{j\gamma})} \tag{6.8}$$

where x^* denotes the conjugate of x.

Takagi et al. [171] assumed that the current distribution factor is a real number ($\gamma = 0$), which facilitates calculations. This simplification is applied since all the impedances involved in (6.6) have approximately the same phases. Otherwise, iterative calculations, which require knowing all the impedances from (6.6), have to be performed.

The fault location algorithm (6.8) was derived for a single phase line. For three-phase lines, the symmetrical components or phase co-ordinates approaches will be considered in successive sections of this chapter.

6.3. Use of fault current distribution factors

6.3.1. Transmission network with single line

Current distribution factors for symmetrical components were introduced in [31]. According to the fault model (4.1), the total fault current ($\underline{I}_F$) is expressed as the

weighted sum of its symmetrical components ($\underline{I}_{F1}$, $\underline{I}_{F2}$, $\underline{I}_{F0}$), which can be determined with the respective fault current distribution factors:

$$\underline{I}_{F1} = \frac{\Delta \underline{I}_{S1}}{\underline{k}_{F1}} = \frac{\underline{I}_{S1} - \underline{I}_{S1}^{pre}}{\underline{k}_{F1}} \tag{6.9}$$

$$\underline{I}_{F2} = \frac{\underline{I}_{S2}}{\underline{k}_{F2}} \tag{6.10}$$

$$\underline{I}_{F0} = \frac{\underline{I}_{S0}}{\underline{k}_{F0}} \tag{6.11}$$

In (6.9)–(6.11) and in Fig. 6.4, the respective subscript denotes: 1 – positive-, 2 – negative-, 0 – zero-sequences. For determining the positive-sequence component ($\underline{I}_{F1}$), equation (6.9), the superimposed positive-sequence circuit (Fig. 6.4a) is considered. For the remaining sequences ((6.10)–(6.11)), the pre-fault sequence currents are not involved in the formulae since they are equal to zero for the completely symmetrical network before the fault occurrence. This is the condition of using the symmetrical components approach.

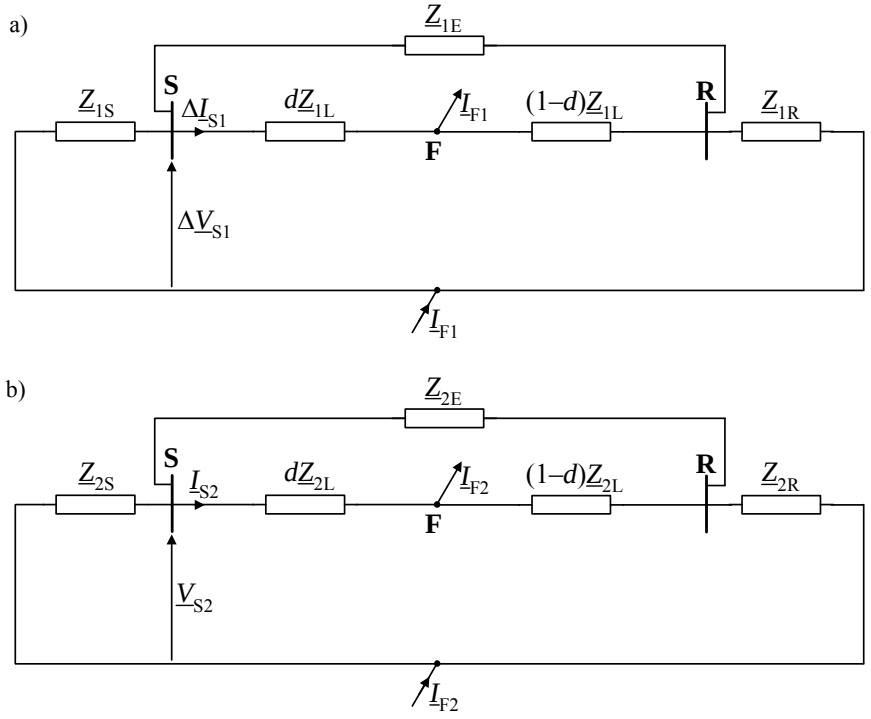

(Fig. 6.4 to be continued)

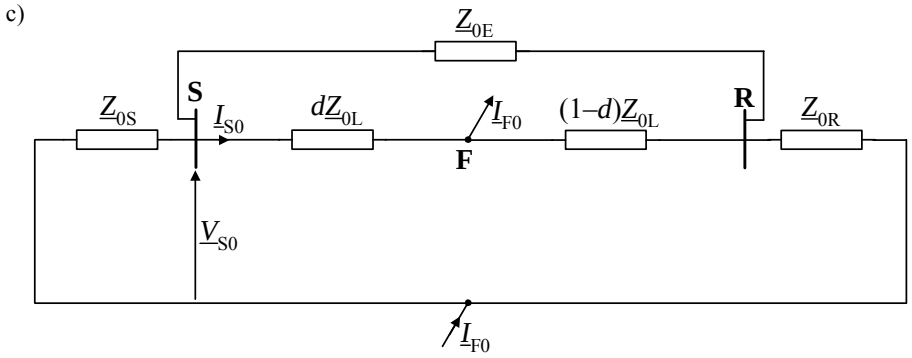

Fig. 6.4. Equivalent circuit diagrams of transmission network with single line ($\underline{Z}_L$) and extra link between the end buses ($\underline{Z}_E$) for: a) superimposed positive-, b) negative-, c) zero- sequence

From the analysis of the circuits presented in Fig. 6.4, and taking into account the fact that the respective network impedances for positive- and negative-sequences are basically identical, one obtains the fault current distribution factors as:

$$\underline{k}_{F1} = \underline{k}_{F2} = \frac{\underline{K}_1 d + \underline{L}_1}{\underline{M}_1} \tag{6.12}$$

$$\underline{k}_{F0} = \frac{\underline{K}_0 d + \underline{L}_0}{\underline{M}_0} \tag{6.13}$$

where:

$\underline{K}_1$, $\underline{L}_1$, $\underline{M}_1$ – complex coefficients dependent on positive-sequence impedances of the network (Table 6.1),

$\underline{K}_0$, $\underline{L}_0$, $\underline{M}_0$ – complex coefficients dependent on zero-sequence impedances of the network, having analogous forms as for the positive-sequence but the positive-sequence impedances are exchanged by the respective zero-sequence impedances.

Table 6.1. Transmission network with single line (Fig. 6.4a, b – complex coefficients used for determining fault current distribution factor for positive- and negative-sequence (6.12)

Extra link	Coefficients
$\underline{Z}_{1E} \neq \infty$ (extra link exists)	$\underline{K}_1 = -\underline{Z}_{1L}\underline{Z}_{1E} - (\underline{Z}_{1S} + \underline{Z}_{1R})\underline{Z}_{1L}$ $\underline{L}_1 = \underline{Z}_{1L}(\underline{Z}_{1S} + \underline{Z}_{1R}) + \underline{Z}_{1E}(\underline{Z}_{1L} + \underline{Z}_{1R})$ $\underline{M}_1 = (\underline{Z}_{1S} + \underline{Z}_{1R})(\underline{Z}_{1E} + \underline{Z}_{1L}) + \underline{Z}_{1L}\underline{Z}_{1E}$
$\underline{Z}_{1E} \to \infty$ (lack of extra link)	$\underline{K}_1 = -\underline{Z}_{1L}$ $\underline{L}_1 = \underline{Z}_{1L} + \underline{Z}_{1R}$ $\underline{M}_1 = \underline{Z}_{1S} + \underline{Z}_{1R} + \underline{Z}_{1L}$

6.3.2. Transmission network with double-circuit line

Figure 6.5 presents equivalent circuit diagrams of transmission network with double-circuit line ($\underline{Z}_{LI}$, $\underline{Z}_{LII}$) for determining the fault current distribution factors for the superimposed positive-sequence (it is analogous for the negative-sequence). Different modes of buses connection at the sending and receiving ends are reflected with the switches: w_S, w_R (switch status: 0 – sections of buses are separated, 1 – sections of buses are connected). Usually, the sections of buses are connected ($w_S w_R = 11$).

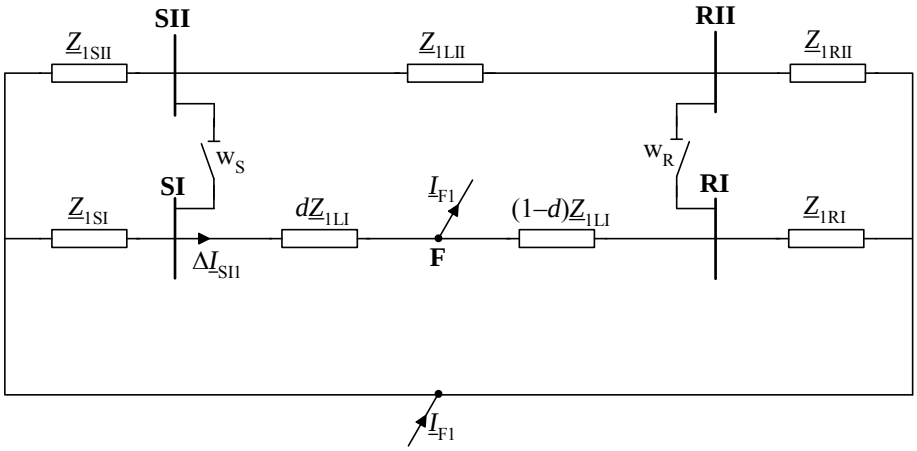

Fig. 6.5. Equivalent circuit diagram of transmission network with double-circuit line ($\underline{Z}_{LI}$, $\underline{Z}_{LII}$) with different modes of buses connection for superimposed positive-sequence

From the analysis of the circuits presented in Fig. 6.5 the fault current distribution factor (6.12) can be derived. In Table 6.2, the coefficients involved in this factor are gathered.

The considerations for the network with a double-circuit line (Fig. 6.5, Table 6.2) have been performed under the assumption that the current from the faulted circuit (connected to the bus SI) only, i.e. $\Delta\underline{I}_{SI1}$ – Fig. 6.5a, $\underline{I}_{SI2}$ – Fig. 6.5b, is measured. However, there are some applications [63, 158, 188, 190] in which the currents from both circuits of the parallel lines (connected to the bus SI and to the bus SII) are available. Such an arrangement is shown in Fig. 6.6.

Comparing the voltage drops across two different routes in the circuit from Fig. 6.6: ROUTE 1, ROUTE 2, one obtains the following formula for the positive- and negative-sequence component of the total fault current:

$$\underline{I}_{F1} = \frac{\underline{I}_{SI1} - \dfrac{\underline{Z}_{1LII}}{\underline{Z}_{1LI}}\underline{I}_{SII1}}{1-d} \tag{6.14}$$

$$\underline{I}_{F2} = \frac{\underline{I}_{SI2} - \dfrac{\underline{Z}_{2LII}}{\underline{Z}_{2LI}}\underline{I}_{SII2}}{1-d} \tag{6.15}$$

Note that in (6.15) the negative-sequence impedances can be replaced by the respective positive-sequence quantities since they are identical.

Table 6.2. Transmission network with double-circuit line (Fig. 6.5) – complex coefficients used for determining fault current distribution factor for positive- and negative-sequence (6.12)

Status of switches	Coefficients
$w_S w_R = 00$	$\underline{K}_1 = -\underline{Z}_{1LI}$ $\underline{L}_1 = \underline{Z}_{1RI} + \underline{Z}_{1LI}$ $\underline{M}_1 = \underline{Z}_{1SI} + \underline{Z}_{1LI} + \underline{Z}_{1RI}$
$w_S w_R = 01$	$\underline{K}_1 = -\underline{Z}_{1LI}(\underline{Z}_{1SII} + \underline{Z}_{1R} + \underline{Z}_{1LII})$ $\underline{L}_1 = \underline{Z}_{1LI}(\underline{Z}_{1LII} + \underline{Z}_{1SII} + \underline{Z}_{1R}) + \underline{Z}_{1LII}(\underline{Z}_{1LII} + \underline{Z}_{1SII})$ $\underline{M}_1 = (\underline{Z}_{1LI} + \underline{Z}_{1SI})(\underline{Z}_{1LII} + \underline{Z}_{1SII}) + \underline{Z}_{1R}(\underline{Z}_{1LI} + \underline{Z}_{1SI} + \underline{Z}_{1LII} + \underline{Z}_{1SII})$
$w_S w_R = 10$	$\underline{K}_1 = -\underline{Z}_{1LI}(\underline{Z}_{1S} + \underline{Z}_{1RII} + \underline{Z}_{1LII})$ $\underline{L}_1 = (\underline{Z}_{1RI} + \underline{Z}_{1LI})(\underline{Z}_{1LII} + \underline{Z}_{1S} + \underline{Z}_{1RII})$ $\underline{M}_1 = (\underline{Z}_{1LI} + \underline{Z}_{1RI})(\underline{Z}_{1S} + \underline{Z}_{1LII} + \underline{Z}_{1RII}) + \underline{Z}_{1S}(\underline{Z}_{1LII} + \underline{Z}_{1RII})$
$w_S w_R = 11$	$\underline{K}_1 = -\underline{Z}_{1LI}(\underline{Z}_{1S} + \underline{Z}_{1R} + \underline{Z}_{1LII})$ $\underline{L}_1 = \underline{Z}_{1LI}(\underline{Z}_{1S} + \underline{Z}_{1R} + \underline{Z}_{1LII}) + \underline{Z}_{1LII}\underline{Z}_{1R}$ $\underline{M}_1 = \underline{Z}_{1LI}\underline{Z}_{1LII} + (\underline{Z}_{1LI} + \underline{Z}_{1LII})(\underline{Z}_{1S} + \underline{Z}_{1R})$
Where: $\underline{Z}_{1S} = \dfrac{\underline{Z}_{1SI}\underline{Z}_{1SII}}{\underline{Z}_{1SI} + \underline{Z}_{1SII}}$, $\underline{Z}_{1R} = \dfrac{\underline{Z}_{1RI}\underline{Z}_{1RII}}{\underline{Z}_{1RI} + \underline{Z}_{1RII}}$	

For the network with a single line (Fig. 6.4a) and with a double-circuit line, but with the current from one circuit only (Fig. 6.5a), the positive-sequence component of the total fault current was determined using the measured superimposed positive-sequence current. Under the availability of measurements such as in Fig. 6.6a, it is possible to determine the positive-sequence component of the total fault current with use of positive-sequence currents. However, it is possible to use also the superimposed positive-sequence currents, obtaining the following formula, which is analogous to (6.14):

$$\underline{I}_{F1} = \frac{\Delta\underline{I}_{SI1} - \dfrac{\underline{Z}_{1LII}}{\underline{Z}_{1LI}}\Delta\underline{I}_{SII1}}{1-d} \tag{6.16}$$

The formula (6.16) can be utilised for fault location if the superimposed currents can be determined, i.e. the pre-fault currents are registered. Use of (6.16), instead of (6.14), in the fault location algorithm derivation is advantageous since for the super-

imposed quantities the line shunt capacitances effect (not taken into account here) has less influence on fault location accuracy, i.e. higher accuracy is achieved.

The advantage of using measurement of currents from both line circuits relies on estimating the total fault current components (6.14)–(6.16) without involving source impedances, as in the case of measuring a current from one circuit only (Table 6.2).

In (6.14)–(6.16), impedances of both line circuits are involved, however, in practice they are identical: $\underline{Z}_{1LI} = \underline{Z}_{1LII}$.

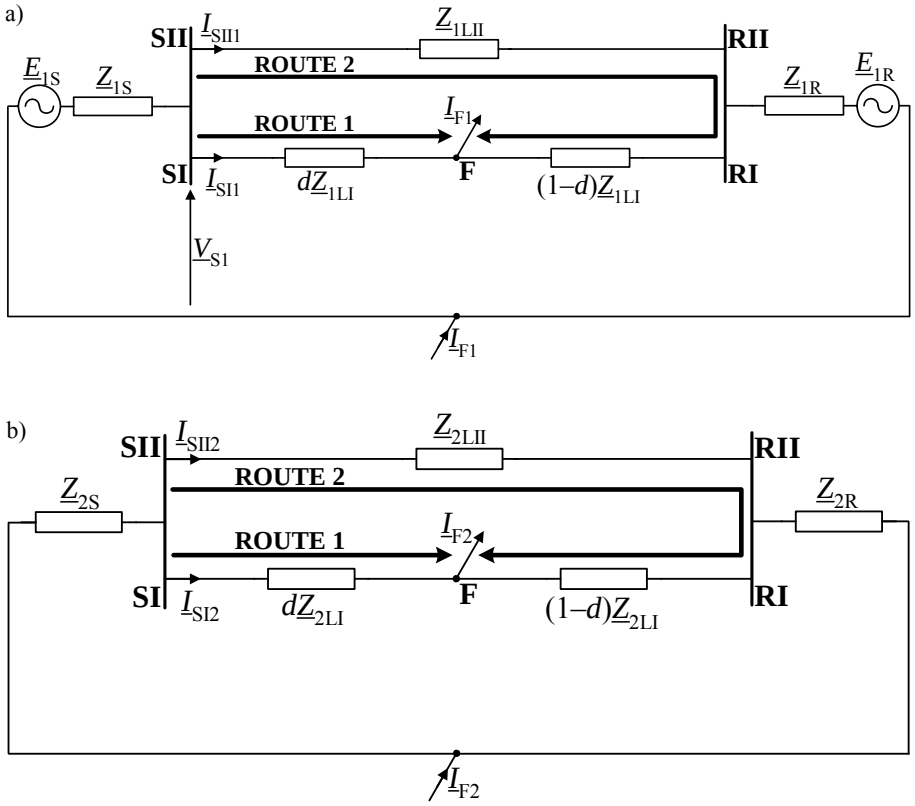

Fig. 6.6. Equivalent circuit diagrams of transmission network with double-circuit line ($\underline{Z}_{LI}$, $\underline{Z}_{LII}$) for availability of measurements of currents from both line circuits: a) for positive-sequence, b) for negative-sequence

The impedance of overhead line for the zero-sequence since it is affected by soil resistivity (difficult to measure and changeable) is considered as uncertain parameter [B.7, B.9]. Therefore, the fault current distribution factors for the positive-(superimposed positive-) and negative-sequence are basically used in fault location algorithms. However, for example in case of the complete lack of measurement of current from the

healthy parallel line [58], there is a need for using also the fault current distribution factor for the zero-sequence. Equivalent circuits of double-circuit line for the zero-sequence, when both circuits are in operation, are presented in Fig. 3.25. The case where the parallel healthy line (line: LII) is switched off and earthed is presented in Fig. 3.26.

Considering the mesh of the circuit from Fig. 3.25b (**both line circuits in operation)** containing the elements: $[\underline{Z}_{0\mathrm{LII}} - \underline{Z}_{0\mathrm{m}}]$; $[d(\underline{Z}_{0\mathrm{LI}} - \underline{Z}_{0\mathrm{m}})]$; $[(1-d)(\underline{Z}_{0\mathrm{LI}} - \underline{Z}_{0\mathrm{m}})]$ yields the compact formula for the zero-sequence component of the total fault current:

$$\underline{I}_{\mathrm{F0}} = \frac{\underline{I}_{\mathrm{SI0}} - \underline{P}'_0 \underline{I}_{\mathrm{SII0}}}{1-d} \tag{6.17}$$

where:

$$\underline{P}'_0 = \frac{\underline{Z}_{0\mathrm{LII}} - \underline{Z}_{0\mathrm{m}}}{\underline{Z}_{0\mathrm{LI}} - \underline{Z}_{0\mathrm{m}}} \tag{6.18}$$

For the case of **the parallel healthy line switched off and earthed** (Fig. 3.26) the consideration of the healthy line path (thus excluding impedances of the equivalent sources) appears to be advantageous. Taking into account that the sum of voltage drops defined in (3.14)–(3.17), across this path is:

$$\underline{V}_0^{\mathrm{E}} + \underline{V}_0^{\mathrm{F}} + \underline{V}_0^{\mathrm{G}} + \underline{V}_0^{\mathrm{H}} = 0 \tag{6.19}$$

yields:

$$\underline{I}_{\mathrm{F0}} = \frac{\underline{I}_{\mathrm{SI0}} - \underline{P}''_0 \underline{I}_{\mathrm{SII0}}}{1-d} \tag{6.20}$$

where:

$$\underline{P}''_0 = -\frac{\underline{Z}_{0\mathrm{LII}}}{\underline{Z}_{0\mathrm{m}}} \tag{6.21}$$

6.4. Models of fault loops

The majority of one-end fault location algorithms are based on considering the fault loops composed accordingly to the identified fault type, analogously as for the distance relays. The distance protective relay, say at the sending line end S, measures apparent impedance of the fault loop under consideration:

$$\underline{Z}_{\mathrm{S\_P}} = \frac{\underline{V}_{\mathrm{S\_P}}}{\underline{I}_{\mathrm{S\_P}}} \tag{6.22}$$

where $\underline{V}_{S\_P}$, $\underline{I}_{S\_P}$ – protective (subscript P) distance relay voltage and current signals, at the sending (subscript S) line end, which are composed as presented in Tables 6.3–6.6.

For solid faults (fault resistance $R_F = 0$), the apparent impedance (6.22) is equal to the positive-sequence impedance of the line segment of the relative distance d (p.u.), i.e. from the measurement point to the fault. Thus, one obtains:

$$\underline{Z}_{S\_P} = d\,\underline{Z}_{1L} \tag{6.23}$$

Otherwise (for resistive faults), due to "the reactance effect" the apparent impedance (6.22) is not a strict measure of the distance to fault. As opposed to protective distance relays, the one-end fault location algorithms compensate for "the reactance effect" by considering the fault loop model, in which the term ($R_F\underline{I}_F$) represents the voltage drop across the fault path resistance:

$$\underline{V}_{S\_P} - d\,\underline{Z}_{1L}\underline{I}_{S\_P} - R_F\underline{I}_F = 0 \tag{6.24}$$

Table 6.3. Composition of fault loop voltage and current signals for single line

Single line		
Fault type	Fault loop voltage: $\underline{V}_{S\_P}$	Fault loop current: $\underline{I}_{S\_P}$
a–E	$\underline{V}_{Sa}$	$\underline{I}_{Sa} + \underline{k}_0\underline{I}_{S0}$
b–E	$\underline{V}_{Sb}$	$\underline{I}_{Sb} + \underline{k}_0\underline{I}_{S0}$
c–E	$\underline{V}_{Sc}$	$\underline{I}_{Sc} + \underline{k}_0\underline{I}_{S0}$
a–b a–b–E a–b–c* a–b–c–E*	$\underline{V}_{Sa} - \underline{V}_{Sb}$	$\underline{I}_{Sa} - \underline{I}_{Sb}$
b–c b–c–E	$\underline{V}_{Sb} - \underline{V}_{Sc}$	$\underline{I}_{Sb} - \underline{I}_{Sc}$
c–a c–a–E	$\underline{V}_{Sc} - \underline{V}_{Sa}$	$\underline{I}_{Sc} - \underline{I}_{Sa}$
Where: $\underline{k}_0 = \dfrac{\underline{Z}_{0L} - \underline{Z}_{1L}}{\underline{Z}_{1L}}$. * – inter-phase fault loop (a–b) is considered, however, the other fault loops (b–c), (c–a) can be taken as well.		

In Table 6.3, the composition of fault loop signals (for the terminal S) for a single line is shown. For example, for the fault loop voltage and current we assume:

– a–E fault:

- voltage from faulted phase 'a': $\underline{V}_{Sa}$,
- current from faulted phase 'a': $\underline{I}_{Sa}$ and additionally the compensation for the zero-sequence component: $\underline{k}_0\underline{I}_{S0}$,

– a–b fault:

- difference of voltages from faulted phases ‘a’ and ‘b’: $\underline{V}_{\mathrm{Sa}} - \underline{V}_{\mathrm{Sb}}$,
- difference of currents from faulted phases ‘a’ and ‘b’: $\underline{I}_{\mathrm{Sa}} - \underline{I}_{\mathrm{Sb}}$.

In the case of single phase-to-earth faults on double-circuit line (Table 6.4) additionally the compensation for the mutual coupling of the circuits: $\underline{k}_{0\mathrm{m}}\underline{I}_{\mathrm{SII0}}$ is included.

Table 6.4. Composition of fault loop voltage and current signals for phase-to-ground faults on double-circuit line

Double-circuit line		
Fault type	Fault loop voltage: $\underline{V}_{\mathrm{S\_P}}$	Fault loop current: $\underline{I}_{\mathrm{S\_P}}$
a–E	$\underline{V}_{\mathrm{Sa}}$	$\underline{I}_{\mathrm{SIa}} + \underline{k}_0\underline{I}_{\mathrm{SI0}} + \underline{k}_{0\mathrm{m}}\underline{I}_{\mathrm{SII0}}$
b–E	$\underline{V}_{\mathrm{Sb}}$	$\underline{I}_{\mathrm{SIb}} + \underline{k}_0\underline{I}_{\mathrm{SI0}} + \underline{k}_{0\mathrm{m}}\underline{I}_{\mathrm{SII0}}$
c–E	$\underline{V}_{\mathrm{Sc}}$	$\underline{I}_{\mathrm{SIc}} + \underline{k}_0\underline{I}_{\mathrm{SI0}} + \underline{k}_{0\mathrm{m}}\underline{I}_{\mathrm{SII0}}$
Where: $\underline{k}_0 = \frac{\underline{Z}_{0\mathrm{LI}} - \underline{Z}_{1\mathrm{LI}}}{\underline{Z}_{1\mathrm{LI}}}$, $\underline{k}_{0\mathrm{m}} = \frac{\underline{Z}_{0\mathrm{m}}}{\underline{Z}_{1\mathrm{LI}}}$. For the remaining fault types the composition of fault loop signals is analogous to the single line case (Table 6.3).		

In turn, in Tables 6.5 and 6.6, the fault loop signals are expressed in terms of the respective symmetrical components of the measured voltages and currents (the last subscript denotes the symmetrical component type):

$$\underline{V}_{\mathrm{S\_P}} = \underline{a}_1\underline{V}_{\mathrm{S1}} + \underline{a}_2\underline{V}_{\mathrm{S2}} + \underline{a}_0\underline{V}_{\mathrm{S0}} \tag{6.25}$$

$$\underline{I}_{\mathrm{S\_P}} = \underline{a}_1\underline{I}_{\mathrm{S1}} + \underline{a}_2\underline{I}_{\mathrm{S2}} + \underline{a}_0\frac{\underline{Z}_{0\mathrm{L}}}{\underline{Z}_{1\mathrm{L}}}\underline{I}_{\mathrm{S0}} \tag{6.26}$$

In the case of a double-circuit line the fault loop current:

$$\underline{I}_{\mathrm{S\_P}} = \underline{a}_1\underline{I}_{\mathrm{SI1}} + \underline{a}_2\underline{I}_{\mathrm{SI2}} + \underline{a}_0\left(\frac{\underline{Z}_{0\mathrm{LI}}}{\underline{Z}_{1\mathrm{LI}}}\underline{I}_{\mathrm{SI0}} + \frac{\underline{Z}_{0\mathrm{m}}}{\underline{Z}_{1\mathrm{LI}}}\underline{I}_{\mathrm{SII0}}\right) \tag{6.27}$$

where $\underline{a}_1$, $\underline{a}_2$, $\underline{a}_0$ – coefficients dependent on fault type, which are the same as for the single line.

The circuit diagrams with the indicated symmetrical component signals used in (6.25)–(6.27) are shown in Fig. 3.24 (single line) and in Figs. 3.25, 3.26 (double-circuit line).

The notation used in (6.25)–(6.27) appears convenient if the compensation for line shunt capacitances is performed [63]. Of course, this notation is fully equivalent to the description traditionally used for distance protection (Tables 6.3 and 6.4).

Table 6.5. Composition of fault loop voltage and current signals in terms of symmetrical components for single line

Single line			
Fault type	Fault loop voltage: $\underline{V}_{S\_P} = \underline{a}_1\underline{V}_{S1} + \underline{a}_2\underline{V}_{S2} + \underline{a}_0\underline{V}_{S0}$ Fault loop current: $\underline{I}_{S\_P} = \underline{a}_1\underline{I}_{S1} + \underline{a}_2\underline{I}_{S2} + \underline{a}_0\frac{\underline{Z}_{0L}}{\underline{Z}_{1L}}\underline{I}_{S0}$		
	$\underline{a}_1$	$\underline{a}_2$	$\underline{a}_0$
a–E	1	1	1
b–E	$-0.5 - j0.5\sqrt{3}$	$-0.5 + j0.5\sqrt{3}$	1
c–E	$-0.5 + j0.5\sqrt{3}$	$-0.5 - j0.5\sqrt{3}$	1
a–b a–b–E a–b–c* a–b–c–E*	$1.5 + j0.5\sqrt{3}$	$1.5 - j0.5\sqrt{3}$	0
b–c b–c–E	$-j\sqrt{3}$	$j\sqrt{3}$	0
c–a c–a–E	$-1.5 + j0.5\sqrt{3}$	$-1.5 - j0.5\sqrt{3}$	0
* – inter-phase fault loop (a–b) is considered, however, the other fault loops: (b–c) and (c–a) can be taken as well.			

Table 6.6. Composition of the fault loop voltage and current signals in terms of symmetrical components, for phase-to-ground faults on double-circuit line

Double-circuit line			
Fault type	Fault loop voltage: $\underline{V}_{S\_P} = \underline{a}_1\underline{V}_{S1} + \underline{a}_2\underline{V}_{S2} + \underline{a}_0\underline{V}_{S0}$ Fault loop current: $\underline{I}_{S\_P} = \underline{a}_1\underline{I}_{SI1} + \underline{a}_2\underline{I}_{SI2} + \underline{a}_0\left(\frac{\underline{Z}_{0LI}}{\underline{Z}_{1LI}}\underline{I}_{SI0} + \frac{\underline{Z}_{0m}}{\underline{Z}_{1LI}}\underline{I}_{SII0}\right)$		
	$\underline{a}_1$	$\underline{a}_2$	$\underline{a}_0$
a–E	1	1	1
b–E	$-0.5 - j0.5\sqrt{3}$	$-0.5 + j0.5\sqrt{3}$	1
c–E	$-0.5 + j0.5\sqrt{3}$	$-0.5 - j0.5\sqrt{3}$	1
For the remaining fault types the composition of fault loop signals is analogous as for the single line case (Table 6.5).			

6.5. Fault location algorithm by Takagi et al.

One of the earliest fault location algorithms has been developed by Takagi et al. [171]. Its form for a single-phase line was presented by the formula (6.8). An extension to the three-phase application can be performed by utilising the general fault loop model (6.24) and the general formula for a total fault current (4.1). Combining them gives:

$$\underline{V}_{\mathrm{S\_P}} - d\underline{Z}_{\mathrm{1L}}\underline{I}_{\mathrm{S\_P}} - R_{\mathrm{F}}(\underline{a}_{\mathrm{F1}}\underline{I}_{\mathrm{F1}} + \underline{a}_{\mathrm{F2}}\underline{I}_{\mathrm{F2}} + \underline{a}_{\mathrm{F0}}\underline{I}_{\mathrm{F0}}) = 0 \tag{6.28}$$

Taking into account such a set of the weighting coefficients that for the zero-sequence: $\underline{a}_{\mathrm{F0}} = 0$ (Tables 4.3, 4.4 or 4.5) and expressing the symmetrical components of the total fault current with use of the current distribution factors (6.9)–(6.10) one obtains:

$$\underline{V}_{\mathrm{S\_P}} - d\underline{Z}_{\mathrm{1L}}\underline{I}_{\mathrm{S\_P}} - R_{\mathrm{F}}\left(\underline{a}_{\mathrm{F1}}\frac{\Delta\underline{I}_{\mathrm{S1}}}{\underline{k}_{\mathrm{F1}}} + \underline{a}_{\mathrm{F2}}\frac{\underline{I}_{\mathrm{S2}}}{\underline{k}_{\mathrm{F2}}}\right) = 0 \tag{6.29}$$

Considering that for the fault current distribution factors for the positive- and negative-sequence, with respect to their magnitude and angle, we have:

$$|\underline{k}_{\mathrm{F}}| = |\underline{k}_{\mathrm{F1}}| = |\underline{k}_{\mathrm{F2}}| \tag{6.30}$$

$$\gamma = \mathrm{angle}(\underline{k}_{\mathrm{F1}}) = \mathrm{angle}(\underline{k}_{\mathrm{F2}}) \tag{6.31}$$

the formula (6.29) transforms to:

$$\underline{V}_{\mathrm{S\_P}} - d\underline{Z}_{\mathrm{1L}}\underline{I}_{\mathrm{S\_P}} - \frac{R_{\mathrm{F}}}{|\underline{k}_{\mathrm{F}}|\,\mathrm{e}^{\mathrm{j}\gamma}}(\underline{a}_{\mathrm{F1}}\Delta\underline{I}_{\mathrm{S1}} + \underline{a}_{\mathrm{F2}}\underline{I}_{\mathrm{S2}}) = 0 \tag{6.32}$$

Multiplying (6.32) by the term: $(\mathrm{e}^{\mathrm{j}\gamma}(\underline{a}_{\mathrm{F1}}\Delta\underline{I}_{\mathrm{S1}} + \underline{a}_{\mathrm{F2}}\underline{I}_{\mathrm{S2}})^*)$ and then rearranging it, the resultant formula for the sought distance to fault (d (p.u.)) is obtained as follows:

$$d = \frac{\mathrm{imag}(\underline{V}_{\mathrm{S\_P}}(\underline{a}_{\mathrm{F1}}\Delta\underline{I}_{\mathrm{S1}} + \underline{a}_{\mathrm{F2}}\underline{I}_{\mathrm{S2}})^*\mathrm{e}^{\mathrm{j}\gamma})}{\mathrm{imag}(\underline{Z}_{\mathrm{1L}}\underline{I}_{\mathrm{S\_P}}(\underline{a}_{\mathrm{F1}}\Delta\underline{I}_{\mathrm{S1}} + \underline{a}_{\mathrm{F2}}\underline{I}_{\mathrm{S2}})^*\mathrm{e}^{\mathrm{j}\gamma})} \tag{6.33}$$

where x^* denotes the conjugate of x.

The signals involved in the fault location algorithm (6.33) are determined from measurements acquired at one line terminal (here, the terminal S). Table 6.7 shows how to set the coefficients.

In formula (6.33), the angle of the current distribution factor (for the positive- or negative-sequence) is involved. Takagi et al. [171] proposed assuming that this angle equals zero ($\gamma = 0$), i.e. that the fault current distribution factor is a real number. In

practice, this assumption is not fulfilled and thus there is a certain error due to this. However, in the case of high voltage network these additional errors are not substantial [B.7, 182].

Table 6.7. Description of signals and coefficients of the fault location algorithm (6.33)

Signals	V_{S_P} – fault loop voltage	Formula (6.25), and Table 6.3 or Table 6.5
	I_{S_P} – fault loop current	Single line: formula (6.26), and Table 6.3 or Table 6.5 Double-circuit line: formula (6.27), and Table 6.4 or Table 6.6
	ΔI_{S1} – superimposed positive-sequence current	Single line: Fig. 6.4a Double-circuit line: Fig. 6.5a
	I_{S2} – negative-sequence current	Single line: Fig. 6.4b Double-circuit line: Fig. 6.5b
Coefficients	a_{F1}, a_{F2} – weighting coefficients	Tables 4.3–4.5, depending on the assumed preference with respect to using the respective sequences

6.6. Fault location algorithm by Wiszniewski

The other fundamental fault location algorithm has been developed by Wiszniewski [182], which is somehow similar to the algorithm by Takagi et al. [171]. However, it is more related to the distance protection technique as impedance measured by a distance relay is involved in the algorithm. The algorithm by Wiszniewski [182] was derived utilising the general fault loop model (6.24) and the general formula for a total fault current (4.1). The same assumptions, as in the Takagi method for obtaining formula (6.32), were assumed. Dividing (6.32) by $\underline{I}_{S\_P}$ yields:

$$\underline{Z}_{S\_P} - d\underline{Z}_{1L} - \frac{R_F}{|\underline{k}_F|}\frac{(\underline{a}_{F1}\Delta\underline{I}_{S1} + \underline{a}_{F2}\underline{I}_{S2})}{\underline{I}_{S\_P}e^{j\gamma}} = 0 \tag{6.34}$$

where:

$\underline{Z}_{S\_P} = \dfrac{\underline{V}_{S\_P}}{\underline{I}_{S\_P}} = R_{S\_P} + jX_{S\_P}$ – fault loop impedance (measured by a distance relay).

Resolving (6.34) into the real and imaginary parts results in:

$$R_{S\_P} - dR_{1L} - \frac{R_F}{|\underline{k}_F|}a = 0 \tag{6.35}$$

$$X_{\mathrm{S\_P}} - dX_{1\mathrm{L}} - \frac{R_{\mathrm{F}}}{|\underline{k}_{\mathrm{F}}|} b = 0 \tag{6.36}$$

where:

$$a = \mathrm{real}\left(\frac{\underline{a}_{\mathrm{F1}} \Delta \underline{I}_{\mathrm{S1}} + \underline{a}_{\mathrm{F2}} \underline{I}_{\mathrm{S2}}}{\underline{I}_{\mathrm{S\_P}} \mathrm{e}^{\mathrm{j}\gamma}} \right) \tag{6.37}$$

$$b = \mathrm{imag}\left(\frac{\underline{a}_{\mathrm{F1}} \Delta \underline{I}_{\mathrm{S1}} + \underline{a}_{\mathrm{F2}} \underline{I}_{\mathrm{S2}}}{\underline{I}_{\mathrm{S\_P}} \mathrm{e}^{\mathrm{j}\gamma}} \right) \tag{6.38}$$

$R_{1\mathrm{L}}$, $X_{1\mathrm{L}}$ – positive-sequence line resistance and reactance, respectively.

One of the possible forms of the solution of the set of two equations (6.35)–(6.36) is as follows [182]:

$$d = \frac{X_{\mathrm{S\_P}}}{X_{1\mathrm{L}}} - \frac{\dfrac{R_{\mathrm{S\_P}}}{X_{1\mathrm{L}}} \mathrm{tg}(\varphi_{1\mathrm{L}}) - \dfrac{X_{\mathrm{S\_P}}}{X_{1\mathrm{L}}}}{\dfrac{a}{b} \mathrm{tg}(\varphi_{1\mathrm{L}}) - 1} \tag{6.39}$$

where $\varphi_{1\mathrm{L}}$ – angle of the positive-sequence line impedance $\underline{Z}_{1\mathrm{L}} = R_{1\mathrm{L}} + \mathrm{j}X_{1\mathrm{L}}$.

The signals involved in the fault location algorithm (6.39) are determined from measurements acquired at one line terminal (here, at the terminal S) and the coefficients are identical with those used in the algorithm by Takagi et al. (Table 6.7).

The formula (6.39) allows for a simple interpretation of the reactance effect. The remarks concerning a need for making an assumption with respect to the angle of the fault current distribution factor are identical with those written for the Takagi et al. method (Section 6.5).

6.7. Fault location method by Saha et al.

In [31], an accurate one-end fault location algorithm has been introduced. High accuracy of fault location is achieved due to taking into account the actual distribution of a fault current in the transmission network. The initial assumptions for deriving this algorithm are identical with those used in Sections 6.5 and 6.6.

The authors of [31] introduced into (6.34) the following form for the fault current distribution factor for the positive- (negative-) sequence:

$$\underline{k}_{\mathrm{F}} = |\underline{k}_{\mathrm{F}}| \mathrm{e}^{\mathrm{j}\gamma} = \frac{\underline{K}_1 d + \underline{L}_1}{\underline{M}_1} \tag{6.40}$$

where $\underline{K}_1$, $\underline{L}_1$, $\underline{M}_1$ – coefficients determined with use of impedances of the transmission network: Table 6.1 (network with a single line) and Table 6.2 (network with a double-circuit line).

Substituting (6.40) into (6.34) yields:

$$\underline{Z}_{S\_P} - d\underline{Z}_{1L} - R_F \frac{\underline{M}_1(\underline{a}_{F1}\Delta\underline{I}_{S1} + \underline{a}_{F2}\underline{I}_{S2})}{(\underline{K}_1 d + \underline{L}_1)\underline{I}_{S\_P}} = 0 \tag{6.41}$$

where Z_{S_P} – fault loop impedance (measured by a distance relay).

After performing the relevant rearrangements of (6.41) one gets:

$$\underline{K}_1\underline{Z}_{1L}d^2 + (\underline{L}_1\underline{Z}_{1L} - \underline{K}_1\underline{Z}_{S\_P})d - L_1\underline{Z}_{S\_P} + R_F\underline{M}_1\frac{(\underline{a}_{F1}\Delta\underline{I}_{S1} + \underline{a}_{F2}\underline{I}_{S2})}{\underline{I}_{S\_P}} = 0 \tag{6.42}$$

Equation (6.42) can be rewritten to the following compact formula for complex numbers, with two unknowns (d (p.u.) – distance to fault, R_F – fault resistance):

$$\underline{A}_2 d^2 + \underline{A}_1 d + \underline{A}_0 + \underline{A}_{00}R_F = 0 \tag{6.43}$$

The fault location formula (6.43) suits both single and double-circuit lines. The signals involved here are determined from measurements performed at one line terminal (here, at the terminal S) and the coefficients are identical with those used in the algorithm by Takagi et al. (Table 6.7). The complex coefficients $\underline{K}_1$, $\underline{L}_1$, $\underline{M}_1$ are gathered in the following tables:

- single line – Table 6.1,
- double-circuit line – Table 6.2.

The formula (6.43) can be written down separately for the real and imaginary parts. Combining them in such a way that fault resistance is eliminated yields the quadratic formula for a sought distance to fault:

$$B_2 d^2 + B_1 d + B_0 = 0 \tag{6.44}$$

where:

$B_2 = \text{real}(\underline{A}_2)\,\text{imag}(\underline{A}_{00}) - \text{imag}(\underline{A}_2)\,\text{real}(\underline{A}_{00})$,

$B_1 = \text{real}(\underline{A}_1)\,\text{imag}(\underline{A}_{00}) - \text{imag}(\underline{A}_1)\,\text{real}(\underline{A}_{00})$,

$B_0 = \text{real}(\underline{A}_0)\,\text{imag}(\underline{A}_{00}) - \text{imag}(\underline{A}_0)\,\text{real}(\underline{A}_{00})$.

There are two solutions of (6.44):

$$d_1 = \frac{-B_1 - \sqrt{B_1^2 - 4B_2B_0}}{2B_2} \tag{6.45}$$

$$d_2 = \frac{-B_1 + \sqrt{B_1^2 - 4B_2B_0}}{2B_2} \tag{6.46}$$

of which only one determines the real distance to fault (d), while the second solution usually lies outside the line range, i.e. outside the range: 0 to 1 (p.u.).

For the specific fault cases it may happen that both solutions (6.45)–(6.46) indicate the fault as occurring within the line range. In such rare cases one has to check the sign of fault resistances R_{F1}, R_{F2}, which correspond to the calculated values of distance to fault: d_1, d_2. In a natural way, the solution which results in negative fault resistance has to be rejected. Fault resistance can be calculated by taking the real or imaginary part of the formula (6.43). With the real part, one obtains:

$$R_{F1} = \frac{-\text{real}(\underline{A}_2)d_1^2 - \text{real}(\underline{A}_1)d_1 - \text{real}(\underline{A}_0)}{\text{real}(\underline{A}_{00})} \tag{6.47}$$

$$R_{F2} = \frac{-\text{real}(\underline{A}_2)d_2^2 - \text{real}(\underline{A}_1)d_2 - \text{real}(\underline{A}_0)}{\text{real}(\underline{A}_{00})} \tag{6.48}$$

It has been suggested in [23] that selection of the valid solution for a distance to fault can also be performed by analysing the relation between the symmetrical components of measured currents, such as presented in formula (4.3) and Table 4.7.

The signals involved in (6.39) are determined from measurements performed at one line terminal (here, at the terminal S) and the coefficients are identical to those of the algorithm by Takagi et al. (Section 6.5) and the Wiszniewski method (Section 6.6). It is important that additionally the positive-sequence source impedances (for the local source $\underline{Z}_{1S}$ and for the remote source $\underline{Z}_{1R}$) are involved in the complex coefficients $\underline{K}_1$, $\underline{L}_1$, $\underline{M}_1$ (see (6.43)), and thus required for solving the resultant quadratic formula (6.44).

The local source impedance can be determined from the superimposed positive-sequence voltage and current:

$$\underline{Z}_{1S} = -\frac{\Delta\underline{V}_{S1}}{\Delta\underline{I}_{S1}} \tag{6.48}$$

or for all the faults, except the three-phase balanced ones, from the negative-sequence quantities:

$$\underline{Z}_{2S} = -\frac{\underline{V}_{S2}}{\underline{I}_{S2}} \tag{6.49}$$

The remote source impedance $\underline{Z}_{1R}$ is the other parameter required by the fault location formula (6.44). This impedance can be determined on condition that exact net-

work topology and parameters are known. Otherwise, its "representative" value has to be provided as the input data [31]. Some mismatch between the actual impedance and the provided "representative" can appear. However, in strong meshed modern networks the equivalent system configuration is fixed [130] and the expected mismatch is rather not too high. Moreover, it follows from the many years' experience [31] that the mismatch causes no problem. So, the need for providing the remote source impedance ($\underline{Z}_{1R}$) cannot be considered as the algorithm limitation.

On the other hand, there is a possibility [49] for improving fault location accuracy by sending the source impedance, which can be measured at the remote end devices (for example, in the recording device RD), with use of simple and even slow communication means (Fig. 6.7).

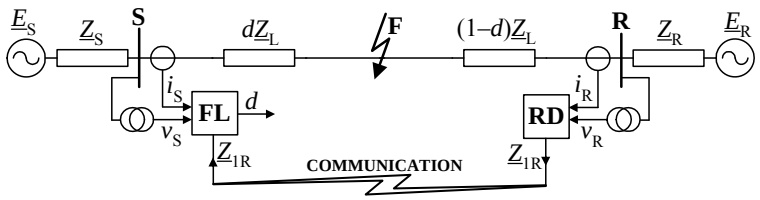

Fig. 6.7. Improving the accuracy of the fault location by measurement of remote source impedance ($\underline{Z}_{1R}$) in recording device and usage of communication for sending it to fault locator (FL)

Figure 6.8 presents an example of fault location on a single 400 kV, 300 km line for the following fault specifications:

- fault type: a–E,
- fault resistance: 10 Ω,
- fault location: 0.7 p.u.

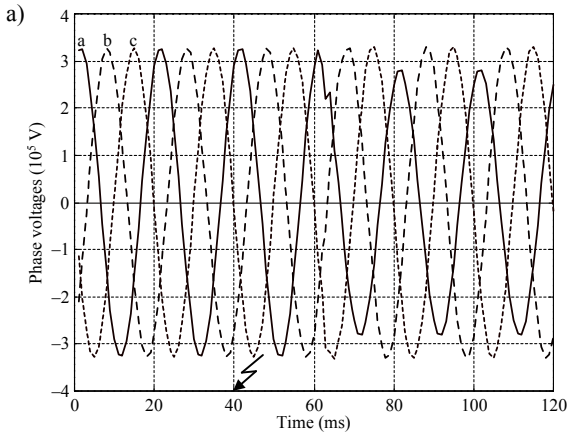

(Fig. 6.8 to be continued)

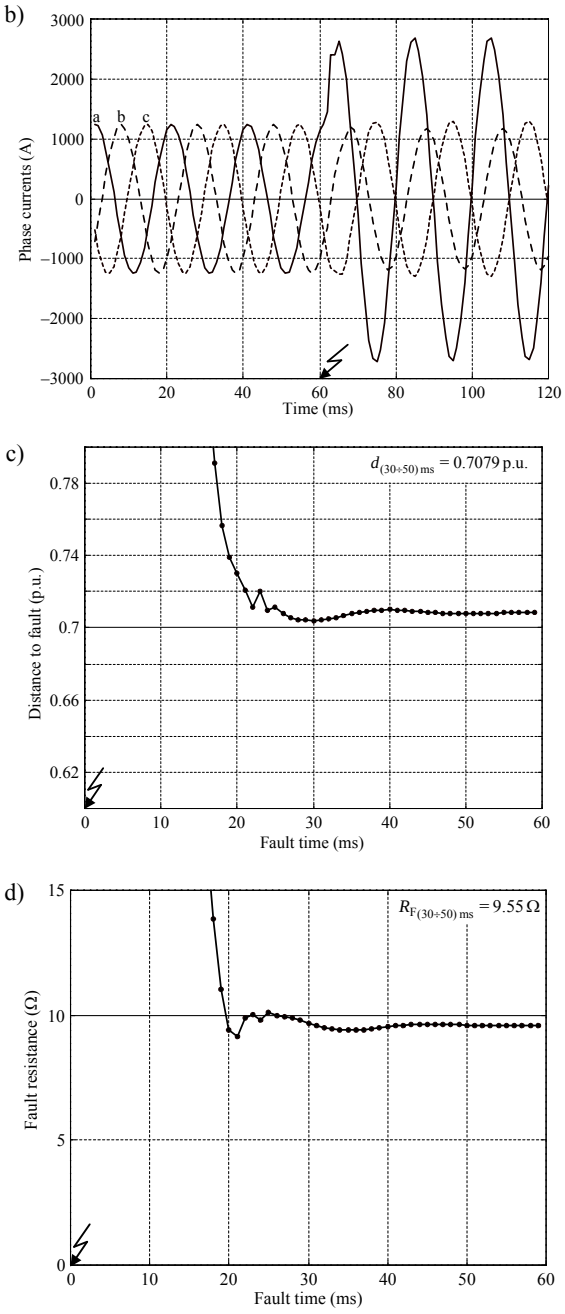

Fig. 6.8. Example of fault location on a single 400 kV, 300 km line with the following fault specifications: fault type: a–E, fault resistance: 10 Ω, fault location: 0.7 p.u.:
a) phase voltages, b) phase currents, c) estimated distance to fault, d) estimated fault resistance

The estimated fault distance (averaged over the time interval lasting from 30 ms up to 50 ms after the fault inception) equals 0.7079 p.u., and thus the error is 0.8%. The accuracy obtained can be improved by introducing the compensation for the line shunt capacitances (Section 6.15).

6.8. Fault location algorithm for a double-circuit line with complete measurements at one line end

A schematic diagram of fault location (FL) on a double-circuit line and distance protection (DP) with measurements of three-phase voltage and three-phase current from both faulted and healthy lines is shown in Fig. 6.9 [63, 158]. There is greater availability of measured signals compared to the standard measurements, for which only zero-sequence current is measured from the healthy parallel line.

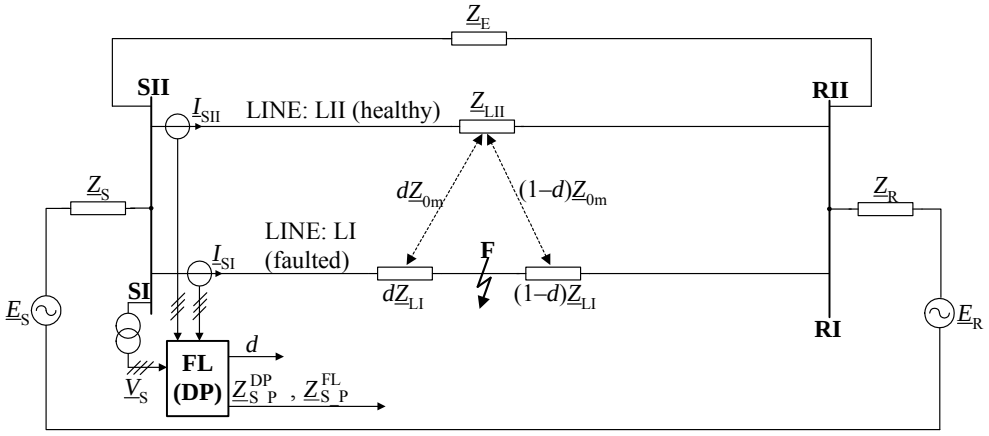

Fig. 6.9. Schematic diagram of fault location (FL) on a double-circuit line and distance protection (DP) with measurements of three-phase voltage and three-phase current from both faulted and healthy lines

The fault current distribution factors for availability of measurements were determined on the basis of equivalent circuit diagrams from Fig. 6.6 and presented by the formulae (6.14)–(6.16). Considering the fault model (4.1), with zero-sequence component being eliminated ($\underline{a}_{F0} = 0$), as in Tables 4.3–4.5, and substituting (6.14)–(6.15) into the fault loop model (6.24) yields:

$$\underline{V}_{S\_P} - d\,\underline{Z}_{1LI}\underline{I}_{S\_P} - \frac{R_F}{1-d}\underline{N}_{12} = 0 \tag{6.50}$$

where:

$$\underline{N}_{12} = \underline{a}_{F1}\left(\underline{I}_{SI1} - \frac{\underline{Z}_{1LII}}{\underline{Z}_{1LI}}\underline{I}_{SII1}\right) + \underline{a}_{F2}\left(\underline{I}_{SI2} - \frac{\underline{Z}_{2LII}}{\underline{Z}_{2LI}}\underline{I}_{SII2}\right).$$

Resolving (6.50) into the real and imaginary parts and then eliminating the component $(R_F/(1-d))$ yields the following formula for a sought distance to fault:

$$d = \frac{\text{imag}(\underline{V}_{S\_P})\,\text{real}(\underline{N}_{12}) - \text{real}(\underline{V}_{S\_P})\,\text{imag}(\underline{N}_{12})}{\text{imag}(\underline{Z}_{1LI}\underline{I}_{S\_P})\,\text{real}(\underline{N}_{12}) - \text{real}(\underline{Z}_{1LI}\underline{I}_{S\_P})\,\text{imag}(\underline{N}_{12})} \tag{6.51}$$

The fault location formula (6.51) can be written down even in a more compact alternative form, which can be implemented with use of digital algorithms developed for reactive power calculation:

$$d = \frac{\text{imag}(\underline{V}_{S\_P}\underline{N}_{12}^{*})}{\text{imag}(\underline{Z}_{1LI}\underline{I}_{S\_P}\underline{N}_{12}^{*})} \tag{6.52}$$

where $\underline{N}_{12}^{*}$ – conjugate of $\underline{N}_{12}$ defined in (6.50).

Table 6.8. Description of signals and coefficients of the fault location algorithm (6.52)

Signals	$\underline{V}_{S\_P}$ – fault loop voltage	Formula (6.25), and Table 6.3 or Table 6.5
	$\underline{I}_{S\_P}$ – fault loop current	Formula (6.27), and Table 6.4 or Table 6.6
	$\underline{I}_{SI1}$ – positive-sequence current from faulted line	Fig. 6.6a
	$\underline{I}_{SII1}$ – positive-sequence current from healthy line	Fig. 6.6a
	$\underline{I}_{SI2}$ – negative-sequence current from faulted line	Fig. 6.6b
	$\underline{I}_{SII2}$ – negative-sequence current from healthy line	Fig. 6.6b
Coefficients	$\underline{a}_{F1}$, $\underline{a}_{F2}$ – weighting coefficients	Tables 4.3–4.5, depending on the assumed preference for using the respective sequence components

Obtaining such compact first order formulae (as (6.51) or (6.52)) appears to be very attractive for application to adaptive distance protection of parallel lines. It is

important here that neither impedances of the equivalent sources are to be known nor the pre-fault measurements are to be used.

It is worthwhile to note that the classic distance relay determines the fault loop impedance from the fault loop signals (6.24), (6.26):

$$\underline{Z}_{\mathrm{S\_P}}^{\mathrm{DP}} = R_{\mathrm{S\_P}}^{\mathrm{DP}} + \mathrm{j}X_{\mathrm{S\_P}}^{\mathrm{DP}} = \frac{\underline{V}_{\mathrm{S\_P}}}{\underline{I}_{\mathrm{S\_P}}} \tag{6.53}$$

The impedance measurement (6.53) is affected by "the reactance effect", relevant for resistive faults, and presence of pre-fault power flow. In consequence, the quality of protection can be adversely influenced. However, the fault loop impedance measurement can be accomplished with the fault location algorithm derived according to:

$$\underline{Z}_{\mathrm{S\_P}}^{\mathrm{FL}} = R_{\mathrm{S\_P}}^{\mathrm{FL}} + \mathrm{j}X_{\mathrm{S\_P}}^{\mathrm{FL}} = \frac{\mathrm{imag}(\underline{V}_{\mathrm{S\_P}}\underline{N}_{12}^{*})}{\mathrm{imag}(\underline{Z}_{\mathrm{1LI}}\underline{I}_{\mathrm{S\_P}}\underline{N}_{12}^{*})}\underline{Z}_{\mathrm{1LI}} \tag{6.54}$$

Results for the sample fault, shown in Figs. 6.10 and 6.11 illustrate the effectiveness of compensation for "the reactance effect", when performing the measurements according to (6.52) and (6.54). The main specifications for the 400 kV, 300 km double-circuit line considered are as follows:

– fault type: a–E,
– fault resistance: 15 Ω,
– fault location: 0.8 pu,
– pre-fault power flow: from the bus R to S ($\underline{E}_{\mathrm{R}}$ leads $\underline{E}_{\mathrm{S}}$ by 35°).

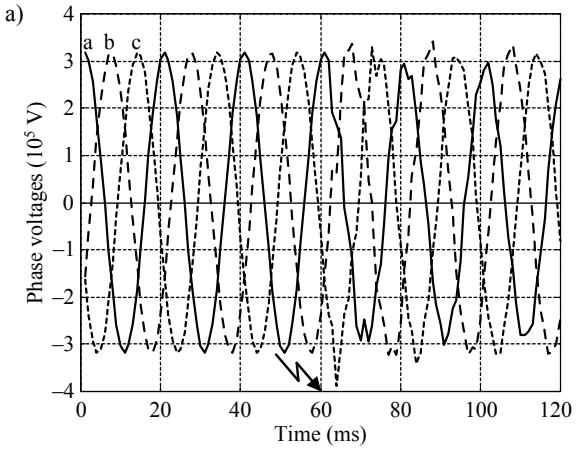

(Fig. 6.10 to be continued)

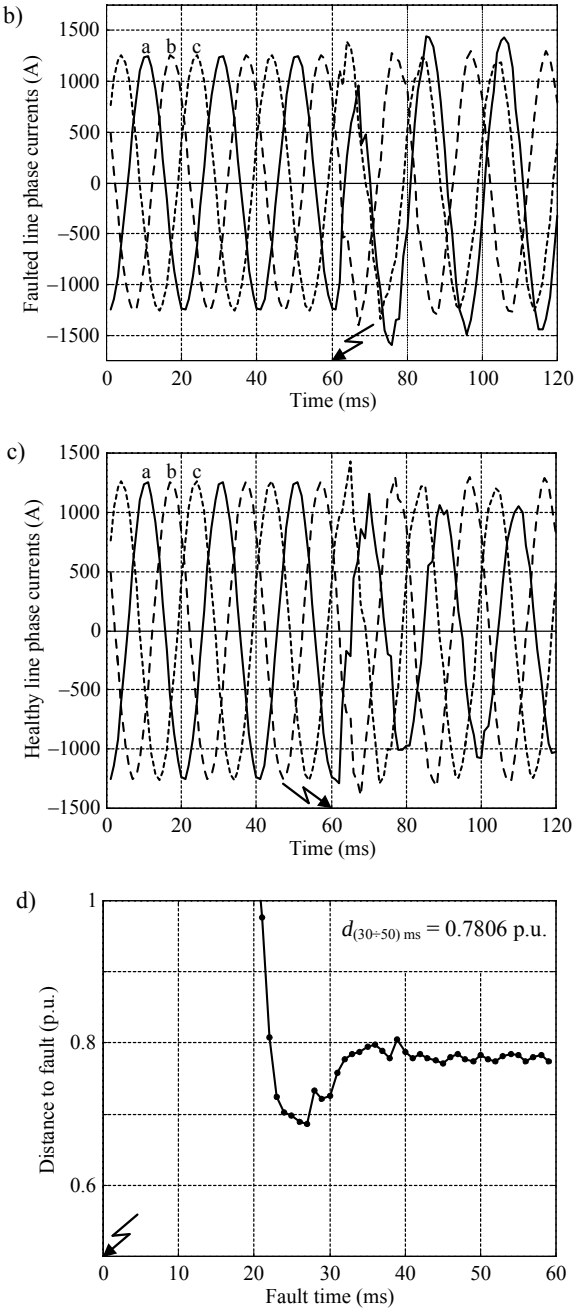

Fig. 6.10. Example of fault location on a double-circuit transmission line with the fault location algorithm (6.52): a) three-phase voltage, b) faulted line three-phase current, c) healthy line three-phase current, d) estimated distance to fault

The estimated value of the distance to fault in the example under consideration is $d = 0.7806$ p.u. ($d_{\text{actual}} = 0.8$ p.u.), and thus around 2% error is obtained. This result can be improved by introducing compensation for the line shunt capacitances (Section 6.15).

Figure 6.11 presents, for the fault location example under study, the fault loop resistance and reactance in two ways:

- classic distance protection principle (6.53) – resistance $R_{\text{S\_P}}^{\text{DP}}$, reactance $X_{\text{S\_P}}^{\text{DP}}$,
- fault location-based method (6.54) – resistance $R_{\text{S\_P}}^{\text{FL}}$, reactance $X_{\text{S\_P}}^{\text{FL}}$.

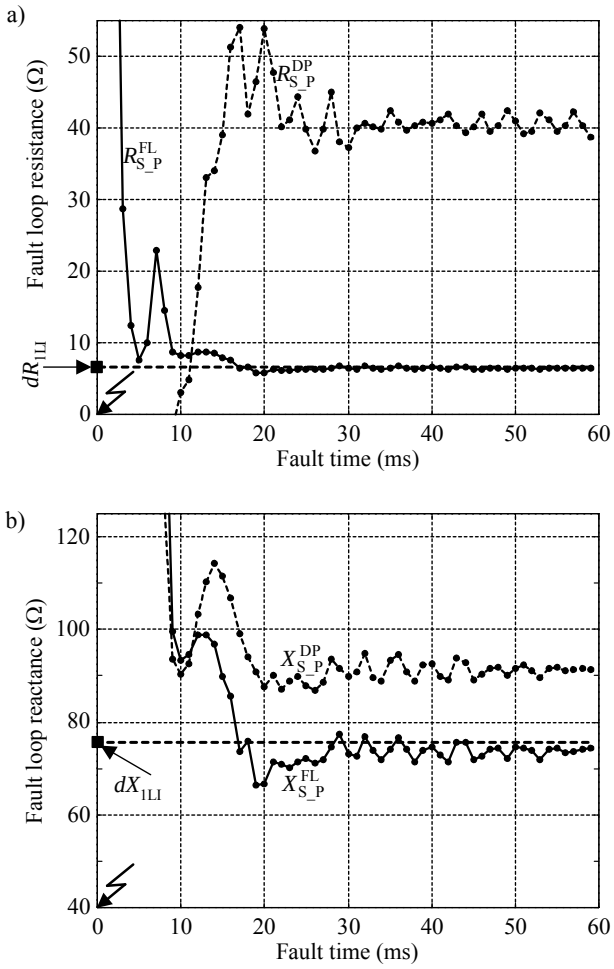

Fig. 6.11. Example of fault location on a double-circuit transmission line, with the measurement of fault loop resistance (a) and reactance (b) being performed according to the classic distance protection (6.53) and fault location-based (6.54) principles

The impedance measurement of the classic distance protection ($R_{S\_P}^{DP}$, $X_{S\_P}^{DP}$) departs very much from the real values (dR_{1LI}, dX_{1LI}). By contrast, using the fault location algorithm presented, one obtains the fault loop impedance components ($R_{S\_P}^{FL}$, $X_{S\_P}^{FL}$), which coincide with the real values of resistance and reactance of the line segment from the measuring point (S) to the fault place (F). The indicates that the distance protection immune to "the reactance effect" can be readily achieved.

6.9. Fault location algorithm for a double-circuit line with limited measurements at one line end

Figure 6.12 presents a schematic diagram of fault location on a double-circuit line with measurement of three-phase voltage and current from faulted line only [58]. It is considered that the healthy parallel line is in operation or switched off and earthed at both ends.

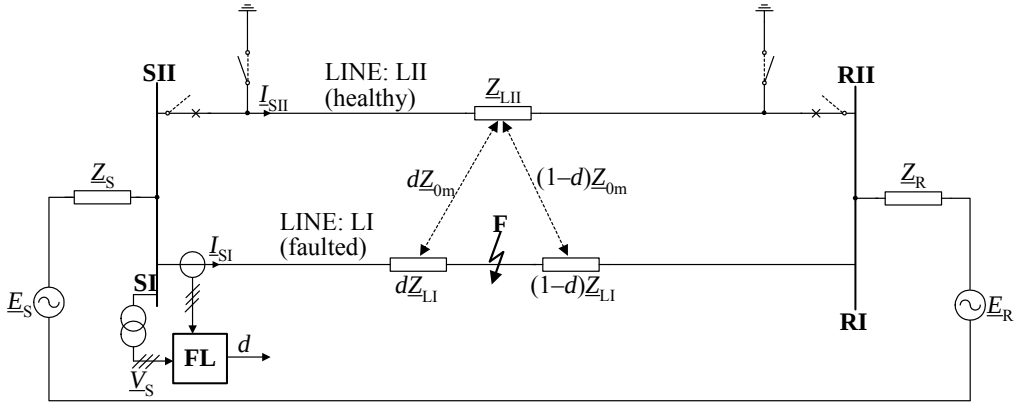

Fig. 6.12. Schematic diagram of fault location on a double-circuit line with measurements of three-phase voltage and current from faulted line only, when healthy parallel line is in operation (status of switches marked with solid line) or switched off and earthed (status of switches marked with dotted line)

Taking the fault loop model (6.23) and expressing the total fault current with use of the symmetrical components of this current and the fault current distribution factors (6.9)–(6.11) one obtains:

$$\underline{V}_{S\_P} - d\,\underline{Z}_{1LI}\underline{I}_{S\_P} - R_F\left(\frac{\underline{a}_{F1}\Delta\underline{I}_{SI1}}{\underline{k}_{F1}} + \frac{\underline{a}_{F2}\underline{I}_{SI2}}{\underline{k}_{F2}} + \frac{\underline{a}_{F0}\underline{I}_{SI0}}{\underline{k}_{F0}}\right) = 0 \tag{6.55}$$

In (6.55), the fault loop voltage ($\underline{V}_{S\_P}$) is determined by (6.24), while the fault loop current can be expressed as:

$$\underline{I}_{S\_P} = \underline{I}_{S\_P}^{SL} + \underline{a}_0 \frac{\underline{Z}_{0m}}{\underline{Z}_{1LI}} \underline{I}_{SII0} \tag{6.56}$$

where the first component represents the fault loop current without taking into account the mutual coupling effect, i.e. as used for the single line (hence the superscript SL):

$$\underline{I}_{S\_P}^{SL} = \underline{a}_1 \underline{I}_{SI1} + \underline{a}_2 \underline{I}_{SI2} + \underline{a}_0 \frac{\underline{Z}_{0LI}}{\underline{Z}_{1LI}} \underline{I}_{SI0} \tag{6.57}$$

Since the zero-sequence current from the healthy line ($\underline{I}_{SII0}$), which is required for making the compensation for the mutual coupling (6.56), is considered here as unavailable from the measurement, it has to be estimated. For this purpose, one takes the formula determining the relations between the symmetrical components of the total fault current (formula (4.3) and Table 4.7), which can be expressed as:

$$\frac{\underline{I}_{SI0} - \underline{P}_0 \underline{I}_{SII0}}{1-d} = \frac{(\underline{b}_{F1} \Delta \underline{I}_{SI1} + \underline{b}_{F2} \underline{I}_{SI2}) \underline{M}_1}{\underline{K}_1 d + \underline{L}_1} \tag{6.58}$$

which is obtained after substituting:

- formulae (6.17)–(6.18) or (6.20)–(6.21) for the zero-sequence current ($\underline{I}_{F0}$), depending on the mode of operation of the healthy parallel line,
- formula (6.12) for the fault current distribution factor for the positive- and negative-sequence.

The unavailable zero-sequence current from the healthy line ($\underline{I}_{SII0}$) can be determined from (6.58) as equal to:

$$\underline{I}_{SII0} = \frac{1}{\underline{P}_0} \left(\underline{I}_{SI0} - \frac{(1-d)(\underline{b}_{F1} \Delta \underline{I}_{SI1} + b_{F2} \underline{I}_{SI2}) \underline{M}_1}{\underline{K}_1 d + \underline{L}_1} \right) \tag{6.59}$$

Substituting (6.59) into the formula for the fault loop current (6.56) and then into the fault loop model (6.55) one obtains the following quadratic complex formula:

$$\underline{A}_2 d^2 + \underline{A}_1 d + \underline{A}_0 + \underline{A}_{00} R_F = 0 \tag{6.60}$$

where:

$$\underline{A}_2 = -\underline{Z}_{1LI} \underline{K}_1 \underline{I}_{S\_P}^{SL} - \frac{\underline{Z}_{0m}}{\underline{P}_0} (\underline{K}_1 \underline{I}_{SI0} - (\underline{b}_{F1} \Delta \underline{I}_{SI1} + \underline{b}_{F2} \underline{I}_{SI2}) \underline{M}_1),$$

$$\underline{A}_1 = \underline{K}_1 \underline{V}_{S\_P} - \underline{Z}_{1LI} \underline{L}_1 \underline{I}_{S\_P}^{SL} - \frac{\underline{Z}_{0m}}{\underline{P}_0} \underline{L}_1 \underline{I}_{SI0}.$$

$\underline{A}_0 = \underline{L}_1 \underline{V}_{S\_P}$,

$\underline{A}_{00} = -\underline{M}_1 (\underline{a}_{F1} \Delta \underline{I}_{SI1} + \underline{a}_{F2} \underline{I}_{SI2})$.

Solution of (6.60) is identical to the solution of the quadratic complex formula (6.43).

Table 6.9. Description of signals and coefficients of the fault location algorithm (6.60)

Signals	$\underline{V}_{S\_P}$ – fault loop voltage	Formula (6.25), and Table 6.3 or Table 6.5
	$\underline{I}_{S\_P}$ – fault loop current (complete)	Formula (6.56)
	$\underline{I}_{S\_P}^{SL}$ – fault loop current without taking into account the mutual coupling effect, being the part of $\underline{I}_{S\_P}$	Formula (6.57), and Table 6.6
	$\Delta \underline{I}_{SI1}$ – superimposed positive-sequence current from faulted line	Fig. 6.5a
	$\underline{I}_{SI2}$ – negative-sequence current from faulted line	Fig. 6.5b
	$\underline{I}_{SI0}$ – zero-sequence current from faulted line	Figs. 3.25 and 3.26
Coefficients	Line LII in operation	Line LII switched off and earthed
	$\underline{K}_1 = -\underline{Z}_{1LI}(\underline{Z}_{1S} + \underline{Z}_{1R} + \underline{Z}_{1LII})$	$\underline{K}_1 = -\underline{Z}_{1LI}$
	$\underline{L}_1 = -\underline{K}_1 + \underline{Z}_{1LII}\underline{Z}_{1R}$	$\underline{L}_1 = \underline{Z}_{1LI} + \underline{Z}_{1R}$
	$\underline{M}_1 = \underline{Z}_{1LI}\underline{Z}_{1LII} + (\underline{Z}_{1LI} + \underline{Z}_{1LII})(\underline{Z}_{1S} + \underline{Z}_{1R})$	$\underline{M}_1 = \underline{Z}_{1S} + \underline{Z}_{1R} + \underline{Z}_{1LI}$
	$\underline{P}_0 = \underline{P}'_0 = \dfrac{\underline{Z}_{0LII} - \underline{Z}_{0m}}{\underline{Z}_{0LI} - \underline{Z}_{0m}}$	$\underline{P}_0 = \underline{P}''_0 = -\dfrac{\underline{Z}_{0LII}}{\underline{Z}_{0m}}$
	$\underline{a}_1$, $\underline{a}_2$, $\underline{a}_0$: Table 6.6	
	$\underline{a}_{F1}$, $\underline{a}_{F2}$, $\underline{a}_{F0}$: The sets with $\underline{a}_{F0} = 0$: Tables 4.3–4.5, accordingly to the assumed preference for using the respective sequence components	
	$\underline{b}_{F1}$, $\underline{b}_{F2}$: formula (4.3) and Table 4.7	

In Fig. 6.13, an example of fault location on a 120 km double-circuit line is shown. The main specifications are as follows: a–E fault, d_{actual} = 0.9 p.u., R_F = 10 Ω, both lines are in operation [58]. Without using the zero-sequence current from the healthy parallel line, the compensation for mutual coupling of the lines is performed accurately (according to (6.60)), ensuring exact location of the fault (Fig. 6.13c).

The zero-sequence current from the healthy parallel line (its real and imaginary parts), estimated according to (6.59), is shown in Fig. 6.14, together with the actual current. The difference between these currents is considerable only during the first cycle after fault inception. However, after completing the data window of the filters (within 20 ms) the difference between the estimated and the actual currents is very small.

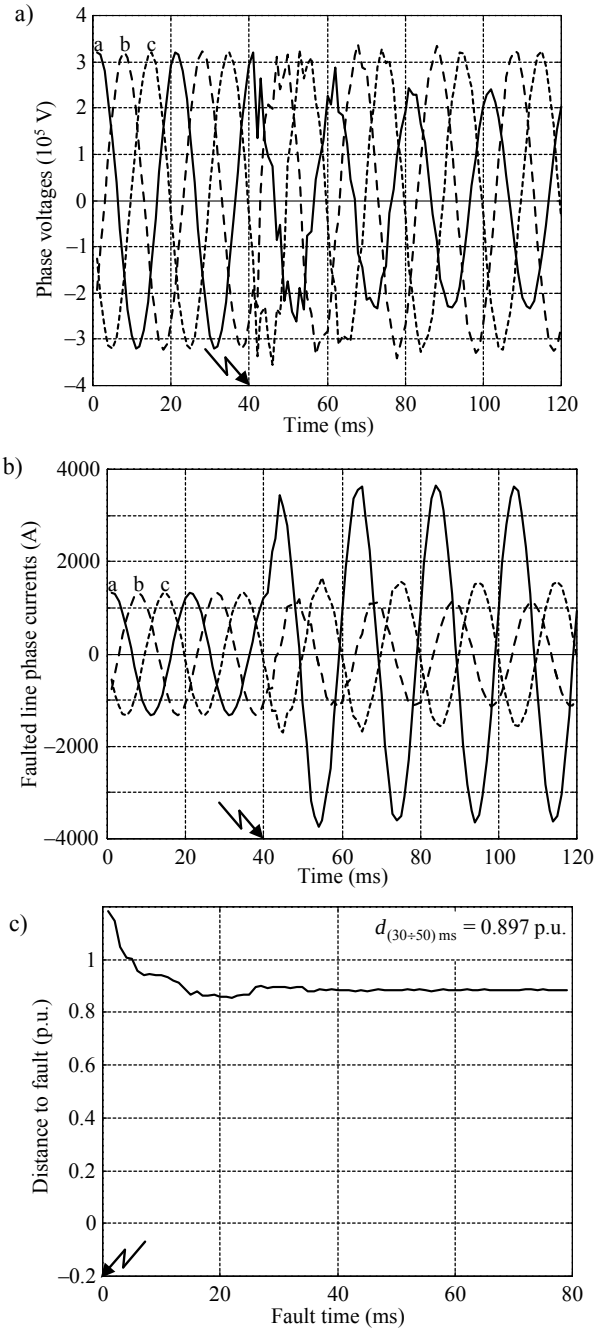

Fig. 6.13. Example of a–E fault location on a 400 kV, 120 km double-circuit line (d_{actual} = 0.9 p.u., R_{F} = 10 Ω): a) three-phase voltage, b) three-phase current from faulted line, c) estimated distance to fault

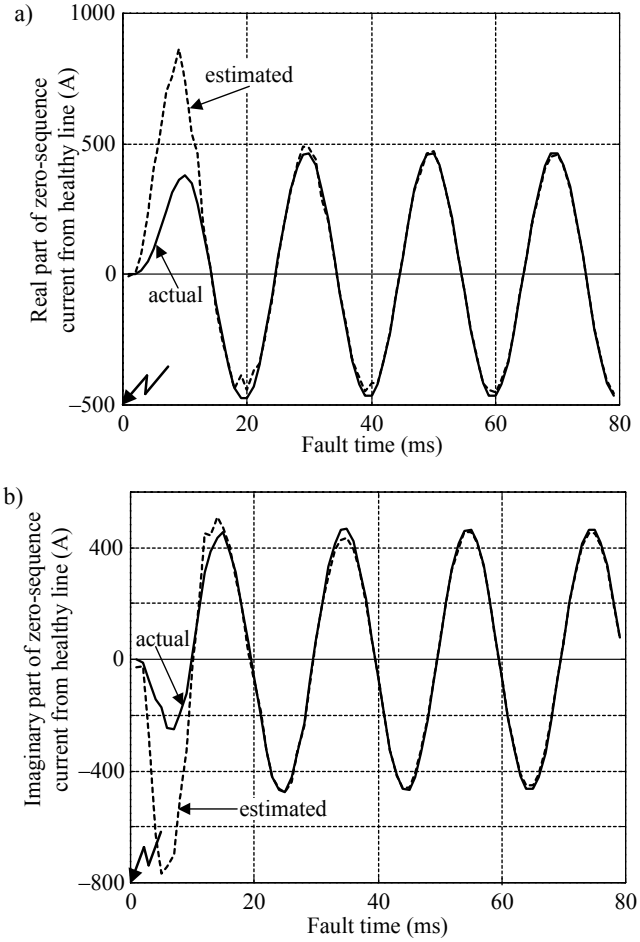

Fig. 6.14. Example of a–E fault location on a 400 kV, 120 km double-circuit line (d_{actual} = 0.9 p.u., R_F = 10 Ω) – estimated zero-sequence current from the healthy parallel line: a) real part, b) imaginary part

Figure 6.15 shows errors of estimation of the distance to fault for the parallel lines of 120 km in length under single phase-to-ground faults applied at different locations (0.1, 0.2, ..., 0.9 p.u.) with fault resistance of 10 Ω. The errors in case of no compensation for mutual coupling between the lines are big, which is very well known. For far end faults the error for such location exceeds 10% (Fig. 6.15a). On the other hand, using the fault location algorithm (6.60), the errors are quite small, especially for the case with the parallel line being in operation, for which the error does not exceed 0.3% (Fig. 6.15b). If the parallel line is switched off and earthed at both ends the errors are slightly bigger, but still acceptable.

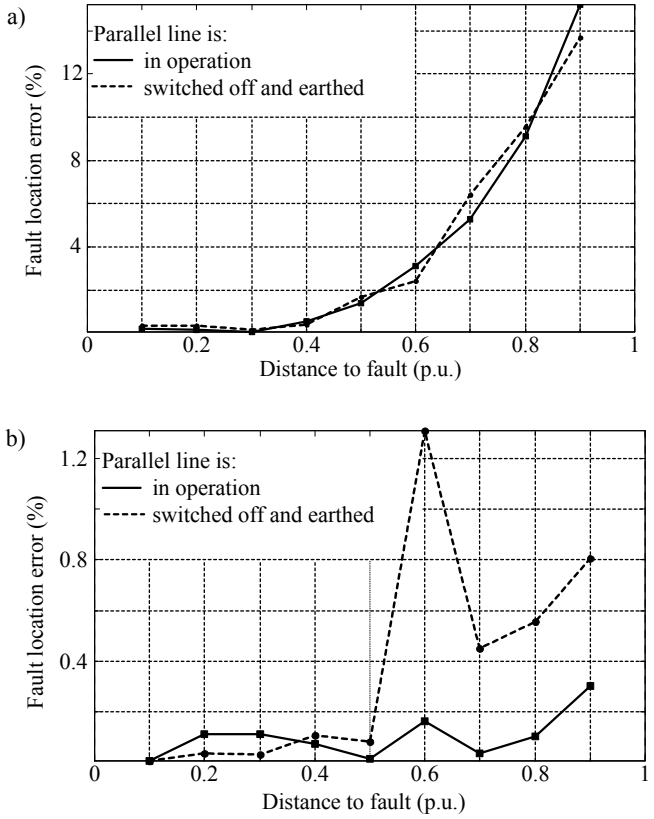

Fig. 6.15. Error in estimated distance to fault for a 120 km transmission line:
a) under no mutual coupling compensation, b) with the compensation according to (6.60)

6.10. Fault location algorithm utilising only phase current phasors

Djuric et al. presented in [23] two fault location algorithms, which use only current signals from one end of a single transmission line as input data. The first algorithm utilises the relation between symmetrical components of the total fault current. As the algorithm covers only the phase-to-earth faults, in order to extend it to the phase-to-phase-to-earth faults, the formula (4.3) and its coefficients gathered in Table 4.7 are recommended. After substituting (6.9)–(6.13) into (4.3) one obtains:

$$\frac{\underline{M}_0 \underline{I}_{S0}}{\underline{K}_0 d + \underline{L}_0} = (\underline{b}_{F1} \Delta \underline{I}_{S1} + \underline{b}_{F2} \underline{I}_{S2}) \frac{\underline{M}_1}{\underline{K}_1 d + \underline{L}_1} \tag{6.61}$$

The distance to fault can be determined from (6.61) as:

$$d = \frac{\underline{L}_1 \underline{M}_0 \underline{I}_{S0} - \underline{L}_0 \underline{M}_1 (\underline{b}_{F1} \Delta \underline{I}_{S1} + \underline{b}_{F2} \underline{I}_{S2})}{\underline{K}_0 \underline{M}_1 (\underline{b}_{F1} \Delta \underline{I}_{S1} + \underline{b}_{F2} \underline{I}_{S2}) - \underline{K}_1 \underline{M}_0 \underline{I}_{S0}} . \tag{6.62}$$

where:

$\Delta \underline{I}_{S1}$, $\underline{I}_{S2}$, $\underline{I}_{S0}$ – superimposed positive-, negative- and zero-sequence components of current from the terminal S,

$\underline{b}_{F1}$, $\underline{b}_{F2}$ – complex coefficients dependent on fault type (Table 4.7),

$\underline{K}_1$, $\underline{L}_1$, $\underline{M}_1$ – complex coefficients determined by the positive-sequence impedances of the network (Table 6.1),

$\underline{K}_0$, $\underline{L}_0$, $\underline{M}_0$ – complex coefficients determined by the zero-sequence impedances of the network (in coefficients from Table 6.1 the positive-sequence impedances have to be replaced by the respective zero-sequence impedances: $\underline{Z}_{1L}$ replaced by $\underline{Z}_{0L}$, etc.).

The first algorithm from [23] covers only the faults for which an earth is involved and thus the zero-sequence current is present. For the phase-to-phase fault one can formulate a relation between the superimposed positive- and negative-sequence currents – the second algorithm from [23]. However, the distance to fault can be determined from this relation only for specific conditions with impedances of the network for the positive- and negative-sequence being not identical. Normally, this is not so and the fault current distribution factors for the superimposed positive- and negative-sequence involved in the relation, being identical are cancelled and the relation becomes useless.

Evaluation of the fault location accuracy performed in [23] has shown the presence of relatively big errors. Fortunately, the errors do not depend on fault resistance and pre-fault power flow direction. Therefore, one can apply the correction factors, calculated in advance, for correcting the results obtained for the particular line and network topology. The other possibility is to derive the relation formula (4.3) taking into account the distributed parameter line model.

The fault location method discussed does not cover all faults, and thus cannot be considered as the only one suitable for implementing into the fault locator. It can be used as the supplement of other methods. Due to the simplicity of the algorithm, it can be utilised not only for fault location (off-line application), but also in the field of distance protection (on-line application).

6.11. Fault location with limited use of current phasors

The need for limiting use of current phasors is considered as one of the remedies for assuring high accuracy of fault location under CT saturation.

The relation between the symmetrical components of the total fault current (6.61) can be used for formulating the fault location algorithm utilising only voltage phasors [B.9]. For this purpose, the symmetrical components of the measured three-phase current are expressed as follows:

$$\Delta \underline{I}_{\mathrm{S1}} = \frac{-\Delta \underline{V}_{S1}}{\underline{Z}_{\mathrm{1S}}} \tag{6.63}$$

$$\underline{I}_{\mathrm{S2}} = \frac{-\underline{V}_{\mathrm{S2}}}{\underline{Z}_{\mathrm{1S}}} \tag{6.64}$$

$$\underline{I}_{\mathrm{S0}} = \frac{-\underline{V}_{\mathrm{S0}}}{\underline{Z}_{\mathrm{0S}}} \tag{6.65}$$

Substituting (6.63)–(6.65) into (6.61) results in the following formula for the distance to fault:

$$d = \frac{\underline{Z}_{\mathrm{1S}}\underline{L}_1\underline{M}_0\underline{V}_{\mathrm{S0}} - \underline{Z}_{\mathrm{0S}}\underline{L}_0\underline{M}_1(\underline{b}_{\mathrm{F1}}\Delta\underline{V}_{\mathrm{S1}} + \underline{b}_{\mathrm{F2}}\underline{V}_{\mathrm{S2}})}{\underline{Z}_{\mathrm{0S}}\underline{K}_0\underline{M}_1(\underline{b}_{\mathrm{F1}}\Delta\underline{V}_{\mathrm{S1}} + \underline{b}_{\mathrm{F2}}\underline{V}_{\mathrm{S2}}) - \underline{Z}_{\mathrm{1S}}\underline{K}_1\underline{M}_0\underline{V}_{\mathrm{S0}}} \tag{6.66}$$

Again, as for the fault location algorithm [23], all impedances of the network, for the positive- and zero-sequence are required to be known and only the faults involving earth are covered.

Pereira et al. presented in [130] an algorithm for fault location on transmission lines, with fault distance calculation based on steady-state measured phasors in local terminal. Voltage phasors from the fault interval only are required, while, the current phasors only from the pre-fault time, when CT saturation does not occur. When use is made of such input signals, the CT saturation does not affect the fault location accuracy. The algorithm covers all faults. It requires impedances of equivalent systems at both line terminals to be known, as well as performing the fault classification, assuming at the same time that the fault impendance is purely resistive.

The solution in [130] consists in comparing the voltage measured at the local terminal (S) with the calculated one, taking into account the objective function of the sum of errors modules:

$$F(d, R_{\mathrm{F}}) = \sum_{i=\mathrm{a,b,c}} |\underline{V}_{\mathrm{S}i}^{\mathrm{calc.}} - \underline{V}_{\mathrm{S}i}^{\mathrm{measur.}}| \tag{6.67}$$

Node voltages under fault condition are calculated [130] using three-phase injected currents in the nodes (line terminals S, R and at the fault F), and a three-phase nodal admittance matrix.

Unknown fault distance (d) and fault resistance (R_{F}) are obtained through an optimisation algorithm at the point of minimum of function (6.67).

6.12. Fault location and arc voltage estimation algorithm

Arcing character of faults is reflected in the algorithm presented in [24, 26]. This numerical algorithm is based on one terminal data and is derived in time domain. The fault location and its nature, in terms of arcing or arc-less fault, are estimated using the least error squares technique. The faulted phase voltage (Fig. 6.16) is modelled as a serial connection of fault resistance (R_F) and arc voltage (v) – represented by the model defined in formula (4.11). The algorithm is derived for the most frequent case of single phase-to earth fault.

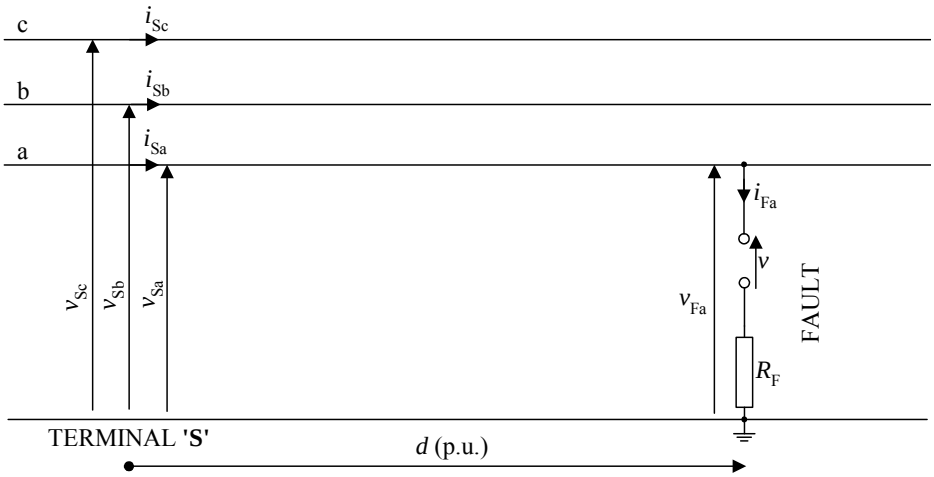

Fig. 6.16. Schematic diagram of three-phase line under phase ‘a’ to-earth fault with electrical arc and linear resistance

Considering the fault loop for the phase ‘a’ one obtains [24, 26]:

$$v_{Sa}(t) = \left[R_{1L}(i_{Sa}(t) - i_{S0}(t)) + \frac{X_{1L}}{\omega_1}\left(\frac{di_{Sa}(t)}{dt} + k_0 \frac{di_{S0}(t)}{dt} \right) \right] d + V_a \,\text{signum}(i_{S0}(t)) + R_e i_{S0}(t) + \xi(t) \tag{6.68}$$

where:

$k_0 = \dfrac{X_{0L} - X_{1L}}{X_{1L}}$, $R_e = R_{0L} d + k_a R_F$, $k_a = \dfrac{i_{Fa}(t)}{i_{S0}(t)}$,

R_{1L}, X_{1L} – positive-sequence resistance and reactance of the line,
R_{0L}, X_{0L} – zero-sequence resistance and reactance of the line,
ω_1 – fundamental radian frequency,
$i_{S0}(t)$ – zero-sequence current,

V_a – magnitude of the rectangular voltage wave: v (see equation (4.11)),
$\xi(t)$ – Gaussian noise with zero average value.
Equation (6.68) involves three unknowns:
- d (p.u.) – distance to fault,
- V_a – magnitude of the rectangular voltage wave,
- quantity R_e.

After transforming (6.68) into the discrete form, an estimation with the use of the least error squares technique [24, 26] is carried out.

Besides the basic feature of the algorithm relying on determining the nature of the fault also the distance to fault is obtained. Moreover, the approach does not require the line zero sequence resistance as input data.

6.13. Fault location on untransposed lines

The symmetrical components approach can be effectively used for locating faults on completely symmetrical lines, i.e. on transposed lines. However, the symmetry of a line can be substantially disturbed, which is the case when there are long segments of a line without transposition of the conductors (untransposed line). The other causes are related with such installations as, for example, series compensating capacitors equipped with MOVs for overvoltage protection, which introduce asymmetry upon the occurrence of unsymmetrical faults.

In order to take into account the asymmetry of a line, the phase co-ordinates approach [B.9, 121, 150, 156] has to be applied for representing a faulted line in the fault location algorithm. Voltage drop across a three phase element, represented by a column matrix of three-phase voltage **V**, can be expressed as a product of an impedance matrix (**Z**) and a column matrix of three-phase current (**I**):

$$\mathbf{V} = \mathbf{Z}\mathbf{I} \tag{6.69}$$

where:

$$\mathbf{V} = \begin{bmatrix} \underline{V}_a \\ \underline{V}_b \\ \underline{V}_c \end{bmatrix}, \quad \mathbf{I} = \begin{bmatrix} \underline{I}_a \\ \underline{I}_b \\ \underline{I}_c \end{bmatrix}, \quad \mathbf{Z} = \begin{bmatrix} \underline{Z}_{aa} & \underline{Z}_{ab} & \underline{Z}_{ac} \\ \underline{Z}_{ab} & \underline{Z}_{bb} & \underline{Z}_{bc} \\ \underline{Z}_{ac} & \underline{Z}_{bc} & \underline{Z}_{cc} \end{bmatrix}.$$

For a power line, which is perfectly transposed, the diagonal components of the impedance matrix **Z** (self impedances: subscript ‘s’) as well as all the off-diagonal elements (mutual impedances: subscript ‘m’) are accordingly equal to each other:

$$\underline{Z}_s = \underline{Z}_{aa} = \underline{Z}_{bb} = \underline{Z}_{cc} \tag{6.70}$$

$$\underline{Z}_{\mathrm{m}} = \underline{Z}_{\mathrm{ab}} = \underline{Z}_{\mathrm{bc}} = \underline{Z}_{\mathrm{ac}} \tag{6.71}$$

and as a result, one obtains the following relations in which impedances of a line for the positive- and zero-sequence are involved:

$$\underline{Z}_{\mathrm{s}} = \frac{\underline{Z}_{0\mathrm{L}} + \underline{Z}_{1\mathrm{L}}}{3} \tag{6.72}$$

$$\underline{Z}_{\mathrm{m}} = \frac{\underline{Z}_{0\mathrm{L}} - \underline{Z}_{1\mathrm{L}}}{3} \tag{6.73}$$

Models of a transmission network with a single line, for pre-fault and fault conditions, respectively, are presented in Figs. 6.17 and 6.18. In Figs. 6.19 and 6.20, a double-circuit line transmission network arrangement is presented. The voltages induced due to mutual coupling of the line circuits are denoted by rhombus symbols, under which the value of the particular voltage induced (contained in a dashed rectangle) is specified.

In the models from Figs. 6.17 through 6.20, only the longitudinal line parameters are taken into account, while the shunt line parameters are neglected. Such simplification is applied with the aim of obtaining compact formulae for the distance to fault. Then, in order to improve fault location accuracy, as required for the lines stretching over long distances, the compensation for the shunt line capacitances (Section 6.15: Compensation for shunt capacitance effect) can be performed.

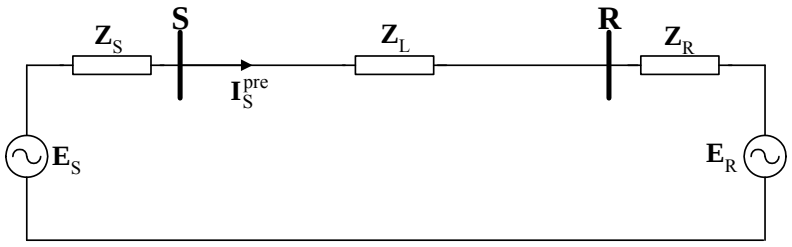

Fig. 6.17. Model of transmission network with single line for pre-fault conditions

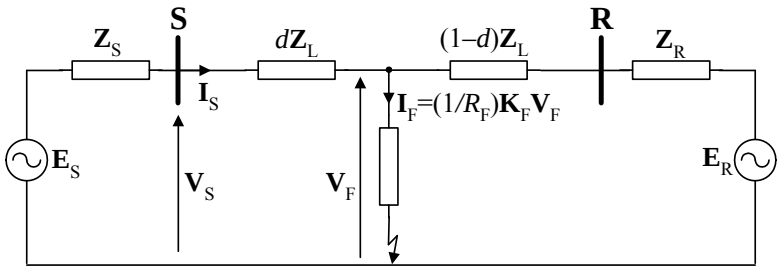

Fig. 6.18. Model of transmission network with single line for fault conditions

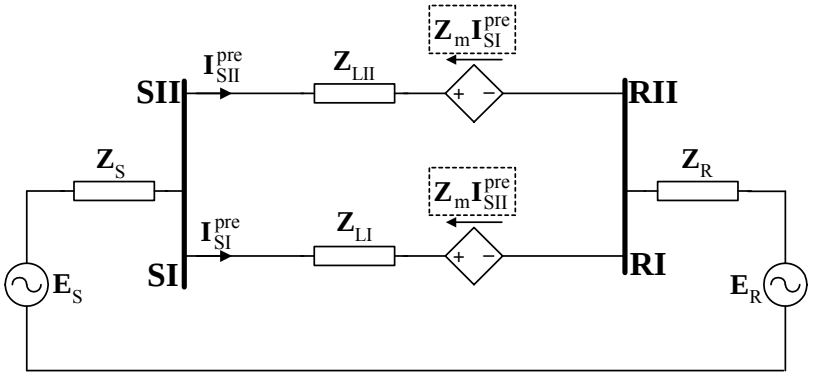

Fig. 6.19. Model of a transmission network with double-circuit line for pre-fault conditions

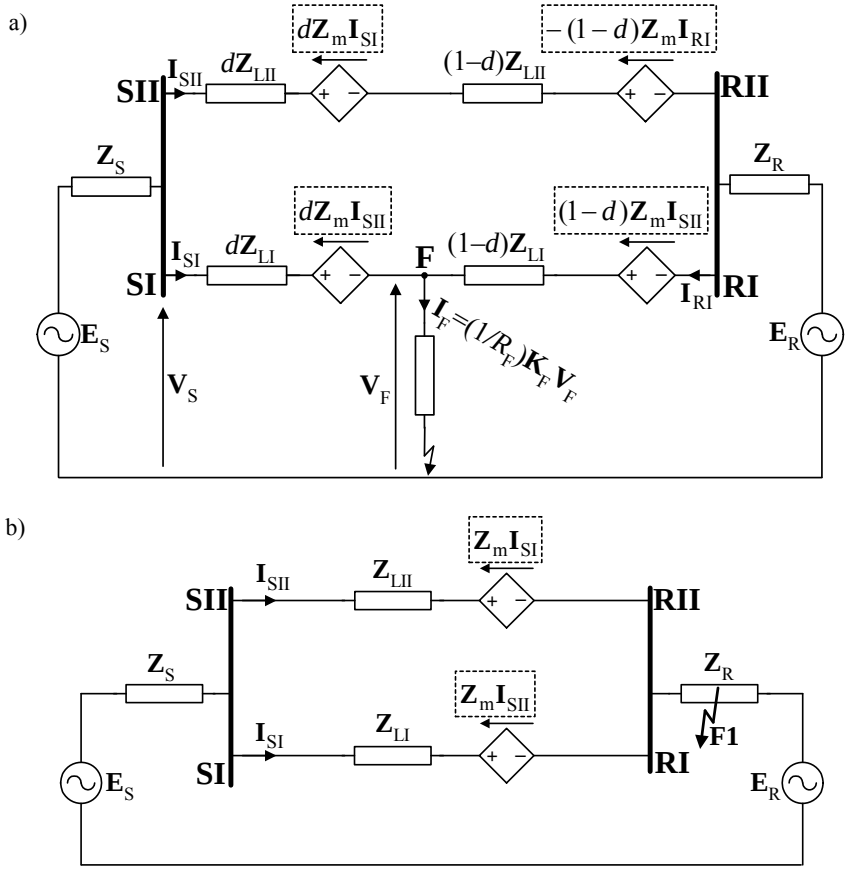

Fig. 6.20. Model of a transmission network with double-circuit line for:
a) fault F on line LI, b) fault F1 overreaching line length

Transmission network with a double-circuit line, as a more general circuit, is taken further for deriving the fault location algorithm. Location is considered as performed on a faulted line LI, utilising the three-phase currents: $\mathbf{I}_{SI}^{pre}$, $\mathbf{I}_{SII}^{pre}$, $\mathbf{I}_{SI}$, $\mathbf{I}_{SII}$ and three-phase voltage $\mathbf{V}_S$ (Figs. 6.19 and 6. 20). So, it is assumed that the one-end fault locator is installed at the terminal S. Besides these input signals of the fault locator, also the total fault current $\mathbf{I}_F$ and the current $\mathbf{I}_{RI}$ from the remote terminal RI are marked in Fig. 6.20a. These currents are immeasurable for the one-end fault locator installed at the bus SI–SII. However, the currents $\mathbf{I}_F$, $\mathbf{I}_{RI}$ will be involved in the fault location algorithm derivation. During the derivation they will be eliminated as a result of being expressed by means of the measurable quantities and network parameters.

Considering the path formed by emfs: $\mathbf{E}_S$, $\mathbf{E}_R$, and impedances: $\mathbf{Z}_S$, $d\mathbf{Z}_{LI}$, $(1-d)\mathbf{Z}_{LI}$, $\mathbf{Z}_R$ in the circuit of Fig. 6.20a, one obtains the following matrix formula:

$$\Delta\mathbf{E} = \mathbf{E}_S - \mathbf{E}_R = (\mathbf{Z}_S + d\mathbf{Z}_{LI})\mathbf{I}_{SI} - ((1-d)\mathbf{Z}_{LI} + \mathbf{Z}_R)\mathbf{I}_{RI} + (\mathbf{Z}_S + \mathbf{Z}_R)\mathbf{I}_{SII} + \mathbf{Z}_m\mathbf{I}_{SII} \quad (6.74)$$

where impedance matrices for the line LI ($\mathbf{Z}_{LI}$) and for mutual coupling between line circuits ($\mathbf{Z}_m$) are:

$$\mathbf{Z}_{LI} = \begin{bmatrix} \underline{Z}_{LI\_aa} & \underline{Z}_{LI\_ab} & \underline{Z}_{LI\_ac} \\ \underline{Z}_{LI\_ab} & \underline{Z}_{LI\_bb} & \underline{Z}_{LI\_bc} \\ \underline{Z}_{LI\_ac} & \underline{Z}_{LI\_bc} & \underline{Z}_{LI\_cc} \end{bmatrix} \qquad \mathbf{Z}_m = \begin{bmatrix} \underline{Z}_{m\_aa} & \underline{Z}_{m\_ab} & \underline{Z}_{m\_ac} \\ \underline{Z}_{m\_ab} & \underline{Z}_{m\_bb} & \underline{Z}_{m\_bc} \\ \underline{Z}_{m\_ac} & \underline{Z}_{m\_bc} & \underline{Z}_{m\_cc} \end{bmatrix}$$

For a completely symmetrical line, the elements of the impedance matrix $\mathbf{Z}_{LI}$ are determined as in (6.72), while all the components of the mutual coupling impedance $\mathbf{Z}_m$ are identical:

$$\underline{Z}_{m\_aa} = \underline{Z}_{m\_bb} = \underline{Z}_{m\_cc} = \underline{Z}_{m\_ab} = \underline{Z}_{m\_ac} = \underline{Z}_{m\_bc} = \frac{\underline{Z}_{0m}}{3} \quad (6.75)$$

where $\underline{Z}_{0m}$ – mutual coupling impedance for the zero-sequence.

Assuming that emfs of the sources do not change due to a fault, the column matrix $\Delta\mathbf{E}$ determined in (6.74) can be expressed based on the pre-fault model (Fig. 6.19) as [156]:

$$\Delta\mathbf{E} = \mathbf{E}_S - \mathbf{E}_R = (\mathbf{Z}_S + \mathbf{Z}_R + \mathbf{Z}_{LI})\mathbf{I}_{SI}^{pre} + (\mathbf{Z}_S + \mathbf{Z}_m + \mathbf{Z}_R)\mathbf{I}_{SII}^{pre} \quad (6.76)$$

The current at the remote substation R flowing in the line LI ($\mathbf{I}_{RI}$), which is immeasurable, can be determined from (6.74) as:

$$\mathbf{I}_{RI} = ((1-d)\mathbf{Z}_{LI} + \mathbf{Z}_R)^{-1}((\mathbf{Z}_S + d\mathbf{Z}_{LA})\mathbf{I}_{SI} + (\mathbf{Z}_S + \mathbf{Z}_R + \mathbf{Z}_m)\mathbf{I}_{SII} - \Delta\mathbf{E}) \quad (6.77)$$

Column matrices of the voltage across a fault path and total fault current (Fig. 6.20a) are determined accordingly:

$$\mathbf{V}_F = \mathbf{V}_S - d\mathbf{Z}_{LI}\mathbf{I}_{SI} - d\mathbf{Z}_m\mathbf{I}_{SII} \tag{6.78}$$

$$\mathbf{I}_F = \mathbf{I}_{SI} + \mathbf{I}_{RI} \tag{6.79}$$

A general fault model with use of the matrix notation was described in Chapter 4: formula (4.4) and Table 4.8. Taking into account the general fault model (4.4) and equations (6.78)–(6.79) one obtains [156]:

$$\frac{1}{R_F}\mathbf{K}_F(\mathbf{V}_S - d\mathbf{Z}_{LI}\mathbf{I}_{SI} - d\mathbf{Z}_m\mathbf{I}_{SII}) = \mathbf{I}_{SI} + \mathbf{I}_{RI} \tag{6.80}$$

Combining (6.77) and (6.80), yields after the arrangements the following matrix equation:

$$\mathbf{A}d^2 - \mathbf{B}d + \mathbf{C} - \mathbf{D}R_F = \mathbf{0} \tag{6.81}$$

where:

$\mathbf{A} = \mathbf{Z}_{LI}\mathbf{K}_F\mathbf{Z}_{LI}\mathbf{I}_{SI} + \mathbf{Z}_{LI}\mathbf{K}_F\mathbf{Z}_m\mathbf{I}_{SII}$,

$\mathbf{B} = \mathbf{Z}_{LI}\mathbf{K}_F(\mathbf{V}_S + \mathbf{Z}_{LI}\mathbf{I}_{SI}) + \mathbf{Z}_R\mathbf{K}_F\mathbf{Z}_{LI}\mathbf{I}_{SI} + \mathbf{Z}_m\mathbf{K}_F(\mathbf{Z}_{LI} + \mathbf{Z}_R)\mathbf{I}_{SII}$,

$\mathbf{C} = (\mathbf{Z}_{LI} + \mathbf{Z}_R)\mathbf{K}_F\mathbf{V}_S$,

$\mathbf{D} = (\mathbf{Z}_S + \mathbf{Z}_{LI} + \mathbf{Z}_R)(\mathbf{I}_{SI} - \mathbf{I}_{SI}^{pre}) + (\mathbf{Z}_S + \mathbf{Z}_R + \mathbf{Z}_m)(\mathbf{I}_{SII} - \mathbf{I}_{SII}^{pre})$.

Transforming (6.81) into the scalar form one obtains the following quadratic formula for complex numbers:

$$\underline{A}_2 d^2 - \underline{A}_1 d + \underline{A}_0 - R_F = 0 \tag{6.82}$$

where:

$$\underline{A}_2 = \mathbf{PA}, \quad \underline{A}_1 = \mathbf{PB}, \quad \underline{A}_0 = \mathbf{PC}, \quad \mathbf{P} = \frac{\mathbf{D}^T}{\mathbf{D}^T\mathbf{D}},$$

superscript T denotes transposition of the matrix.

The scalar quadratic equation (6.82) can be resolved into the real and imaginary parts, from which one calculates the distance to fault (d) and fault resistance (R_F), analogously as was presented for the formula (6.43).

In the case of a double-circuit line arrangement one ought to discriminate faults overreaching a total line length, i.e. occurring in a remote system (Fig. 6.20b: fault F1). This can be performed by analysing the following column matrix:

$$\mathbf{F}_1 = (\mathbf{Z}_{LI} - \mathbf{Z}_m)\mathbf{I}_{SI} - (\mathbf{Z}_{LII} - \mathbf{Z}_m)\mathbf{I}_{SII} \tag{6.83}$$

which for such faults has to possess all the components equal to zero. However, in practice, due to the presence of measurement errors, some threshold has to applied.

Adaptation of the fault location formula (6.82) (derived for a double-circuit line) to the case of a single line requires deleting all the components relevant to mutual coupling of the line circuits ($\mathbf{Z}_m$) as well as all the components involving currents from the sound line ($\mathbf{I}_{SII}$, $\mathbf{I}_{SII}^{pre}$).

In [B.9], a quantitative evaluation of the fault location accuracy, with use of ATP-EMTP generated fault data has been performed. It was shown that for the transmission system studied there, the presented algorithm allows the fault location accuracy to be improved up to 2%, compared to the symmetrical components approach (applied after averaging the diagonal and off-diagonal elements of the line impedance matrix). Note that such improvement was obtained for comparatively small asymmetry of the line under consideration [B.9]. In the presence of larger asymmetry of the line, the expected improvement can be considerably higher.

6.14. Fault location on series-compensated lines

6.14.1. Representation of SC&MOV bank

Series capacitors equipped with MOVs (Fig. 6.21) create certain problems for transmission line protective devices and fault locators. In order to cope with them, adequate representations of SCs&MOVs have to be developed, being required for both distance protection and fault location purposes.

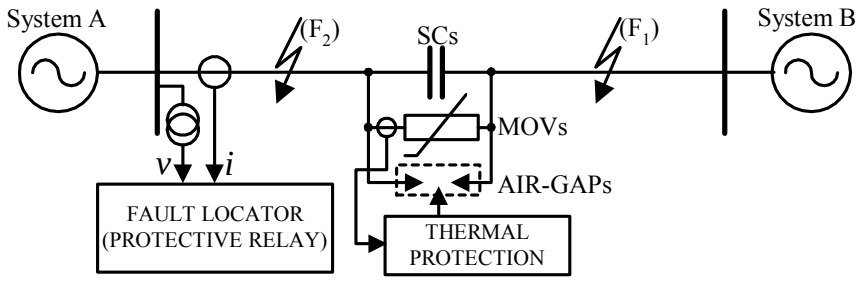

Fig. 6.21. Scheme of transmission line with series compensation in mid-line

The fundamental frequency concept has been utilised for representing SCs&MOVs for fault location purposes in [55, 150]. In turn, a digital algorithm for estimating a voltage drop across the bank of SC&MOV has been considered for application to fault location in [140] and for protective relaying purposes in [153]. This estimation algorithm is based on the on-line solving of the strongly non-linear differential equation and is of recursive form.

Fundamental frequency equivalenting of SC&MOV

Figure 6.22 presents the equivalenting principle [55, 150]. The parallel connection of a fixed series capacitor (C) and its non-linear protecting resistor MOV (Fig. 6.22a) is represented for the steady state by the fundamental frequency equivalent (Fig. 6.22b). The equivalent is of the form of a series branch with the resistance (R_v) and the capacitive reactance (X_v), both dependent on the amplitude of a current ($|\underline{I}_v|$) entering the SC&MOV bank. Fundamental frequency currents and voltage drops denoted in the original scheme (Fig. 6.22a) and in the equivalent (Fig. 6.22b) must match each other. The equivalenting has to be done by scanning through different amplitudes of the fault current entering the parallel connection of the SC and MOV. This can be achieved, for example, by changing the voltage magnitude of the supplying source (Fig. 6.23).

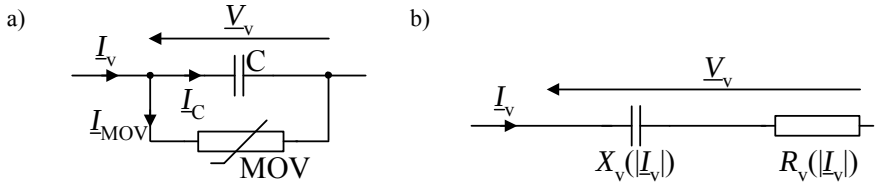

Fig. 6.22. Principle of SC&MOV equivalenting:
a) original circuit, b) scheme of the fundamental frequency equivalent

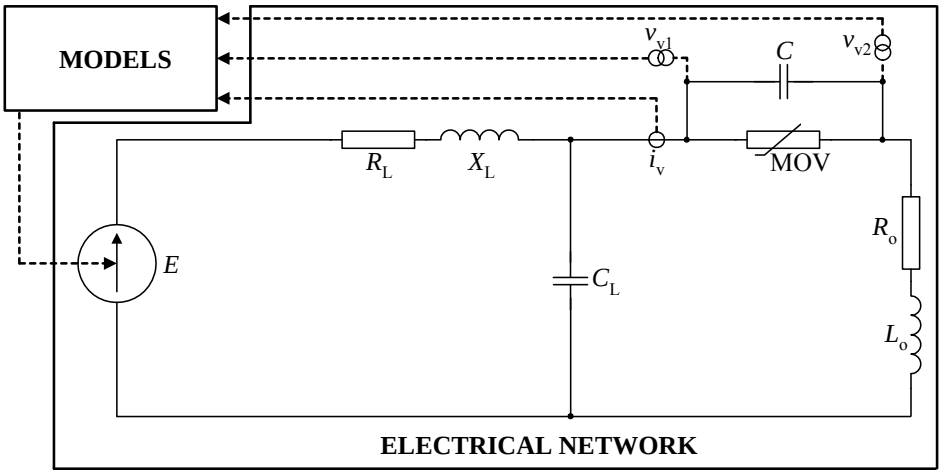

Fig. 6.23. Principle of using ATP-EMTP for equivalenting

Figure 6.23 presents the principle of equivalenting performed with use of ATP-EMTP [B.5] simulations. The circuit considered is supplied by a source for which the voltage magnitude (E) is controlled in the MODELS unit. The inductive impedance (R_L, X_L)

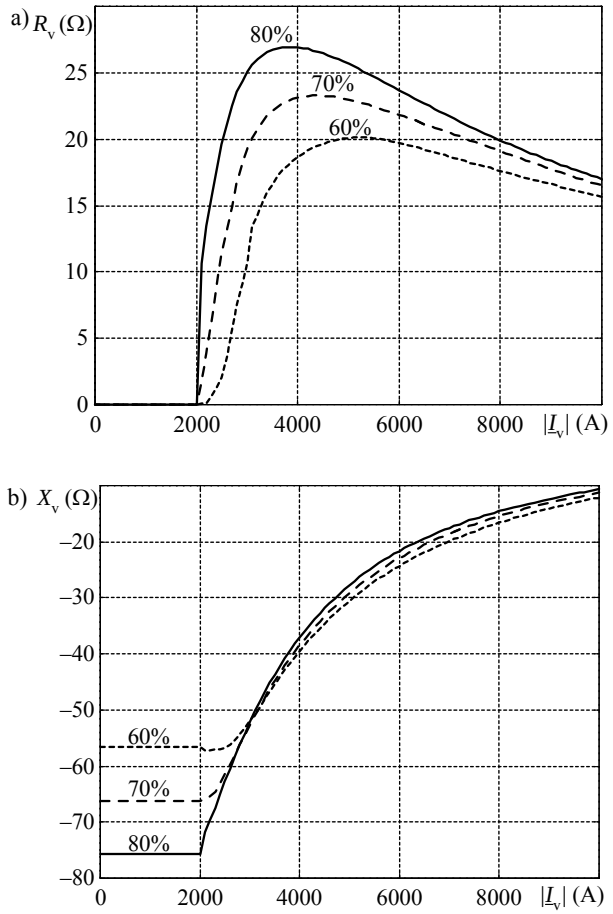

Fig. 6.24. Fundamental frequency equivalents under different compensation rates for a 400 kV, 300 km line: a) equivalent resistance, b) equivalent reactance

represents the resultant impedance of the source and the line segment from the measuring point up to the SC&MOV installation point. The capacitance (C_L) represents the shunt capacitance of this line segment, while R_o and X_o – the equivalent impedance for the remote faulted line segment, together with the remote supplying system. Exchange of the signals, between the units of ATP-EMTP: the MODELS and the Electrical Network, is shown in Fig. 6.23. The simulation time interval is subdivided into subintervals with different magnitudes of the voltage source (the number of subintervals is equal to the required number of points on the equivalent characteristics). The voltage magnitude is determined in the MODELS unit and sent to the Electrical Network. Length of the simulation subintervals is set in such a way that steady state measurement is achieved in each subinterval. This requires setting wider subintervals for smaller voltage magnitudes

when long lasting transients are present due to linear operation of MOVs. On the other hand, for higher supplying voltage magnitudes, the MOVs operate in a non-linear range and the transients are damped faster, and thus shorter subintervals can be designated. Voltages at both terminals of the compensating capacitor (v_{v1}, v_{v2}) and the current entering the SC&MOV complex (i_V) are picked up from the Electrical Network and sent to the MODELS unit. Then, these signals are transferred to Matlab program for determining fundamental frequency phasors of the processed signals: $\underline{V}_v$, $\underline{I}_v$. From these phasors the equivalent characteristics (Fig. 6.24) are determined.

Results of the equivalenting for different rates of the capacitor compensation, namely for 60%, 70% and 80% rates, applied to a 400 kV, 300 km transmission line are shown in Fig. 6.24. When determining the equivalents presented in Fig. 6.24, it was assumed that the MOVs have identical characteristics, while different SCs are applied for providing 60%, 70% or 80% compensation of the line, respectively. It is seen that the capacitance of the SC influences mainly the equivalent resistance (R_v). For the analysed compensation rates the equivalent reactance (X_v) differs only for low amplitudes of the fault current (when the MOVs operate linearly or almost linearly).

Using the phase co-ordinates approach, the three-phase equivalent of SCs&MOVs can be presented with the following matrix [150]:

$$\mathbf{Z}_v(|\mathbf{I}|) = \begin{bmatrix} \underline{Z}_{va}(|\underline{I}_a|) & 0 & 0 \\ 0 & \underline{Z}_{vb}(|\underline{I}_b|) & 0 \\ 0 & 0 & \underline{Z}_{vc}(|\underline{I}_c|) \end{bmatrix} \tag{6.84}$$

Digital algorithm for estimation of voltage drop across SC&MOV

Let us consider a parallel connection of the series capacitor SC, and the MOV shown in Fig. 3.13a and also in Fig. 6.21. Assuming the analytical approximation of the MOV characteristic in the form of (3.4), the non-linear circuit of SC&MOV can be described by the following non-linear differential equation [153]:

$$C\frac{dv_v}{dt} + P\left(\frac{v_v}{V_{REF}}\right)^q - i_v = 0 \tag{6.85}$$

In this equation, all the parameters are known and constant; the current i_v entering the bank is available (since neglecting the shunt parameters of the line, this is the current in the substation where the fault locator is installed); while the voltage drop v_v is to be calculated. Thus, one needs to transform the continuous-time differential equation (6.85) into its algebraic discrete-time form. The 2nd order Gear differentiation rule has been taken for this purpose. The following substitutions apply to (6.85):

$$i_v(t) \to i_{v(n)} \qquad v_v(t) \to v_{v(n)} \tag{6.86}$$

$$\frac{dv_{\mathrm{v}}(t)}{dt} \to \mathrm{D}\,(3v_{\mathrm{v}(n)} - 4v_{\mathrm{v}(n-1)} + v_{\mathrm{v}(n-2)}) \tag{6.87}$$

where:

$$\mathrm{D} = \frac{2\pi f_1}{2\sqrt{(1-\cos(\alpha))^4 + (2\sin(\alpha) - 0.5\sin(2\alpha))^2}} \text{ or}$$

$$\mathrm{D} = \frac{2\pi f_1}{\sqrt{26 - 32\cos(\alpha) + 6\cos(2\alpha)}},$$

$\alpha = 2\pi f_1 T_{\mathrm{s}}$,

f_1 – rated fundamental frequency,

T_{s} – sampling period,

n – discrete time index.

Substituting (6.86)–(6.87) into (6.85) yields the discrete-time equation:

$$F(x_{(n)}) = A_{\mathrm{q}} x_{(n)}^{q} + A_1 x_{(n)} - A_0 = 0 \tag{6.88}$$

in which:

$$x_{(n)} = \frac{v_{\mathrm{v}(n)}}{V_{\mathrm{REF}}}, \qquad A_{\mathrm{q}} = P, \qquad A_1 = 3\,\mathrm{D}\,C V_{\mathrm{REF}}, \qquad A_0 = i_{\mathrm{v}(n)} + \frac{A_1}{3}(4x_{(n-1)} - x_{(n-2)}).$$

Equation (6.88) is to be solved for $x_{(n)}$ (the p.u. value of the sought voltage drop $v_{\mathrm{v}(n)}$ at the current sampling instant n). The two parameters of this equation: A_{q} and A_1 are the constants, while A_0 depends on the sample of the current ($i_{\mathrm{v}(n)}$) entering the bank and the two historical samples of the p.u. voltage drop $(x_{(n-1)}, x_{(n-2)})$. In order to ensure good convergence of the algorithm, appropriately modified Newton–Raphson method has been used. The form (6.88) of the equation is numerically efficient for "*small*" values of A_0 while for "*large*" values of A_0, it should be re-written to:

$$F(y_{(n)}) = A_{\mathrm{q}} y_{(n)} + A_1 (y_{(n)})^{\frac{1}{q}} - A_0 = 0 \tag{6.89}$$

(where: $y_{(n)} = x_{(n)}^{q}$) and solved for $y_{(n)}$.

The threshold value of A_0 alternating the two optimal formulae (6.88) and (6.89) is:

$$A_0^{\#} = A_{\mathrm{q}} \left(\left(\frac{A_1}{qA_{\mathrm{q}}} \right)^{\frac{1}{q-1}} \right)^{q} + A_1 \left(\left(\frac{A_1}{qA_{\mathrm{q}}} \right)^{\frac{1}{q-1}} \right) \tag{6.90}$$

The formula (6.88) is solved iteratively with the Newton–Raphson method by applying the following algorithm:

$$x_{(n)\text{new}} = x_{(n)\text{old}} - \frac{A_\text{q} x_{(n)\text{old}}{}^{q} + A_\text{l} x_{(n)\text{old}} - A_0}{q A_\text{q} x_{(n)\text{old}}{}^{q-1} + A_\text{l}} \tag{6.91}$$

The formula (6.89) is solved iteratively with the Newton–Raphson method by applying:

$$y_{(n)\text{new}} = y_\text{old} - \frac{A_\text{q} y_{(n)\text{old}} + A_\text{l} y_{\text{old}(n)}{}^{\frac{1}{q}} - A_0}{A_\text{q} + \frac{A_\text{l}}{q} y_{\text{old}(n)}{}^{\left(\frac{1-q}{q}\right)}} \tag{6.92}$$

Certainly, if (6.88) is applied, the sought voltage drop (in Volts) is eventually computed from:

$$v_{\text{v}(n)} = x_{(n)} V_\text{REF} \tag{6.93}$$

while, if (6.89) is applied, the voltage drop (in Volts) is obtained from:

$$v_{\text{v}(n)} = (y_{(n)})^{(q^{-1})} V_\text{REF} \tag{6.94}$$

The algorithm is accurate and numerically efficient owing to the following factors [153]:

- The difference in the signal levels (voltage in thousands while current in tens or hundreds) is removed by applying the p.u. value of the voltage drop.
- The strong non-linearity of the equation is moderated by using either of the two optimal formulae: (6.88) or (6.89), depending on the operating point on the characteristic of the MOV.
- The algorithm ensures satisfactory accuracy for time steps as large as 1/20th of the fundamental frequency cycle (it needs 2–3 iterations to find a solution). For shorter time steps (sampling frequency over 1000 Hz) the algorithm performs even better.

It is assumed that the pre-fault current is available and the estimation algorithm is started *a posteriori*, few samples before detecting the fault. Thus, the algorithm is initiated in the pre-fault steady state using the zero conditions, i.e. assuming:

$$x_{(n-1)} = 0 \qquad x_{(n-2)} = 0 \tag{6.95}$$

In the pre-fault conditions, the compensating bank is a pure capacitance (since the MOV almost does not conduct a current) and when using the algorithm with zero initial conditions (6.95), a certain constant offset to the accurate solution is added. In order to remove this offset, it is recommended to apply the following filter:

$$\lambda_{(n)} = \frac{1}{2(\cos(\alpha)-1)}(x_{(n)} - 2x_{(n-1)} + x_{(n-2)}) \tag{6.96}$$

where angle α, as in (6.87).

Implementation of the estimation algorithm, for the case where only the first form (6.88) is utilised, into the Matlab function [B.27] follows. The task of incorporating the second form (6.89) to this Matlab function is left for the reader.

% Matlab function for estimating voltage drop across SC&MOV

```
function vMOVa=MOV_fun(ia);    % 'ia' is the input current of the algorithm
n_iter=2;   % here fixed number of iterations (for example: 2) for solving equation is set
C=4.8119e-005;      % capacitance of series capacitor
P=1000.0;           % reference current of MOV characteristic
q=23;               % exponent of MOV characteristic
V_REF=150000.0;  % reference voltage of MOV characteristic
f=50;               % rated power system frequency
fs=1000;            % sampling frequency
omega1=2*pi*f;      % rated power system angular frequency
a=omega1/fs;        % angle corresponding to single sampling interval
kF=0.5/(cos(a)–1);  % gain for the filter used for rejecting the DC component
D=omega1/sqrt(26–32*cos(a)+6*cos(2*a));    % constant for the 2nd order GEAR rule
A_q=P;                  % constant
A_1=3*D*C*V_REF;        % constant
l=size(ia);             % size of input current
x=[0;0;0];              % initial conditions
        for n=1:l(1),       % processing with time
        A_0=ia(n)+A_1*[0 4 –1]*x/3;   % quantity from the numeric formula
                for k=1:n_iter,          % perform iterative calculations
                z=abs(x(1));
                        if z,
                        z=log(z);
                        z=A_q*exp(q*z);
                                if x(1)<0, z=–z; end;
```

```
                    z1=q*z/x(1);
                else,
                z1=0;
                end;
                x(1)=x(1)–(z+A_1*x(1)–A_0)/(z1+A_1);
        end,
        if n<4,                 % reject the constant offset
        xF(n)=kF*[1 –2 1]*x;
        end,
        if n==3,
        xF(n)=kF*[1 –2 1]*x;
        x(1)=ia(n)/A_1+(4*xF(n)–xF(n–1))/3;
        x(2)=xF(n);
        end,
        x(3)=x(2);
        x(2)=x(1);
        vMOVa_pu(n,1)=x(1);             % result in per units
        end;
vMOVa=vMOVa_pu*V_REF;           % result in Volts
```

Figure 6.25 illustrates operation of the presented estimation algorithm for a 400 kV 300 km line under a single phase-to-earth fault just behind the compensating bank (as seen from the bus S), with 5 Ω fault resistance.

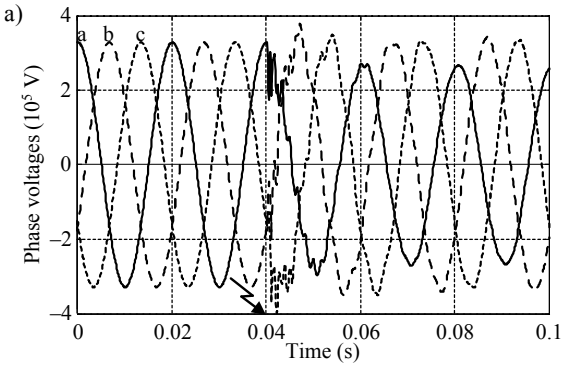

(Fig. 6.25 to be continued)

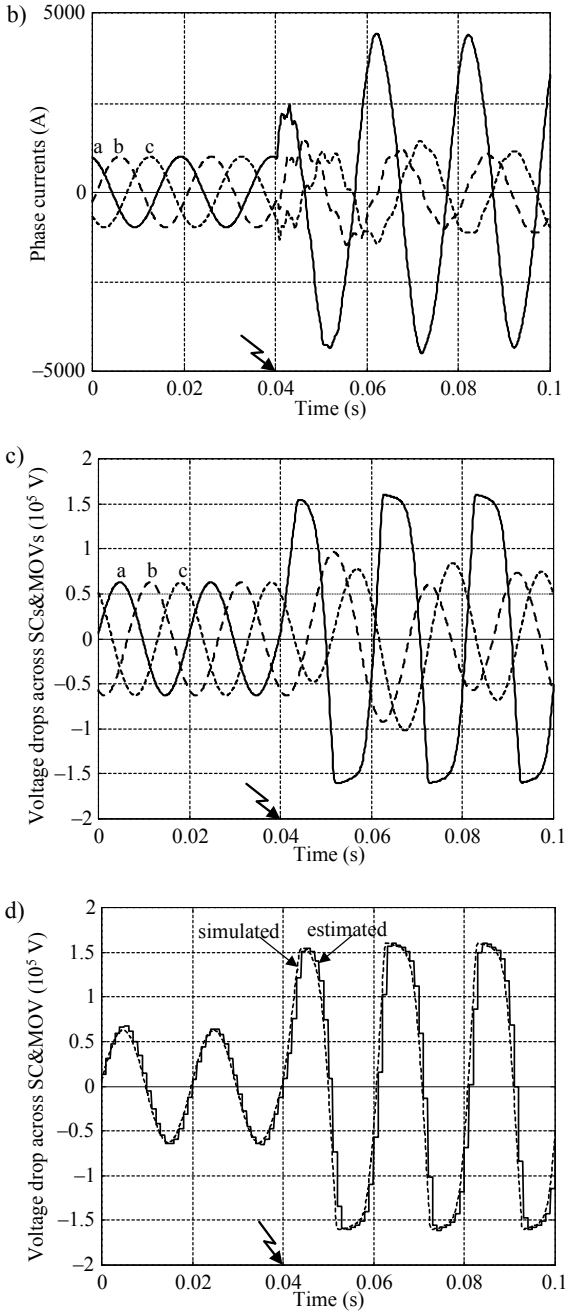

Fig. 6.25. Sample fault: a) measured phase voltages, b) measured phase currents (input to the algorithm), c) voltage drops across SCs&MOVs from simulation, d) voltage drop across SC&MOV in the faulted phase – from simulation, and estimated (output from the algorithm)

In the measured phase voltages (Fig. 6.25a) and phase currents (Fig. 6.25b) one observes the characteristic distortion of the waveforms. It is distinctive that, in contrast to uncompensated line case, there are no DC components in currents. Limiting of the voltage drop across SC&MOV from the faulted phase to the level equal to around the reference voltage of MOV (V_{REF}) is observed (Fig. 6.25c). On the other hand, the MOVs from the sound phases operate linearly, which results in slowly decaying sub-harmonic oscillations (Fig. 6.25c). Figure 6.25d shows the actual voltage drop across the SC&MOV from the faulted phase (EMTP simulation) and the signal estimated with the algorithm presented. The accuracy of the voltage reconstruction is very high and the difference between the actual and calculated values is very small. Note that the voltage drop is calculated at the sampling instants only (1000 Hz sampling frequency was assumed here) and therefore the calculated voltage drop is presented as a stair waveform.

6.14.2. Fault location algorithm for single series-compensated lines

Let us consider the one-end fault location on a single-circuit transmission line with series compensation inserted at the mid-line: at the distance d_{SC} (p.u.) from the terminal S. It is assumed that the fault locator is installed at the bus S (Fig. 6. 21). For such a configuration of the series-compensated line there is a need for applying two subroutines, which are designed for locating faults:

- behind SCs&MOVs (fault F1, Fig. 6. 21) – the subroutine SUB_1,
- in front of SCs&MOVs (fault F2, Fig. 6. 21) – the subroutine SUB_2.

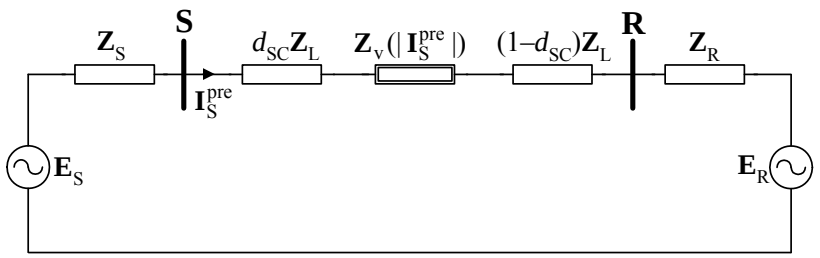

Fig. 6.26. Equivalent diagram for a transmission system with single line compensated at midpoint, for pre-fault conditions (superscript: pre)

The position of a fault with respect to the SCs&MOVs (behind or in front of them) is of random nature, therefore, in order to get the final result, the selection of the valid subroutine, i.e. the subroutine which yields the result consistent with the real fault, is necessary.

The fault location algorithm presented here belongs to the phasor-based category [285]. In this algorithm, the SCs&MOVs are represented by the three-phase fundamental frequency equivalent (6.84). In the following circuit diagrams they are pre-

sented by the rectangle impedance symbol, but drawn with double line, with the equivalent impedance being specified. For example, in the equivalent circuit diagram for pre-fault conditions (Fig. 6.26) the SCs&MOVs equivalent is denoted by $\mathbf{Z}_{\mathrm{v}}(|\mathbf{I}_{\mathrm{S}}^{\mathrm{pre}}|)$.

Subroutine SUB_1 – for faults behind SCs

In this case (Fig. 6.27), the current flowing through the SCs&MOVs is directly measured by the fault locator at the terminal S. The following applies to the faulted network (Fig. 6.27):

$$\mathbf{E}_{\mathrm{S}} - \mathbf{E}_{\mathrm{R}} = (\mathbf{Z}_{\mathrm{L}} + d_1\mathbf{Z}_{\mathrm{L}} + \mathbf{Z}_{\mathrm{v}}(|\mathbf{I}_{\mathrm{S}}|))\mathbf{I}_{\mathrm{S}} - ((1-d_1)\mathbf{Z}_{\mathrm{L}} + \mathbf{Z}_{\mathrm{R}})\mathbf{I}_{\mathrm{R}} \tag{6.97}$$

$$\mathbf{V}_{\mathrm{S}} - \mathbf{V}_{\mathrm{F}} = (d_1\mathbf{Z}_{\mathrm{L}} + \mathbf{Z}_{\mathrm{v}}(|\mathbf{I}_{\mathrm{S}}|))\mathbf{I}_{\mathrm{S}} \tag{6.98}$$

$$\mathbf{I}_{\mathbf{F}} = \mathbf{I}_{\mathrm{S}} + \mathbf{I}_{\mathrm{R}} \tag{6.99}$$

where $d_{\mathrm{SC}} < d_1 < 1$ is the sought fault distance (p.u.).

The pre-fault network (Fig. 6.26) is described by:

$$\mathbf{E}_{\mathrm{S}} - \mathbf{E}_{\mathrm{R}} = (\mathbf{Z}_{\mathrm{S}} + \mathbf{Z}_{\mathrm{L}} + \mathbf{Z}_{\mathrm{v}}(|\mathbf{I}_{\mathrm{S}}^{\mathrm{pre}}|) + \mathbf{Z}_{\mathrm{R}})\mathbf{I}_{\mathrm{S}}^{\mathrm{pre}} \tag{6.100}$$

where the superscript ‘pre’ stands for the pre-fault values of three-phase current.

The fault equation (4.4) completes the model:

$$\mathbf{I}_{\mathrm{F}} = \frac{1}{R_{\mathrm{F1}}}\mathbf{K}_{\mathrm{F}}\mathbf{V}_{\mathrm{F}} \tag{6.101}$$

where R_{F1} – unknown resistance involved in the fault.

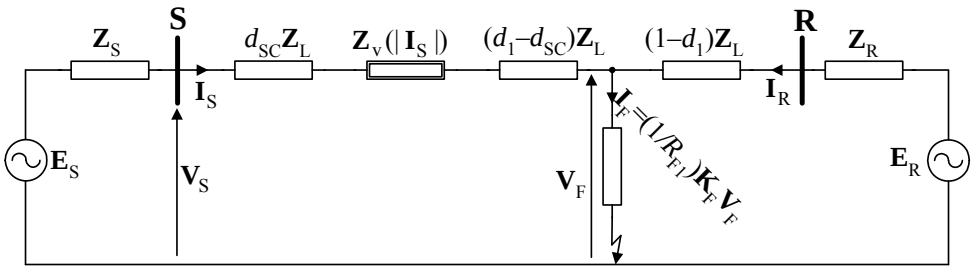

Fig. 6.27. Subroutine SUB_1 for faults occurring behind the compensating capacitors – equivalent circuit diagram for transmission network with single line compensated at midpoint

Combining (6.97)–(6.101) results in the following matrix formula:

$$\mathbf{A}d_1^2 - \mathbf{B}d_1 + \mathbf{C} - \mathbf{D}R_{\mathrm{F1}} = \mathbf{0} \tag{6.102}$$

where:

$\mathbf{A} = \mathbf{Z}_L\mathbf{K}_F\mathbf{Z}_L\mathbf{I}_S$,

$\mathbf{B} = \mathbf{Z}_L\mathbf{K}_F(\mathbf{V}_S + (\mathbf{Z}_L - \mathbf{Z}_v(|\mathbf{I}_S|))\mathbf{I}_S) + \mathbf{Z}_R\mathbf{K}_F\mathbf{Z}_L\mathbf{I}_S$,

$\mathbf{C} = (\mathbf{Z}_L + \mathbf{Z}_R)\mathbf{K}_F(\mathbf{V}_S - \mathbf{Z}_v(|\mathbf{I}_S|)\mathbf{I}_S)$,

$\mathbf{D} = (\mathbf{Z}_S + \mathbf{Z}_L + \mathbf{Z}_R)(\mathbf{I}_S - \mathbf{I}_S^{pre}) + \mathbf{Z}_v(|\mathbf{I}_S|)\mathbf{I}_S - \mathbf{Z}_v(|\mathbf{I}_S^{pre}|)\mathbf{I}_S^{pre}$.

Transforming (6.102) into the scalar form yields the following quadratic formula (for complex numbers) in two unknowns: distance to fault (d_1), such that: $d_{SC} < d_1 < 1$ (p.u.) and fault resistance (R_{F1}):

$$\underline{A}_2 d_1^2 - \underline{A}_1 d_1 + \underline{A}_0 - R_{F1} = 0 \tag{6.103}$$

where:

$$\underline{A}_2 = \mathbf{PA}, \qquad \underline{A}_1 = \mathbf{PB}, \qquad \underline{A}_0 = \mathbf{PC}, \qquad \mathbf{P} = \frac{\mathbf{D}^T}{\mathbf{D}^T\mathbf{D}},$$

superscript T denotes transposition of the matrix.

The scalar quadratic equation (6.103) can be resolved into the real and imaginary parts, from which one calculates the distance to fault (d_1) and fault resistance (R_{F1}), analogously to that presented for the formula (6.43)

There are, certainly, two roots of the scalar quadratic formula, but one of them being constant (depending only on the system parameters) can be easily identified and rejected. Eventually, the first subroutine SUB_1 delivers the solution (d_1, R_{F1}) assuming the fault behind the SCs&MOVs.

Subroutine SUB_2 – for faults in front of SCs

The case of a fault between the substation and the SCs&MOVs is more involved because the current flowing through the SCs&MOVs ($\mathbf{I}_R$) is not directly available to the locator (since here the one-end measurement at the terminal S is considered).

The following equations apply to the faulted network (Fig. 6.28):

$$\mathbf{E}_S - \mathbf{E}_S = (\mathbf{Z}_S + d_2\mathbf{Z}_L)\mathbf{I}_S - ((1 - d_2)\mathbf{Z}_L + \mathbf{Z}_v(|\mathbf{I}_R|) + \mathbf{Z}_R)\mathbf{I}_R \tag{6.104}$$

$$\mathbf{V}_S - \mathbf{V}_F = d_2\mathbf{Z}_L\mathbf{I}_S \tag{6.105}$$

but now, $0 < d_2 < d_{SC}$.

The model of the pre-fault network (6.100) and also the fault model (6.101), but with fault resistance R_{F2} instead of R_{F1}, remain valid.

In this case, one also obtains the quadratic matrix equation:

$$\mathbf{A}d_2^2 - \mathbf{B}d_2 + \mathbf{C} - \mathbf{D}R_{F2} = \mathbf{0} \tag{6.106}$$

where:

$$\mathbf{A} = \mathbf{Z}_\mathrm{L}\mathbf{K}_\mathrm{F}\mathbf{Z}_\mathrm{L}\mathbf{I}_\mathrm{S},$$

$$\mathbf{B} = \mathbf{Z}_\mathrm{L}\mathbf{K}_\mathrm{F}\mathbf{V}_\mathrm{S} + (\mathbf{Z}_\mathrm{L} + \mathbf{Z}_\mathrm{v}(|\,\mathbf{I}_\mathrm{R}\,|) + \mathbf{Z}_\mathrm{R})\mathbf{K}_\mathrm{F}\mathbf{Z}_\mathrm{L}\mathbf{I}_\mathrm{S},$$

$$\mathbf{C} = (\mathbf{Z}_\mathrm{L} + \mathbf{Z}_\mathrm{R} + \mathbf{Z}_\mathrm{v}(|\,\mathbf{I}_\mathrm{R}\,|))\mathbf{K}_\mathrm{F}\mathbf{V}_\mathrm{S},$$

$$\mathbf{D} = (\mathbf{Z}_\mathrm{S} + \mathbf{Z}_\mathrm{L} + \mathbf{Z}_\mathrm{R})(\mathbf{I}_\mathrm{S} - \mathbf{I}_\mathrm{S}^\mathrm{pre}) + \mathbf{Z}_\mathrm{v}(|\,\mathbf{I}_\mathrm{R}\,|)\mathbf{I}_\mathrm{S} - \mathbf{Z}_\mathrm{v}(|\,\mathbf{I}_\mathrm{S}^\mathrm{pre}\,|)\mathbf{I}_\mathrm{S}^\mathrm{pre}.$$

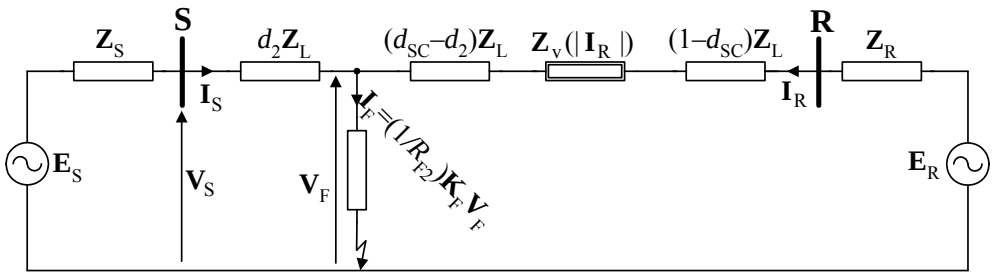

Fig. 6.28. Subroutine SUB_2 for faults occurring in front of the compensating capacitors – equivalent circuit diagram for transmission network with single line compensated at midpoint

Transforming matrix formula (6.106) into the scalar form is performed analogously as for the subroutine SUB_1. Then, the unknowns d_2, R_F2 are calculated, but an iterative numerical solution (Fig. 6.29b) is required because the coefficients depend on the unknown current from the remote substation R.

Eventually, the second subroutine delivers the solution (d_2, R_F2) assuming the fault in front of the SCs&MOVs.

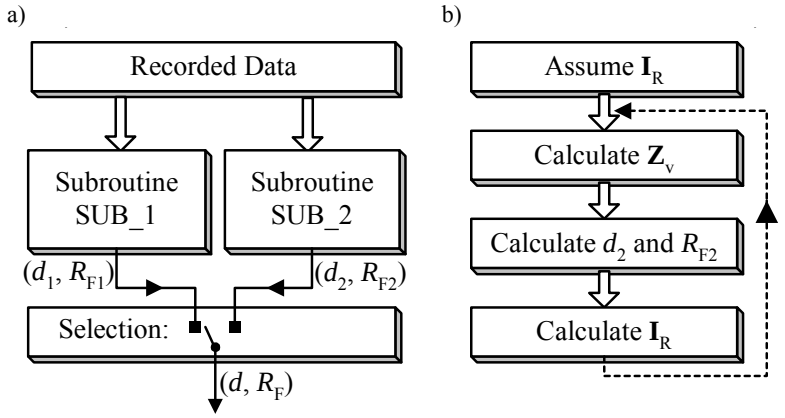

Fig. 6.29. Fault location algorithm: a) two subroutines compute two conditional fault locations and resistances, which undergo selection, b) iterative solution applies to the subroutine SUB_2

Selection algorithm

Locating a fault with respect to the SCs&MOVs in the system of Fig. 6.21, i.e. selecting either SUB_1 or SUB_2 as a valid subroutine, is a separate issue. Here, however, the problem narrows to the selection of the correct pair (d, R_F) out of two alternatives (d_1, R_{F1}) and (d_2, R_{F2}), as depicted in Fig. 6.29a. The simple and straightforward algorithm:

if d_1 is out of $[d_{SC}, 1]$ **and** d_2 is in $[0, d_{SC}]$ **then**
accept (d_2, R_{F2}) as the valid solution **otherwise**
if d_1 is in $[d_{SC}, 1]$ **and** d_2 is out of $[0, d_{SC}]$ **then**
accept (d_1, R_{F1}) as the valid solution **otherwise** select the alternative with lower R_F as the valid solution.

This selecting algorithm works in most cases. In order to avoid false selection, which could happen in some rare cases, an additional selection criterion has been proposed. This criterion is based on calculating currents at fault place, according to both subroutines: SUB_1, SUB_2, substituting the obtained distances to fault, d_1, d_2. Ideally, for the valid subroutine the calculated currents from healthy phases at fault have to be equal to zero (since in the healthy phases there is no current flow at all). In practice, due to the presence of the errors, certain threshold has to be assumed for indicating that these currents are close to zero (the valid subroutine) or far away from zero (the false subroutine). Certainly, this criterion can be applied for all fault types, except three-phase faults under which there are no healthy phases.

Improvements of the one-end fault location algorithm

The fault algorithm has been presented in its very basic form. The important enhancements for its field implementation may include:

- the impedance of the local system should be traced on-line based on the sequence voltages and currents; owing to this, the local impedance is always perfectly matched,
- more involved techniques should be used for phasor estimation and dealing with the off-nominal frequencies,
- advanced post-processing techniques for output filtering and elaborated methods for selecting the final result from the available data window should be applied,
- the remote end source impedance may also be accurately measured by the remote end relays or fault locators and transmitted to the local substation; no sampling synchronisation is needed (the voltage and current act as reference for each other),
- the amplitude of the remote current may also be measured and transmitted enabling iterative calculations to be avoided for the subroutine SUB_2 and improving the accuracy.

Example of fault location (Fig. 6.30a–f):

The following specifications of the fault on a 400 kV, 300 km transmission line, compensated at 70% rate with the three-phase compensating bank installed at mid-line (d_{SC} = 0.5 p.u.) were assumed:

- fault type: a–E,
- distance to fault: $d = 0.5^{+}$ p.u. (just behind SCs&MOVs),
- fault resistance: $R_F = 10\ \Omega$.

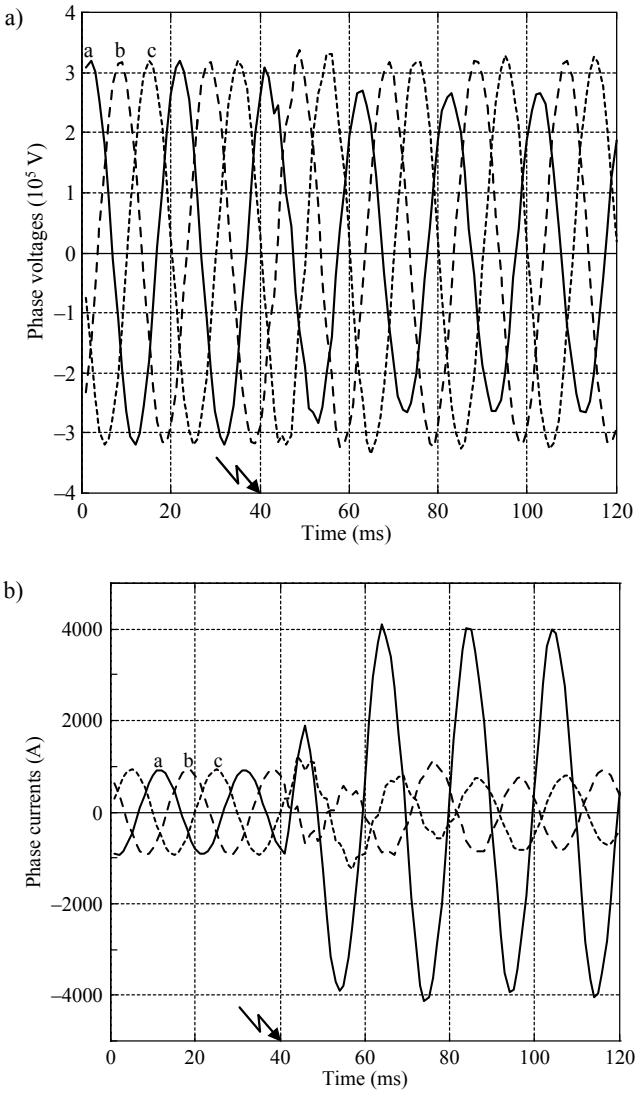

(Fig. 6.30 to be continued)

c)

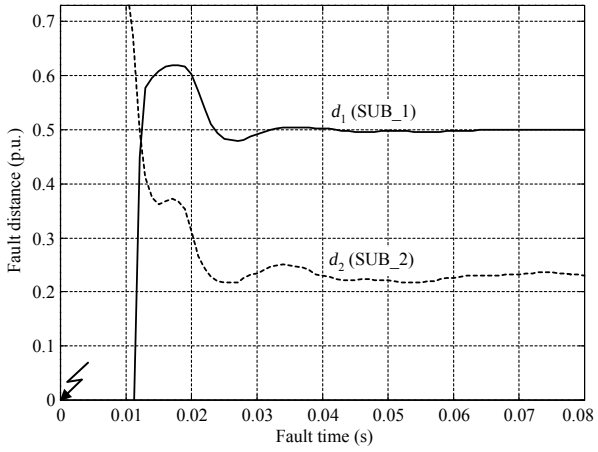

d)

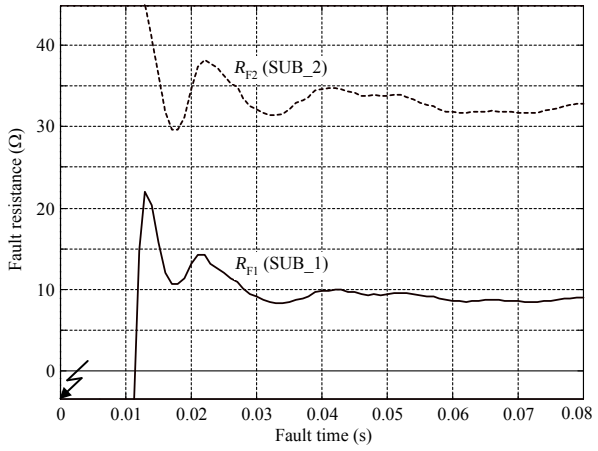

e)

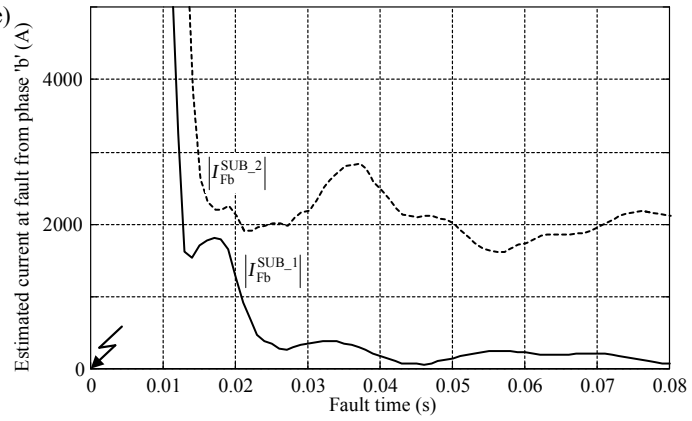

(Fig. 6.30 to be continued)

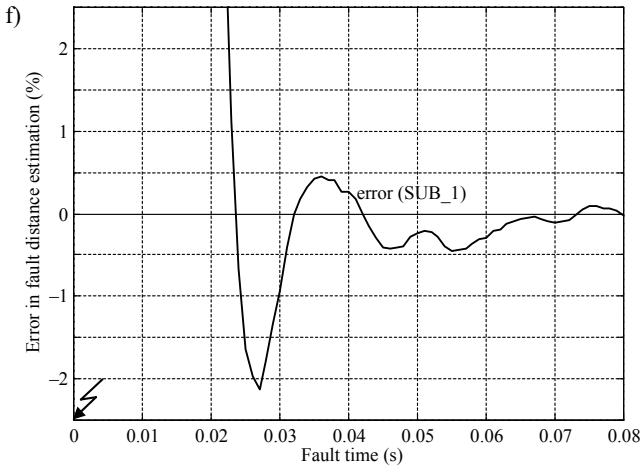

Fig. 6.30. Example of fault location (a–E fault, $d = 0.5^{+}$ p.u., $R_F = 10\ \Omega$):
a) three-phase input voltage, b) three-phase input current, c) distance to fault, d) fault resistance,
e) magnitude of total fault current from healthy phase 'b' according to SUB_1 and SUB_2,
f) fault distance estimation error for valid subroutine (SUB_1)

The fault locator input signals are shown in Fig. 6.30a, b. Results for estimated distance to fault from both subroutines (Fig. 6.30c) could be accepted and thus selection of the valid result is required. Lower positive fault resistance (Fig. 6.30d) is yielded by the subroutine SUB_1 and this supports selection of it as the valid subroutine. Also the selection criterion based on calculating the healthy phase total fault current (Fig. 6.30e) indicates the subroutine SUB_1 as the valid one. The estimation error for the fault distance (from the valid subroutine SUB_1) shown in Fig. 6.30f is definitely acceptable, as it does not exceed 0.5% after around 1.5 fundamental frequency cycle since fault incipience. Note: full cycle Fourier filtration was applied for determining the phasors of the processed signals.

6.15. Application of distributed-parameter line model to one-end fault location algorithms

The varieties of fault location algorithms presented above (Sections 6.2–6.14) were derived assuming the lumped model of a transmission line and neglecting the line shunt parameters (predominantly the shunt capacitances). The fault loop formula (6.28) was used for deriving those algorithms. Introducing in (6.28) the fault loop current for the single line (6.26) one obtains the following form for the fault loop formula [63]:

$$\underline{V}_{\mathrm{S\_P}} - d\,\underline{Z}_{1\mathrm{L}}\left(\underline{a}_1 I_{\mathrm{S1}} + \underline{a}_2 \underline{I}_{\mathrm{S2}} + \underline{a}_0 \frac{\underline{Z}_{0\mathrm{L}}}{\underline{Z}_{1\mathrm{L}}} \underline{I}_{\mathrm{S0}}\right) - R_{\mathrm{F}}(\underline{a}_{\mathrm{F1}}\underline{I}_{\mathrm{F1}} + \underline{a}_{\mathrm{F2}}\underline{I}_{\mathrm{F2}} + \underline{a}_{\mathrm{F0}}\underline{I}_{\mathrm{F0}}) = 0 \qquad (6.145)$$

in which there are coefficients dependent on fault type (gathered in Table 6.5 and Tables 4.3–4.5).

Using (6.145) accurate location of faults on transmission lines of comparatively short length can be performed. In order to keep the fault location errors in the case of long lines (usually considered as exceeding 150 km) on the acceptable level, the distributed-parameter line model has to be incorporated.

Distributed-parameter model of faulted line for the *i*-th symmetrical component from Fig. 2.25 will be utilised for simplified introduction of the distributed-parameter line model into the fault loop formula (6.145). This model is simplified (not strict) since in order to avoid solving non-linear equations, the iterative calculations are performed. Performing the current iteration (the iteration number *n*), the shunt parameters (capacitances) for the faulted line section are determined not by accurate value of the distance to fault but by the value obtained in the last but one iteration (the iteration number: $(n-1)$). Also the longitudinal line impedance for the line section in the model from Fig. 2.25 is determined using the distance to fault value obtained in the previous iteration of the calculations. In order to start the iterative calculations, the distance to fault obtained for the lumped line model has to be taken.

Introducing into (6.145) the distributed-parameter line model from Fig. 2.25 one obtains:

$$\underline{V}_{\mathrm{S\_P}} - d_{(n)}\underline{Z}_{1\mathrm{L}}\left(\underline{a}_1 \underline{A}^{\mathrm{sh}}_{1_{(n-1)}} \underline{I}^{\mathrm{comp}}_{\mathrm{S1}} + \underline{a}_2 \underline{A}^{\mathrm{sh}}_{2(n-1)} \underline{I}^{\mathrm{comp}}_{\mathrm{S2}} + \underline{a}_0 \underline{A}^{\mathrm{sh}}_{0(n-1)} \frac{\underline{Z}_{0\mathrm{L}}}{\underline{Z}_{1\mathrm{L}}} \underline{I}^{\mathrm{comp}}_{\mathrm{S0}}\right)$$
$$- R_{\mathrm{F}_{(n)}}(\underline{a}_{\mathrm{F1}}\underline{I}^{\mathrm{comp}}_{\mathrm{F1}} + \underline{a}_{\mathrm{F2}}\underline{I}^{\mathrm{comp}}_{\mathrm{F2}} + \underline{a}_{\mathrm{F0}}\underline{I}^{\mathrm{comp}}_{\mathrm{F0}}) = 0 \qquad (6.146)$$

where:

$d_{(n)}$, $d_{(n-1)}$ – distance to fault from current and previous iterations,

$R_{\mathrm{F}_{(n)}}$ – fault resistance from current iteration,

$\underline{A}^{\mathrm{sh}}_{1_{(n-1)}} = \underline{A}^{\mathrm{sh}}_{2_{(n-1)}} = \dfrac{\sinh(\underline{\gamma}_1 d_{(n-1)}\ell)}{\underline{\gamma}_1 d_{(n-1)}\ell}$ – correction factor for determining the positive-sequence (negative-sequence) longitudinal impedance of line section having the length d (p.u.),

$\underline{A}^{\mathrm{sh}}_{0_{(n-1)}} = \dfrac{\sinh(\underline{\gamma}_0 d_{(n-1)}\ell)}{\underline{\gamma}_0 d_{(n-1)}\ell}$ – as above, but for the zero-sequence.

The positive-, negative- and zero-sequence currents after deducing the shunt capacitance currents equal:

$$\underline{I}_{\mathrm{S1}}^{\mathrm{comp}} = \underline{I}_{\mathrm{S1}} - 0.5 d_{(n-1)} \ell \underline{Y}'_{\mathrm{1L}} \, \underline{A}_{\mathrm{l}_{(n-1)}}^{\mathrm{th}} \underline{V}_{\mathrm{S1}}$$

$$\underline{I}_{\mathrm{S2}}^{\mathrm{comp}} = \underline{I}_{\mathrm{S2}} - 0.5 d_{(n-1)} \ell \underline{Y}'_{\mathrm{2L}} \, \underline{A}_{2_{(n-1)}}^{\mathrm{th}} \underline{V}_{\mathrm{S2}}$$

$$\underline{I}_{\mathrm{S0}}^{\mathrm{comp}} = \underline{I}_{\mathrm{S0}} - 0.5 d_{(n-1)} \ell \underline{Y}'_{\mathrm{0L}} \, \underline{A}_{0_{(n-1)}}^{\mathrm{th}} \underline{V}_{\mathrm{S0}}$$

where:

$\underline{A}_{\mathrm{l}_{(n-1)}}^{\mathrm{th}} = \underline{A}_{2_{(n-1)}}^{\mathrm{th}}$ – correction factor for determining the positive-(negative-)sequence shunt admittance of line section having the length d (p.u.),

$\underline{A}_{0_{(n-1)}}^{\mathrm{th}}$ – as above, but for the zero-sequence,

$\underline{I}_{\mathrm{F1}}^{\mathrm{comp}}$, $\underline{I}_{\mathrm{F2}}^{\mathrm{comp}}$, $\underline{I}_{\mathrm{F0}}^{\mathrm{comp}}$ – symmetrical components of total fault current determined with considering the distributed-parameter line model, however, it is a common practice [142, 143] that they are identical with the currents estimated using the lumped line model.

The fault loop formula (6.146) is solved iteratively for the unknowns: $d_{(n)}$, $R_{\mathrm{F}_{(n)}}$ with checking the convergence of iterative calculations (this requires setting the convergence threshold) or applying the pre-defined number of iterations. Usually, performance of two iterations appears to be sufficient.

Analogously as for the symmetrical components approach (6.146), the distributed-parameter line model can be introduced for the phase co-ordinates approach.

7. Two-end and multi-end fault location algorithms

7.1. Introduction

In this chapter, two-end and multi-end fault location algorithms are considered. Both, synchronised [B.8, 33, 53, 71, 72, 91, 92, 133, 180, 181] and unsynchronised [20, 60, 70, 103, 104, 126, 127, 132, 165, 177, 178] measurements are taken into account. In the case of unsynchronised measurements, different ways of dealing with the unknown synchronisation angle are presented. Use of both complete (two-end voltages and currents) and incomplete (two-end voltages and current from one end or two-end currents and one-end voltage) measurements is considered. Also, use of measurements from distance relays at both line terminals is considered for deriving a fault location algorithm designed for post-fault analysis of operation of the relays [64, 69, 142, 143, 148].

Different options with respect to availability of measurements from the terminals of three-terminal and multi-terminal lines are considered.

7.2. Fault location with use of two-end synchronised measurements

7.2.1. Phasor-based approach

The distributed-parameter model of faulted line for the *i*-th symmetrical component, with use of the correction factors for representing series and shunt parameters, as in Fig. 3.30, is taken into consideration. Voltage at fault point (F), viewed from the terminals S and R, respectively, is as follows:

$$\underline{V}_{\mathrm{F}i}^{\mathrm{S}} = \cosh(\underline{\gamma}_i d\ell)\underline{V}_{\mathrm{S}i} - \sinh(\underline{\gamma}_i d\ell)\underline{Z}_{\mathrm{c}i}\underline{I}_{\mathrm{S}i} \tag{7.1}$$

$$\underline{V}_{\mathrm{F}i}^{\mathrm{R}} = \cosh(\underline{\gamma}_i (1-d)\ell)\underline{V}_{\mathrm{R}i} - \sinh(\underline{\gamma}_i (1-d)\ell)\underline{Z}_{\mathrm{c}i}\underline{I}_{\mathrm{R}i} \tag{7.2}$$

where $\underline{V}_{\mathrm{S}i}$, $\underline{I}_{\mathrm{S}i}$, $\underline{V}_{\mathrm{R}i}$, $\underline{I}_{\mathrm{R}i}$ – phasors of the *i*-th symmetrical component of voltages and currents obtained from synchronous measurements at the line terminals.

After taking into account the following trigonometric identities:

$$\cosh(\underline{\gamma}_i(1-d)\ell) = \cosh(\underline{\gamma}_i\ell)\cosh(\underline{\gamma}_i d\ell) - \sinh(\underline{\gamma}_i\ell)\sinh(\underline{\gamma}_i d\ell) \tag{7.3}$$

$$\sinh(\underline{\gamma}_i(1-d)\ell) = \sinh(\underline{\gamma}_i\ell)\cosh(\underline{\gamma}_i d\ell) - \cosh(\underline{\gamma}_i\ell)\sinh(\underline{\gamma}_i d\ell) \tag{7.4}$$

and performing the rearrangements, the formula (7.2) can be presented as:

$$\underline{V}_{\mathrm{F}i}^{\mathrm{R}} = \underline{A}_i\cosh(\underline{\gamma}_i d\ell) + \underline{B}_i\sinh(\underline{\gamma}_i d\ell) \tag{7.5}$$

where:

$\underline{A}_i = \underline{V}_{\mathrm{R}i}\cosh(\underline{\gamma}_i\ell) - \underline{Z}_{\mathrm{c}i}\underline{I}_{\mathrm{R}i}\sinh(\underline{\gamma}_i\ell)$,

$\underline{B}_i = -\underline{V}_{\mathrm{R}i}\sinh(\underline{\gamma}_i\ell) + \underline{Z}_{\mathrm{c}i}\underline{I}_{\mathrm{R}i}\cosh(\underline{\gamma}_i\ell)$.

The voltages (7.1) and (7.5), as present at the same point (F), are to be compared:

$$\underline{V}_{\mathrm{F}i}^{\mathrm{S}} = \underline{V}_{\mathrm{F}i}^{\mathrm{R}} \tag{7.6}$$

As a result of this comparison one obtains:

$$\begin{aligned}&(\underline{V}_{\mathrm{R}i}\sinh(\underline{\gamma}_i\ell) - \underline{Z}_{\mathrm{c}i}\underline{I}_{\mathrm{R}i}\cosh(\underline{\gamma}_i\ell) - \underline{Z}_{\mathrm{c}i}I_{\mathrm{S}i})\sinh(\underline{\gamma}_i d\ell)\\ &= (\underline{V}_{\mathrm{R}i}\cosh(\underline{\gamma}_i\ell) - \underline{Z}_{\mathrm{c}i}\underline{I}_{\mathrm{R}i}\sinh(\underline{\gamma}_i\ell) - \underline{V}_{\mathrm{S}i})\cosh(\underline{\gamma}_i d\ell)\end{aligned} \tag{7.7}$$

From (7.7) one obtains the following formula for the distance to fault for two-end synchronous measurements of voltages and currents [74]:

$$d = \frac{1}{\underline{\gamma}_i\ell}\tanh^{-1}\left(\frac{\underline{V}_{\mathrm{R}i}\cosh(\underline{\gamma}_i\ell) - \underline{Z}_{\mathrm{c}i}\underline{I}_{\mathrm{R}i}\sinh(\underline{\gamma}_i\ell) - \underline{V}_{\mathrm{S}i}}{\underline{V}_{\mathrm{R}i}\sinh(\underline{\gamma}_i\ell) - \underline{Z}_{\mathrm{c}i}\underline{I}_{\mathrm{R}i}\cosh(\underline{\gamma}_i\ell) - \underline{Z}_{\mathrm{c}i}\underline{I}_{\mathrm{S}i}}\right) \tag{7.8}$$

The obtained fault location formula (7.8) can also be applied for the modal quantities [74].

7.2.2. Time domain approach

In Chapter 3, the modified Telegrapher's Equations of the long line model were formulated. Such first order partial differential equations can be solved using the method of characteristics [B.2]. This method discovers lines (called characteristic lines or characteristics) along which the partial differential equation degenerates into an ordinary differential equation.

Using the characteristics [B.2], the partial differential equations relating *u* and *i* (3.29)–(3.30) can be written as ordinary differential equations:

$$\frac{du}{ds} - \chi \frac{di}{ds} = \frac{\eta i}{\sqrt{1+\chi^2}} \tag{7.9}$$

$$\frac{du}{d\rho} + \chi \frac{di}{d\rho} = \frac{-\eta i}{\sqrt{1+\chi^2}} \tag{7.10}$$

where s, ρ – length along the two characteristics: $t \pm \chi x = \text{const}$ (straight lines in the distance–time plane).

The solution of equations (7.9)–(7.10) requires the discretization of the continuous time system. Assuming [46] that the distance (x) axis is discretized by the index j and the time (t) axis by the index k, the following expressions for the voltage and current are obtained:

$$v_{j,k} = \frac{1}{2}(v_{j-1,k-1} + v_{j-1,k+1}) + \frac{Z_c}{2}(i_{j-1,k-1} - i_{j-1,k+1}) + \frac{R'_L \Delta x}{4}(i_{j-1,k-1} + i_{j-1,k+1}) + \frac{R'_L \Delta x}{2} i_{j,k} \tag{7.11}$$

$$i_{j,k} = \frac{1}{2Z_c}(v_{j-1,k-1} - v_{j-1,k+1}) + \frac{1}{2}(i_{j-1,k-1} + i_{j-1,k+1}) + \frac{R'_L \Delta x}{4Z_c}(i_{j-1,k-1} - i_{j-1,k+1}) \tag{7.12}$$

where $Z_c = \sqrt{L'_L / C'_L}$ – surge impedance of the transmission line.

Starting from the ends of the line, one can compute the voltage and current profile along the line, applying equations (7.11)–(7.12).

If in equations (7.11)–(7.12), the series resistance R'_L is neglected, they will reduce to the well known Bergeron equations for a transmission line. Instead of computing the profile point by discrete point, the voltage and current at any point on the line can be determined knowing the voltage and current at the end of the line and the distance to the point.

The Bergeron equations for the voltage and current at a point x_j and time instant t_k are then given by:

$$v_{j,k} = \frac{1}{2}(v_{0,k-j} + v_{0,k+j}) + \frac{Z_c}{2}(i_{0,k-1} - i_{0,k+j}) \tag{7.13}$$

$$i_{j,k} = \frac{1}{2Z_c}(v_{0,k-j} + v_{0,k+j}) + \frac{1}{2}(i_{0,k-j} + i_{0,k+j}) \tag{7.14}$$

Steps in Fault Location

Using the voltage and current profiles, calculated by means of the method of characteristics, the fault location procedure described in [46] consists of the following steps:

• Modal decomposition used for obtaining three decoupled single phase transmission lines (from a three phase coupled system), to which the method of characteristics can be applied.

• Discretization of the transmission line: Based on the sampling frequency of the data acquisition, each mode of the transmission line is discretized into a finite number of points.

• Location of the approximate fault point: For each discrete point determined above, compute the voltage due to the sending end voltage and current. Then, the procedure using the receiving end data is repeated and the approximate fault point is found (the point with the least error).

• Refining the fault location performed with use of reconstructed voltage and current values transformed back to the phase domain.

7.3. Fault location with use of two-end unsynchronised measurements

In the case the phasors of voltages and currents are obtained from digital measurements acquired asynchronously at the line terminals, there is no common time reference. This happens when the GPS facility is not used or for some reasons the signal from the GPS is not received. In order to make use of such measurements for fault location, a common time reference has to be provided. Different approaches for that follow in the next sections. The measurements from the terminal R will be assumed as the base, while all phasors for voltage and current from the end S (acquired asynchronously) will be multiplied by the synchronisation operator $e^{j\delta}$.

7.3.1. Fault location with measurement of synchronisation angle

Application of (7.8) requires earlier determination of the synchronisation operator $e^{j\delta}$. This can be accomplished using the distributed parameter line model for the pre-fault positive sequence quantities (superscript 'pre' and subscript '1' in Fig. 7.1) [149].

In the pre-fault circuit (Fig. 7.1) there are the following phasors of signals measured asynchronously during pre-fault state, which after analytical synchronisation, performed with use of the synchronisation operator $e^{j\delta}$, take the form:

• at the terminal R: $\underline{I}_{R1}^{pre}$, $\underline{V}_{R1}^{pre}$,

• at the terminal S: $\underline{I}_{S1}^{pre}e^{j\delta}$, $\underline{V}_{S1}^{pre}e^{j\delta}$.

Different options with regard to using these phasors can be considered, as presented in the next sections. Note that in Fig. 7.1, the phasors which are to be calculated are

marked by dashed boxes, in order to distinguish them from those obtained from measurement.

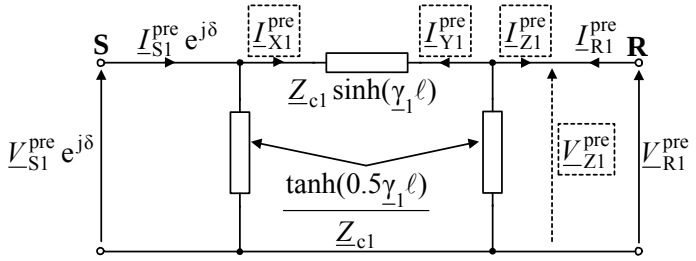

Fig. 7.1. Distributed-parameter model of line for the pre-fault positive-sequence (the calculated signals are marked by dashed boxes)

Use of pre-fault positive-sequence voltage and current from two ends

Using the equivalent π circuit model (Fig. 7.1), the current $\underline{I}_{X1}^{pre}$ is obtained by deducing the shunt current from the current at bus S:

$$\underline{I}_{X1}^{pre} = \underline{I}_{S1}^{pre} e^{j\delta} - \frac{\tanh(0.5\underline{\gamma}_1\ell)}{\underline{Z}_{c1}} \underline{V}_{S1}^{pre} e^{j\delta} \tag{7.15}$$

Analogously, the current $\underline{I}_{Y1}^{pre}$ is calculated as:

$$\underline{I}_{Y1}^{pre} = \underline{I}_{R1}^{pre} - \frac{\tanh(0.5\underline{\gamma}_1\ell)}{\underline{Z}_{c1}} \underline{V}_{R1}^{pre} \tag{7.16}$$

The currents determined (7.15)–(7.16) satisfy:

$$\underline{I}_{X1}^{pre} = -\underline{I}_{Y1}^{pre} \tag{7.17}$$

From (7.17), one obtains the following formula for the synchronisation operator:

$$e^{j\delta} = \frac{-\underline{I}_{R1}^{pre}\underline{Z}_{c1} + \tanh(0.5\underline{\gamma}_1\ell)\underline{V}_{R1}^{pre}}{\underline{I}_{S1}^{pre}\underline{Z}_{c1} - \tanh(0.5\underline{\gamma}_1\ell)\underline{V}_{S1}^{pre}} \tag{7.18}$$

Use of pre-fault positive-sequence voltage from two ends and current from one end

The positive-sequence pre-fault voltage $\underline{V}_{Z1}^{pre}$ can be calculated by transferring signals from the bus S towards the bus R:

$$\underline{V}_{Z1}^{pre} = \cosh(\underline{\gamma}_1 \ell)\underline{V}_{S1}^{pre} e^{j\delta} - \underline{Z}_{c1} \sinh(\underline{\gamma}_1 \ell)\underline{I}_{S1}^{pre} e^{j\delta} \tag{7.19}$$

The calculated voltage (7.19) is equal to the voltage at bus R:

$$\underline{V}_{Z1}^{pre} = \underline{V}_{R1}^{pre} \tag{7.20}$$

From (7.20), one obtains the following formula for the synchronisation operator:

$$e^{j\delta} = \frac{\underline{V}_{R1}^{pre}}{\cosh(\underline{\gamma}_i \ell)\underline{V}_{S1}^{pre} - \underline{Z}_{c1} \sinh(\underline{\gamma}_i \ell)\underline{I}_{S1}^{pre}} \tag{7.21}$$

Use of pre-fault positive-sequence current from two ends and voltage from one end

Transferring signals measured at the bus S towards the bus R one obtains:

$$\underline{I}_{Z1}^{pre} = -\frac{1}{\underline{Z}_{c1}} \sinh(\underline{\gamma}_i \ell)\underline{V}_{S1}^{pre} e^{j\delta} + \cosh(\underline{\gamma}_i \ell)\underline{I}_{S1}^{pre} e^{j\delta} \tag{7.22}$$

The calculated current (7.22) and that measured at the bus R satisfy:

$$I_{Z1}^{pre} = -I_{R1}^{pre} \tag{7.23}$$

From (7.23), one obtains the following formula for the synchronisation operator:

$$e^{j\delta} = \frac{-\underline{Z}_{c1}\underline{I}_{R1}^{pre}}{-\sinh(\underline{\gamma}_1 \ell)\underline{V}_{S1}^{pre} + \cosh(\underline{\gamma}_1 \ell)\underline{Z}_{c1}\underline{I}_{S1}^{pre}} \tag{7.24}$$

The unknown synchronisation operator can be determined from pre-fault positive-sequence currents and voltages measured asynchronously at the line terminals, applying (7.18) or (7.21) or (7.24).

Alternatively, the synchronisation operator can be determined using only fault quantities (measured within the fault period). For this purpose, the boundary conditions of particular faults can be explored [65]. In the case of three-phase balanced faults, the positive sequence components are the only ones present in the measured currents and voltages. For this reason, the boundary conditions will be considered for all faults, but except three-phase balanced faults, for which the synchronisation operator can be determined with use of pre-fault positive-sequence quantities, applying (7.18) or (7.21) or (7.24).

Use of two-end voltages and one-end current

For analysis of boundary conditions of faults the symmetrical components of the total fault current have to be determined. This will be done using the distributed parameter line model (Fig. 7.2).

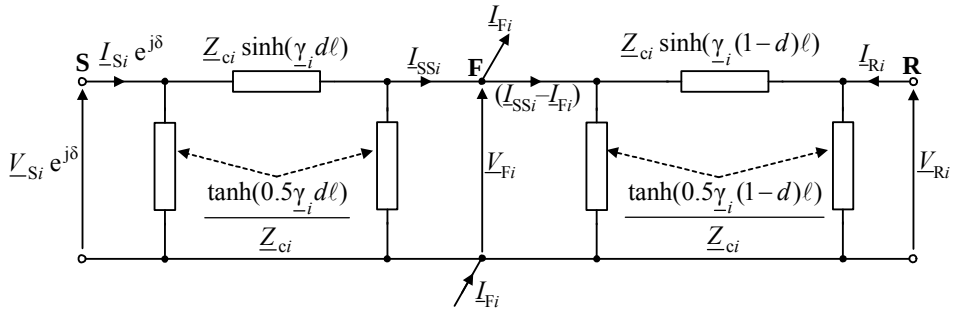

Fig. 7.2. Distributed parameter model of faulted transmission line for the *i*-th symmetrical component

Transferring analytically signals from the bus S towards the fault point F (Fig. 7.2) one obtains:

$$\underline{V}_{Fi} = (\underline{V}_{Si}\cosh(\underline{\gamma}_i d\ell) - \underline{Z}_{ci}\underline{I}_{Si}\sinh(\underline{\gamma}_i d\ell))e^{j\delta} \tag{7.25}$$

$$\underline{I}_{SSi} = (-(1/\underline{Z}_{ci})\underline{V}_{Si}\sinh(\underline{\gamma}_i d\ell) + \underline{I}_{Si}\cosh(\underline{\gamma}_i d\ell))e^{j\delta} \tag{7.26}$$

Taking (7.25) and (7.26), the voltage at the remote terminal R (Fig. 7.2) can be determined as follows:

$$\underline{V}_{Ri} = \underline{V}_{Fi}\cosh(\underline{\gamma}_i(1-d)\ell) - \underline{Z}_{ci}(\underline{I}_{SSi} - \underline{I}_{Fi})\sinh(\underline{\gamma}_i(1-d)\ell) \tag{7.27}$$

Substituting (7.25)–(7.26) into (7.27) and performing tedious manipulations on hyperbolic functions (with use of the trigonometric identities (7.3)–(7.4)) one obtains the following formula for the *i*-th symmetrical component of the total fault current [65]:

$$\underline{I}_{Fi} = \frac{\underline{V}_{Ri} + \underline{N}_{Si}e^{j\delta}}{\underline{Z}_{ci}\sinh(\underline{\gamma}_i(1-d)\ell)} \tag{7.28}$$

where:

$\underline{N}_{Si} = -\underline{V}_{Si}\cosh(\underline{\gamma}_i\ell) + \underline{Z}_{ci}\underline{I}_{Si}\sinh(\underline{\gamma}_i\ell)$,

$\underline{V}_{Si}$, $\underline{V}_{Ri}$, $\underline{I}_{Si}$ – the *i*-th symmetrical component of the signals obtained from asynchronous measurements of two-end voltages and one-end current.

The total fault current is a composition of its respective components, using the share coefficients dependent on the fault type (in Tables 4.3–4.6, alternative sets of the weighting coefficients for different faults are gathered, depending on the assumed priority for using respective sequences). Two characteristic sets of the

share coefficients for the phase-to-ground and phase-to-phase faults are collected in Table 7.1.

Table 7.1. Two sets of share coefficients for phase-to-ground and phase-to-phase faults

Fault type	SET I (from Table 4.3)		SET II (from Table 4.4)	
	$\underline{a}_{F1}^{SET\ I}$	$\underline{a}_{F2}^{SET\ I}$	$\underline{a}_{F1}^{SET\ II}$	$\underline{a}_{F2}^{SET\ II}$
a–E	0	3	3	0
b–E	0	$-1.5+\mathrm{j}1.5\sqrt{3}$	$-1.5-\mathrm{j}1.5\sqrt{3}$	0
c–E	0	$-1.5-\mathrm{j}1.5\sqrt{3}$	$-1.5+\mathrm{j}1.5\sqrt{3}$	0
a–b	0	$1.5-\mathrm{j}1.5\sqrt{3}$	$1.5+\mathrm{j}0.5\sqrt{3}$	0
b–c	0	$\mathrm{j}\sqrt{3}$	$-\mathrm{j}\sqrt{3}$	0
c–a	0	$-1.5-\mathrm{j}0.5\sqrt{3}$	$-1.5+\mathrm{j}0.5\sqrt{3}$	0

Applying the share coefficients from Table 7.1, the total fault current can be expressed as follows:

$$\underline{I}_{F} = \underline{a}_{F1}^{SET\ I}\,\underline{I}_{F1} + \underline{a}_{F2}^{SET\ I}\,\underline{I}_{F2} \tag{7.29}$$

or alternatively as:

$$\underline{I}_{F} = \underline{a}_{F1}^{SET\ II}\,\underline{I}_{F1} + \underline{a}_{F2}^{SET\ II}\,\underline{I}_{F2} \tag{7.30}$$

Considering (7.28) for $i = 1$ (positive-sequence) and $i = 2$ (negative-sequence) one can take into account that for these sequences the propagation constants are identical, and the surge impedances are identical, too. As a result of comparing (7.29) with (7.30) one gets the following formula for the synchronisation operator, valid for all faults listed in Table 7.1 (phase-to-earth and phase-to-phase faults):

$$[\mathrm{e}^{\mathrm{j}\delta}]_{\mathrm{ph-E,\,ph1-ph2}} = \frac{\underline{a}_{F2}^{SET\ I}\,\underline{V}_{R2} - \underline{a}_{F1}^{SET\ II}\,\underline{V}_{R1}}{\underline{a}_{F1}^{SET\ II}\,\underline{N}_{S1} - \underline{a}_{F2}^{SET\ I}\,\underline{N}_{S2}} \tag{7.31}$$

where:

$$\underline{N}_{S1} = -\underline{V}_{S1}\cosh(\underline{\gamma}_1\ell) + \underline{Z}_{c1}\underline{I}_{S1}\sinh(\underline{\gamma}_1\ell),$$

$$\underline{N}_{S2} = -\underline{V}_{S2}\cosh(\underline{\gamma}_1\ell) + \underline{Z}_{c1}\underline{I}_{S2}\sinh(\underline{\gamma}_1\ell).$$

In (7.31), the positive- and negative-sequence quantities from a fault period are involved. Thus, one avoids using the pre-fault measurements.

For phase-to-phase-to-ground faults the relation between the zero-sequence component of the total fault current and the remaining components (formula (4.3) and Table 4.7) is utilised. Substituting (7.28) into (4.3) gives:

$$\frac{\underline{V}_{\mathrm{R0}} + \underline{N}_{\mathrm{S0}}[\mathrm{e}^{\mathrm{j}\delta}]_{\mathrm{ph1-ph2-E}}}{\underline{Z}_{\mathrm{c0}} \sinh(\underline{\gamma}_0(1-d)\ell)} = \frac{\underline{b}_{\mathrm{F1}}\underline{V}_{\mathrm{R1}} + \underline{b}_{\mathrm{F2}}\underline{V}_{\mathrm{R2}} + (\underline{b}_{\mathrm{F1}}\underline{N}_{\mathrm{S1}} + \underline{b}_{\mathrm{F2}}\underline{N}_{\mathrm{S2}})[\mathrm{e}^{\mathrm{j}\delta}]_{\mathrm{ph1-ph2-E}}}{\underline{Z}_{\mathrm{c1}} \sinh(\underline{\gamma}_1(1-d)\ell)} \tag{7.32}$$

where:

$\underline{b}_{\mathrm{F1}}, \underline{b}_{\mathrm{F2}}$ – coefficients from Table 4.7,

$\underline{N}_{\mathrm{S0}} = -\underline{V}_{\mathrm{S0}} \cosh(\underline{\gamma}_0 \ell) + \underline{Z}_{\mathrm{c0}} \underline{I}_{\mathrm{S0}} \sinh(\underline{\gamma}_0 \ell)$,

$\underline{N}_{\mathrm{S1}}$, $\underline{N}_{\mathrm{S2}}$ as in (7.31).

Direct determination of the synchronisation operator from (7.32), i.e. without knowing the distance to fault (d), cannot be accomplished. Therefore, the solution of (7.32) can be considered together with the fault location algorithm. Approximate determination of the synchronisation operator from (7.32) can be performed by linearizing the formula, i.e. by applying the substitution for the positive- and zero-sequence ($i = 1$ and $i = 0$):

$$\sinh(\underline{\gamma}_i(1-d)\ell) \to (\underline{\gamma}_i(1-d)\ell) \tag{7.33}$$

Use of two-end currents and one-end voltage

Considering the line section (F–R) (Fig. 7.2) one obtains the following formula for the i-th sequence of the remote bus current:

$$\underline{I}_{\mathrm{R}i} = \frac{1}{\underline{Z}_{ci}} \underline{V}_{\mathrm{F}i} \sinh(\underline{\gamma}_i(1-d)\ell) - (\underline{I}_{\mathrm{SS}i} - \underline{I}_{\mathrm{F}i}) \cosh(\underline{\gamma}_i(1-d)\ell) \tag{7.34}$$

Substituting (7.25)–(7.26) into (7.34) and performing tedious manipulations on hyperbolic functions, with use of the trigonometric identities (7.3)–(7.4), one obtains the following formula for the i-th symmetrical component of the total fault current:

$$\underline{I}_{\mathrm{F}i} = \frac{\underline{I}_{\mathrm{R}i} + \underline{N}_{\mathrm{S}i}\mathrm{e}^{\mathrm{j}\delta}}{\cosh(\underline{\gamma}_i(1-d)\ell)} \tag{7.35}$$

where:

$$\underline{N}_{\mathrm{S}i} = \underline{I}_{\mathrm{S}i} \cosh(\underline{\gamma}_i \ell) - \frac{1}{\underline{Z}_{\mathrm{c}i}} \underline{V}_{\mathrm{S}i} \sinh(\underline{\gamma}_i \ell),$$

$\underline{I}_{\mathrm{S}i}$, $\underline{I}_{\mathrm{R}i}$, $\underline{V}_{\mathrm{S}i}$ – phasors of the i-th symmetrical component of the signals obtained from asynchronous measurements of two-end currents and one-end voltage.

Using (7.35) one can determine the synchronisation operator, analogously to the method presented in the previous section, where formula (7.28) was used for determining the i-th symmetrical component of the total fault current.

7.3.2. Fault location algorithm with elimination of synchronisation angle

The algorithm presented here starts with considering the lumped model of the faulted line (Fig. 7.3). Then, the distributed parameter line model (Fig. 7.4) is taken into account.

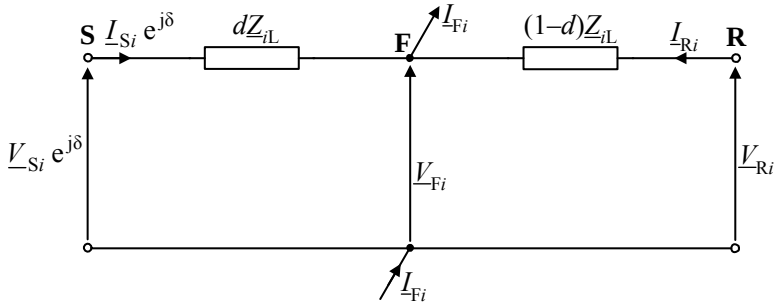

Fig. 7.3. Lumped model of faulted line for the *i*-th symmetrical component

Comparing the *i*-th symmetrical component of voltage at fault point ($\underline{V}_{Fi}$), viewed from both S and R sides gives:

$$\underline{V}_{Si}\,e^{j\delta} - d\,\underline{Z}_{iL}\,\underline{I}_{Si}\,e^{j\delta} = \underline{V}_{Ri} - (1-d)\underline{Z}_{iL}\,\underline{I}_{Ri} \tag{7.36}$$

From (7.36) one obtains the following formula for the synchronisation operator:

$$e^{j\delta} = \frac{\underline{V}_{Ri} - \underline{Z}_{iL}\,\underline{I}_{Ri} + d\,\underline{Z}_{iL}\,\underline{I}_{Ri}}{\underline{V}_{Si} - d\,\underline{Z}_{iL}\,\underline{I}_{Si}} \tag{7.37}$$

Taking into account that for the absolute value of the synchronisation operator:

$$|\,e^{j\delta}\,| = 1 \tag{7.38}$$

after using (7.37) and tedious rearrangements one obtains:

$$A_{2i}d^2 + A_{1i}d + A_{0i} = 0 \tag{7.39}$$

where:

$A_{2i} = |\,\underline{Z}_{iL}\,\underline{I}_{Si}\,|^2 - |\,\underline{Z}_{iL}\,\underline{I}_{Ri}\,|^2$,

$A_{1i} = -2\,\mathrm{real}(\underline{V}_{Si}(\underline{Z}_{iL}\,\underline{I}_{Si})^* + (\underline{V}_{Ri} - \underline{Z}_{iL}\,\underline{I}_{Ri})(\underline{Z}_{iL}\,\underline{I}_{Ri})^*)$,

$A_{0i} = |\,\underline{V}_{Si}\,|^2 - |\,\underline{V}_{Ri} - \underline{Z}_{iL}\,\underline{I}_{Ri}\,|^2$,

X^* – conjugate of X.

Solution of (7.39), formulated with the *i*-th type of the symmetrical components, yields two results for the distance to fault (p.u.): (d_{1i}, d_{2i}). Usually, one of them lies in

the line range: from 0 to 1 p.u., and in a natural way such result is selected as the valid one, i.e. corresponding to the actual fault. In some rare cases it can happen that both results (d_{1i}, d_{2i}) lie within the line range and in order to select the valid result, additional calculations, with use of another type of symmetrical components, have to be performed:

$$A_{2j}d^2 + A_{1j}d + A_{0j} = 0 \tag{7.40}$$

where j – subscript denoting that the j-th type symmetrical components ($j \neq i$) are utilised, i.e. in (7.39) the i-th type is replaced by the j-th type of symmetrical components.

In order to improve the fault location accuracy achieved using (7.39) or (7.40), the distributed parameter line model has to be included into the formula (7.36), which was used for deriving (7.39). Applying the distributed parameter line model suitable for simple iterative calculations (as in Fig. 3.31), the circuit diagram as in Fig. 7.4 is obtained and the following substitutions apply:

$$d\underline{Z}_{i\mathrm{L}} \rightarrow d_{(n)}\ell\underline{Z}'_{i\mathrm{L}}\,\underline{A}^{\mathrm{sh}}_{i(n-1)} \tag{7.41}$$

$$\underline{I}_{\mathrm{S}i} \rightarrow \underline{I}^{\mathrm{comp}}_{\mathrm{S}i} = \underline{I}_{\mathrm{S}i} - 0.5d_{(n-1)}\ell\underline{Y}'_{i\mathrm{L}}\,\underline{A}^{\mathrm{th}}_{i(n-1)}\underline{V}_{\mathrm{S}i} \tag{7.42}$$

$$(1-d)\underline{Z}_{i\mathrm{L}} \rightarrow (1-d_{(n)})\ell\underline{Z}'_{i\mathrm{L}}\,\underline{B}^{\mathrm{sh}}_{i(n-1)} \tag{7.43}$$

$$\underline{I}_{\mathrm{R}i} \rightarrow \underline{I}^{\mathrm{comp}}_{\mathrm{R}i} = \underline{I}_{\mathrm{R}i} - 0.5(1-d_{(n-1)})\ell\underline{Y}'_{i\mathrm{L}}\,\underline{B}^{\mathrm{th}}_{i(n-1)}\underline{V}_{\mathrm{R}i} \tag{7.44}$$

where:

$d_{(n)}$, $d_{(n-1)}$ – distance to fault in the 'current' and 'previous' iterations,

$\underline{A}^{\mathrm{sh}}_{i(n-1)}$, $\underline{A}^{\mathrm{th}}_{i(n-1)}$, $\underline{B}^{\mathrm{sh}}_{i(n-1)}$, $\underline{B}^{\mathrm{th}}_{i(n-1)}$ – values determined in the 'previous' iteration using (3.39)–(3.42).

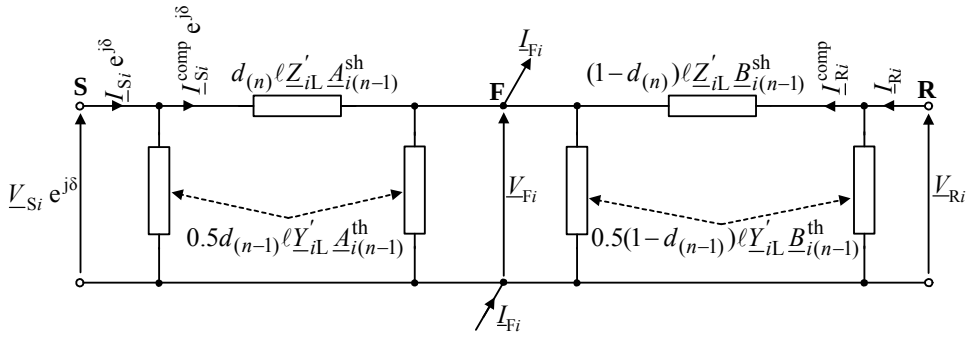

Fig. 7.4. Distributed parameter model of faulted line for the i-th symmetrical component suitable for iterative calculations of distance to fault

7.3.3. Fault location algorithm by Novosel et al.

In [127], a fault location algorithm utilising two-end unsynchronised measurement has been introduced. It is formulated in symmetrical components. Since different types of the components can be utilised, the algorithm will be presented in general form, i.e. for the *i*-th symmetrical component (subscript *i*). The algorithm is derived [127] by substituting the synchronisation operator:

$$e^{j\delta_i} = \cos(\delta_i) + j\sin(\delta_i) \tag{7.45}$$

into (7.36), thus obtaining:

$$\underline{V}_{Si}(\cos(\delta_i) + j\sin(\delta_i)) - d\underline{Z}_{iL}\underline{I}_{Si}(\cos(\delta_i) + j\sin(\delta_i)) - \underline{V}_{Ri} + (1-d)\underline{Z}_{iL}\underline{I}_{Ri} = 0 \tag{7.46}$$

Resolving (7.46) into the real/imaginary parts and eliminating the unknown distance to fault results in the following compact formula for the unknown synchronisation angle:

$$A_i \cos(\delta_i) + B_i \sin(\delta_i) = C_i \tag{7.47}$$

where:

$A_i = \text{imag}(\underline{Z}_{iL}^{*}((\underline{V}_{Ri} - \underline{Z}_{iL}\underline{I}_{Ri})\underline{I}_{Si}^{*} - \underline{V}_{Si}\underline{I}_{Ri}^{*}))$,

$B_i = \text{real}(-\underline{Z}_{iL}^{*}((\underline{V}_{Ri} - \underline{Z}_{iL}\underline{I}_{Ri})\underline{I}_{Si}^{*} + \underline{V}_{Si}\underline{I}_{Ri}^{*}))$,

$C_i = \text{imag}(-\underline{Z}_{iL}^{*}((\underline{V}_{Ri} - \underline{Z}_{iL}\underline{I}_{Ri})\underline{I}_{Ri}^{*} - \underline{V}_{Si}\underline{I}_{Si}^{*}))$,

x^{*} – conjugate of x.

Note that formula (7.47) is completely equivalent to the original formula from reference [127]. However, it contains more compact description of the quantities: A_i, B_i, C_i.

In [127], the formula (7.47) is solved iteratively, applying the Newton–Raphson method. The iterative calculations are stopped when the difference between the last two values of the synchronisation angle is smaller than a pre-assigned limit. An initial value for the unknown synchronisation angle is required. In [127], setting the initial value to zero has been recommended. This is due to the fact that in practice, the synchronisation angle is contained within a limited range around zero. The calculations have been observed to converge rapidly in numerous cases.

Once the synchronisation angle is known, the distance to fault can be calculated from the real or imaginary part of (7.46).

7.3.4. Optimal fault location algorithm

In order to avoid iterative calculations at the stage of using the lumped line model, rewriting (7.46) to the following form has been proposed in [60]:

$$\sin(\delta_{i\_1(2)} + \alpha_i) = \frac{C_i}{\sqrt{A_i^2 + B_i^2}} \tag{7.48}$$

where:

$$\sin(\alpha_i) = \frac{A_i}{\sqrt{A_i^2 + B_i^2}}, \quad \cos(\alpha_i) = \frac{B_i}{\sqrt{A_i^2 + B_i^2}}.$$

Two solutions of the trigonometric equation (7.48) from the range $(-\pi, \pi)$ are as follows (Fig. 7.5):

$$\delta_{i\_1} = \operatorname{asin}\left(\frac{C_i}{\sqrt{A_i^2 + B_i^2}}\right) - \operatorname{atan2}(\sin(\alpha_i),\ \cos(\alpha_i)) \tag{7.49}$$

$$\delta_{i\_2} = -\operatorname{asin}\left(\frac{C_i}{\sqrt{A_i^2 + B_i^2}}\right) - \operatorname{atan2}(\sin(\alpha_i),\ \cos(\alpha_i)) - \pi \tag{7.50}$$

where 'atan2' – four-quadrant arctangent function for calculating the angle with setting the sine and cosine values of this angle (note: 'atan2' is a function which is used in Matlab program [B.13]).

Performing calculations according to (7.49)–(7.50) one has to:

- take the real part from the arcsine function since in the presence of transient errors the term: $C_i \Big/ \sqrt{A_i^2 + B_i^2}$ could get out of the permissible range: (–1, 1),
- limit the values for the synchronisation angle $\delta_{i-1(2)}$ to the range $(-\pi, \pi)$ by adding or subtracting 2π, should it happen that the values $\delta_{i-1(2)}$ get outside the range $(-\pi, \pi)$.

Limitation of the synchronisation angle to the range $(-\pi, \pi)$ is reasonable, since the synchronisation angle is considered to have a small value [3].

In Fig. 7.5, an illustration of the solution of trigonometric formula (7.48) is given. In the case when only one solution is close to zero, while the latter is far away from zero, the selection of the valid synchronisation angle becomes straightforward. The solution being close to zero can be selected as the valid one (in Fig. 7.5a, the solution δ_{i_1}) and further taken for determining the distance to fault. In contrast, if both solutions lie close to zero (Fig. 7.5b), none of them can be rejected and there is a need for performing the selection. This will be explained when presenting the fault location example for the method from [60].

After determination of the synchronisation angle, the distance to fault can be calculated:

$$d_{i\_1(2)} = \text{real}\left(\frac{\underline{V}_{\text{S}i}\, \text{e}^{\text{j}\delta_{i\_1(2)}} - (\underline{V}_{\text{R}i} - \underline{Z}_{i\text{L}}\, \underline{I}_{\text{R}i})}{\underline{Z}_{i\text{L}}\, (\underline{I}_{\text{S}i}\, \text{e}^{\text{j}\delta_{i\_1(2)}} + \underline{I}_{\text{R}i})} \right) \tag{7.51}$$

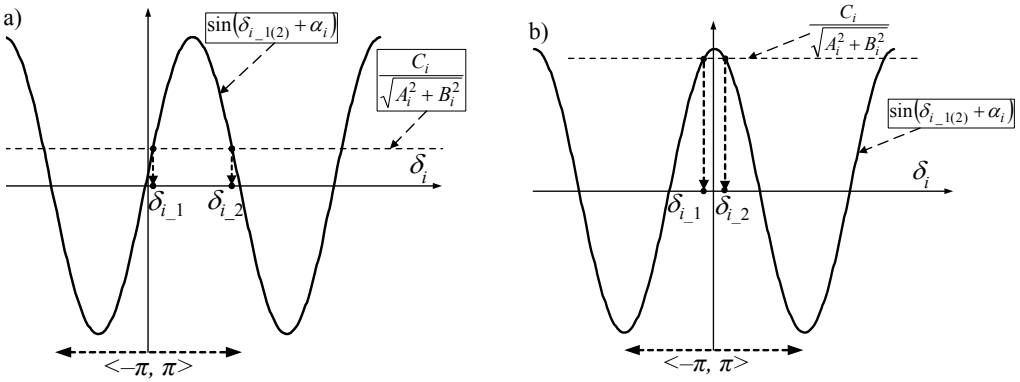

Fig. 7.5. Illustration of the solution of trigonometric formula (7.48):
a) only one solution is close to zero, b) both solutions are close to zero

Again, there are two solutions for the distance to fault (d_{i_1}, d_{i_2}). The solution, which is obtained for the earlier selected valid solution of the synchronisation angle, is the valid solution for the distance to fault. Otherwise, further selection is required.

Optimal fault location algorithm – use of distributed parameter line model

Applying the distributed parameter line model (Fig. 7.2), the voltage at the fault point F for the *i*-th symmetrical component, viewed from the terminals S and R, is determined as follows:

$$\underline{V}_{\text{F}i}^{\text{S}}(d, \delta) = (\underline{V}_{\text{S}i} \cosh(\underline{\gamma}_i d\ell) - \underline{Z}_{\text{c}i}\, \underline{I}_{\text{S}i} \sinh(\underline{\gamma}_i d\ell)) \cdot (\cos(\delta) + \text{j}\sin(\delta)) \tag{7.52}$$

$$\underline{V}_{\text{F}i}^{\text{R}}(d) = \underline{V}_{\text{R}i} \cosh(\underline{\gamma}_i (1-d)\ell) - \underline{Z}_{\text{c}i}\, \underline{I}_{\text{R}i} \sinh(\underline{\gamma}_i (1-d)\ell) \tag{7.53}$$

Comparison of (7.52) with (7.53) does not result in direct solution for the synchronisation angle and the distance to fault, as was the case for the lumped line model. This can be obtained by performing iterative calculations utilising the Newton–Raphson method. For this purpose, the following function of the sought unknowns is considered:

$$\underline{F}(d, \delta) = \underline{V}_{\text{F}i}^{\text{S}}(d, \delta) - \underline{V}_{\text{F}i}^{\text{R}}(d) = 0 \tag{7.54}$$

The iterative calculations are performed according to the following matrix formula:

$$\mathbf{X}_{\text{new}} = \mathbf{X}_{\text{old}} - \mathbf{J}^{-1}(\mathbf{F}_{\text{old}}) * \mathbf{F}_{\text{old}} \tag{7.55}$$

where:

$$\mathbf{X}_{\text{new}} = \begin{bmatrix} d_{\text{new}} \\ \delta_{\text{new}} \end{bmatrix}, \quad \mathbf{X}_{\text{old}} = \begin{bmatrix} d_{\text{old}} \\ \delta_{\text{old}} \end{bmatrix}, \quad \mathbf{F}_{\text{old}} = \begin{bmatrix} F_{\text{real}}(d_{\text{old}}, \delta_{\text{old}}) \\ F_{\text{imag}}(d_{\text{old}}, \delta_{\text{old}}) \end{bmatrix},$$

$$\mathbf{J}(\mathbf{F}_{\text{old}}) = \begin{bmatrix} \dfrac{\partial F_{\text{real}}(d_{\text{old}}, \delta_{\text{old}})}{\partial d_{\text{old}}} & \dfrac{\partial F_{\text{real}}(d_{\text{old}}, \delta_{\text{old}})}{\partial \delta_{\text{old}}} \\ \dfrac{\partial F_{\text{imag}}(d_{\text{old}}, \delta_{\text{old}})}{\partial d_{\text{old}}} & \dfrac{\partial F_{\text{imag}}(d_{\text{old}}, \delta_{\text{old}})}{\partial \delta_{\text{old}}} \end{bmatrix}.$$

The respective elements of the vector $\mathbf{F}_{\text{old}}$ are defined as follows:

$$F_{\text{real}}(d_{\text{old}}, \delta_{\text{old}}) = \text{real}[\underline{V}_{\text{F}i}^{\text{S}}(d_{\text{old}}, \delta_{\text{old}}) - \underline{V}_{\text{F}i}^{\text{R}}(d_{\text{old}})] \tag{7.56}$$

$$F_{\text{imag}}(d_{\text{old}}, \delta_{\text{old}}) = \text{imag}[\underline{V}_{\text{F}i}^{\text{S}}(d_{\text{old}}, \delta_{\text{old}}) - \underline{V}_{\text{F}i}^{\text{R}}(d_{\text{old}})] \tag{7.57}$$

After taking into account (7.52) and (7.54) one obtains:

$$F_{\text{real}}(d_{\text{old}}, \delta_{\text{old}}) = \text{real}[\underline{V}_{\text{F}i}^{\text{S\_unsynchr.}}(d_{\text{old}})]\cos(\delta_{\text{old}}) - \text{imag}[\underline{V}_{\text{F}i}^{\text{S\_unsynchr.}}(d_{\text{old}}]\sin(\delta_{\text{old}}) - \text{real}[\underline{V}_{\text{F}i}^{\text{R}}(d_{\text{old}})] \tag{7.58}$$

$$F_{\text{imag}}(d_{\text{old}}, \delta_{\text{old}}) = \text{imag}[\underline{V}_{\text{F}i}^{\text{S\_unsynchr.}}(d_{\text{old}})]\cos(\delta_{\text{old}}) + \text{real}[\underline{V}_{\text{F}i}^{\text{S\_unsynchr.}}(d_{\text{old}})]\sin(\delta_{\text{old}}) - \text{imag}[\underline{V}_{\text{F}i}^{\text{R}}(d_{\text{old}})] \tag{7.59}$$

Applying (7.58) and (7.59), the respective components of the Jacobian matrix $\mathbf{J}(\mathbf{F}_{\text{old}})$ can be determined.

The results for the synchronisation angle (7.49) and (7.50) and the distance to fault (7.51), obtained considering the lumped model of the line, are used as the initial values for $\delta_{\text{old}}, d_{\text{old}}$ in the calculations according to (7.55), (7.58)–(7.59). The iterative calculations are performed for the pre-defined fixed number of iterations or until the required convergence for the sought results is achieved.

Example 7.1. Location with optimal fault location algorithm

In Figs. 7.6 through 7.8, the results for the fault location performed according to the fault location algorithm from [60] are presented. The specifications of the fault on a 400 kV, 300 km line are as follows:

- a–E fault,
- distance to fault d = 0.8 p.u.,
- fault resistance R_{F} = 10 Ω,

• actual synchronisation angle $\delta = 36°$ (obtained by introducing a delay of signals from the side S by two samples at the sampling frequency $f_s = 1000$ Hz and the fundamental frequency $f_1 = 50$ Hz).

The digital values for the synchronisation angle (Fig. 7.7) and distance to fault (Fig. 7.8) are singled out by averaging (subscript: av.) within the interval lasting from 30 to 50 ms after the fault inception.

Using positive-sequence quantities the following averaged values of the synchronisation angle have been obtained: 94.28°, 37.42° (Fig. 7.7a), while using the negative-sequence components: 36.11°, –143.78° (Fig. 7.7a). Of the four possible pairs of the calculated angles:

• (94.28°, 36.11°),
• (94.28°, –143.78°),
• (37.42°, 36.11°),
• (37.42°, –143.78°),

the pair (37.42°, 36.11°) consists of the synchronisation angle values, which are the closest to each other and do not differ too much. Such a pair with coincident results indicates the valid solution for the synchronisation angle. Taking the values 37.42° for the positive-sequence and 36.11° for the negative-sequence, respectively, the distance to fault (Fig. 7.8) was determined. In the case of using the positive-sequence quantities one gets:

• for the lumped line model: 0.8964 p.u.
• for the distributed parameter line model: 0.8003 p.u.

Applying the negative-sequence components as the fault locator input signals, the following results have been obtained:

• for the lumped line model: 0.7948 p.u.
• for the distributed parameter line model: 0.7998 p.u.

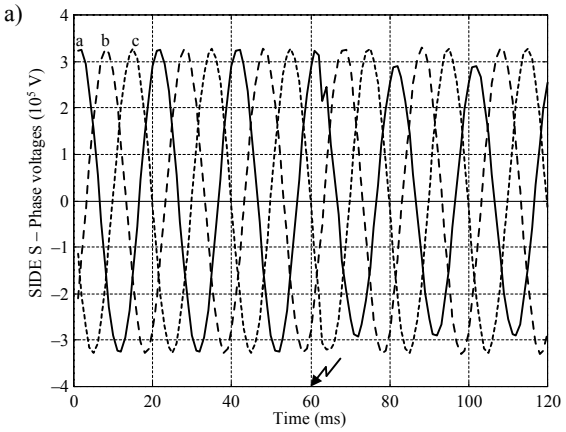

(Fig. 7.6 to be continued)

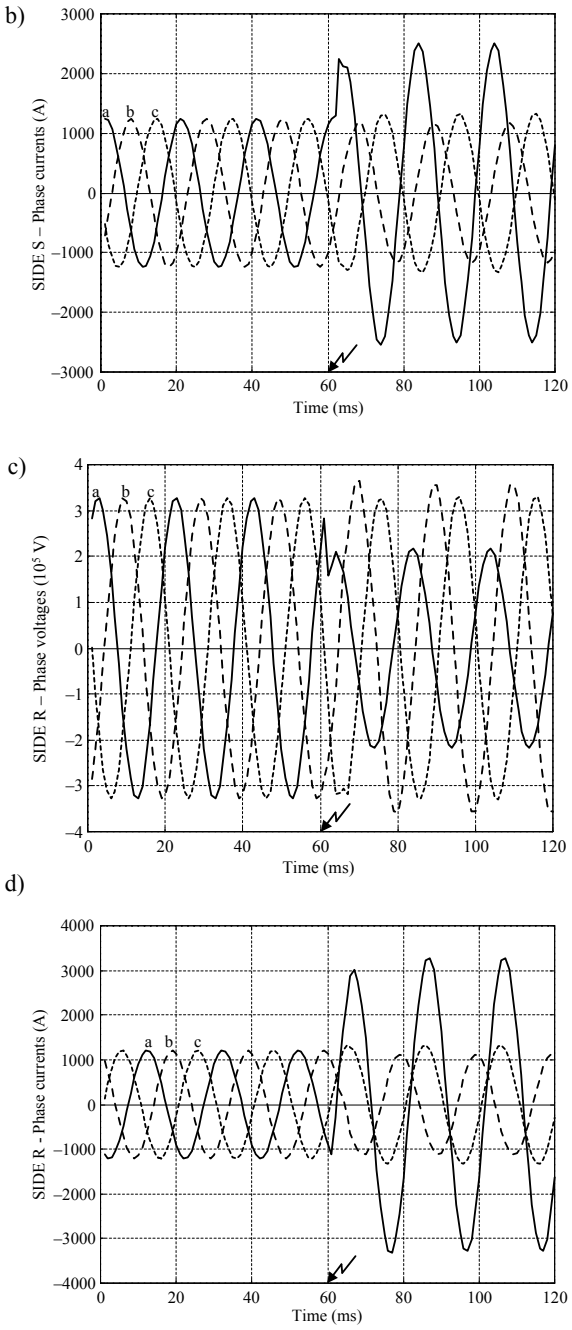

Fig. 7.6. Example of fault location – input signals of the fault locator:
a) side S voltage, b) side S current, c) side R voltage, d) side R current

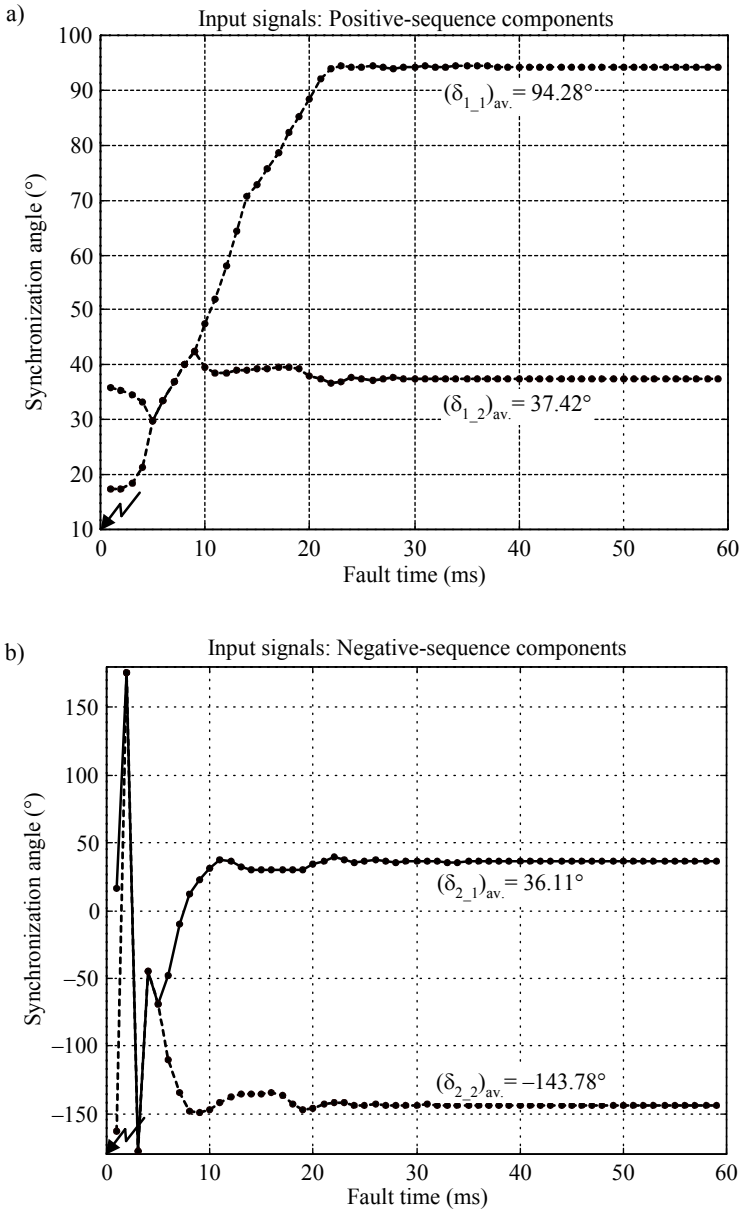

Fig. 7.7. Example of fault location – determination of the synchronisation angle using: a) positive-sequence components, b) negative-sequence components

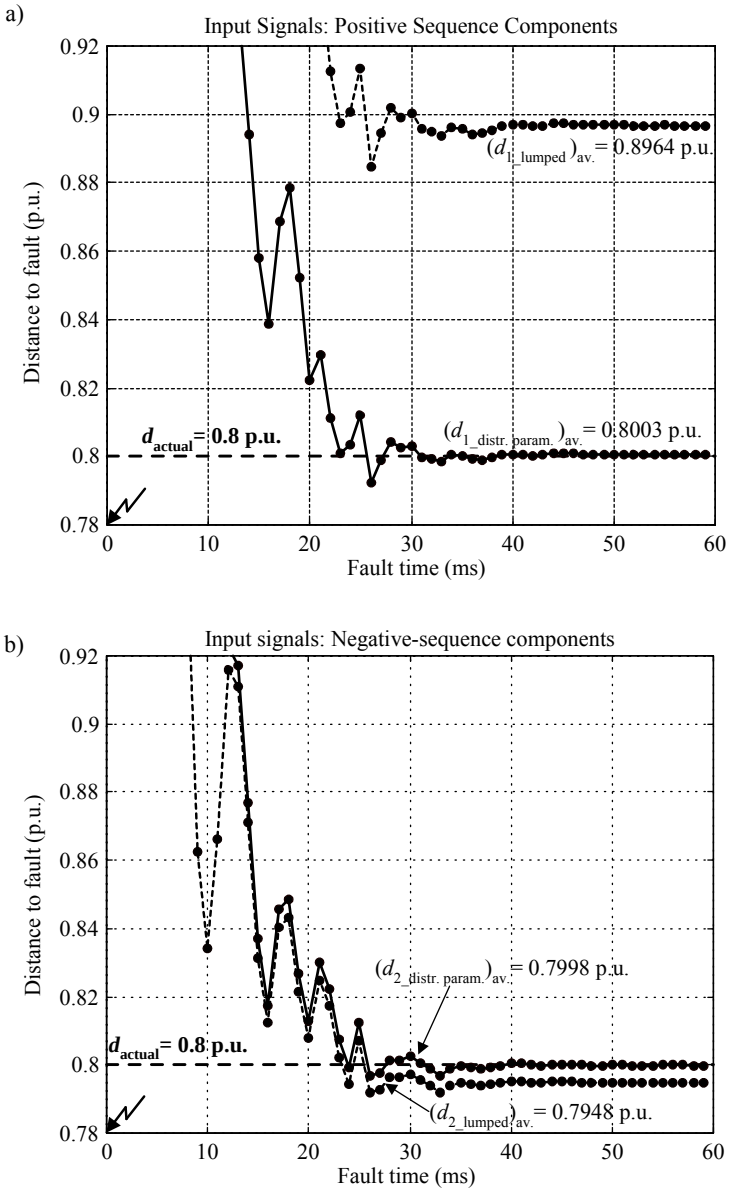

Fig. 7.8. Example of fault location – determination of the distance to fault applying lumped and distributed parameter line models, using:
a) positive-sequence components, b) negative-sequence components

Applying the distributed parameter line model for both types of symmetrical components accurate results for the distance to fault are obtained. When using the lumped

line model, application of the negative-sequence components as the fault locator input signals assures much more accurate result than for the positive-sequence components.

7.3.5. Fault location with analytical synchronisation of measurements of distance relays from line terminals

Figure 7.9 presents the idea for the post-fault analysis of protective distance relays ($Relay_S$, $Relay_R$) installed at the terminals (S, R) of the line. The voltage and current signals measured by the relays are sent to the computer performing the analysis. Versatile methods for processing the input signals have been included in the post-fault analysis program developed. Then, the fault loop impedance measurement performed in the distance relays is taken into account. The other part of the program utilises the fault loop impedance measurements which are based on the two-end fault location principle. Prior to the fault location the processed two-end signals are analytically synchronised.

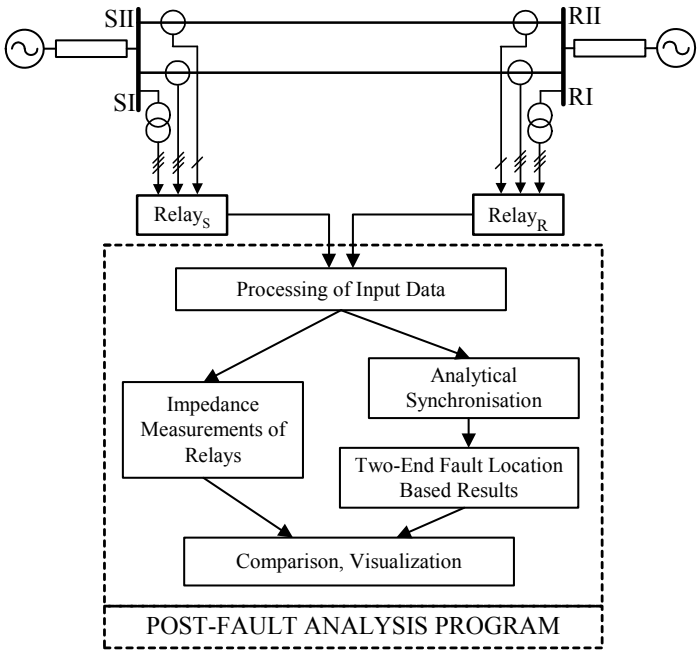

Fig. 7.9. Structure of post-fault analysis program for protective distance relays from transmission line ends

Distance relays measure the apparent impedance of the appropriate fault loop using the relaying voltage ($\underline{V}_{S\_P}$) and current ($\underline{I}_{S\_P}$) signals. These signals are composed according to the identified fault type, as shown in:

- Tables 6.3 and 6.5: for single-circuit line,
- Tables 6.4 and 6.6: for double-circuit line.

For the side S relay the fault loop can be described with the following formula for the phasor notation:

$$\underline{V}_{\mathrm{S\_P}} - d\,\underline{Z}_{\mathrm{1L}}\underline{I}_{\mathrm{S\_P}} - R_{\mathrm{F}}\underline{I}_{\mathrm{F}} = 0 \tag{7.60}$$

where:

d – distance to fault (p.u.), measured from the bus S up to fault point F,

R_{F} – fault path resistance,

$\underline{I}_{\mathrm{F}}$ – total fault current.

The measurements of distance relays from both sides (S and R) are considered as performed asynchronously. Assuming the measurements of the relay R as the reference, the signals of the relay S are multiplied by the synchronisation operator $\mathrm{e}^{\mathrm{j}\delta}$.

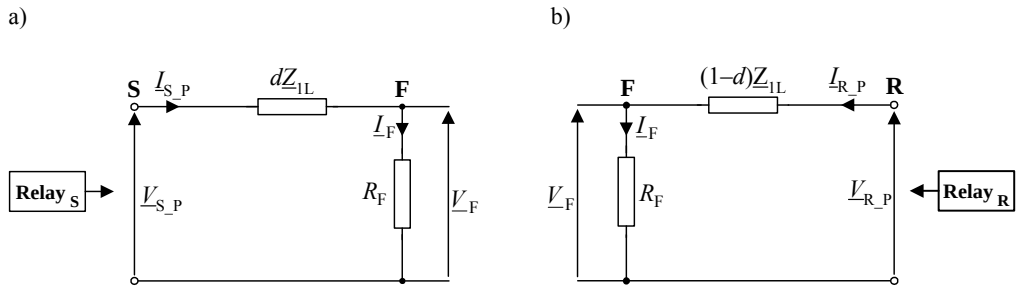

Fig. 7.10. Models of fault-loop measurement for: a) relay at bus S, b) relay at bus R

In the models from Fig. 7.10a (for the relay S) and Fig. 7.10b (for the relay R) there are longitudinal branches represented by the positive-sequence impedances of the line sections S–F and F–R. The transverse branch in these models represents the fault path through which the total fault current flows. Merging the models of measurements of these two relays (from Figs. 7.10a and b), one obtains a general model with a fictitious transverse branch (Fig. 7.11). Through this fictitious branch the following sum of the relaying currents flows:

$$\underline{I}_{\mathrm{SR}} = \underline{I}_{\mathrm{S\_P}}\mathrm{e}^{\mathrm{j}\delta} + \underline{I}_{\mathrm{R\_P}} \tag{7.61}$$

It has been proposed in [64, 148] to define the impedance of this **fictitious branch** $\underline{Z}_{\mathrm{FLT}}$ as a function of the real fault path resistance R_{F} (see fault models in Fig. 3.1) and the fault type coefficient $\underline{P}_{\mathrm{FLT}}$:

$$\underline{Z}_{\mathrm{FLT}} = \frac{R_{\mathrm{F}}}{\underline{P}_{\mathrm{FLT}}} \tag{7.62}$$

The fault type coefficient $\underline{P}_{\mathrm{FLT}}$ has to be set to such a value that the voltage drop ($\underline{V}_{\mathrm{F}}$) across the fault path in the model from Fig. 7.10a or Fig. 7.10b is identical with the drop across the impedance $\underline{Z}_{\mathrm{FLT}}$ (7.62) in the model from Fig. 7.11. This condition results in the following formula:

$$R_{\mathrm{F}}\underline{I}_{\mathrm{F}} = \frac{R_{\mathrm{F}}}{\underline{P}_{\mathrm{FLT}}}(\underline{I}_{\mathrm{S\_P}}\mathrm{e}^{\mathrm{j}\delta} + \underline{I}_{\mathrm{R\_P}}) \tag{7.63}$$

From (7.63) one obtains:

$$\underline{P}_{\mathrm{FLT}} = \frac{\underline{I}_{\mathrm{S\_P}}\mathrm{e}^{\mathrm{j}\delta} + \underline{I}_{\mathrm{R\_P}}}{\underline{I}_{\mathrm{F}}} \tag{7.64}$$

Expressing the relaying currents from the nominator of (7.64) and the total fault current from the denominator of (7.64) in terms of the respective symmetrical components allows the coefficient $\underline{P}_{\mathrm{FLT}}$ to be determined for different fault types, as gathered in Table 7.2.

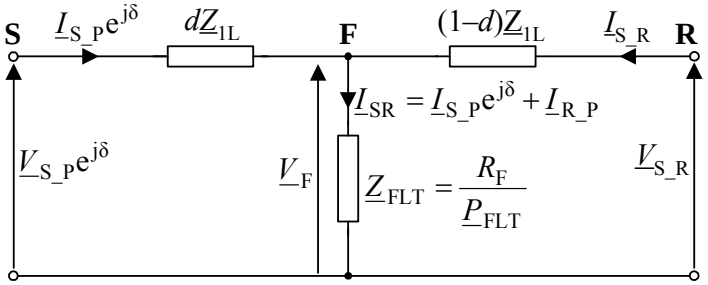

Fig. 7.11. General model of measurements of relays obtained by merging the models from Figs. 7.10a, b, assuming the time reference of measurements of $\mathrm{Relay_R}$ to be the base

Table 7.2. Coefficient $\underline{P}_{\mathrm{FLT}}$ for different fault types

Fault type (Models: Fig. 4.1)	$\underline{P}_{\mathrm{FLT}}$
a–E, b–E, c–E	$\frac{2\underline{Z}_{1\mathrm{L}} + \underline{Z}_{0\mathrm{L}}}{3\underline{Z}_{1\mathrm{L}}}$
a–b, b–c, c–a	2
a–b–E, b–c–E, c–a–E, a–b–c, a–b–c–E	1

Example 7.2. Determination of $\underline{P}_{\mathbf{FLT}}$ for a–E fault

According to Table 6.5, the relaying currents for the single-circuit transmission line and a–E fault are determined as follows:

$$[\underline{I}_{\mathrm{S\_P}}\mathrm{e}^{\mathrm{j}\delta}]_{(\mathrm{a-E})} = \left(\underline{I}_{\mathrm{S1}} + \underline{I}_{\mathrm{S2}} + \frac{\underline{Z}_{\mathrm{0L}}}{\underline{Z}_{\mathrm{1L}}}\underline{I}_{\mathrm{S0}}\right)\mathrm{e}^{\mathrm{j}\delta}$$

$$[\underline{I}_{\mathrm{R\_P}}]_{(\mathrm{a-E})} = \underline{I}_{\mathrm{R1}} + \underline{I}_{\mathrm{R2}} + \frac{\underline{Z}_{\mathrm{0L}}}{\underline{Z}_{\mathrm{1L}}}\underline{I}_{\mathrm{R0}}$$

The total fault current for a–E fault can be expressed as the following sum of its symmetrical components:

$$\underline{I}_{\mathrm{F}} = \underline{I}_{\mathrm{F1}} + \underline{I}_{\mathrm{F2}} + \underline{I}_{\mathrm{F0}}$$

Substitution of the above three formulae into (7.64) yields:

$$[\underline{P}_{\mathrm{FLT}}]_{(\mathrm{a-E})} = \frac{\left(\underline{I}_{\mathrm{S1}} + \underline{I}_{\mathrm{S2}} + \frac{\underline{Z}_{\mathrm{0L}}}{\underline{Z}_{\mathrm{1L}}}\underline{I}_{\mathrm{S0}}\right)\mathrm{e}^{\mathrm{j}\delta} + \underline{I}_{\mathrm{R1}} + \underline{I}_{\mathrm{R2}} + \frac{\underline{Z}_{\mathrm{0L}}}{\underline{Z}_{\mathrm{1L}}}\underline{I}_{\mathrm{R0}}}{\underline{I}_{\mathrm{F1}} + \underline{I}_{\mathrm{F2}} + \underline{I}_{\mathrm{F0}}}$$

Taking into account that the symmetrical components of the total fault current can be expressed as the respective sums of components of currents from both ends (with shunt capacitances being neglected):

$$\underline{I}_{\mathrm{F1}} = \underline{I}_{\mathrm{S1}}\mathrm{e}^{\mathrm{j}\delta} + \underline{I}_{\mathrm{R1}}$$

$$\underline{I}_{\mathrm{F2}} = \underline{I}_{\mathrm{S2}}\mathrm{e}^{\mathrm{j}\delta} + \underline{I}_{\mathrm{R2}}$$

$$\underline{I}_{\mathrm{F0}} = \underline{I}_{\mathrm{S0}}\mathrm{e}^{\mathrm{j}\delta} + \underline{I}_{\mathrm{R0}}$$

the fault type coefficient equals:

$$[\underline{P}_{\mathrm{FLT}}]_{(\mathrm{a-E})} = \frac{\underline{I}_{\mathrm{F1}} + \underline{I}_{\mathrm{F2}} + \frac{\underline{Z}_{\mathrm{0L}}}{\underline{Z}_{\mathrm{1L}}}\underline{I}_{\mathrm{F0}}}{\underline{I}_{\mathrm{F1}} + \underline{I}_{\mathrm{F2}} + \underline{I}_{\mathrm{F0}}}$$

Consideration of the boundary conditions for a–E fault:

$$\underline{I}_{\mathrm{Fb}} = \underline{I}_{\mathrm{Fc}} = 0 \text{ and } \underline{I}_{\mathrm{F}} = \underline{I}_{\mathrm{Fa}} \neq 0$$

results in the following relation between the symmetrical components of the total fault current:

$$\underline{I}_{\mathrm{F1}} = \underline{I}_{\mathrm{F2}} = \underline{I}_{\mathrm{F0}}$$

Finally, the fault type coefficient for a–E fault is equal to:

$$[\underline{P}_{\mathrm{FLT}}]_{(\mathrm{a-E})} = \frac{2\underline{Z}_{1\mathrm{L}} + \underline{Z}_{0\mathrm{L}}}{3\underline{Z}_{1\mathrm{L}}}$$

The same value of $\underline{P}_{\mathrm{FLT}}$ one also obtains for the other single phase-to-earth faults (Table 7.2):

$$[\underline{P}_{\mathrm{FLT}}]_{(\mathrm{a-E})} = [\underline{P}_{\mathrm{FLT}}]_{(\mathrm{b-E})} = [\underline{P}_{\mathrm{FLT}}]_{(\mathrm{c-E})} = \frac{2\underline{Z}_{1\mathrm{L}} + \underline{Z}_{0\mathrm{L}}}{3\underline{Z}_{1\mathrm{L}}}$$

Since impedances of transmission lines for the positive- and zero-sequence, with respect to both magnitude and phase angle, are not identical, thus the fault type coefficient $\underline{P}_{\mathrm{FLT}}$ for phase-to-earth faults is a complex number.

In the case of parallel (double-circuit) transmission lines the fault type coefficient $\underline{P}_{\mathrm{FLT}}$ for single phase-to-earth faults is determined identically as for the single-circuit line. This results from the fact that after taking into account that under neglecting shunt capacitances of the line, the sum of the zero-sequence currents from both ends of parallel healthy line equals zero:

$$\frac{\underline{Z}_{0\mathrm{m}}}{\underline{Z}_{1\mathrm{L}}}\underline{I}_{\mathrm{SII0}}\mathrm{e}^{\mathrm{j}\delta} + \frac{\underline{Z}_{0\mathrm{m}}}{\underline{Z}_{1\mathrm{L}}}\underline{I}_{\mathrm{RII0}} = 0$$

The coefficient $\underline{P}_{\mathrm{FLT}}$ for other fault types can be determined analogously (Table 7.2) and one also obtains identical values for both single and parallel lines.

Example 7.3. Fault location with analytical synchronisation of measurements of distance relays from line terminals

Figures 7.12 through 7.17 present the results for the a–E fault on a 400 kV, 300 km single-circuit transmission line (the EMFs at the bus R assumed as the leading EMFs of the side S by 30°): distance to fault from the terminal S: d = 0.8 p.u., fault resistance: $R_{\mathrm{F}} = 10\ \Omega$.

The distance relay at the terminal S using the input signals as shown in Fig. 7.12 determines the fault-loop resistance (Fig. 7.13a) and reactance (Fig. 7.13b). Due to the presence of the reactance effect, the determined values differ from the actual resistance and reactance of the transmission line section from the measuring point (S) up to the fault point (F). A full-cycle Fourier filtering was applied to the measurement. Polar plots of the impedance measurements are shown in Fig. 7.14a (for the first 20 samples) and Fig. 7.14b (for the next 20 samples). One observes that due to the reactance effect the trajectory of the measured fault-loop impedance does not enter the MHO impedance characteristic, for which the reach of 85% of the line positive-sequence impedance was set. The reactance effect causes that the fault occurring at 80% of the line length is not detected by the first zone MHO element set at 85%.

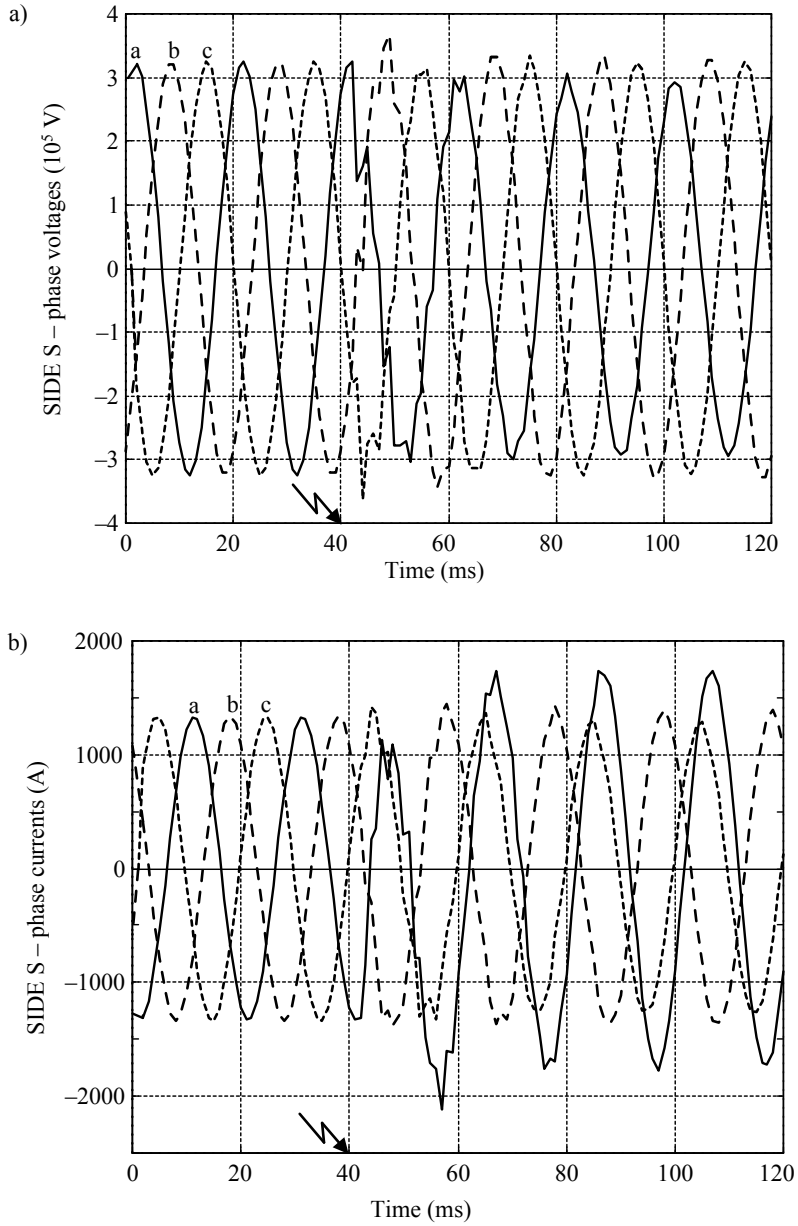

Fig. 7.12. Example of fault location: a) voltage at side S, b) current at side S

Application of the two-end fault location algorithm allows accurate location of the fault. It starts with determination of the synchronisation angle using the relaying signals (fault-loop voltage and current), Fig. 7.15a, or the negative-sequence signals, Fig. 7.15b.

This allows us to select the valid values for the synchronisation angle (18.47°, 18.15°), which are very close to the introduced intentional de-synchronisation (δ_{actual} = 18°). Taking the synchronisation angle the distance to fault (*d* [p.u.]) was determined. Then, the fault-loop impedance using the fault location principle (Fig. 7.16) was calculated: $\underline{Z}_{FL} = d\underline{Z}_{1L}$, the trajectory of which surely enters the MHO characteristic. Figure 7.17 shows a comparison of the fault-loop resistance (Fig. 7.17a) and reactance (Fig. 7.17b) determined in two different ways (according to classic distance relay measurement and using the two-end fault location principle). It is clearly shown that using the two-end fault location principle, the influence of the reactance effect is fully compensated for.

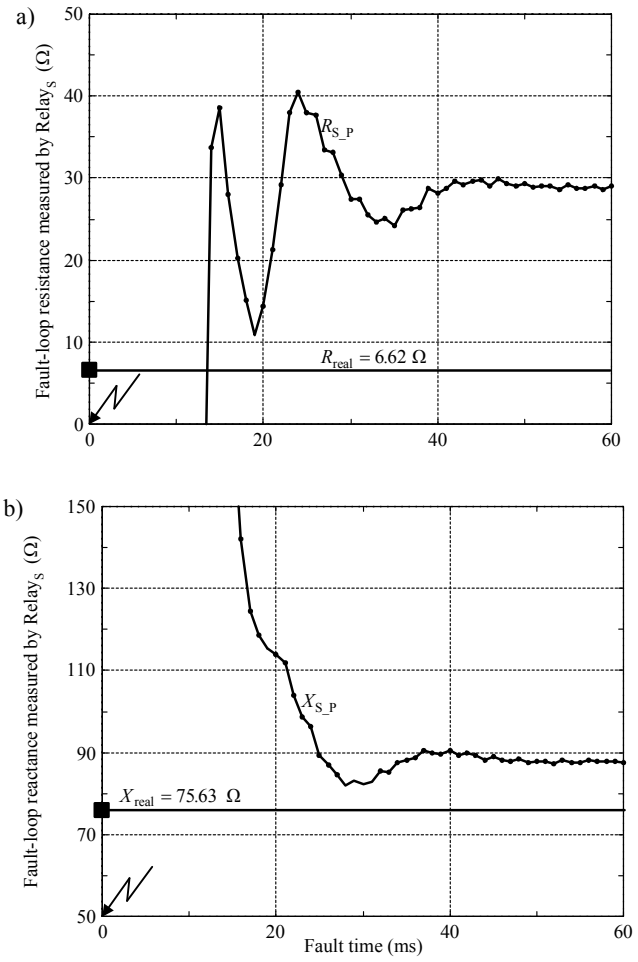

Fig. 7.13. Example of fault location: a) fault-loop resistance measured by relay at S, b) fault-loop reactance measured by relay at S

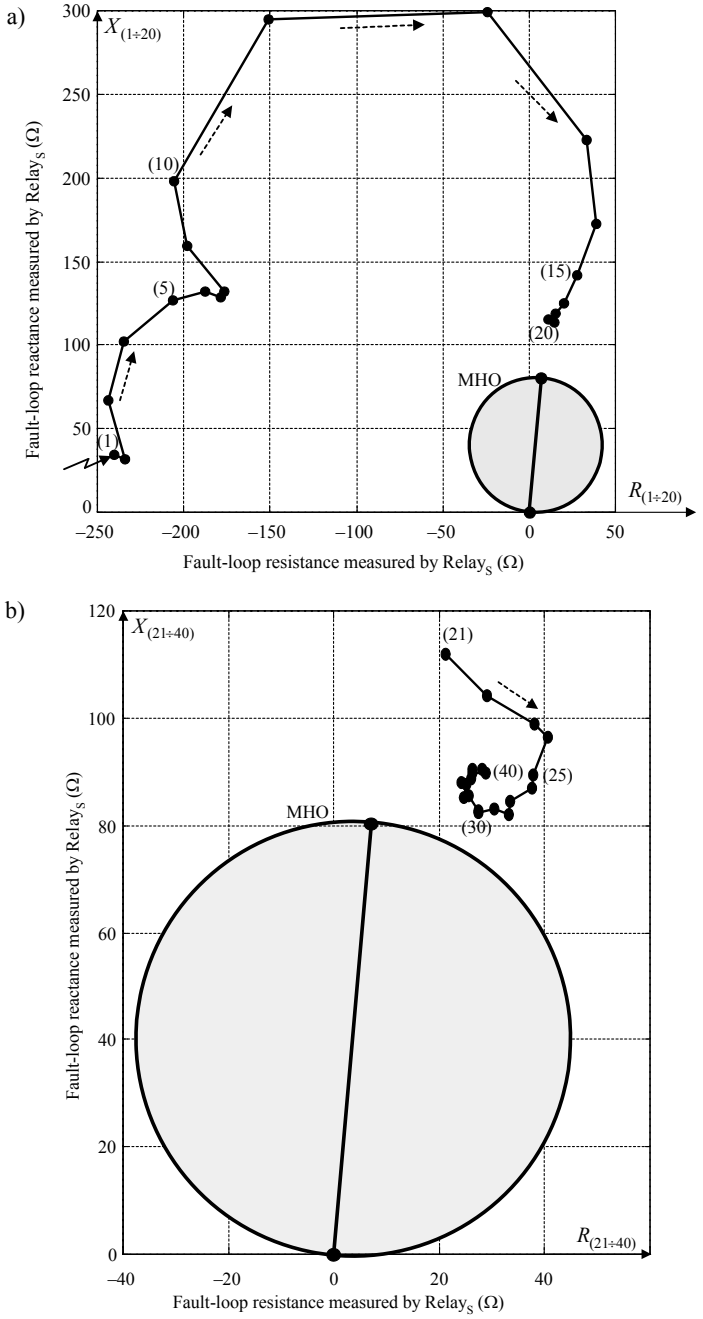

Fig. 7.14. Example of fault location: a) polar plot of fault-loop impedance measured by relay at S – first 20 samples since fault inception, b) polar plot of fault-loop impedance measured by relay at S – next 20 samples since fault inception

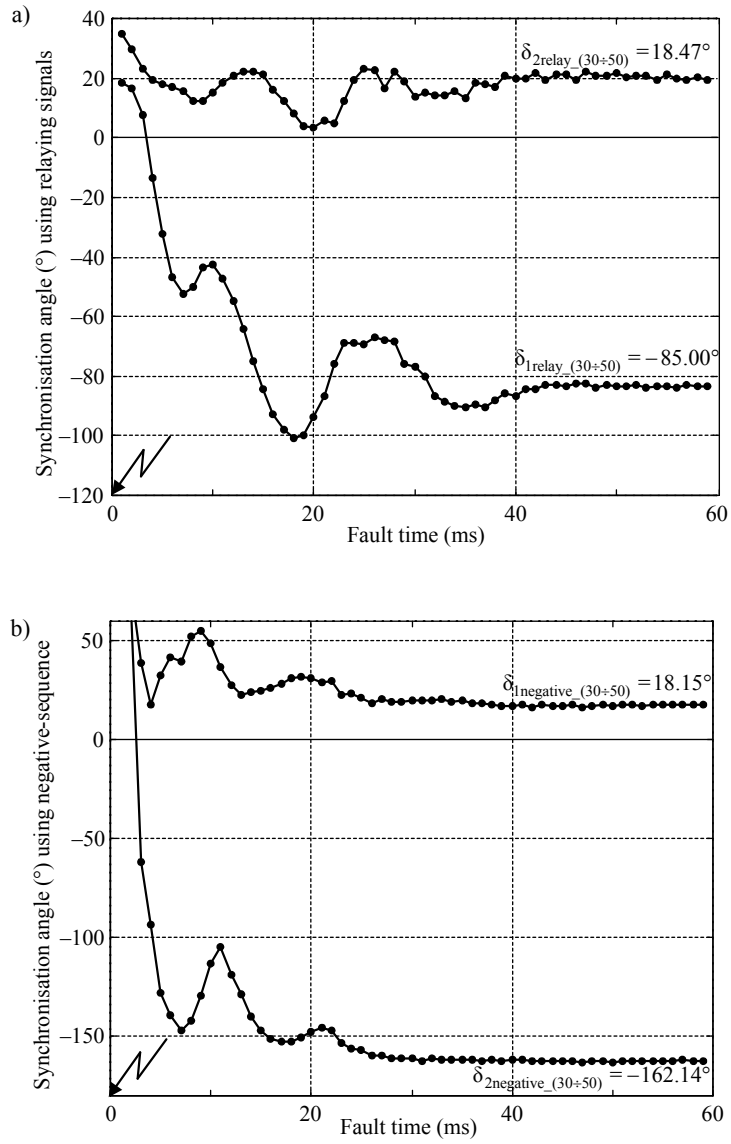

Fig. 7.15. Example of fault location – determination of synchronisation angle using: a) relaying signals, b) negative-sequence components

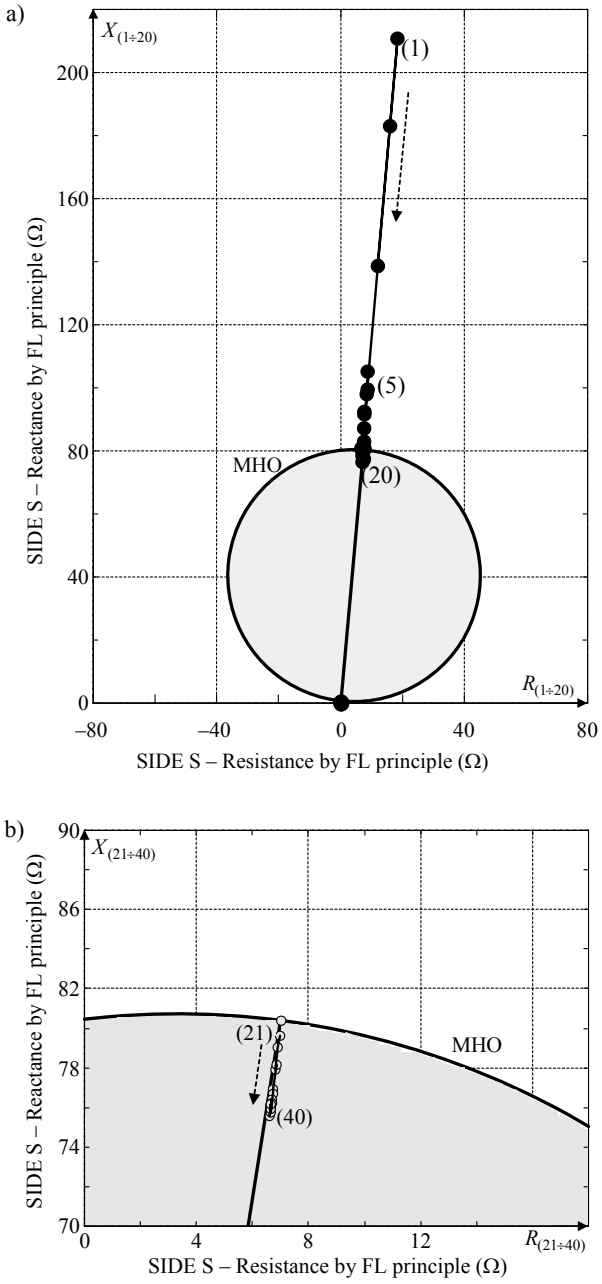

Fig. 7.16. Example of fault location – determination of fault-loop impedance by applying the fault location principle: a) for the first 20 samples since fault inception, b) for the next 20 samples since fault inception

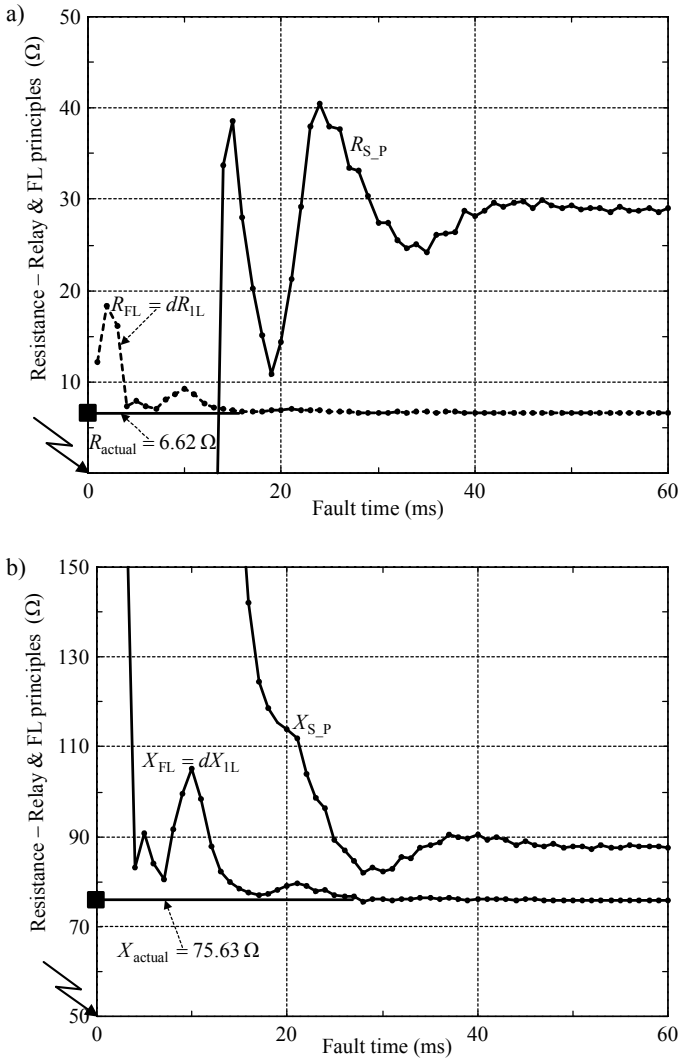

Fig. 7.17. Example of fault location – comparison of fault-loop impedance determined by distance relay measurement and by applying the fault location principle: a) fault-loop resistance, b) fault-loop reactance

7.3.6. Fault location with use of unsynchronised measurements of distance relays from line terminals

Applying the general model derived, depicted in Fig. 7.11, one can describe the measurements performed by impedance relays from both terminals of the faulted line as:

$$\underline{V}_{\mathrm{S\_P}}\,\mathrm{e}^{\mathrm{j}\delta} - d\,\underline{Z}_{1\mathrm{L}}\,\underline{I}_{\mathrm{S\_P}}\,\mathrm{e}^{\mathrm{j}\delta} - \frac{R_{\mathrm{F}}}{\underline{P}_{\mathrm{FLT}}}(\underline{I}_{\mathrm{S\_P}}\,\mathrm{e}^{\mathrm{j}\delta} + \underline{I}_{\mathrm{R\_P}}) = 0 \tag{7.65}$$

$$\underline{V}_{\mathrm{R\_P}} - (1-d)\underline{Z}_{1\mathrm{L}} I_{\mathrm{R\_P}} - \frac{R_{\mathrm{F}}}{\underline{P}_{\mathrm{FLT}}}(\underline{I}_{\mathrm{S\_P}}\,\mathrm{e}^{\mathrm{j}\delta} + \underline{I}_{\mathrm{R\_P}}) = 0 \tag{7.66}$$

Introducing the apparent impedances measured by the impedance relays:

$$\underline{Z}_{\mathrm{S\_P}} = \frac{\underline{V}_{\mathrm{S\_p}}\,\mathrm{e}^{\mathrm{j}\delta}}{\underline{I}_{\mathrm{S\_P}}\,\mathrm{e}^{\mathrm{j}\delta}} \tag{7.67}$$

$$\underline{Z}_{\mathrm{R\_P}} = \frac{\underline{V}_{\mathrm{R\_P}}}{\underline{I}_{\mathrm{R\_P}}} \tag{7.68}$$

equations (7.65)–(7.66) transform to:

$$\underline{Z}_{\mathrm{S\_P}} - d\,\underline{Z}_{1\mathrm{L}} - \frac{R_{\mathrm{F}}}{\underline{P}_{\mathrm{FLT}}}\frac{(\underline{I}_{\mathrm{S\_P}}\,\mathrm{e}^{\mathrm{j}\delta} + \underline{I}_{\mathrm{R\_P}})}{\underline{I}_{\mathrm{S\_P}}\,\mathrm{e}^{\mathrm{j}\delta}} = 0 \tag{7.69}$$

$$\underline{Z}_{\mathrm{R\_P}} - (1-d)\underline{Z}_{1\mathrm{L}} - \frac{R_{\mathrm{F}}}{\underline{P}_{\mathrm{FLT}}}\frac{(\underline{I}_{\mathrm{S\_P}}\,\mathrm{e}^{\mathrm{j}\delta} + \underline{I}_{\mathrm{R\_P}})}{\underline{I}_{\mathrm{R\_P}}} = 0 \tag{7.70}$$

Combining (7.69)–(7.70), and eliminating the fault loop currents, one obtains the following quadratic formula for the complex numbers with the unknowns d, R_{F}:

$$\underline{D}_2 d^2 + \underline{D}_1 d + \underline{D}_0 + \frac{R_{\mathrm{F}}}{\underline{P}_{\mathrm{FLT}}}\underline{N}_0 = 0 \tag{7.71}$$

where:

$\underline{D}_2 = \underline{Z}_{1\mathrm{L}}\underline{Z}_{1\mathrm{L}}$,

$\underline{D}_1 = \underline{Z}_{1\mathrm{L}}\underline{Z}_{\mathrm{R\_P}} - \underline{Z}_{1\mathrm{L}}\underline{Z}_{1\mathrm{L}} - \underline{Z}_{1\mathrm{L}}\underline{Z}_{\mathrm{S\_P}}$,

$\underline{D}_0 = \underline{Z}_{1\mathrm{L}}\underline{Z}_{\mathrm{S\_P}} - \underline{Z}_{\mathrm{S\_P}}\underline{Z}_{\mathrm{R\_P}}$,

$\underline{N}_0 = \underline{Z}_{\mathrm{S\_P}} + \underline{Z}_{\mathrm{R\_P}} - \underline{Z}_{1\mathrm{L}}$,

$\underline{P}_{\mathrm{FLT}}$ – as in Table 7.2.

Analysis of the quantity $\underline{N}_0$ from (7.71) allows for distinguishing the solid faults (or involving comparatively low fault resistances) from those evidently resistive. In the second case (resistive faults), after resolving (7.71) into the real and imaginary components, respectively, the following quadratic formula for a sought fault distance is obtained:

$$F_A(d) = A_2 d^2 + A_1 d + A_0 = 0 \tag{7.72}$$

where A_2, A_1, A_0 – real number coefficients (derived accordingly from (7.71)), involving only the apparent impedances – defined in Equations (7.67)–(7.68), and the fault type coefficient $\underline{P}_{FLT}$ (Table 7.2).

One of the roots of (7.72) gives the valid solution for a distance to fault. In some cases it may happen that both roots are within the line length. In order to cope with such troublesome cases an extra formula has to be derived. This can be accomplished by combining (7.69)–(7.70) with elimination of the quantity $R_F/\underline{P}_{FLT}$. As a result, one obtains:

$$d = \frac{1 - \dfrac{\underline{Z}_{R\_P}}{\underline{Z}_{1L}} + \dfrac{\underline{Z}_{S\_P}}{\underline{Z}_{1L}}\underline{W}}{\underline{W} + 1} \tag{7.73}$$

where:

$$\underline{W} = \frac{\underline{I}_{S\_P} e^{j\delta}}{\underline{I}_{R\_P}} = |\underline{W}| e^{jw},$$

$$|\underline{W}| = \left| \frac{\underline{I}_{S\_P} e^{j\delta}}{\underline{I}_{R\_P}} \right| = \left| \frac{\underline{I}_{S\_P}}{\underline{I}_{R\_P}} \right|,$$

$$w = \text{angle}\left(\frac{\underline{I}_{S\_P} e^{j\delta}}{\underline{I}_{R\_P}} \right) = \text{angle}\left(\frac{\underline{I}_{S\_P}}{\underline{I}_{R\_P}} \right) + \delta.$$

A sought distance to fault can be calculated from (7.73) if besides the apparent impedances, defined in (7.67)–(7.68), the ratio of the phasors of the fault loop currents of both relays ($\underline{W}$) is provided. The magnitude of this ratio ($|\underline{W}|$) is not affected by the synchronisation angle (δ). In contrast, calculation of the angle (w) requires knowing this angle. There are different possibilities of measuring this angle, as for example, with utilising the pre-fault measurements. However, setting the angle (w) in (7.73) by trial and error method, so that the right-hand side of (7.73) is the real number, may be a good alternative.

7.4. Fault location with use of incomplete two-end measurement

7.4.1. Fault location with use of two-end voltages

In [13], a fault-location method utilising only synchronised measurements of two-end voltages was proposed. It has been assumed that currents should be excluded

completely in order to obtain a fault location algorithm free from CT errors. Thus, the fault location algorithm from [13] appears to be completely immune to CT saturation, which is an important advantage of it. On the other hand, the need of providing source impedances from both line ends is a serious drawback. This is so since a mismatch between the data provided and the actual source impedances may happen and thus the fault location accuracy can be deteriorated. The algorithm from [13] is formulated using matrix description of the transmission network.

In [103], several algorithms utilising only the voltages, dispensing with current transformers and thus eliminating the errors caused by saturation of current transformers are presented. The algorithms are applicable to line to earth faults, line to line faults, and line to line to earth faults. The algorithms utilise unsynchronised fault voltage measurements from two ends of a line and do not require pre-fault data. Shunt capacitances of the line are fully considered.

In [187], a method for locating faults on two-terminal transmission lines based on the fundamental components of fault and pre-fault voltage measured at the two ends of a transmission line has been introduced. This methodology allows one to establish a direct calculation procedure that is independent of fault and pre-fault currents, fault type, fault resistance, synchronisation condition of register devices located on line ends, and pre-fault condition, either balanced or not. This is achieved by defining a new concept called 'distance factor' in relation to the circuit diagram of the transmission network for the superimposed positive sequence:

$$K_{\mathrm{V}} = \left| \frac{\Delta \underline{V}_{\mathrm{S1}} \mathrm{e}^{\mathrm{j}\delta}}{\Delta \underline{V}_{\mathrm{R1}}} \right| \tag{7.74}$$

where $\Delta \underline{V}_{\mathrm{S1}}$, $\Delta \underline{V}_{\mathrm{R1}}$ – superimposed positive-sequence voltage obtained from asynchronous measurements of voltages at both line ends (S, R).

Taking into account that for the synchronisation operator we have $|\mathrm{e}^{\mathrm{j}\delta}| = 1$, one can see that the distance factor (7.74) is a real number function of:

- positive-sequence impedance and admittance of the transmission line,
- positive-sequence impedances of the sources (S, R) and extra link between the buses S, R (Fig. 7.18),
- distance to fault (d).

In general, the distance factor can be expressed as the following function:

$$K_{\mathrm{V}} = f(\underline{Z}'_{\mathrm{1L}}, \underline{Y}'_{\mathrm{1L}}, \underline{Z}_{\mathrm{1S}}, \underline{Z}_{\mathrm{1R}}, \underline{Z}_{\mathrm{1EQ}}, d) \tag{7.75}$$

Knowing the impedance/admittance data involved in (7.75) one can draw the plot for the distance factor as in Fig. 7.19: $(K_{\mathrm{V}})_{\mathrm{theoretical}}$. The same can be done with use of a simulation tool, by applying faults at subsequent locations and calculating the distance factor according to the definition (7.74).

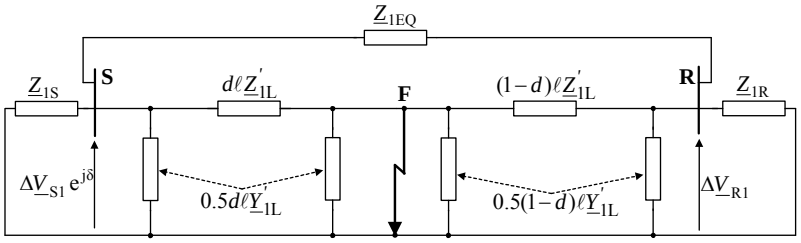

Fig. 7.18. Equivalent circuit-diagram for two-end unsynchronised measurement of superimposed positive-sequence voltage

The distance to fault can be determined by finding the intersection of the distance factor obtained from theoretical considerations ($(K_V)_{theoretical}$) and that measured according to the definition (7.74), as shown in Fig. 7.19.

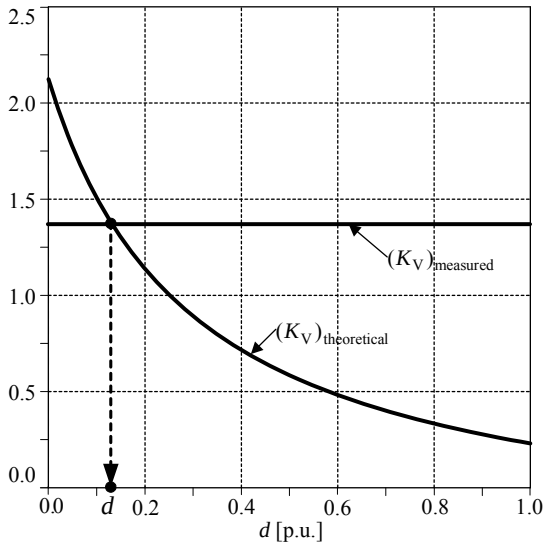

Fig. 7.19. Plots of the distance factors determined theoretically and obtained from measurement

The fault location algorithm from [187], similarly to the algorithm proposed in [13], is completely immune to CT saturation. However, also the source impedances are required to be known.

7.4.2. Fault location with use of two-end voltages and one-end current

It is well known from the experience and literature [162] that if the CT saturation occurs, it basically occurs at one side of the line only. Therefore, it appears favourable

to include the secondary currents of the CTs from the line side with no CT saturation to the fault locator input signals, besides voltages acquired at both line sides, which were utilised in the methods introduced in [13, 187]. As a result, still incomplete two-end signals are utilised, but more information can be gained from the signals. The fault location algorithm utilising such incomplete two-end signals measured asynchronously was introduced in [65, 149].

Let us present the fault location algorithm for the case with CT saturation occurring at the line side R (the other case: saturation of CTs at the side S can be resolved analogously). For the purpose of recognizing saturation, the algorithms known from literature have to be applied. As a result of identifying the CT saturation at the line end R, the three-phase current phasors measured at the side R $\{\underline{I}_{\mathrm{Ra}}, \underline{I}_{\mathrm{Rb}}, \underline{I}_{\mathrm{Rc}}\}$ are further rejected, regardless of how many CTs (only one, or two, or all three CTs) have become saturated. Finally, the following three-phase phasors are applied for determining the distance to fault:

- voltages at the bus S: $\{\underline{V}_{\mathrm{Sa}}, \underline{V}_{\mathrm{Sb}}, \underline{V}_{\mathrm{Sc}}\}$,
- voltages at the bus R: $\{\underline{V}_{\mathrm{Ra}}, \underline{V}_{\mathrm{Rb}}, \underline{V}_{\mathrm{Rc}}\}$,
- currents at the bus S: $\{\underline{I}_{\mathrm{Sa}}, \underline{I}_{\mathrm{Sb}}, \underline{I}_{\mathrm{Sc}}\}$.

Since asynchronous measurements are considered in this algorithm [65], an analytical synchronisation is performed by multiplying all phasors from the side S (the side R measurement is assumed here as the basis) by the synchronisation operator $\mathrm{e}^{\mathrm{j}\delta}$.

In relation to Fig. 7.2, where the distributed parameter model of faulted transmission line for the *i*-th symmetrical component is presented, the following generalised model, describing the fault loop seen from the terminal S, can be formulated:

$$\underline{V}_{\mathrm{F\_P}}(d, \mathrm{e}^{\mathrm{j}\delta}) - R_{\mathrm{F}}\underline{I}_{\mathrm{F}} = 0 \tag{7.76}$$

where:

$\underline{V}_{\mathrm{F\_P}}(d, \mathrm{e}^{\mathrm{j}\delta})$ – fault-loop voltage (composed accordingly to the fault type) after having been transferred from the measuring point S to the fault point F (Fig. 7.2),

d – unknown distance to fault (p.u.), as measured from the terminal S,

R_F – unknown fault path resistance,

I_F – fault path current (total fault current).

The fault-loop voltage at the fault point F can be composed as follows:

$$\underline{V}_{\mathrm{F\_P}}(d, \mathrm{e}^{\mathrm{j}\delta}) = \underline{a}_1\underline{V}_{\mathrm{F1}} + \underline{a}_2\underline{V}_{\mathrm{F2}} + \underline{a}_0\underline{V}_{\mathrm{F0}} \tag{7.77}$$

where $\underline{a}_1$, $\underline{a}_2$, $\underline{a}_0$ – weighting coefficients dependent on fault type (Table 6.5).

Applying the distributed parameter model of the line (Fig. 7.2), the *i*-th symmetrical component of voltages at the fault point, involved in (7.77), equals:

$$\underline{V}_{\mathrm{F}i} = (\underline{V}_{\mathrm{S}i}\cosh(\underline{\gamma}_i d\ell) - \underline{Z}_{\mathrm{c}i}\underline{I}_{\mathrm{S}i}\sinh(\underline{\gamma}_i d\ell))\mathrm{e}^{\mathrm{j}\delta} \tag{7.78}$$

Then, the total fault current ($\underline{I}_F$) is determined as a composition of its positive- and negative-sequence components:

$$\underline{I}_F = \frac{\underline{M}_{12}(e^{j\delta})}{\underline{Z}_{c1}\sinh(\underline{\gamma}_1(1-d)\ell)} \tag{7.79}$$

where:

$\underline{M}_{12}(e^{j\delta}) = \underline{a}_{F1}(\underline{V}_{R1} + \underline{N}_{S1}e^{j\delta}) + \underline{a}_{F2}(\underline{V}_{R2} + \underline{N}_{S2}e^{j\delta})$,

$\underline{N}_{S1}$, $\underline{N}_{S2}$ – as in (7.28),

$\underline{a}_{F1}$, $\underline{a}_{F2}$ – share coefficients dependent on fault type (any set taken from Tables 4.3–4.5 can be applied).

Substituting the total fault current (7.79) into the general fault loop model (7.76) yields:

$$\underline{V}_{F\_P}(d, e^{j\delta}) - R_F \frac{\underline{M}_{12}(e^{j\delta})}{\underline{Z}_{c1}\sinh(\underline{\gamma}_1(1-d)\ell)} = 0 \tag{7.80}$$

In order to solve (7.80) for the distance to fault (d) and fault resistance (R_F), the synchronisation operator $e^{j\delta}$ has to be determined as well. In [65], it has been proposed to determine this operator for particular faults as follows:

- *single-phase and phase-to-phase faults* – by utilising formula (7.31), obtained from analysis of boundary conditions of the faults,
- *phase-to-phase-to-ground faults* – with use of formula (7.32), obtained by considering the relation between the zero-sequence component of the total fault current and the remaining components,
- *three-phase balanced faults* – by utilising formula (7.21) involving pre-fault positive-sequence voltages from both line sides and one-end current (from bus S).

Note that the most complex solution appears for the case of phase-to-phase-to-ground faults since here the Newton–Raphson iterative calculations have to be applied for the formulae (7.80) and (7.32). Resolving them into the real and imaginary parts one obtains four real number equations, which have to be solved for the following unknowns: d, R_F, $\sin(\delta)$, $\cos(\delta)$.

For the other fault types, i.e. all, except phase-to-phase-to-ground faults, the Newton–Raphson calculations are applied only to (7.80), which after having been resolved into the real and imaginary parts gives two equations.

7.4.3. Fault location with use of two-end currents and one-end voltage

Modern microprocessor-based current differential relays exchange locally measured current phasors over long distances. For this purpose different forms of communication

means are utilised. The current differential protection principle requires synchronisation of digital measurements performed at different line terminals. This is accomplished using the well-known Global Positioning System (GPS) or other techniques [B.8].

This fault location method is aimed at application to current differential protective relays of the two-terminal power transmission or distribution line, analogously as in [66] for a three-terminal line. It is assumed that such a fault locator apart from three-phase currents from both ends of the line is additionally provided with three-phase voltages from the local line terminal (Fig. 7.20). The signals provided from both ends of the line are considered as synchronised. In case this is not so, the synchronisation angle can be determined with use of the already known algorithms.

Distinctive availability of the measurement signals for this method has been assumed since the fault location algorithm (being of off-line regime nature) is designed as the added feature for the current differential protection relay. The differential relay when applied to protect the two-terminal line utilises phase currents measured synchronously at both line terminals. Therefore, in order to incorporate the fault location function additionally to the protection function itself, the local phase voltages (from the terminal S in further considerations) have to be supplied to the relay. In this way, the differential relay, with the fault location added, can identify the fault not only indicating whether it has occurred within the zone or outside it (which is performed by the differential relay principle itself), but also stating precisely at what distance from the particular line terminal (performed with the fault location principle).

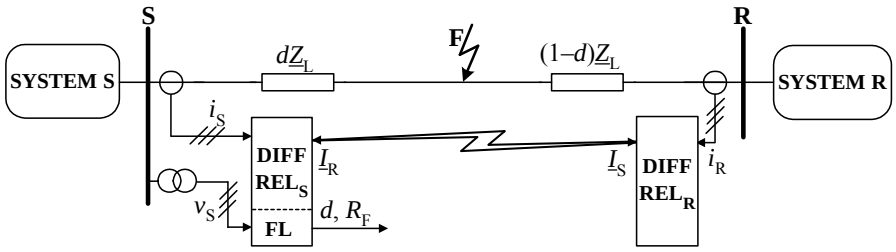

Fig. 7.20. Fault locator added to the current differential protective relays of two-terminal line

The generalised fault loop model, expressed in terms of phasors, can be utilised for deriving the fault location algorithm. This is a single universal formula covering different fault types, obtained with coefficients dependent on a fault type:

$$\underline{V}_{S\_P} - d\underline{Z}_{1L}\underline{I}_{S\_P} - R_F\underline{I}_F = 0 \tag{7.81}$$

where:

$\underline{V}_{S\_P}$, $\underline{I}_{S\_P}$ – fault-loop voltage and current, composed as shown in Tables 6.5 and 6.6,

d – unknown distance to fault (p.u.), measured from the bus S,

R_F – unknown fault resistance,

$\underline{I}_F$ – total fault current.

Since currents at both line ends are available (measured synchronously), the total fault current ($\underline{I}_F$) can be easily determined by adding, in particular phases (a, b, c), currents flowing from both ends towards the fault:

$$\underline{I}_{Fa} = \underline{I}_{Sa} + \underline{I}_{Ra} \tag{7.82}$$

$$\underline{I}_{Fb} = \underline{I}_{Sb} + \underline{I}_{Rb} \tag{7.83}$$

$$\underline{I}_{Fc} = \underline{I}_{Sc} + \underline{I}_{Rc} \tag{7.84}$$

The respective phase current from (7.82)–(7.84) (for single phase-to-ground faults) or respective difference of phase currents (for inter-phase faults) is then substituted to (7.81).

As an alternative to the direct addition, as presented in (7.82)–(7.84), the total fault current can be determined from the respective sequence currents from both line ends.

For all the faults, but with exception of three-phase balanced faults, it is advantageous to utilise the negative- and zero-sequence components, while avoiding the positive-sequence (choosing a set of share coefficients, for which $\underline{a}_{F1} = 0$):

$$[\underline{I}_F]_{ph-E,\, ph1-ph2,\, ph1-ph2-E} = \underline{a}_{F2}(\underline{I}_{S2} + \underline{I}_{R2}) + \underline{a}_{F0}(\underline{I}_{S0} + \underline{I}_{R0}) \tag{7.85}$$

where $\underline{a}_{F2}$, $\underline{a}_{F0}$ – share coefficients for all the faults except three-phase balanced ones, Table 4.6.

For three-phase balanced faults, there are no negative- nor zero-sequence quantities, and the total fault current can be determined from the positive-sequence components, or alternatively and more accurately from the superimposed positive-sequence components:

$$[\underline{I}_F]_{3-ph} = \underline{a}_{F1}(\Delta\underline{I}_{S1} + \Delta\underline{I}_{R1}) \tag{7.86}$$

where $\underline{a}_{F1}$ – share coefficient for three-phase balanced faults from Table 4.6.

Having determined the total fault current (7.85)–(7.86), the generalised fault loop model can be solved for the unknowns d and R_F.

The fault location accuracy of the method presented can be improved by introducing the distributed parameter line model, similarly as for the algorithm from Section 7.4.2 (fault location with use of two-end voltages and one-end current). The total fault current ($\underline{I}_F$) can be determined as the following composition of its positive- and negative-sequence components:

$$\underline{I}_{\mathrm{F}} = \frac{\underline{M}_{12}}{\cosh(\underline{\gamma}_1(1-d)\ell)} \tag{7.87}$$

where:

$\underline{M}_{12} = \underline{a}_{\mathrm{F1}}(\underline{I}_{\mathrm{R1}} + \underline{N}_{\mathrm{S1}}) + \underline{a}_{\mathrm{F2}}(\underline{I}_{\mathrm{R2}} + \underline{N}_{\mathrm{S2}})$

$\underline{N}_{\mathrm{S1}}$, $\underline{N}_{\mathrm{S2}}$ – as in (7.35),

$\underline{a}_{\mathrm{F1}}$, $\underline{a}_{\mathrm{F2}}$ – share coefficients dependent on fault type (any set from Tables 4.3–4.5 can be applied).

7.4.4. Fault location with exchange of limited information

In [177, 178], a fault location system for two-terminal and also multi-terminal transmission lines has been introduced. The algorithm used by this system is suitable for inclusion in a numerical protection relay, which communicates with remote relay(s) and exchanges information over a protective relaying channel. The data volume communicated between relays is sufficiently small to be easily transmitted using a digital protection channel. The algorithm does not require data alignment, pre-fault load flow information, phase selection information, and does not perform iterations to calculate the distance to the fault. Pre-fault load flow, zero-sequence mutual coupling, fault resistance, power system non-homogeneity, and current infeeds from other line terminals or tapped loads do not affect the fault location accuracy.

In relation to Fig. 7.21, one can write down the formula, which comes from comparison of the negative-sequence voltage at the fault point F, viewed from both line terminals S, R, respectively:

$$(\underline{Z}_{2\mathrm{S}} + d\underline{Z}_{2\mathrm{L}})\underline{I}_{\mathrm{S2}}\mathrm{e}^{\mathrm{j}\delta} = (\underline{Z}_{2\mathrm{R}} + (1-d)\underline{Z}_{2\mathrm{L}})\underline{I}_{\mathrm{R2}} \tag{7.88}$$

Application of negative-sequence components in (7.88) implies that this algorithm is for all faults, except three-phase balanced ones, for which the superimposed positive sequence can be applied.

The absolute value of the negative-sequence current from the remote bus R is determined from (7.88) as:

$$|\underline{I}_{\mathrm{R2}}| = \frac{|\underline{Z}_{2\mathrm{S}}I_{\mathrm{S2}} + d\underline{Z}_{2\mathrm{L}}\underline{I}_{\mathrm{S2}}|}{|\underline{Z}_{2\mathrm{R}} + \underline{Z}_{2\mathrm{L}} - d\underline{Z}_{2\mathrm{L}}|} \tag{7.89}$$

This leads to cancelling the synchronisation operator. Finally, the following quadratic formula for the distance to fault is obtained:

$$A_2 d^2 + A_1 d + A_0 = 0 \tag{7.90}$$

where A_2, A_1, A_0 – coefficients dependent on negative-sequence quantities measured by each relay and impedance data of the network.

It is distinctive that the relay at each line terminal of the two-terminal line must transmit a minimal amount of information. The information sent by the relay at side S for a two-terminal application includes:

- magnitude of the negative-sequence current: $|\underline{I}_{S2}|$,
- magnitude of the negative-sequence source impedance: $|\underline{Z}_{2S}|$,
- angle of negative-sequence source impedance: angle($\underline{Z}_{2S}$).

Using the above information combined with the negative-sequence quantities measured by each relay, we can determine the fault location at each terminal without iterations. However, the lumped line model is applied and thus acceptable accuracy is achieved for lines being not too long.

This algorithm is also extended to three-terminal line application, which was presented in [177, 178].

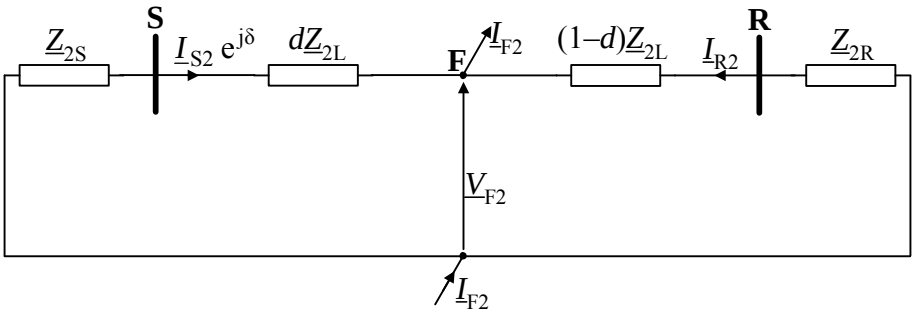

Fig. 7.21. Circuit diagram of transmission network for negative-sequence

7.5. Fault location on three-terminal lines

7.5.1. Fault location on three-terminal lines with use of three-end measurements

A circuit diagram of three-terminal line for considering a fault location using three-end measurements is presented in Fig. 7.22 (synchronised measurements) and in Fig. 7.23 (unsynchronised measurements). Different types of signals can be processed and in Figs. 7.22–7.23 the type is marked by the subscript *i*.

In the case of unsynchronised measurements, the measurements at one end have to be assumed as the basis (in Fig. 7.23: from the end B), while those from the buses A and C have to be analytically synchronised, with use of the synchronisation operators $e^{j\delta_1}$ and $e^{j\delta_2}$, respectively. Thus, two additional unknowns: syn-

chronisation angles δ_1 and δ_2 appear in comparison to the case of synchronised measurements.

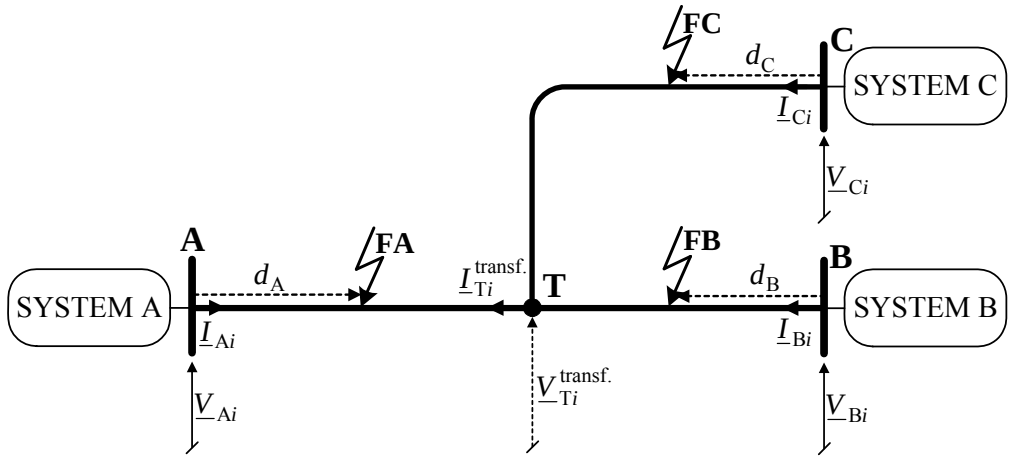

Fig. 7.22. Circuit diagram of three-terminal line for considering fault location using three-end synchronised measurements

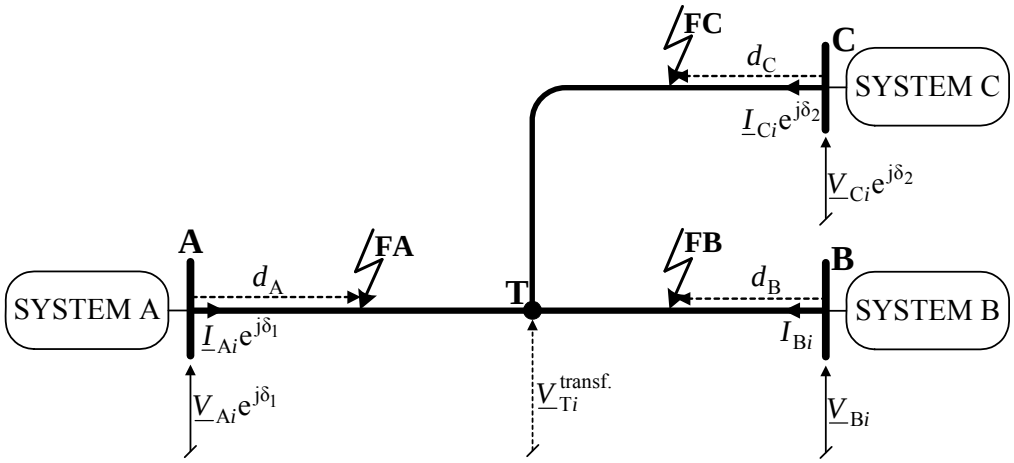

Fig. 7.23. Circuit diagram of three-terminal line for considering fault location using three-end unsynchronised measurements: the measurements from the bus B are assumed as the base, while analytical synchronisation is performed for the measurements from the buses A and C

The fault may occur at any of the three line sections (faults: FA, FB or FC in Figs. 7.22 and 7.23). The distance to the particular fault, measured from the particular bus (A, B or C) up to the fault point is denoted by d_A, d_B, d_C, respectively. So, there are

three hypotheses regarding placement of the fault in particular line section: AT, TB or TC. In general, one can distinguish the following approaches:

- all three hypotheses regarding indication of the faulted line section are considered and after calculating the distances to fault (d_A, d_B, d_C) with use of three subroutines, the judgement on selecting only one solution (the valid solution), which corresponds to the actual fault position is performed,
- first, the faulted line section is identified and then the distance to fault for this section is determined.

In [42], a fault location method for two- and three-terminal lines has been presented. As the input signals of the fault locator, complete two- and three-terminal measurements, both synchronised and unsynchronised, have been considered. Three-phase voltage and current phasors from the line terminals are processed for determining the distance to fault (d) and the synchronisation angle (δ) if unsynchronised measurements are considered. So, there is one unknown (d) and two unknowns (d and δ) in the case of synchronised and unsynchronised measurements, respectively. However, using complete three-phase voltage and current measurement at all line terminals, a redundancy of the fault location equations is assured. For example, in the case of two-terminal line and synchronised measurements, the distance to fault is calculated applying the least-squares estimates from three complex equations or six real number equations in one unknown, d. Similarly, the redundancy of the fault location equations is assured for fault location on three-terminal line.

In the fault location method from [42], the line sections are represented with the line series impedance matrix only. Thus, the line capacitances are neglected, which could affect the calculation of the fault location. However, the authors of this method state that the fault location error is minimised due to the redundancy of the fault location equations, which leads to a squares estimate of the fault location. Important advantages of the fault location algorithm rely in that it is independent of fault type, insensitive to fault resistance, and does not require any information on source impedance. Neither does it assume transposition.

Another important contribution to fault location on three-terminal lines is due to the authors of reference [3]. The technique described there makes use of superimposed, modal components (the phase values are transformed into three modes: an Earth mode and two Aerial modes) of voltages and currents rather than total, phase values, as it was for the method presented in [42]. Aggarwal et al. [3] base their approach on the accurate fault location method developed earlier for two-terminal line [74]. Thus, the distributed parameter line model is fully utilised and the fault location formula such as (7.8), developed for two-terminal line is applied.

The fault location algorithm [3] is designed for both synchronised and unsynchronised three-end measurement of voltage and current. In the case of unsynchronised measurement, the shifting of the data at the unsynchronised end(s) is considered. For this purpose, the voltage at the tee point (T), based on the knowledge of the pre-fault

power frequency voltage and current phasors at all the line terminals is determined, applying the distributed parameter models of all line sections.

It is important to identify the faulted leg of the tee (the faulted line section) before determining the distance to fault [3]. The technique consists in evaluating the voltages at the tee point based on the knowledge of the fault current and voltage phasors at the three ends. With reference to Fig. 7.22, one can state that the fault is in the section AT if the voltage at the T point transferred analytically from the buses B and C (superscript: B and C):

$$\underline{V}_{\mathrm{T}i}^{\mathrm{transf.\,B}} = \cosh(\underline{\gamma}_{i\mathrm{LB}}\ell_{\mathrm{LB}})\underline{V}_{\mathrm{B}i} - \underline{Z}_{ci\mathrm{LB}}\sinh(\underline{\gamma}_{i\mathrm{LB}}\ell_{\mathrm{LB}})\underline{I}_{\mathrm{B}i} \tag{7.91}$$

$$\underline{V}_{\mathrm{T}i}^{\mathrm{transf.\,C}} = \cosh(\underline{\gamma}_{i\mathrm{LC}}\ell_{\mathrm{LC}})\underline{V}_{\mathrm{C}i} - \underline{Z}_{ci\mathrm{LC}}\sinh(\underline{\gamma}_{i\mathrm{LC}}\ell_{\mathrm{LC}})\underline{I}_{\mathrm{C}i} \tag{7.92}$$

is identical, whereas that attained from the end A:

$$\underline{V}_{\mathrm{T}i}^{\mathrm{transf.\,A}} = \cosh(\underline{\gamma}_{i\mathrm{LA}}\ell_{\mathrm{LA}})\underline{V}_{\mathrm{A}i} - \underline{Z}_{ci\mathrm{LA}}\sinh(\underline{\gamma}_{i\mathrm{LA}}\ell_{\mathrm{LA}})\underline{I}_{\mathrm{A}i} \tag{7.93}$$

is much different, indicating that the faulted line section is AT.

Note that in (7.91)–(7.93), the distributed parameters of the respective line sections (having length: ℓ_{LA}, ℓ_{LB}, ℓ_{LC}) are used:

$\underline{\gamma}_{i\mathrm{LA}}$, $\underline{\gamma}_{i\mathrm{LB}}$, $\underline{\gamma}_{i\mathrm{LC}}$ – propagation constants,

$\underline{Z}_{ci\mathrm{LA}}$, $\underline{Z}_{ci\mathrm{LB}}$, $\underline{Z}_{ci\mathrm{LC}}$ – surge impedance.

The other faulted line sections can be similarly identified. If, however, there is no discernable difference in the voltages attained with data from all three ends, then it can be safely assumed that the fault is at the tee point itself [3]. Having identified the faulted line section, the distance to fault can be calculated. As for example, for the faulted section AT, the distance to fault (d_{A}) is calculated using the signals from the bus A ($\underline{V}_{\mathrm{A}i}$, $\underline{I}_{\mathrm{A}i}$) and at the tee point T ($\underline{V}_{\mathrm{T}i}^{\mathrm{transf.}}$, $\underline{I}_{\mathrm{T}i}^{\mathrm{transf.}}$) – obtained after analytical transfer (Fig. 7.22):

$$d_{\mathrm{A}} = \frac{1}{\underline{\gamma}_{i\mathrm{LA}}\ell_{\mathrm{LA}}}\tanh^{-1}\left(\frac{\underline{V}_{\mathrm{T}i}^{\mathrm{transf.}}\cosh(\underline{\gamma}_{i\mathrm{LA}}\ell_{\mathrm{LA}}) - \underline{Z}_{ci\mathrm{LA}}\underline{I}_{\mathrm{T}i}^{\mathrm{transf.}}\sinh(\underline{\gamma}_{i\mathrm{LA}}\ell_{\mathrm{LA}}) - \underline{V}_{\mathrm{A}i}}{\underline{V}_{\mathrm{T}i}^{\mathrm{transf.}}\sinh(\underline{\gamma}_{i\mathrm{LA}}\ell_{\mathrm{LA}}) - \underline{Z}_{ci\mathrm{LA}}\underline{I}_{\mathrm{T}i}^{\mathrm{transf.}}\cosh(\underline{\gamma}_{i\mathrm{LA}}\ell_{\mathrm{LA}}) - \underline{Z}_{ci\mathrm{LA}}\underline{I}_{\mathrm{A}i}}\right) \tag{7.94}$$

where $\underline{V}_{\mathrm{T}i}^{\mathrm{transf.}}$ – voltage transferred analytically to the tee point T, from the bus B (7.91) or the bus C (7.92),

$$\underline{I}_{\mathrm{T}i}^{\mathrm{transf.}} = -\frac{\sinh(\underline{\gamma}_{i\mathrm{LB}}\ell_{\mathrm{LB}})\underline{V}_{\mathrm{B}i}}{\underline{Z}_{ci\mathrm{LB}}} + \cos(\underline{\gamma}_{i\mathrm{LB}}\ell_{\mathrm{LB}})\underline{I}_{\mathrm{B}i}$$

$$-\frac{\sinh(\underline{\gamma}_{i\mathrm{LC}}\ell_{\mathrm{LC}})\underline{V}_{\mathrm{C}i}}{\underline{Z}_{ci\mathrm{LC}}} + \cos(\underline{\gamma}_{i\mathrm{LC}}\ell_{\mathrm{LC}})\underline{I}_{\mathrm{C}i} \tag{7.95}$$

Analogously to (7.94)–(7.95), the distance to fault in the section TB and in the section TC is calculated.

In the case of unsynchronised measurements, the synchronisation operators ($e^{j\delta_1}$, $e^{j\delta_2}$) have to be determined. In [3], it is proposed to determine them by processing the pre-fault quantities. The synchronisation operator $e^{j\delta_1}$ can be determined by comparing the pre-fault voltage at the tee point T, transferred analytically from the bus A and the bus B:

$$\underline{V}_{\mathrm{T}i}^{\mathrm{pre\_transf.\,A}} = (\cosh(\underline{\gamma}_{i\mathrm{LA}}\ell_{\mathrm{LA}})\underline{V}_{\mathrm{A}i}^{\mathrm{pre}} - \underline{Z}_{ci\mathrm{LA}}\sinh(\underline{\gamma}_{i\mathrm{LA}}\ell_{\mathrm{LA}})\underline{I}_{\mathrm{A}i}^{\mathrm{pre}})e^{j\delta_1} \tag{7.96}$$

$$\underline{V}_{\mathrm{T}i}^{\mathrm{pre\_transf.\,B}} = \cosh(\underline{\gamma}_{i\mathrm{LB}}\ell_{\mathrm{LB}})\underline{V}_{\mathrm{B}i}^{\mathrm{pre}} - \underline{Z}_{ci\mathrm{LB}}\sinh(\underline{\gamma}_{i\mathrm{LB}}\ell_{\mathrm{LB}})\underline{I}_{\mathrm{B}i}^{\mathrm{pre}} \tag{7.97}$$

Analogously, the other synchronisation operator $e^{j\delta_2}$ can be determined by comparing the pre-fault voltage at the tee point T, transferred analytically from the bus C and the bus B.

7.5.2. Fault location on three-terminal lines associated with current differential protective relays

In Section 7.4.3, the fault location method using two-end currents and one-end voltage, aimed at application to current differential protective relays of the two-terminal power transmission or distribution line was presented. Analogously, this method can be applied in association with current differential relays protecting a three-terminal line [66], as shown in Fig. 7.24. In this case, the fault location (FL) function is supplemented to the current differential relay from the substation A (Fig. 7.24). For this purpose, phasors of three-phase current from all line terminals: $\underline{I}_{\mathrm{A}}$, $\underline{I}_{\mathrm{B}}$, $\underline{I}_{\mathrm{C}}$ – exchanged by the current differential relays A, B, C, together with the locally measured three-phase voltage phasor ($\underline{V}_{\mathrm{A}}$) are taken as the fault locator input signals. In a natural way, these measurements are considered as synchronised.

The fault location technique proposed [66] is based on using three subroutines: SUB_A, SUB_B, SUB_C. They are designed for locating faults: FA, FB, FC at hypothetical fault spots within particular line sections: AT, TB, TC, respectively. Note that any of the sections may be faulted at random. Therefore, the position of a fault is a random factor, and thus, the faulted line section is not known in advance. The faulted section will be indicated using a special selection procedure.

The subroutine SUB_A, designed for locating faults (FA) within the line section AT (Fig. 7.25), is based on the following generalised fault loop model:

$$\underline{V}_{\mathrm{A\_P}} - d_{\mathrm{A}}\underline{Z}_{1\mathrm{LA}}\underline{I}_{\mathrm{A\_P}} - R_{\mathrm{FA}}\underline{I}_{\mathrm{F}} = 0 \tag{7.98}$$

where:

$\underline{V}_{A\_P}$, $\underline{I}_{A\_P}$ – fault loop voltage and current, composed as shown in Tables 6.5 and 6.6,

$\underline{I}_F$ – total fault current (fault path current).

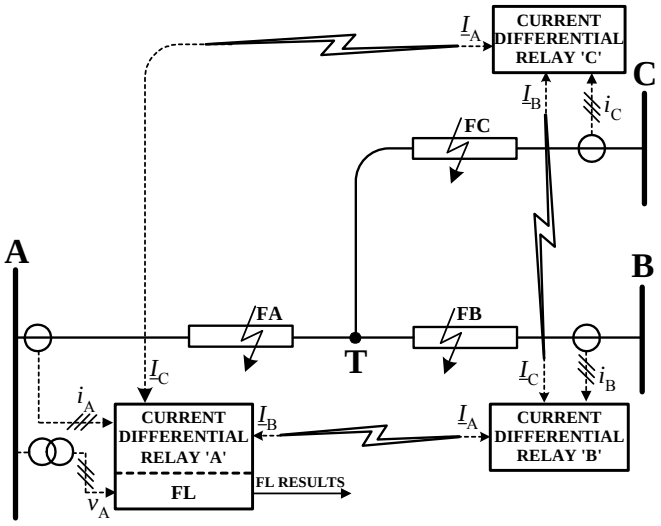

Fig. 7.24. Fault location on three-terminal line included into one of the current differential relays

Before calculating from (7.98) the unknowns: d_A – distance to fault, R_{FA} – fault path resistance, one has to determine the total fault current $\underline{I}_F$. This can be accomplished analogously as for the two-terminal line (7.85)–(7.86), but instead of adding currents from two line ends, the respective symmetrical components of currents from three line ends are added.

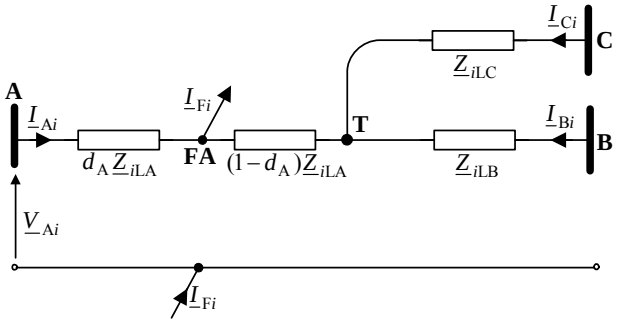

Fig. 7.25. Circuit diagram of three-terminal line under fault in section AT, for the *i*-th symmetrical component

The remaining subroutines SUB_B, SUB_C complete the location procedures. An illustration for deriving the subroutine SUB_B is shown in Fig. 7.26. An analytic transfer of three-phase measurements: $\underline{V}_A$, $\underline{I}_A$, $\underline{I}_C$ to the beginning of the section LB, with the distributed parameter line model being strictly taken into account, is performed. The superscript 'transf.' is used to distinguish the analytically transferred signals from the measured ones. Certainly, such transfer has to be performed separately for each of the *i*-th type symmetrical components of three-phase voltage and current, as presented in (7.93) and (7.95).

Using the transferred signals $\underline{V}_{Ti}^{\text{transf.}}$ and $\underline{I}_{TBi}^{\text{transf.}}$, the fault loop voltage $\underline{V}_{T\_P}$ and current $\underline{I}_{TB\_P}$ are composed. Then, as in (7.98), the fault loop model for the subroutine SUB_B is formulated, and the unknown distance to fault d_B and fault resistance R_{FB} are determined. The subroutine SUB_C, desiged for locating faults on the line section TC, is derived analogously to the subroutine SUB_B.

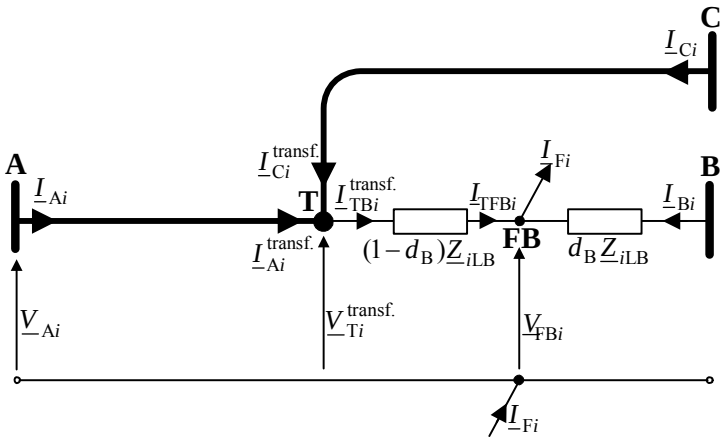

Fig. 7.26. Circuit diagram of three-terminal line under fault in section TB, for the *i*-th symmetrical component

Three fault estimates are calculated assuming the fault to be on the AT, TB or TC segment of the line, respectively.

A selection procedure is required to indicate the faulted line segment, i.e. which of the subroutines (SUB_A, SUB_B or SUB_C) is valid, i.e. corresponds to the real fault. In the first step of the selection procedure, the results of the fault distance and resistance calculations are utilised. The subroutine which yields the distance to fault indicating the fault as occurring outside the section range (outside the range: 0 to 1.0 p.u.) or/and the calculated fault resistance of negative value, is surely rejected.

The second step of the selection is used when the first step is not sufficient. In the second step, the remote source impedances (behind the terminals B and C – if it is

considered that the fault locator is installed at the station A (Fig. 7.24)), are calculated for different subroutines [66]. Having calculated the impedances of the sources behind the remote buses B, C – in relation to both subroutines (SUB_B, SUB_C), first it is checked in which quadrant of the complex plane they are placed. The actual equivalent source impedance is of the form of R–L branch, i.e. is considered as placed in the I quadrant of the impedance plane. If the calculated source impedance lies outside the I quadrant, then this subroutine is false and has to be rejected. Otherwise, if at least two subroutines (out of three) still remain, then the selection has to be continued. The particular subroutine can be rejected also if the calculated value of the remote source differs from the actual impedance. For this rare fault cases a certain knowledge about the actual equivalent sources behind the line terminals is necessary. Note that in the case of the other fault location algorithms which utilise incomplete three-end measurements [12, 61, 107, 118], the impedances of the sources are involved even in calculation of the distance to fault.

7.5.3. Fault location on three-terminal lines with use of two-end measurements

The demand and importance of developing fault locators for three-terminal lines under the availability of two-end synchronised measurements of voltages and currents (Fig. 7.27) has been introduced and justified in [107]. This is of practical importance since the measurement infrastructure of the tapped line is usually rather poor, or there are no communication channels for sending measurements from the end of the tapped line.

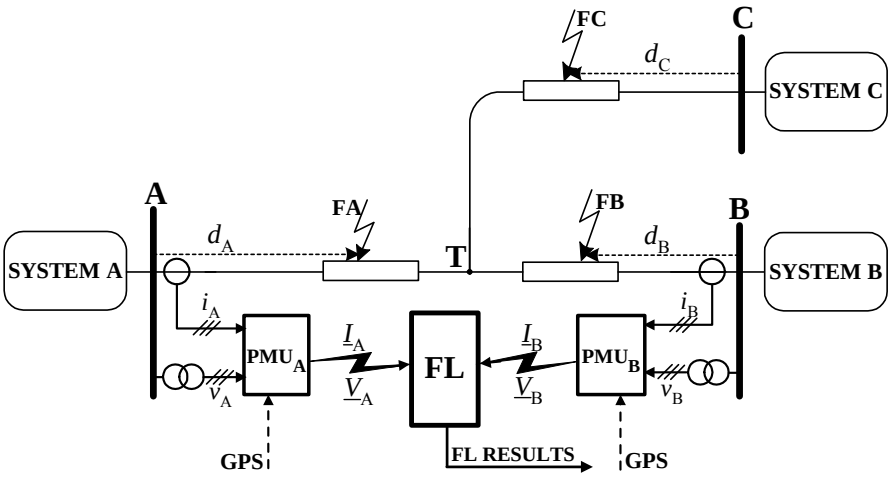

Fig. 7.27. Fault location on three-terminal line using two-end synchronised measurements

It is considered in the fault location methods presented in [59] and [107] that phasor measurement units from two line ends (PMU_A, PMU_B) provide the fault locator (FL) with three-phase phasors of voltage and current ($\underline{V}_A$, $\underline{I}_A$, $\underline{V}_B$, $\underline{I}_B$) measured synchronously (Fig. 7.27). Fault location is based on using three subroutines, designed for locating particular faults (FA, FB, FC) and selecting the valid subroutine.

Comparison of the voltage at the tee point T, obtained by analytical transfer of signals measured at the end A (according to (7.93)) and at the end B (according to (7.91)) allows preliminary selection of the faulted line section. If these voltages match each other, then there is a fault FC on the tapped line. Otherwise, there is a fault FA or FB on the main route of the line (sections: A–T and T–B). Distinguishing between the fault FA and FB can be performed on the basis of the calculated distance to fault [59, 107].

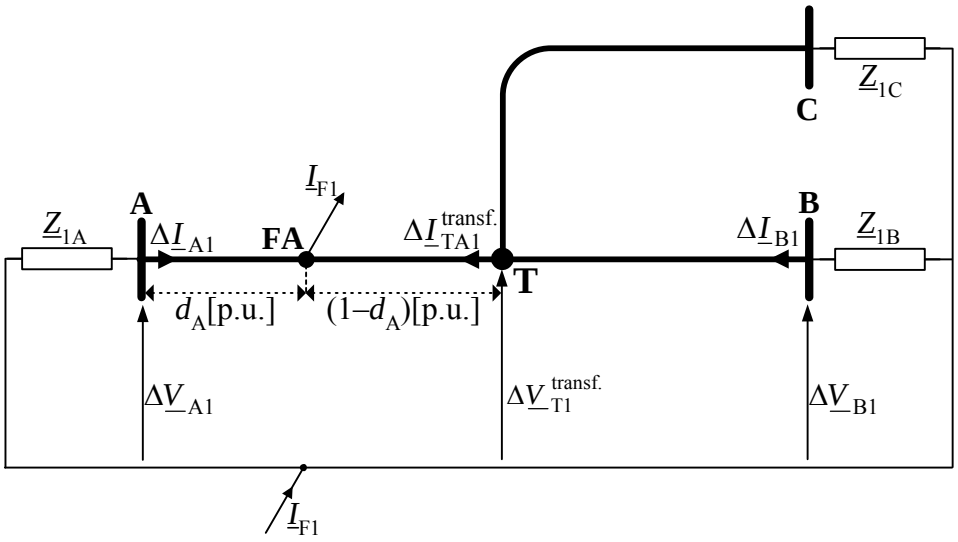

Fig. 7.28. Three-terminal line network – illustration for subroutine SUB_A according to approach from [107]

Figure 7.28 shows a three-terminal line network with fault on the section A–T for illustrating the subroutine SUB_A according to the approach presented in [107]. The subroutine SUB_B is derived analogously to the subroutine SUB_A, for which the derivation follows. It was proposed in [107] to apply accurate fault location algorithm (7.8), which applies complete two-end synchronised measurements for locating faults on a two-terminal line. Lin et al. [107] proposed to apply (7.8) in order to locate faults (FA) on the section A–T using as the input signals:

- superimposed positive-sequence components of signals from the side A: $\Delta\underline{V}_{A1}$, $\Delta\underline{I}_{A1}$

• superimposed positive-sequence components of signals transferred to the tee point T: $\Delta\underline{V}_{\mathrm{T1}}^{\mathrm{transf.}}$ (obtained according to (7.91)), and $\Delta\underline{I}_{\mathrm{TA1}}^{\mathrm{transf.}}$ derived using a current division theory as the following function:

$$\Delta\underline{I}_{\mathrm{TA1}}^{\mathrm{transf.}} = f(\Delta\underline{I}_{\mathrm{B1}}, \underline{\gamma}_{\mathrm{1LB}}, \underline{\gamma}_{\mathrm{1LC}}, \underline{Z}_{\mathrm{c1LB}}, \underline{Z}_{\mathrm{c1LC}}, \ell_{\mathrm{LB}}, \ell_{\mathrm{LC}}, \underline{Z}_{\mathrm{1B}}, \underline{Z}_{\mathrm{1C}}) \tag{7.99}$$

The required current (7.99) is dependent on measured superimposed current: $\Delta\underline{I}_{\mathrm{B1}}$, the parameters of the line section T–B: $\underline{\gamma}_{\mathrm{1LB}}, \underline{Z}_{\mathrm{c1LB}}, \ell_{\mathrm{LB}}$, the line section T–C: $\underline{\gamma}_{\mathrm{1LC}}, \underline{Z}_{\mathrm{c1LC}}, \ell_{\mathrm{LC}}$ and the source impedances behind the buses B, C: $\underline{Z}_{\mathrm{1B}}, \underline{Z}_{\mathrm{1C}}$. Inaccuracy in providing these source impedances is a source of certain additional fault location errors. In order to assure the highest possible accuracy of fault location, a new approach, not requiring these source impedances as the input parameters, was proposed in [59]. This algorithm applies two-end voltages and one-end current and is based on the generalised fault-loop model (7.76) and its final form (7.80), derived with strict consideration being given to the distributed parameter line model. The formula (7.80) applied to two-terminal line requires two-end voltages ($\underline{V}_{\mathrm{S}}$, $\underline{V}_{\mathrm{R}}$) and one-end current ($\underline{I}_{\mathrm{S}}$). When applying it to the subroutine SUB_A for locating faults FA on the section A–T of a three-terminal line (Fig. 7.27, Fig. 7.28) the following input signals are considered:

• signals measured at the bus A: $\underline{V}_{\mathrm{A}}$, $\underline{I}_{\mathrm{A}}$,

• voltage at the tee point T: $\underline{V}_{\mathrm{T}}^{\mathrm{transf.}}$, obtained after analytic transfer of signals from the bus B with use of (7.91).

Analogously, the formula (7.80) can be applied to the subroutine SUB_B for locating faults FB on the section T–B.

Use of the fault location algorithm (7.80) for locating faults (faults FA, FB in Fig. 7.27) on the main route of a three-terminal line [59] is advantageous since the source impedances are for this algorithm not involved, in contrast to the method introduced in [107].

Faults on the line section T–C (fault FC in Fig. 7.27) are located using the subroutine SUB_C, for which an illustration is given in Fig. 7.29. The signals measured at the buses A, B are transferred analytically to the tee point T, applying the distributed parameter line section model, performing it separately for each symmetrical component (positive-sequence: $i = 1$, negative-sequence: $i = 2$, zero-sequence: $i = 0$). The transferred voltage: $\underline{V}_{\mathrm{T1}}^{\mathrm{transf.}}$, $\underline{V}_{\mathrm{T2}}^{\mathrm{transf.}}$, $\underline{V}_{\mathrm{T0}}^{\mathrm{transf.}}$, and sums of transferred currents: $(\underline{I}_{\mathrm{TA1}}^{\mathrm{transf.}} + \underline{I}_{\mathrm{TB1}}^{\mathrm{transf.}})$, $(\underline{I}_{\mathrm{TA2}}^{\mathrm{transf.}} + \underline{I}_{\mathrm{TB2}}^{\mathrm{transf.}})$, $(\underline{I}_{\mathrm{TA0}}^{\mathrm{transf.}} + \underline{I}_{\mathrm{TB0}}^{\mathrm{transf.}})$ are the input signals for the subroutine SUB_C. Thus, we deal with the one-end voltage and current in this case. Two alternative formulations of the subroutine SUB_C have been presented in [59, 107].

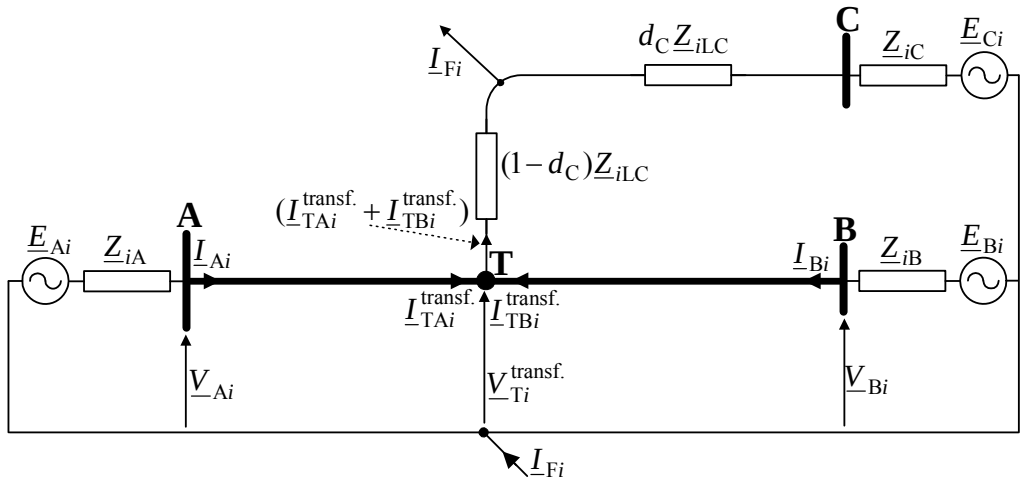

Fig. 7.29. Three-terminal line network – illustration for subroutine SUB_C designed for locating faults on section T–C

7.5.4. Fault location on three-terminal lines with use of minimal measurements

In [61], the fault location algorithm for three-terminal lines using the limited measurements in comparison to the earlier known approaches has been presented. One-end measurements of three-phase current and voltage, and additional information on amplitudes of pre-fault currents, i.e. amplitudes of pre-fault positive-sequence currents under the symmetry assumption, from the remaining sections of the line are utilised as the fault locator input signals (Fig. 7.30). Moreover, detailed impedance data of the network (for both the line sections and equivalent sources behind the line terminals) has to be provided as the fault locator input data. The method is based on the symmetrical components approach applied for formulating all three subroutines designed for locating faults on the respective line sections.

The final step in the fault location algorithm relies on selecting a valid subroutine, i.e. on indicating which of the subroutines yields results corresponding to the real distance to fault and fault resistance. The subroutine which yields distance to fault outside its line section, and/or negative fault resistance, is surely false and has to be rejected. If it is not so, other criteria have to be considered. In the study carried out the following criteria quantities were utilised: – total fault currents in faulted phases (ought to correspond to the measured currents), – amplitudes of the total fault current in healthy phases (ought to be close to zero), – boundary conditions for faults involving earth.

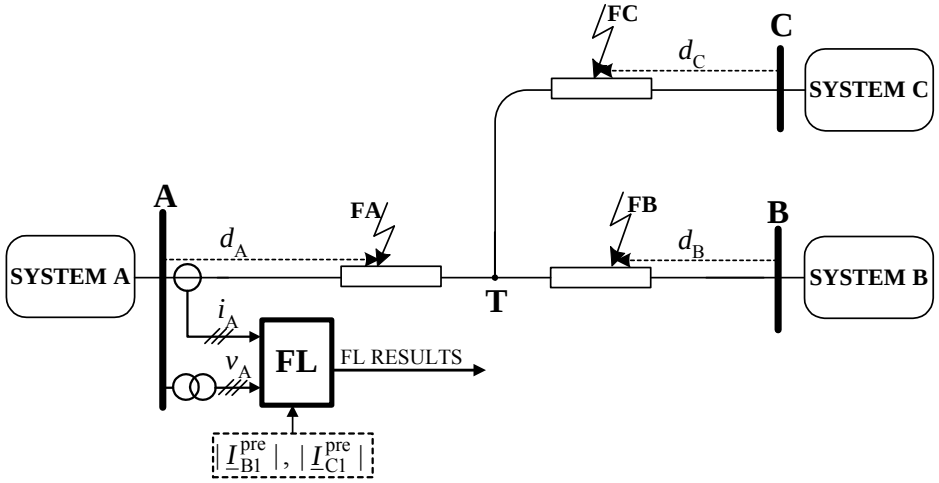

Fig. 7.30. Fault location on three-terminal line with use of minimal measurements

7.6. Fault location on multi-terminal and tapped lines

In Chapter 3, basic models of multi-terminal and tapped lines were introduced. The networks presented there were limited to three-terminal line case (Figs. 3.7 and 3.8) and the network with one tapped line (Fig. 3.9). In real power networks, however, we can find lines with numbers of terminals higher than three and also lines with more than one tap for feeding the load. Use of the fault location algorithms, which were presented in Section 7.5 is limited to a three-terminal line or to a line with a single tap.

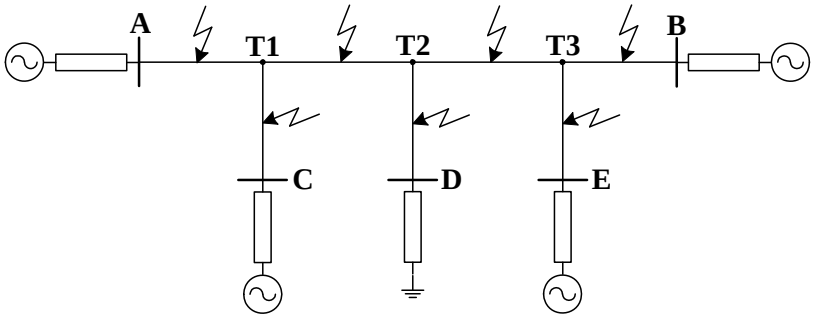

Fig. 7.31. Fault location on a five-terminal line

In Figure 7.31, a scheme of the multi-terminal line is shown. It has four terminals with power generation, and thus not less than three, as required in the definition of

multi-terminal lines given in [B.23]. In the case of five terminals there are three tap points (T1, T2, T3) to which the tapped lines (T1-C, T3-E) are connected with the sources of power generation, and the tapped line (T2-D) feeding the load. Distributed generation included into distributed systems changes the power flow, normally radial in distribution systems, to multidirectional one [43]. For the five-terminal lines there are four hypothetical locations of faults on the main route of the line (A-T1-T2-T3-B) and three hypothetical locations on the tapped lines (T1-C, T2-D, T3-E).

Figure 7.32 shows an example of the tapped line with a source of generation at the bus A and alternatively also at the bus B [2]. Thus, generation is at two of the terminals, which is in compliance with the definition of the tapped line given in [B.23]. There are also four tapped lines feeding the loads, which are usually balanced three-phase ones, but also a single phase load can be met in distribution systems [17].

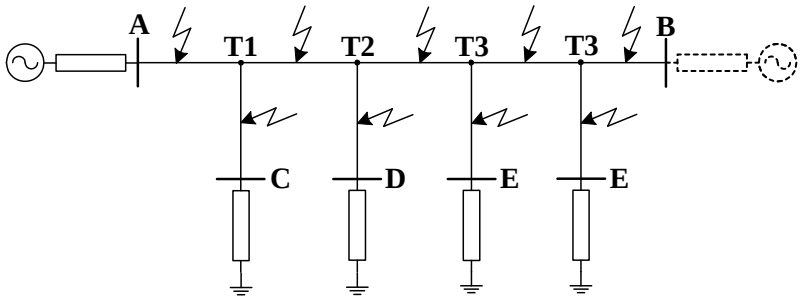

Fig. 7.32. Fault location on line A-B with four tapped lines feeding loads

A variety of algorithms for locating faults on multi-terminal and tapped lines have been developed so far. For example, fault location on a multi-terminal line has been reported in [123]. This method uses magnitudes of differential current at all terminals for locating faults on multi-terminal two parallel lines. The method is based on a three-terminal fault location algorithm and an equivalent conversion from an n-terminal to a three-terminal system is applied.

Abe et al. [1] use synchronised three-phase voltages and currents at all terminals. They apply the algorithm using voltage differentials at terminals to gradually reduce a multi-terminal line into a two-terminal line containing the faulted section. Then, a reactive power-based method is used to locate the fault.

Funabashi et al. [34] use synchronised current inputs from all terminals and use two different methods to locate the fault on parallel double-circuit multi-terminal transmission lines:

- impedance relay method (employs an impedance calculation),
- current diversion ratio method.

In [172], an analysis and evaluation of multi-terminal fault location have been presented. The technique proposed there uses the voltage from two terminals and the

current data from all terminals of the line. The measurements are considered as performed synchronously with use of the GPS.

Brahma in [12] delivers a fault location method for a multi-terminal transmission line using synchronised voltage measurements. It contains a simple new procedure for identifying the faulted line section first. Then, to exactly locate the fault on this section, a method is described that uses the synchronised voltage measurements at all terminals. The main advantage of this method [12] is that the current-transformer errors in the current measurements can be avoided. The method assumes that the source impedances are available. The method readily lends itself to untransposed lines and is free from the pre-fault conditions.

Aggarwal et al. in [2] presented an interactive approach to fault location on distribution overhead lines with load taps. However, the approach can be applied to transmission networks as well. The cited paper presents a novel technique in single-ended fault location for overhead systems based on the concept of superimposed components of voltages and currents rather than total quantities. The superimposed fault-path current at the assumed fault point is determined. In order to find the actual fault point, the assumed fault position is shifted in an interactive fashion in such a way as to obtain the minimum value of the fault-path currents from healthy phases. It is shown [2] that the fault locator is highly insensitive to variations in source impedances (both local and remote) and to the presence of taps with variable loads.

Afterword

Recommendations

In this book, a variety of impedance-based fault location algorithms have been presented. In Chapter 6, the one-end algorithms, and in Chapter 7, the two-end (multi-end) fault location algorithms have been delivered. Which algorithm to choose for a particular application depends on the configuration of the line considered and the availability of measurement signals for the fault location.

Much superior algorithms are offered for the two-end (multi-end) measurements, as presented in Chapter 7, especially when using synchronised measurements – Section 7.2. In the case where only the one-end measurements are at one's disposal, the choice of the algorithm depends on the knowledge of the impedance parameters of the system in the vicinity of the line. If the equivalents for the components from the vicinity of the line cannot be reliably determined, then the simplified algorithms, as presented in Sections 6.5 and 6.6, are recommended. Otherwise, the flow of fault current in the whole network can be fully accounted for, which is assured by the algorithm from Section 6.7. A very attractive fault location on double-circuit line can be performed under availability of complete measurements from one line end – the fault location algorithm delivered in Section 6.8.

For proper understanding of the majority of fault location algorithms from Chapters 6 and 7, it is recommended to go through fault models presented in Chapter 4. The author also believes that deep understanding of the fault models and fault location algorithms presented will help those who intend to work on development and improvement of digital protective distance algorithms for transmission lines.

In relation to practical usage of fault locators one can emphasise that in the course of faults occurring, the user will gain knowledge about the network, i.e. about its points with the most frequent faults and also the network parameters. For example, use of the two-end (multi-end) measurements allows, in addition to its fault location function, the line impedance to be determined. By this, the line impedance calculated from the line geometry can be verified, which is also useful for setting protective relays.

Future of fault location

The author of this book is of the opinion that there is still much room for further development of the fault location techniques; expresses his strong desire to participate

in the future research. On the other hand, in today's competitive market, manufactures and utilities will try to maximise the benefit of technology undergoing permanent development, while continually exploring new ways to implement advanced technologies and algorithms into products. Especially, rapid development of the communication means for sending the measurement data acquired at the remote line terminal (terminals) to the fault locator device will promote usage of the fault location algorithms based on the distributed (wide area) measurements.

Improvement in the accuracy of the fault location can be expected if new unconventional instrument transformers become predominant in transforming signals from a power system to fault location devices. Also, one can expect that the fault location techniques relying on knowledge-based approaches will come step-by-step into usage in much wider range than at present.

References – Books & Guides & Monographs

B.1. ANDERSON P.M., *Power system protection*, IEEE Press Power Engineering Series, Part I–VI, McGraw-Hill, 1999.

B.2. COLLATZ L., *Numerical treatment of differential equations*, New York, Springer Verlag, 1960.

B.3. COOK V., *Analysis of distance protection*, Research Studies Press Ltd., John Wiley & Sons Inc., 1985.

B.4. CHEN W.K., (ed.), *The circuits and filters handbook*, CRC Press LLC, Boca Raton, 2003.

B.5. DOMMEL H., *Electro-Magnetic Transients Program*, BPA, Portland, Oregon, 1986.

B.6. GLOVER J.D., SARMA M., *Power system analysis and design*, PWS Publishing Company, Boston, 2nd ed., 1994.

B.7. IEEE Std C37.114,:*IEEE guide for determining fault location on AC transmission and distribution lines*, IEEE Power Engineering Society Publ., 8 June 2005.

B.8. IEEE Std. C37.118: *IEEE standard for synchrophasors for power systems*, IEEE Power Engineering Society Publ., 22 March 2006.

B.9. IŻYKOWSKI J., *Impedancyjne algorytmy lokalizacji zwarć w liniach przesyłowych* (Impedance-based fault location algorithms), Prace Naukowe Instytutu Energoelektryki Politechniki Wrocławskiej Nr 92, Seria: Monografie, Nr 28, 2001, (in Polish).

B.10. KACEJKO P., MACHOWSKI J., *Zwarcia w systemach elektroenergetycznych* (Power system faults), Wydawnictwa Naukowo-Techniczne WNT, Warszawa, 2002, (in Polish).

B.11. KEZUNOVIC M., *Fault location*, Wiley Encyclopedia of Electrical and Electronics Terminology, Vol. 7, John Wiley, 1999, pp. 276–285.

B.12. KUJSZCZYK SZ., BROCIEK S., FLISOWSKI Z., GRYKO J., NAZARKO J., ZDUN Z., *Elektroenergetyczne układy przesyłowe*, Podręczniki Akademickie – Elektrotechnika (Power transmission networks, Academic Textbook – Electrical Engineering), Wydawnictwa Naukowo-Techniczne WNT, Warszawa, 1997, (in Polish).

B.13. *MATLAB user's guide*, The Math Works Inc., Natick, MA.

B.14. OPPENHEIM A.V., SCHAFER R.W., BUCK J.R., *Discrete-time signal processing*, Prentice-Hall Signal Processing Series, 1999.

B.15. ROSOŁOWSKI E., *Cyfrowe przetwarzanie sygnałów w automatyce elektroenergetycznej* (Digital signal processing for power system protection and control), Akademicka Oficyna Wydawnicza EXIT, Warszawa, 2002, (in Polish).

B.16. SACHDEV M.S. (Coordinator), *Advancement in microprocessor based protection and communication*, IEEE Tutorial Course, Power Engineering Education Committee and the Power System Relaying Committee of the IEEE Power Engineering Society, IEEE Catalog Number: 97TP120-0, 1997.

B.17. SMITH S.W., *The scientist and engineer's guide to digital signal processing*, 2nd ed., 1999.

B.18. SZAFRAN J., WISZNIEWSKI A., *Algorytmy pomiarowe i decyzyjne cyfrowej automatyki elektroenergetycznej* (Measurement and decision making algorithms for digital protection and control), Wydawnictwa Naukowo-Techniczne WNT, Warszawa, 2001, (in Polish).

B.19. SZCZERSKI R., *Lokalizacja uszkodzeń w sieciach elektroenergetycznych. Zagadnienia wybrane* (Location of faults in electrical power networks. Selected problems), Wydawnictwa Naukowo-Techniczne WNT, Warszawa, 1990, (in Polish).
B.20. TARCZYŃSKI W., *Metody impulsowe w lokalizacji uszkodzeń w liniach elektroenergetycznych* (Pulse methods for locating faults on power lines), Oficyna Wydawnicza Politechniki Opolskiej: Studia i Monografie, z. 191, Opole, 2006, (in Polish).
B.21. UNGRAD H., WINKLER W., WISZNIEWSKI A., *Protection techniques in electrical energy systems*, Marcel Dekker, Inc., 1995.
B.22. WISZNIEWSKI A., *Przekładniki w elektroenergetyce* (Instrument transformers in power systems), Wydawnictwa Naukowo-Techniczne WNT, Warszawa, 1992, (in Polish).
B.23. ZIEGLER G. (Convener), *Application guide on protection of complex transmission network configuration*, CIGRE SC34-WG04, 1990.
B.24. ZIEGLER G., *Numerical distance protection. Principles and applications*, Editor: Siemens AG, Publicis MCD Verlag, 2nd ed., 2006.
B.25. ŻYDANOWICZ J., *Elektroenergetyczna automatyka zabezpieczeniowa*, t. 1, 2, 3 (Power system protection and control, vol. 1, 2, 3), Wydawnictwa Naukowo-Techniczne WNT, Warszawa, 1979, (in Polish).

Papers

1. ABE M., OTSUZUKI N., EMURA T., TAKEUCHI M., *Development of a new fault location system for multi-terminal single transmission lines*, IEEE Transactions on Power Delivery, Vol. 10, No. 1, 1995, pp. 159–168.
2. AGGARWAL R.K., ASLAN Y., JOHNS A.T., *An interactive approach to fault location on overhead distribution lines with load taps*, Proceedings of the International Conference on Developments in Power System Protection, March 1997, Conference Publication No. 434, 1997, pp. 184–187.
3. AGGARWAL R.K., COURY D.V., JOHNS A.T., KALAM A., *A practical approach to accurate fault location on extra high voltage teed feeders*, IEEE Transactions on Power Delivery, Vol. 8, No. 3, July 1993, pp. 874–883.
4. AGGARWAL R.K., COURY D.V., JOHNS A.T., KALAM A., *Computer-aided design and testing of an accurate fault location for EHV teed feeders*, Proceedings of the International Conference on Developments in Power System Protection, York, 1993, pp. 60–64.
5. AGGARWAL R.K., XUAN Q.Y., DUNN R.W., JOHNS A.J., BENNETT A., *A novel fault classification technique for double-circuit lines based on a combined unsupervised/supervised neural network*, IEEE Transactions on Power Delivery, Vol. 14, No. 4, 1999, pp. 1250–1256.
6. AHN S.-P., KIM C.-H., AGGARWAL R.K., JOHNS, A.T., *An alternative approach to adaptive single pole auto-reclosing in high voltage transmission systems based on variable dead time control*, IEEE Transactions on Power Delivery, Vol. 16, No. 4, October 2001, pp. 676–686.
7. AL-DABBAGH M., KAPUDUWAGE S.K., *Using instantaneous values for estimating fault locations on series compensated transmission lines*, Electric Power Systems Research, Vol. 76, No. 1–3, September 2005, pp. 25–32.
8. AURANGZEB M., CROSSLEY P.A., GALE P., *Fault location using high frequency travelling waves measured at a single location of a transmission line*, Proceedings of the International Conference on Developments in Power System Protection, No. 479. IEE (UK), 2001.
9. BO Z.Q., JOHNS A.T., AGGARWAL R.K., *A new non-unit protection scheme based on fault generated high frequency current travelling waves*, APSCOM–95, International Conference on Advance in Power System Control, Operation & Management, Hong Kong Convention & Exhibition Centre, November 1995.

10. BO Z.O., WELLER G., REDFERN M.A., *Accurate fault location technique for distribution system using fault-generated high frequency transient voltage signals*, IEE Proceedings – Generation Transmission Distribution, Vol. 146, No. 1, January 1999, pp. 73–79.
11. BRADLEY D.A., GRAY C.B., O'KELLY D., *Transient compensation of current transformers*, IEEE Transactions on PAS., Vol. PAS–97, July/August 1978, pp. 1264–1271.
12. BRAHMA S.M., *Fault location scheme for a multi-terminal transmission line using synchronized voltage measurements*, IEEE Transactions on Power Delivery, Vol. 20, No. 2, April 2005, pp. 1325–1331.
13. BRAHMA S.M., GIRGIS A.A., *Fault location on a transmission line using synchronized voltage measurements*, IEEE Transactions on Power Delivery, Vol. 19, No. 4, October 2004, pp. 1619–1622.
14. BUNYAGUL T., CROSSLEY P.A., *Design and evaluation of an overcurrent relay suitable for operation with measurement current transformers*, Proceedings of Seventh International Conference on Developments in Power System Protection, April 2001, Conference Publication No. 479, pp. 201–204.
15. CHEN C.-S., LIU C.-W., JIANG J.-A., *A new adaptive PMU based protection scheme for transposed/untransposed parallel transmission lines*, IEEE Transactions on Power Delivery, Vol. 17, No. 2, April 2002, pp. 395–404.
16. CHEONG W.J., AGGARWAL R.K., *A novel fault location technique based on current signals only for thyristor controlled series compensated transmission lines using wavelet analysis and self organising map neural networks*, Eighth IEE International Conference on Developments in Power System Protection, Vol. 1, April 2004, pp. 224–227.
17. CHOI M.-S., LEE S.-J., LEE D.-S., JIN B.-G., *A new fault location algorithm using direct circuit analysis for distribution systems*, IEEE Transactions on Power Delivery, Vol. 19, No. 1, January 2004, pp. 35–41.
18. COOK V., *Fundamental aspects of fault location algorithms used in distance protection*, IEE Proceedings, Vol. 133, Pt. C, No. 6, September 1986, pp. 359–368.
19. CROSSLEY P.A., SOUTHERN E., *The impact of the global positioning system (GPS) on protection & control*, Proceedings of the 11th International Conference on Power System Protection – PSP '98, Bled, Slovenia, 1998, pp. 1–5.
20. DALCASTAGNE A.L., FILHO S.N., ZUIRN H.H., SEARA R., *A two-terminal fault location approach based on unsynchronized phasors*, 2006 International Conference on Power System Technology, 7 p.
21. DAS R., NOVOSEL D., *Review of fault location techniques for transmission and sub-transmission lines*, Proceedings of Georgia Tech Conference, April 2000, pp. 1–16.
22. DASH P.K., PRADHAN A.K., PANDA G., LIEW A.C., *Adaptive relay setting for flexible AC transmission systems (FACTS)*, IEEE Transactions on Power Delivery, Vol. 15, No. 1, January 2000, pp. 38–43.
23. DJURIC M.B., RADOJEVIC Z.M., TERZIJA V.V., *Distance protection and fault location utilizing only phase current phasors*, Transactions on Power Delivery, Vol. 13, No. 4, October 1998, pp. 1020–1026.
24. DJURIC M.B., RADOJEVIC Z.M., TERZIJA V.V., *Time domain solution of fault distance estimation and arcing fault detection on overhead lines*, IEEE Transactions on Power Delivery, Vol. 14, No. 1, January 1999, pp. 60–65.
25. DJURIC M.B., TERZIJA V.V., *A new approach to the arcing faults detection for autoreclosure in transmission systems*, IEEE Transactions on Power Delivery, Vol. 10, No. 4, 1995, pp. 1793–1798.
26. DJURIC M.B., TERZIJA V., RADOJEVIC Z.M., *Overhead lines fault location and arc voltage estimation numerical algorithm derived in time domain*, Electrical Engineering, Vol. 81, 1998, pp. 45–53.

27. DJURIC M.B., TERZIJA V., SKOLJEV I., *Transmission line arcing faults recognition from the voltage signal*, Proceedings of the 11th Power System Computations Conference – PSCC '93, September 1993, pp. 1037–1040.
28. DOMMEL H., *Digital computer solution of electromagnetic transients in single- and multi-phase networks*, IEEE Transactions on Power Apparatus and Systems, Vol. PAS–88, No. 4, April 1969, pp. 338–396.
29. DUDURYCH I., ROSOŁOWSKI E., *Analysis of overvoltages in overhead ground wires of EHV power transmission line shield under single phase-to-ground faults*, Electric Power Systems Research, Vol. 53/2, December 1999, pp. 105–111.
30. EREZZAGHI M.EL., CROSSLEY P.A., ELFERES R., *Design and evaluation of an adaptive distance protection scheme suitable for series compensated transmission feeders*, Proceedings of Developments in Power System Protection, Amsterdam, 2004, pp. 454–456.
31. ERIKSSON L., SAHA M.M., ROCKEFELLER G.D., *An accurate fault locator with compensation for apparent reactance in the fault resistance resulting from remote-end infeed*, IEEE Transactions on Power Apparatus and Systems, Vol. PAS–104, No. 2, February 1985, pp. 424–436.
32. EVRENOSOGLU C.Y., ABUR A., *Fault location for teed circuits with mutually coupled lines and series capacitors*, Proceedings of IEEE Bologna Power Tech Conference, CD Rom, IEEE Catalog Number 03EX719C, June 2003.
33. FARDANESH B., ZELINGHER S., MELIOPOLOS A.P.S., COKKINIDES G., INGLESON J., *Multifunctional synchronized measurement network*, IEEE Computer Applications in Power, January 1998, pp. 26–30.
34. FUNABASHI T., OTOGURO H., MIZUMA Y., DUBE L., AMETANI A., *Digital fault location for parallel double-circuit multi-terminal transmission lines*, IEEE Transactions on Power Delivery, Vol. 15, No. 2, April 2000, pp. 531–537.
35. FUNABASHI T., OTOGURO H., MIZUMA Y., DUBE L., KIZILCAY M., AMETANI A., *Influence of fault arc characteristics on the accuracy of digital fault locators*, IEEE Transactions on Power Delivery, Vol. 16, No. 2, April 2001, pp. 195–199.
36. FUNK A.T., MALIK O.P., *Impedance estimation including ground fault resistance error correction for distance protection*, Electrical Power and Energy Systems, Vol. 22, 2000, pp. 59–66.
37. GANGADHARAN P.K., SIDHU T.S., FINLAYSON G.J., *Current transformer dimensioning for numerical protection relays*, IEEE Transactions on Power Delivery, Vol. 22, No. 1, January 2007, pp. 108–115.
38. GARCIA-GRACIA M, OSAL W., COMECH M.P., *Line protection based on the differential equation algorithm using mutual coupling*, Electric Power Systems Research, Vol. 77, 2007, pp. 566–573.
39. GHASSEMI F., GOODARZI J., JOHNS A.T., *Method to improve digital distance relay impedance measurement when used in SC lines protected by a metal oxide varistor*, IEE Proceedings Transmission Distribution, Vol. 145, No. 4, July 1998, pp. 403–408.
40. GHASSEMI F., JOHNS A.T., GODDARZI J., *A method for eliminating the effect of MOV operation on digital distance relays when used in series compensated lines*, Proceedings of 32nd Universities Power Engineering Conference – UPEC '97, Manchester, UK, 1997, pp. 113–116.
41. GILANY M.I., MALIK O.P., HOPE G.S., *A digital protection technique for parallel transmission lines using a single relay at each end*, IEEE Transactions on Power Delivery, Vol. 7, No. 1, January 1992, pp. 118–123.
42. GIRGIS A.A., HART D.G., PETERSON W.L., *A new fault location technique for two- and three-terminal lines*, IEEE Transactions on Power Delivery, Vol. 7, No. 1, January 1992, pp. 98–107.
43. GIRGIS A.A., KING D., *Fault location in distribution feeders in the presence of distributed generation*, Proceedings CIGRE Study Committee B5 Colloquium, Sydney, Australia, September/October 2003, paper 217.

44. GIRGIS A.A., SALLAM A.A., EL-DIN A.K., *An adaptive protection scheme for advanced series compensated (ASC) transmission lines*, IEEE Transactions on Power Delivery, Vol. 13, No. 2, April 1998, pp. 414–420.
45. GOLDSWORTHY D.L., *A linearized model for MOV-protected series capacitors*, IEEE Transactions on Power Systems, Vol. 2, No. 4, November 1987, pp. 953–958.
46. GOPALAKRISHNAN A., KEZUNOVIC M., MCKENNA S.M., HAMAI D.M., *Fault Location Using the Distributed Parameter Transmission Line Model*, IEEE Transactions on Power Delivery, Vol. 15, No. 4, October 2000, pp. 1169–1174.
47. GRACIA J., MAZON A., ZAMORA I., *Best ANN structures for fault location in single- and double-circuit transmission lines*, IEEE Transactions Power Delivery, Vol. 20, No. 4, 2005, pp. 2389–2395.
48. GU J.C., SHEN K.Y., YU S.L. et al., *Removal of dc offset and subsynchronous resonance in current signals for series compensated transmission lines using a novel Fourier filter algorithm*, Electric Power Systems Research, Vol. 76, No. 5, March 2006, pp. 327–335.
49. HARMEET S.K., RAGHUVEER T., *A new design distance to fault locator for power transmission lines*, Proceedings of the International Conference on Modern Trends in the Protection Schemes of Electric Power Apparatus and Systems, October 1998, New Delhi, India, pp. VI-7–11.
50. HE B., LI Y., BO Z.Q., *An adaptive distance relay based on transient error estimation of CVT*, IEEE Transactions on Power Delivery, Vol. 21, No. 4, October 2006, pp. 1856–1861.
51. HERRMANN H.J., *Design numerical relays with regard to CT saturation*, Proceedings of CIGRE 2001 S.C. 34 Colloquium, Sibiu, September 2001, Conference Publication No. 301, pp. 1–7.
52. HOSEMANN G., STEIGERWALD H.M., *Modal saturation detector for digital differential protection*, IEEE Transactions on Power Delivery, Vol. 8, No. 3, July 1993, pp. 933–940.
53. IEEE Working Group Report, Power System Relaying Committee, *Synchronized sampling and phasor measurements for relaying and control*, IEEE Transactions on Power Delivery, PWRD–9, 1994, pp. 442–449.
54. IŻYKOWSKI J., BALCEREK P., KAWECKI R., *Location of single phase-to-ground faults combined with broken conductor failure in single power transmission lines*, Proceedings of the International Symposium on Modern Electric Power Systems – MEPS'02, Wrocław, Poland, September 2002, pp. 313–318.
55. IŻYKOWSKI J., KASZTENNY B., ROSOŁOWSKI E., SAHA M.M., *Fundamental frequency equivalenting of series capacitors equipped with MOVs under fault conditions of a series-compensated line*, Proceedings of the 8th International Symposium on Short-Circuit Currents in Power Systems, Brussels, Belgium, October 1998, pp. 13–18.
56. IŻYKOWSKI J., KASZTENNY B., ROSOŁOWSKI E., SAHA M.M., HILLSTROM B., *Dynamic compensation of capacitive voltage transformers*, IEEE Transactions on Power Delivery, Vol. 113, No. 1, January 1998, pp. 116–122.
57. IŻYKOWSKI J., KAWECKI R., *Location of faults in partially parallel transmission networks*, Proceedings of 2001 IEEE Porto Power Tech Conference, Porto, Portugal, September 2001, Volume III, Chapter EDT4-EMS/DMS TOOLS 4, paper EDT4-230, 6 p.
58. IŻYKOWSKI J., KAWECKI R., ROSOŁOWSKI E., SAHA M.M., *Accurate location of faults in parallel transmission lines under availability of measurements from one circuit only*, Proceedings of Power Systems Computation Conference (CD Rom), Sevilla, June 2002, session 08, paper 6.
59. IŻYKOWSKI J., MOLĄG R., BOŻEK M., *Fault location on three-terminal overhead lines with using two-terminal synchronized voltage and current phasors*, International Symposium: Modern Electric Power Systems – MEPS, Wrocław, September 2006.
60. IŻYKOWSKI J., MOLĄG R., ROSOŁOWSKI E., SAHA M.M., *Accurate location of faults on power transmission lines with use of two-end unsynchronized measurements*, IEEE Transactions on Power Delivery, Vol. 21, No. 2, April 2006, pp. 627–633

61. IŻYKOWSKI J., MOLĄG R., ROSOŁOWSKI E., SAHA M.M., *Fault location in three-terminal line with use of limited measurements*, PowerTech, St. Petersburg, Proceedings – CD, June 2005.
62. IŻYKOWSKI J., ROSOŁOWSKI E., SAHA M.M., *Adaptive digital distance algorithm for parallel transmission lines*, 2003 IEEE Power Tech, Bolonia, June 2003, CD Rom, IEEE Catalog Number 03EX719C, ISBN 0-7803-7968-3, paper 343.
63. IŻYKOWSKI J., ROSOŁOWSKI E., SAHA M.M., *Locating faults in parallel transmission lines under availability of complete measurements at one end*, IEE Generation, Transmission and Distribution, Vol. 151, No. 2, March 2004, pp. 268–273.
64. IŻYKOWSKI J., ROSOŁOWSKI E., SAHA M.M., *Post-fault analysis of operation of distance protective relays of power transmission lines*, IEEE Transactions on Power Delivery, Vol. 22, No. 1, January 2007, pp. 74–81.
65. IŻYKOWSKI J., ROSOŁOWSKI E., SAHA M.M, BALCEREK P., *Accurate algorithm for locating faults in power transmission lines under saturation of current transformers*, Proceedings (CD) of Power Systems Computation Conference (PSCC), Liege, August 2005.
66. IŻYKOWSKI J., ROSOŁOWSKI E., SAHA M.M., FULCZYK M., BALCEREK P., *A fault location method for application with current differential relays of three-terminal lines*, IEEE Transactions on Power Delivery, Vol. 22, No. 4, October 2007.
67. JAYASINGHE J.A.S.B., AGGARWAL R.K., JOHNS A.T., BO Z.Q., *A novel non-unit protection for series compensated EHV transmission lines based on fault generated high frequency voltage signals*, IEEE Transactions on Power Delivery, Vol. 13, No. 2, 1998, pp. 405–413.
68. JEYASURYA B., *Accurate distance relaying with error compensation*, Electric Machines and Power Systems, No. 25, 1997, pp. 29–40.
69. JEYASURYA B., BATH C.A., *An accurate algorithm for transmission line fault location using digital relay measurements*, Electric Machines and Power Systems, No. 16, 1989, pp. 25–34.
70. JIALE S., SONG G.B., XU Q.Q. et al., *Time-domain fault location algorithm for parallel transmission lines using unsynchronized currents*, International Journal of Electrical Power and Energy Systems, Vol. 28, No. 4, May 2006, pp. 253–260.
71. JIANG J.-A., LIN Y.-H., YANG J.-Z., TOO T.-M., LIU C.-W., *An adaptive PMU based fault detection/location technique for transmission lines – Part II*: *PMU implementation and performance evaluation*, IEEE Transactions on Power Delivery, Vol. 15, No. 4, October 2000, pp. 1136–1146.
72. JIANG J.-A., YANG J.-Z., LIN Y.-H., YANG J.-Z., LIU C.-W., MA J.-C., *An adaptive PMU based fault detection/location technique for transmission lines – Part I*: *Theory and algorithms*, IEEE Transactions on Power Delivery, Vol. 15, No. 2, April 2000, pp. 486–493.
73. JOHNS A.T., AGGARWAL R.K., SONG Y.H., *Improved techniques for modelling fault arcs on faulted EHV transmission systems*, IEE Proceedings – Generation Transmission Distribution, Vol. 141, No. 2, March 1994, pp. 148–154.
74. JOHNS A.T., JAMALI S., *Accurate fault location technique for power transmission lines*, IEE Proceedings C, November 1990, Vol. 137, No. 6, pp. 395–402.
75. JOHNS A.T., MOORE P.J., WHITTARD R., *New technique for the accurate location of earth faults on transmission systems*, IEE Proceedings Generation Transmission Distribution, Vol. 142, No. 2, 1995, pp. 119–127.
76. KANG S.-H., LEE S.-J., KWON Y.-J., *A fault location algorithm for parallel transmission line with a teed circuit*, Proceedings of IEEE PSE Summer Meeting 2001.
77. KANG Y.-C., LIM U.-J., KANG S.-H., CROSSLEY P.A., *Compensation of the distortion in the secondary current caused by saturation and remanence in a CT*, IEEE Transactions on Power Delivery, Vol. 19, No. 4, October 2004, pp. 1642–1649.

78. KANG Y.-C., KANG S.-H., PARK J.-K., JONES A.T., AGGARWAL R.K., *Development and hardware implementation of a compensating algorithm for the secondary current of current transformers*, IEE Proceedings – Electric Power Applications, Vol. 43, No. 1, January 1996, pp. 41–49.
79. KANG Y.-C., OK S.-H., KANG S.-H.. *A CT saturation detection algorithm*, IEEE Transactions on Power Delivery, Vol. 19, No. 1, January 2004, pp. 78–85.
80. KANG Y.-C., OK S.-H., KANG S.-H., CROSSLEY P.A., *Design and evaluation of an algorithm for detecting current transformer saturation*, IEE Proceedings Generation, Transmission and Distribution, Vol. 151, No. 1, January 2004, pp. 27–35.
81. KANG Y.-C., PARK J.-K., KANG S.-H., JOHNS A.T., AGGARWAL R.K., *An algorithm for compensating secondary currents of current transformers*, IEEE Transactions on Power Delivery, Vol. 12, No. 1, January 1997, pp. 116–124.
82. KASZTENNY B., *Distance protection of series compensated lines – problems and solutions*, Proceedings of 28th Annual western Protective Relay Conference, Spokane, USA, 2001, pp. 1–34.
83. KASZTENNY B., HATZIADONIU C., FUNK A., *VSI-based series compensation scheme for transmission lines*, ETEP-European Transactions on Electrical Power, Vol. 9, No. 2, March–April 1999, pp. 101–108.
84. KASZTENNY B., IŻYKOWSKI J., ROSOŁOWSKI E., *Algorithms for protection of series compensated lines – the comparative analysis*, Proceedings of the 32nd Universities Power Engineering Conference – UPEC '97, Manchester, UK, 10–12 September 1997, Vol. 1, pp. 299–302.
85. KASZTENNY B., ROSOŁOWSKI E., ŁUKOWICZ M., IŻYKOWSKI J., *Current related relaying algorithms immune to saturation of current transformers*, Proceedings of Sixth Int. Conference on Developments in Power System Protection, Publication No. 434, Nottingham 1997, pp. 365–369.
86. KASZTENNY B., SHARPLES D., ASARO V., POZZUOLI M., *Distance relays and capacitive voltage transformers – balancing speed and transient overreach*, 55-th Annual Georgia Tech. Protective Relaying Conference, Atlanta, May 2–4, 2001, 22 p.
87. KAWADY T., STENZEL J., *A practical fault location approach for double circuit transmission lines using single end data*, IEEE Transactions on Power Delivery, Vol. 18, No. 4, 2003, pp. 1166–1173.
88. KEZUNOVIC M., AGANAGIC M., MCKERNNS S., HAMAI D., *Computing responses of series compensation capacitors with MOV protection in real time*, IEEE Transactions on Power Delivery, Vol. 10, No. 1, January 1995, pp. 244–251.
89. KEZUNOVIC M., KOJOVIC L.A., ABUR A., FROMEN C.W., SEVCIK D.R., PHILLIPS F., *Experimental evaluation of EMTP-based current transformer models for protective relay transient study*, IEEE Transactions on Power Delivery, Vol. 9, No. 1, January 1994, pp. 405–413.
90. KEZUNOVIC M., KOJOVIC L.A., SKENDZIC V., FROMEN C.W., SEVCIK D.R., NILSSON S.L., *Digital models of coupling capacitor voltage transformers for protective relay transient studies*, IEEE Transactions on Power Delivery, Vol. 7, No. 4, October 1992, pp. 1927–1935.
91. KEZUNOVIC M., MRKIC J., PERUNICIC B., *An accurate fault location algorithm using synchronized sampling*, Electric Power System Research, No. 29, 1994, pp. 161–169.
92. KEZUNOVIC M., PERUNICIC B., *Automated transmission line fault analysis using synchronized sampling at two ends*, IEEE Transactions on Power Systems, Vol. 11, No. 1, February 1996, pp. 441–447.
93. KIZILCAY M., KOCH K.-H., *Numerical fault arc simulation based on power arc test*, ETEP – European Transactions on Electrical Power, Vol. 4, No. 3, May/June 1994, pp. 177–185.
94. KIZILCAY M., PNIOK T., *Digital simulation of fault arcs in power systems*, ETEP-European Transactions on Electrical Power, Vol. 1, No. 1, January/February 1991, pp. 55–60.
95. KOGLIN H.-J., LOBOS T., *Recognition of arcing faults on transmission lines using a neural network*, Proceedings of the 12th Power System Computations Conference – PSCC '96, Dresden, August 1996, pp. 688–693.

96. KOJOVIC L.A., *PCB Rogowski coils benefit relay protection*, IEEE Computer Applications in Power, Vol. 15, No. 3, July 2002, pp. 50–53.
97. KOJOVIC L.A., BISHOP M.T., SKENDZIC V., *Coiled for protection*, IEEE Power and Energy Magazine, Vol. 1, No. 3, May/June 2003, pp. 43–48.
98. KOREJWO E., SYNAL B., TROJAK J., *Short HV transmission lines problems*, Proceedings of Second International Conference on Development in Power System Protection, IEE Conference Publication No. 185, London, 1980, pp. 196–200.
99. KUMAI T., NAKABAYASHI H., HIRATA Y., TAKAHASHI M., TERAI K., KAMINISHI T., UEHARA K., *Field trial of optical current transformer using optical fiber as Faraday sensor*, Power Engineering Society Summer Meeting, 2002 IEEE, Vol. 2, 2002, pp. 920–925.
100. LAWRENCE D.J., CABEZA L.Z., HOCHBERT L.T., *Development of an advanced transmission line fault location system. Part I: Input transducer analysis and requirements*, IEEE Transactions on Power Delivery, Vol. 7, No. 4, October 1992, pp. 1963–1971.
101. LEE C.J., PARK J.B., SHIN J.R., RADOJEVIC Z.M., *A new two-terminal numerical algorithm for fault location, distance protection, and arcing fault recognition*, IEEE Transactions on Power Systems, Vol. 21, No. 3, August 2006, pp. 1460–1462.
102. LI F., LI Y., AGGARWAL R.K., *Combined wavelet transform and regression technique for secondary current compensation of current transformers*, IEE Proceedings, Vol. 149, No. 4, July 2002, pp. 497–503.
103. LIAO Y., *Fault location utilizing unsynchronized voltage measurements during fault*, Electric Power Components and Systems, Vol. 34, No. 12, December 2006, pp. 1283–1293.
104. LIAO Y., ELANGOVAN S., *Unsynchronised two-terminal transmission-line fault-location without using line parameters*, IEE Proceedings – Generation Transmission Distribution, Vol. 153, No. 6, November 2006, pp. 639–643.
105. LIN Y.-H., LIU C.-W., CHEN C.-S., *A new PMU-based fault detection/location technique for transmission lines with consideration of arcing fault discrimination – Part I: Theory and algorithms*, IEEE Transactions on Power Delivery, Vol. 19, No. 4, October 2004, pp. 1587–1593.
106. LIN Y.-H., LIU C.-W., CHEN C.-S., *A new PMU-based fault detection/location technique for transmission lines with consideration of arcing fault discrimination – Part II: Performance evaluation*, IEEE Transactions on Power Delivery, Vol. 19, No. 4, October 2004, pp. 1594–1601.
107. LIN Y.-H., LIU C.-W., YU C.-S., *A new fault locator for three-terminal transmission lines – using two-terminal synchronized voltage and current phasors*, IEEE Transactions on Power Delivery, Vol. 17, No. 2, April 2002, pp. 452–459.
108. LUCAS J.R., MCLAREN P.G., *A computationally efficient MOV model for series compensation studies*, IEEE Transactions on Power Delivery, Vol. 6, No. 4, October 1991, pp. 1491–1497.
109. MAGNAGO F.H., ABUR A., *Advanced techniques for transmission and distribution system fault location*, CIGRE – Study Committee 34 Colloquium and Meeting, Preferential Subject 2 – Fault Location and System Restoration, 1999, Florence, Italy, Paper 215.
110. MAGNAGO F.H., ABUR A., *A new fault location technique for radial distribution systems based on high frequency signals*, IEEE PES Summer Meeting, 1999.
111. MARTI J.R., *Accurate modeling of frequency-dependent transmission lines in electromagnetic transient simulations*, IEEE Transactions on Power Apparatus and Systems, Vol. PAS–101, No. 1, 1982, pp. 147–155.
112. MARUSIC A., CAVLOVIC M., *Application of fuzzy logic to digital fault locator algorithm*, Proceedings of the 11th International Conference on Power System Protection – PSP '98, Bled, Slovenia, 1998, pp. 71–76.
113. MAUN J.-C., PHILIPPOT L., COEMANS J., MOUVET M., *Power system modelling for the design of advanced fault locators and line protections*, Paper SPT IC 12–01–0381, Proceedings of the IEEE/KTH Stockholm Power Tech Conference, Stockholm, Sweden, June 18–22, 1995, pp. 394–399.

114. MAZON A.J., MINAMBRES J.F., ZORROZUA M.B., ZAMORA I., ALVAREZ-ISASI R., *New method of fault location on double-circuit two-terminal transmission lines*, Electric Power Systems Research, No. 35, 1995, pp. 213–219.
115. MAZON A.J., ZAMORA I., GRACIA J., SAGASTABEITIA K., EGUIA P., JURADO F., SAENZ J.R., *Fault location system on double circuit two-terminal transmission lines based on ANN's*, 2001 IEEE Porto Power Tech Conference, 10th–13th September, Porto, Portugal, 0-7803-7139-9/01.
116. MCKENNA S.M., HAMAI D., KEZUNOVIC M., GOPALAKRISHNAN A., *Transmission line modeling requirements for testing new fault location algorithms using digital simulators*, Proceedings of the Second International Conference on Digital Power System Simulators – ICDS '97, Montreal, Canada, May 28–30, 1997, pp. 63–69.
117. MCLAREN P.G., MARCH G., *A saturation detector and its application to differential current protection*, Proceedings of the 4th International Conference Developments in Power System Protection, IEE Publication No. 302, 1980, pp. 15–19.
118. MINAMBRES J.F., ZAMORA I., MAZON A.J., ZORROZUA M.A., ALVAREZ-ISASI R., *A new technique, based on voltages, for fault location on three-terminal transmission lines*, Electric Power Systems Research, Vol. 37, No. 2, May 1996, pp. 143–151.
119. MOORE P.J., BO Z.Q., AGGARWAL R.K., *Digital distance protection for composite circuit applications*, IEE Proceedings – Generation Transmission Distribution, Vol. 152, No. 2, March 2005, pp. 283–290.
120. MOORE P.J., JOHNS A.T., *Performance of adaptive distance protection under high resistance earth faults*, CIGRE 1992, paper 34–203.
121. MOORE P.J., WHITTARD R., JOHNS A.T., *A novel earth fault location technique utilizing single ended measurements*, Proceedings of the IEEE/KTH Stockholm Power Tech Conference, Stockholm, Sweden, June 18–22, 1995, paper SPT IC 12–03–0515, pp. 406–410.
122. MUSIEROWICZ K., BANDURSKI W., *Estimation of protection's criterion values during arc distortion*, Electrical Power & Energy Systems, 24, 2002, pp. 734–742.
123. NAGASAWA T., ABE M., OTSUZUKI N., EMURA T., JIKIHARA Y., TAKEUCHI M., *Development of a new fault location algorithm for multi-terminal two parallel transmission lines*, IEEE Transactions on Power Delivery, Vol. 7, No. 3, July 1992, pp. 1516–1529.
124. NIE Y.X., YIN X.G., LI K.C. et al., *Development of an optical voltage transformer for power protection relays*, Electric Power Systems Research, Vol. 61, No. 2, March 2002, pp. 127–131.
125. NOVOSEL D., BACHMANN B., HART D., HU Y., SAHA M.M., *Algorithms for locating faults on series compensated lines using neural network and deterministic methods*, IEEE Transactions on Power Delivery, Vol. 11, No. 4, October 1996, pp. 1728–1736.
126. NOVOSEL D., HART D.G., SAHA M.M., GRESS S., *Optimal fault location for transmission systems*, ABB Review, No. 8, 1994, pp. 20–27.
127. NOVOSEL D., HART D.G., UDREN E., GARITTY J., *Unsynchronized two-terminal fault location estimation*, IEEE Transactions on Power Delivery, Vol. 11, No. 1, January 1996, pp. 130–138.
128. NOVOSEL D., PHADKE A., SAHA M.M., LINDAHL S., *Problems and solutions for microprocessor protection of series compensated lines*, Proceedings of Sixth International Conference on Developments in Power System Protection, 25–27 March 1997, Nottingham, UK; Conference Publication No. 434, IEE 1997, pp. 18–23.
129. NOVOSEL D., SAHA M.M., *Locating faults on series compensated lines using intelligent methods*, International Journal of Engineering Intelligent Systems for Electrical Engineering and Communications, Vol. 5, No. 4, December 1997, CRL Publishing Ltd., pp. 259–264.
130. PEREIRA M.C.E., ZANETTA L.C., *Fault location in transmission lines using one-terminal post-fault voltage data*, IEEE Transactions on Power Delivery, Vol. 19, No. 2, April 2004, pp. 570–575.

131. PEREIRA C.E.M., ZANETTA L.C. JR., *Optimization algorithm for fault location in transmission lines considering current transformers saturation*, IEEE Transactions on Power Delivery, Vol. 20, No. 2, April 2005, pp. 603–608.
132. PETERSON W., NOVOSEL D., HART D., CEASE T.W., SCHNEIDER J., *Tapping IED data to find transmission faults*, IEEE Computer Application in Power, Vol. 12, No. 2, April 1999, pp. 36–42.
133. PHADKE A.G., *Synchronized phasor measurements for protection and local control*, CIGRE, 1998, pp. 34–106.
134. PILCH Z., WINKLER W., *Phase-comparison and distance protection performance during simultaneous double faults*, Proceedings of the Third International Conference on Developments in Power System Protection, Conference Publication Number 249, 1985, pp. 42–45.
135. PRADHAN A.K., ROUTRAY A., PATI S., PRADHAN D.K., *Wavelet fuzzy combined approach for fault classification of a series-compensated transmission line*, IEEE Transactions on Power Delivery, Vol. 19, No. 4, October 2004, pp. 1–7.
136. RADOJEVIC Z.M., TERZIJA V.V., *Two-stage numerical algorithm for distance protection, fault location and arcing faults recognition*, Electrical Engineering, No. 88, 2006, pp. 289–295.
137. RICHARDS G.G., TAN O.T., *Fault location for transmission lines with current-transformer saturation*, IEE Proceedings Pt. C, Vol. 130, No. 1, January 1983.
138. RIOUL O., VETTERLI M., *Wavelets and signal processing*, IEEE SP Magazine, October 1991, pp. 14–38.
139. ROSOŁOWSKI E., IŻYKOWSKI J., KASZTENNY B., SAHA M.M., *Differential equation based impedance measurement for series-compensated lines*, Proceedings of IEEE Power Tech Conference, Budapest, Hungary, 29.08–02.10.1999, paper BPT99–316–16.
140. ROSOŁOWSKI E., IŻYKOWSKI J., SAHA M.M., *Differential equation based fault location algorithm for series-compensated transmission line*, Proceedings of Power Systems Computation Conference PSCC, Liege, 22–26 August, 2005.
141. ROSOŁOWSKI E., KASZTENNY B., IŻYKOWSKI J., SAHA M.M., *Fault loop impedance analysis for a transmission line with series capacitors and their overvoltage protection*, Proceedings of the 10th International Conference on Power System Protection – PSP ’96, Bled, Slovenia, 1998, pp. 21–26.
142. SACHDEV M., AGARWAL R., *Accurate fault location estimates from digital impedance relay measurements*, Proceedings of Third International Conference on Developments in Power System Protection, London, 17–19 April 1985, Conference Publication No. 249, pp. 180–184.
143. SACHDEV M.S., AGARWAL R., *A technique for estimating line fault locations from digital distance relay measurements*, IEEE Transactions on Power Delivery, Vol. 3, No. 1, January 1988, pp. 121–129.
144. SADEH J., HADJSAID N., RANJBAR A.M., FEUILLET R., *Accurate fault location algorithm for series compensated transmission lines*, IEEE Transactions on Power Delivery, Vol. 15, No. 3, July 2000, pp.1027–1033.
145. SAHA M.M., IŻYKOWSKI J., KASZTENNY B., ROSOŁOWSKI E., *Modeling fault conditions for protection of series compensated lines*, Proceedings of the International Conference on Power Systems Transients – IPST ’97, Seattle, Washington, USA, June 22–26, 1997, pp. 383–388.
146. SAHA M.M., IŻYKOWSKI J., KASZTENNY B. ROSOŁOWSKI E., *Improving protective relaying by on-line dynamic compensation of capacitive voltage transformers*, Proceedings of the 33rd Universities Power Engineering Conference – UPEC ’98, Edinburgh, UK, 8–18 September 1998, Vol. 1, pp. 336–339.
147. SAHA M.M., IŻYKOWSKI J., KASZTENNY B., ROSOŁOWSKI E., PALKI B.S., *Relaying algorithms for protection of series-compensated lines*, Proceedings of the International Conference on Modern Trends in the Protection Schemes of Electric Power Apparatus and Systems, October 28–30, 1998, New Delhi, India, pp. V-50–61.

148. SAHA M.M., IŻYKOWSKI J., ROSOŁOWSKI E., *A method of fault location based on measurements from impedance relays at the line ends*, Proceedings of IEE Eighth International Conference on Developments in Power System Protection, Amsterdam, 2004, pp. 176–179.
149. SAHA M.M., IŻYKOWSKI J., ROSOŁOWSKI E., *A two-end method of fault location immune to saturation of current transformers*, IEE Eighth International Conference on Developments in Power System Protection, Amsterdam, 2004, pp. 172–175.
150. SAHA M.M., IŻYKOWSKI J., ROSOŁOWSKI E., KASZTENNY B., *A new accurate fault locating algorithm for series compensated lines*, IEEE Transactions on Power Delivery, Vol. 14, No. 3, July 1999, pp. 789–797.
151. SAHA M.M., IŻYKOWSKI J., ROSOŁOWSKI E., PALKI B.S., *Fault location technique for a transmission line compensated with series capacitors at both ends*, Proceedings of 3rd International Conference on Power System Protection and Automation, 2004, New Delhi, India.
152. SAHA M.M., KASZTENNY B., IŻYKOWSKI J., ROSOŁOWSKI E., *A novel fault locating technique for transmission lines with series-compensation*, Proceedings of the Power Systems Computations Conference, PSCC'99, Trondheim, Norway, 1999, pp. 679–685.
153. SAHA M.M., KASZTENNY B., ROSOŁOWSKI E., IŻYKOWSKI J., *First zone algorithm for protection of series compensated lines*, IEEE Transactions on Power Delivery, Vol. 16, No. 2, 2001, pp. 200–207.
154. SAHA M.M., ROSOŁOWSKI E., IŻYKOWSKI J., *ATP-EMTP investigation of a new distance protection principle for series compensated lines*, Proceedings of International Conference on Power Systems Transients–IPST, New Orleans, September/October 2003, CD Rom, paper 5b-1.
155. SAHA M.M., ROSOŁOWSKI E., IŻYKOWSKI J., *Differential equation algorithm for locating faults on parallel series-compensated lines*, Proceedings of Third International Symposium: Modern Electric Power Systems – MEPS, Wrocław, Poland, 2006, pp. 289–295.
156. SAHA M.M., WIKSTROM K., IŻYKOWSKI J., ROSOŁOWSKI E., *Fault location in uncompensated and series-compensated parallel lines*, Proceedings of 2000 IEEE Power Engineering Society Winter Meeting, Singapore, January 2000, CD-ROM.
157. SAHA M.M., WIKSTROM K., IŻYKOWSKI J., ROSOŁOWSKI E., *New concept for fault location in series-compensated parallel lines*, Proceedings of 2001 IEEE Power Engineering Society Winter Meeting, Columbus, Ohio, USA, 2001, 6 p., CD-ROM.
158. SAHA M.M., WIKSTROM K., IŻYKOWSKI J., ROSOŁOWSKI E., *New fault location algorithm for parallel lines*, Proceedings of Seventh International Conference on Developments in Power System Protection, Amsterdam, April 2001, pp. 407–410.
159. SAHA M.M., WIKSTROM K., LIDSTROM S., KOPPARI L., *Implementation of new fault location technique for series-compensated lines*, CIGRE – Study Committee 34 Colloquium and Meeting, Preferential Subject 2 – Fault Location and System Restoration, October 1999, Florence, Italy, Paper 212.
160. SANDERSON J.V.H., PEREIRA P.S., *A device for the detection of CT saturation*, Proceedings of the 4th International Conference Developments in Power System Protection, IEE Publication No. 302, 1989, pp. 20–23.
161. SANT M.T., PAITHANKAR Y.G., *Online digital fault locator for overhead transmission line*, IEE Proceedings, 1979, Vol. 126, No. 11, pp. 1181–1185.
162. SCHWEITZER E.O. III, *A review of impedance-based fault locating experience*, Proceedings of the 14th Annual Iowa–Nebraska System Protection Seminar, 16.10.1990, Omaha, Nebraska, pp. 1–31.
163. SHENG L.B., ELANGOVAN S., *A fault location method for parallel transmission lines*, International Journal of Electrical Power and Energy Systems, Vol. 21, No. 4, May 1999, pp. 253–259.

164. SHENGFANG L., CHUNJU F., WEIYONG Y., HUARONG C., *A new phasor measurement unit (PMU) based fault location algorithm for double circuit lines*, Proceedings in Conference Publications of The Eighth International Conference on Developments in Power System Protection, April 2004, Amsterdam.
165. SILVEIRA E.G., PEREIRA C., *Transmission line fault location using two-terminal data without time synchronization*, IEEE Transactions on Power Systems, Vol. 22, No. 1, February 2007, pp. 498–499.
166. SONG Y.H., AGGARWAL R.K., JOHNS A.T., *Digital simulation of fault arcs on long-distance compensated transmission systems with particular reference to adaptive autoreclosure*, ETEP – European Transactions on Electric Power, Vol. 5, September/October 1995, pp. 315–324.
167. SONG G.B., SUONAN J., XU Q.Q. et al., *Parallel transmission lines fault location algorithm based on differential component net*, IEEE Transactions on Power Delivery, Vol. 20, No. 4, October 2005, pp. 2396–2406.
168. STRINGFIELD T.W., MARIHART D.J., STEVENS R.F., *Fault location methods for overhead lines*, Transactions of the AIEE, Part III, Power Apparatus and Systems, Vol. 76, August 1957, pp. 518–530.
169. STYVAKTAKIS E., BOLLEN M.H.J., GU I.Y.H., *A fault location technique for two and three terminal lines using high frequency fault clearing transients*, Proceedings of IEEE PowerTech Conference, Budapest, Hungary, August/September 1999, paper BPT99–410–22.
170. TAG ELDIN E.M., GILANY M.I., ABDELAZIZ M.M., IBRAHIM D.K., *An accurate fault location scheme for connected aged cable lines in double-fed systems*, Electrical Engineering, (2006) 88, pp. 431–439.
171. TAKAGI T., YAMAKOSI Y., YAMURA M., KONDOW R., MATSUSHIMA T., *Development of new type fault locator using the one–terminal voltage and current data*, IEEE Transactions on Power Apparatus and Systems, Vol. PAS–101, No. 8, August 1982, pp. 2892–2898.
172. TAKANI H., KUROSAWA Y., IM AI S., INUKAI M., *Analysis and evaluation of multi terminal fault location using actual fault data*, Proceedings in Conference Publications of The Eighth International Conference on Developments in Power System Protection, Amsterdam, April 2004, Vol. 1, pp. 208–211.
173. TANG Y.,WANG H.F., AGGARWAL R.K., JOHNS A.T., *Fault indicators in transmission and distribution systems*, Proceedings International Conference on Electric Utility Deregulation and Restructuring and Power Technologies – DRPT 2000, April 2000, pp. 238–243.
174. TERZIJA V.V., KOGLIN H.-J., *A new approach to arc resistance calculation*, Electrical Engineering, No. 83, 2001, Springer-Verlag, pp. 187–192.
175. TZIOUVARAS D.A., BENMOUYAL G., ROBERTS J., HOU D., *The effect of conventional instrument transformer transients on numerical relay elements*, Proceedings of Cigre 2001 S.C. 34 Colloquium, Sibiu, September 2001, Conference Publication No. 308, pp. 1–5.
176. TZIOUVARAS D.A., MCLAREN P., ALEXANDER G., *Mathematical models for current, voltage, and coupling capacitor voltage transformers*, IEEE Transactions on Power Delivery, Vol. 15, No. 1, January 2000, pp. 62–72.
177. TZIOUVARAS D.A., ROBERTS J., BENMMOUYAL G., *New multi-ended fault location design for two- or three-terminal lines*, CIGRE – Study Committee 34 Colloquium and Meeting, Preferential Subject 2 – Fault Location and System Restoration, 11–15.10.1999, Florence, Italy, Paper 213.
178. TZIOUVARAS D.A., ROBERTS J., BENMMOUYAL G., *New multi-ended fault location design for two- or three-terminal lines*, Proceedings of the International Conference on Developments in Power System Protection, 2001, Amsterdam.
179. VAUGHAN M., MOORE P.J., *A digital signal processing technique utilising VLF radio spectra for the detection of power system arcing faults*, Proceedings of the 13th Power systems Computations Conference – PSCC '99, Trondheim, Norway, June/July 1999, pp. 693–699.

180. WANG C., DOU C.X., LI X.B., JIA Q.Q., *A WAMS/PMU-based fault location technique*, Electric Power Systems Research, Vol. 77, 2007, pp. 936–945.
181. WILSON R.E., ZEVENBERGEN G.A., MAH D., MURPHY A.J., *Calculation of transmission line parameters from synchronized measurements*, Electric Machines and Power Systems, Vol. 27, No. 12, December 1999, pp. 1269–1278.
182. WISZNIEWSKI A., *Accurate fault impedance locating algorithm*, IEE Proceedings – Part C, Vol. 130, No. 6, 1983, pp. 311–315.
183. WISZNIEWSKI A., *Fault location correction of errors due to current transformers*, Proceedings of the Third International Conference on Developments in Power System Protection, April 1985, London, UK, Conference Publication, No. 249, pp. 185–187.
184. WISZNIEWSKI A., IŻYKOWSKI J., *Influence of ferroresonance suppression circuits upon the transient response of capacitive voltage transformers*, IEE Conference Publ. No. 125, Developments in Power System Protection, London 1975.
185. WISZNIEWSKI A., SZAFRAN J., *Distance algorithm immune to saturation of current transformers*, Proceedings of the International Conference on Developments in Power System Protection, London, 1989, pp. 196–199.
186. YU C.-S., LIU C.-W., YU S.-L., JIANG J.-A., *A new PMU-based fault location algorithm for series compensated lines*, IEEE Transactions on Power Delivery, Vol. 17, No. 1, January 2002, pp. 33–46.
187. ZAMORA I., MINAMBRES J.F., MAZON A.J., ALVAREZ-ISASI R., LAZARO J., *Fault location on two-terminal transmission lines based on voltages*, IEE Proceedings – Generation Transmission Distribution, Vol. 143, No. 1, January 1996, pp. 1–6.
188. ZHANG Q., ZHANG Y., SONG W., YU Y., *Transmission line fault location for phase-to-earth fault using one-terminal data*, IEE Proceedings – Generation Transmission Distribution, Vol. 146, No. 2, March 1999, pp. 121–124.
189. ZHANG Y., ZHANG Q., SONG W., YU Y., LI X., *Transmission line fault location for double phase-to-earth fault on non-direct-ground neutral system*, IEEE Transactions on Power Delivery, Vol. 15, No. 2, April 2000, pp. 520–524.
190. ZHANG Q., ZHANG Y., SONG W., YU Y., WANG Z., *Fault location of two-parallel transmission line for nonearth fault using one-terminal data*, IEEE Transactions on Power Delivery, Vol. 14, No. 3, July 1999, pp. 863–867.
191. ZIMMERMAN K. COSTELLO D., *Impedance-based fault location experience*, IEEE Rural Electric Power Conference, April 2006, pp. 1–16.

This book deals with impedance-based algorithms for locating faults on power transmission lines for inspection-repair purposes. A large group of one-end fault location algorithms are presented in a uniform way. To this end, the generalised models of fault loops and faults have been introduced. Extensive presentation of fault location algorithms, which apply the measurements performed at different line terminals, is a highlight of this book. Apart from synchronised measurements carried out with the satellite system GPS, the unsynchronised measurements are broadly presented. Analytical synchronisation of unsychronised measurements is discussed in relation to different options concerning fault locator input signals.

Material which is supplementary to the main issues of the book is also provided. In particular, configurations of transmission networks together with transmission line models are reviewed. Performance of the main components of fault locator measurement chains: capacitive voltage transformers, current transformers and analogue antialiasing filters, is analyzed.

This book meets the demands of courses taught at undergraduate and postgraduate levels. It is aimed at students who wish to familiarise themselves with the subject of transmission line faults, fault location, and distance protection.

Wydawnictwa Politechniki Wrocławskiej
są do nabycia w księgarni „Tech"
plac Grunwaldzki 13, 50-377 Wrocław
budynek D-1 PWr., tel. 071 320 29 35
Prowadzimy sprzedaż wysyłkową

ISBN 978-83-7493-430-5